Investigations on 1,2$\sigma^3\lambda^3$-Oxaphosphetanes

Dissertation

zur

Erlangung des Doktorgrades (Dr. rer. nat.)

der

Mathematisch-Naturwissenschaftlichen Fakultät

der

Rheinischen Friedrich-Wilhelms-Universität Bonn

vorgelegt von

Florian Gleim

aus

Neuwied

Bonn, 2024

Angefertigt mit Genehmigung der Mathematisch-Naturwissenschaftlichen Fakultät

der Rheinischen Friedrich-Wilhelms-Universität Bonn

Gutachter/Betreuer: Prof. Dr. Dr. h. c. Rainer Streubel

Gutachter: Prof. Dr. Robert Glaum

Tag der Promotion: 15.05.2025

Erscheinungsjahr: 2025

Die vorliegende Arbeit wurde im Zeitraum von November 2018 bis Dezember 2024 im Arbeitskreis von Prof. Dr. Dr. h.c. R. Streubel am Institut für Anorganische Chemie der Rheinischen Friedrich-Wilhelms-Universität in Bonn angefertigt.

Hiermit versichere ich, dass ich diese Arbeit selbst verfasst und keine anderen als die angegebenen Quellen und Hilfsmittel verwendet habe.

To my parents

“You can never know everything, and part of what you know is always wrong.
Perhaps even the most important part. A portion of wisdom lies in knowing that.
A portion of courage lies in going on anyways.“

- Robert Jordan, The Wheel of Time, Book One: The Eye of the World

-

Teilergebnisse aus dieser Arbeit wurden mit Genehmigung der Mathematisch Naturwissenschaftlichen Fakultät der Universität Bonn vorab veröffentlicht.

Veröffentlichungen:

1) 1,2$\sigma^3\lambda^3$-Oxaphosphetanes and Their P-Chalcogenides—A Combined Experimental and Theoretical Study, F. Gleim, A. García Alcaraz, G. Schnakenburg, A. Espinosa Ferao, R. Streubel, Molecules, **2022**, *27*, 3345-3356. DOI: 10.3390/molecules27103345
2) Where Wittig and Arbuzov meet: transient 1,2-oxaphosphetan-2-ium compounds and cationic oligomerization reactions, F. Gleim, A. García Alcaraz, G. Schnakenburg, A. Espinosa Ferao, R. Streubel, Chem. Commun., **2024**, *60*, 2625-2628. DOI: 10.1039/D4CC00254G

Tagungsbeiträge:

1) F. Gleim, R. Streubel, MHC-10 PhD Workshop, Tübingen (Germany) March 15th – 17th **2019**: "*On synthesis and oxidation of 1,2$\sigma^3\lambda^3$-oxaphosphetanes*" (oral contribution).
2) F. Gleim, R. Streubel, 16th European Workshop on Phosphorus Chemistry, Bristol (United Kingdom), April 24th – 27th **2019**: "*Synthesis and new reactions of 1,2$\sigma^3\lambda^3$-Oxaphosphetanes*" (poster contribution).
3) F. Gleim, R. Streubel, 17th European Workshop on Phosphorus Chemistry, Rennes (France), February 26th – 28th **2020**: "*Synthesis and P-oxidations of 1,2$\sigma^3\lambda^3$-Oxaphosphetanes*" (poster contribution).
4) F. Gleim, A. García Alcaraz, G. Schnakenburg, A. Espinosa Ferao, R. Streubel, 23rd International Conference on Phosphorus Chemistry, Online, July 5th – 9th **2021**, "*Synthesis and P-oxidations of 1,2$\sigma^3\lambda^3$-Oxaphosphetanes*" (poster contribution).
5) F. Gleim, R. Streubel, MHC-11 PhD Workshop, Bonn (Germany), September 3rd – 5th **2021**: "*On reactions of 1,2$\sigma^3\lambda^3$-oxaphosphetanes*" (oral contribution).
6) F. Gleim, R. Streubel, 16th International Symposium on Inorganic Ring Systems, Graz (Austria), July 24th – 29th, **2022**: "Synthesis and reactions of non-diastereomeric 1,2$\sigma^3\lambda^3$-oxaphosphetanes" (poster contribution).
7) F. Gleim, R. Streubel, 18th European Workshop on Phosphorus Chemistry, Rostock (Germany), September 14th – 16th **2022**: "Arbuzov meets Wittig: Alkylation of 1,2-Oxaphosphetanes" (poster contribution).

8) F. Gleim, A. Espinosa Ferao, R. Streubel, 19th European Workshop on Phosphorus Chemistry, Donostia-San Sebastián (Spain), March 28th – 30th **2023**: "Ring Opening Reactions of *1,2$\sigma^3\lambda^3$*-Oxaphosphetanes" (oral contribution).
9) F. Gleim, A. Espinosa Ferao, R. Streubel, 20th European Workshop on Phosphorus Chemistry, Würzburg (Germany), March 4th – 6th **2024**: "Ring Opening Reactions of 1,2$\sigma^3\lambda^3$-Oxaphosphetanes" (poster contribution).

Acknowledgment

There are many people that helped me in one way or another during the last years, people I am very grateful for and without their help I would not have had the strength and endurance to finish this project. Thank you all!

First of all, I want to thank Prof. Dr. Dr. h.c. Rainer Streubel for the supervision of this thesis, and the possibility to attend several international conferences and to have a research stay in Japan. Dear Rainer, I know it's not always been easy, but I appreciate that you pulled through this project together with me. Thank you, a lot.

I thank Prof. Dr. Robert Glaum for being my second reviewer, as well as Prof. Dr. Arne Lützen and Prof. Dr. Diana Imhof for being part of my examination committee.

I want to thank Prof. Dr. Arturo Espinosa Ferao (University of Murcia, Spain) for performing theoretical calculations on my project and providing new interesting input; and especially for some last minute calculations. I want to thank Prof. Dr. Norihiro Tokitoh (Kyoto University, Japan) for hosting me for two months in his work group in Uji, and him and Prof. Dr. Yoshiyuki Mizuhata (Kyoto University, Japan) for supervision during this stay.

I'd like to thank the analytical departments of the University of Bonn. I want to thank Dr. Gregor Schnakenburg and Charlotte Rödde for the measurement and solution of various X-ray crystal structures. I thank the NMR department and especially graduate engineer Karin Prochnicki for many, many NMR-measurements. I thank the mass spectrometry department, Dr. Marianne Engeser, Christine Sondag, Karin Peters-Pflaumbaum and Annette Reiner for measuring samples on various spectrometers and high helpfulness even on short terms.

Also, I'd like to express my gratitude to Dr. Ralf Weisbarth and Dr. Jürgen Tirrée, who always provided hands on help when something in the lab wasn't working. I also thank Dr. Wilfried Assenmacher, for the pleasant working conditions when supervising the undergrad lab course (my yearly "vacations in the solid state chemistry").

I want to thank Dr. Andreas Kyri and Dr. Robert Kunzmann for supervision during my focusing lab course and master thesis that lead to this project, and Robert for his helpfulness during my research stay in Kyoto.

I also want to thank my colleagues. We had many productive discussions, some even on chemistry, a vast number of shared coffee breaks (all, well, mostly all, documented and analysed), several evenings with stronger drinks and conference stays with too many people in Airbnbs. My years in the workgroup were often strenuous, frustrating and exhausting; they were, however, never boring. First and foremost, this is due to Dr. Philipp Brehm, my long-time lab mate and in personal union curse and blessing of my PhD time. I also have to thank him for contributing quantum chemical calculations to this thesis. The other cursed blessing of my PhD time would be Dr. Tim Kalisch. Although these two know no personal boundaries and their energetic behaviour doesn't always interact well with my slightly lethargic ground state, I count myself very lucky to be part of this triumvirate. We spent a lot of time together in and out of the lab, usually over coffee (entered into the coffee list and meticulously evaluated) or beer (preferably crafted), and I'm glad to call them friends (since all our contracts expired, the term "colleagues" was no longer fitting). I also want to thank, for discussions, a good working atmosphere, general fun on conferences or here in Bonn, and the occasional pen and paper session: Dr. David Biskup, Dr. Shahriar Kermanshahian, Dr. Tatjana Terschüren, Dr. Philip Junker, and Dr. Mridhul Ram. I also thank the PhD students of the Glaum group for adopting me into their social events, especially the Dönerstage. Another thanks goes to the members of the "Anorganiker Stammtisch" and the "Kekulé Kegel Klub".

So, these were all the university related people. Now, off to the private relations. I'm glad to call many people my friends, and all of them had to bear with my endless nagging and self-loathing. Thank you all for staying anyway and all the support I got from you! For keeping me focused and pushing me on when necessary and for distraction when reality came too close. I thank my P&P play groups: Dennis Werner, Dr. Denise Meinberger, Thomas Fröhlich, Jan Werner, Sina Werner, Sascha Werner and Philipp Nechterschen; Dominik Delle, Kathi Peschetz, Elena Melcher, Artur Malyi and Jan Thimm. I especially thank each poor soul who ever DM'ed a game for me. Another special thanks goes to Denise, for keeping each other company in many Zoom sessions while writing up our respective theses. Another group of persons I'm very thankful for are my "Girls' Night" girls, for many shared evenings in front of computer screens during Covid curfew and after, most of all Tabea Lohrmann (for each and every medieval fair, cooking session and long nights on the couch with Doctor Who, for being there for each other), but also: Sandra Czypionka, Kristin Gratzfeld, Anna Jonczyk, Frederike Kohrs, Dr. Kim Schuppener, and Sandra Trapp. I also want to thank my long-time and long-distant friend Stefanie Falldorf, who matches my sarcasm level to well. Thanks for all the time spent silently on Skype, the "Finteler Bettspieltage" and all the other trips. I also want to add a thank you to all the friends I don't see as often as they deserve it, but who accompanied me during my studies: Patrick Michalke (for half-

drunken studying sessions, for making me pass physics, for aftercare after that one chemists' party), Kai Ranke and Marius Burschka.

Now, for the last, and most important, I want to thank my family. First and foremost, my parents for always supporting me on my way; from Latin vocabulary and simple math problems to supporting me during my years of studying and the whole dissertation process, I thank you from the depths of my heart. I'm also grateful to my brother Maximilian, especially as he also doubles as my first level tech support and car mechanic, two things in which I'm inappropriately inept in.

Table of Contents

Used Abbreviations

12-crown-4	1,4,7,10-tetraoxacyclododecane
1D	one dimensional
2D	two dimensional
Ø	diameter
°	angular degree
°C	degree Celsius
Δ	thermal energy, difference
Δ	chemical shift
η^n	hapticity n
Θ	Bragg angle
λ^n	number n of all bonds
$\tilde{\nu}$	wavenumber
Ξ	frequency ratio
P	density
Σ	sum
σ^n	number n of all binding partners
Å	Ångström (10^{-10} m)
a, b, c, α, β, γ	unit cell parameters
Ac	acyl,
Ad	1-adamantyl, tricyclo[3.3.1.$1^{3,7}$]dec-1-yl
APCI	atmospheric pressure chemical ionization
Ar	aryl
ATR	attenuated total reflection
br	broad
Bu	*n*-butyl
C	concentration
cat.	catalyst, catalytic amounts
cf.	confer, compare
COSY	correlated spectroscopy
Cp	cyclopentadienyl
Cp*	pentamethylcyclopentadienyl
Cy	cyclohexyl

D	doublet or bond distance
DBU	1,8-diazabicyclo[5.4.0]undec-7-ene
DFT	density functional theory
DPPE	1,2-bis(diphenylphosphino)ethane
e.g.	exempli gratia, for example
EI	electron impact ionization
eq.	equivalent
ESI	electron spray ionization
Et	ethyl
EWG	electron withdrawing group
exp.	experimental
F(000)	structure factor evaluated in the zeroth order case h = k = l = 0
FTIR	Fourier-transform infrared
G	Gibbs free energy
g	gram
H	hour
HMQC	heteronuclear multiple quantum correlation
HOMO	highest occupied molecular orbital
HRMS	high resolution mass spectrometry
HSQC	heteronuclear single quantum coherence
hv	irradiation, photochemical reaction
Hz	Hertz
i.e.	id est, it is
iPr	iso-propyl
IR	infrared
kbar	kilobar
kcal	kilocalories
L	ligand
LIFDI	liquid injection field desorption
LUMO	lowest unoccupied molecular orbital
M	metal
m	meta
Me	methyl
Mes	2,4,6-trimethylphenyl

Mes*	2,4,6-tri-*tert*-butylphenyl
min	minuets
mL	millilitres
mmol	millimole
mol	mole
MS	mass spectrometry
^{n}Bu	*n*-butyl
NHC	N-heterocyclic carbene
$^{n}J_{X\text{-}Y}$	coupling constant
NMR	nuclear magnetic resonance
o	ortho
o-chloranil	3,4,5,6-tetrachlorocyclohexa-3,5-diene-1,2-dione
OTf^{-}	trifluoromethanesulfonate
p	para
PEG	poly ethlene glycole
Ph	phenyl
ppm	parts per million
q	quartet
R, R^1, R^2, R^3 ...	organic substituent
R^2	coefficient of determination
r.t.	room temperature, ambient temperature
s	singlet or strong
sat	satellites
SNR	signal-to-noise-ratio
SPS	solvent purification system
T	temperature
t	Triplet
^{t}Bu	*tert*-butyl
TEMPO	2,2,6,6-tetramethylpiperidin-1-oxyl
theor.	theoretical
THF	tetrahydrofuran
Tip	2,4,6-triisopropylphenyl
TMEDA	N,N,N',N'-tetramethylethane-1,2-diamine
trityl	triphenylmethyl

Tsi	trisyl, tris(trimethylsilyl)methyl
V	volume
vs	very strong
VT	variable temperature
w	weak
X	halogen, halide
xs.	excess
Z	number of formula units in unit cell

1 Introduction

1.1 Phosphorus, the versatile element

Phosphorus is the eleventh most abundant element of the earth crust.[1] In the free nature, it mainly occurs in the form as phosphates in minerals, the most common being apatite $Ca_5X(PO_4)_3$ (X= OH, F, Cl).[2] This mineral is of special interest, since bones and teeth are composed of hydroxyl apatite $Ca_5(OH)(PO_4)_3$.[3] But it doesn't stop there, phosphorus is one of the elements of life,[4] and is also found in different parts of the human body. The backbone of our DNA is connected *via* phosphate units,[5] our cell membranes consist of phospholipids,[6] and adenosine triphosphate (ATP) is the main product of the cellular respiration and the energy currency of our body.[7] So, phosphorus is in our body, and since its discovery in 1669 by Henning Brand,[8] we found a lot of other uses for it. From matches[9] to warfare (*e.g.* smoke screens[10], incendiaries and tracer bullets[11]), to flame retardants[12] and food additives (*e.g.* as melting salts and acid regulators)[13], as ligands in transition metal chemistry[14] or on its own as organo-catalyst[15], and maybe most important, as phosphate fertilizer[16].

Phosphorus (and its compounds) come in many different forms and properties. Elemental phosphorus alone has a number of allotropes. Phosphorus was first discovered as white phosphorus, which consists of P_4 tetrahedrons. In the solid phase, four modifications of white phosphorus are known, with the cubic α-form being the most stable at room temperature.[17] White phosphorus evaporates at 280°C, and at 1200°C mostly decomposes to P_2 molecules (analogous to N_2).[18] White phosphorus is by far the most reactive allotrope, being prone to self-ignition under air and oxidizing first to P_4O_6 and then to P_4O_{10}.[19] If white phosphorus is heated under exclusion of oxygen for an elongated time at 260°C, it transforms to red phosphorus. Red phosphorus consists of various amorphous and crystalline structures.[19] If further heated at 550°C for several days, red phosphorus transforms to violet or Hittorf's phosphorus. Violet phosphor consists of layers of tube-like structures which are perpendicularly connected to the next layer of tubes. Violet phosphorus is insoluble and non-conductive. Black phosphorus is the high-pressure modification and is formed when heating white phosphorus at 200°C at very high pressures (12 kbar). It consists of a two-layer structure, forming folded six-membered rings. This modification possesses semi-conductor properties similar to graphene, due to similar structural features.[19]

But the versatility of phosphorus doesn't end at the various modifications of the element. Phosphorus forms numerous compounds, having oxidation states which range from −III to +V. The preferred

oxidation states are −III (PH_3, metal phosphides), +III (triorganophosphanes, triorganophosphites, etc.), and the thermodynamically most stable +V (phosphane oxides, phosphates). Phosphorus forms compounds with a broad spectrum of other elements, be it inorganic (*e.g.*: Na_3P, PCl_3, P_4S_3, $Ca_5[(OH)(PO_4)_3]$) or organic (*e.g.*: PPh_3, $PCl(NEt_2)_2$, $P(OEt)_3$, $O{=}P(OEt)_3$). Since its discovery in 1669, scientist have further investigated phosphorus and its various compounds, always looking for new academic insights and practical applications.

This thesis will focus on the synthesis and reactivity of 1,2$\sigma^3\lambda^3$-oxaphosphetanes, a beforehand elusive and only shortly before this thesis reported four-membered heterocycle sharing a P-O bond. Before the experimental results will be discussed, this thesis will give a closer introduction to small phosphorus heterocycles and selected phosphaorganic reactions.

1.2 Synthesis of phosphorus heterocycles

1.2.1 Carbocycles containing only one heteroatom

1.2.1.1 General introduction and early developments

Heterocycles are named according to the Hantzsch-Widman nomenclature. In this, the ring size and saturation is given by a suffix (*e.g.* -etane for a saturated, -ete for a maximal unsaturated, four-membered ring), and the contained heteroatoms are listed as prefixes (*e.g.* phospha- for phosphorus, oxa- for oxygen). If more than one heteroatom is contained, their positions are given by locants. *E.g.*, a saturated cyclic compound with the atom arrangement -O-PH-CH_2-CH_2- would be an 1,2-oxa-phosph(a)-etane.[20] Following this nomenclature, a size-dependent series of heterocyclic compounds containing one phosphorus atom can be named (see Figure 1.1).

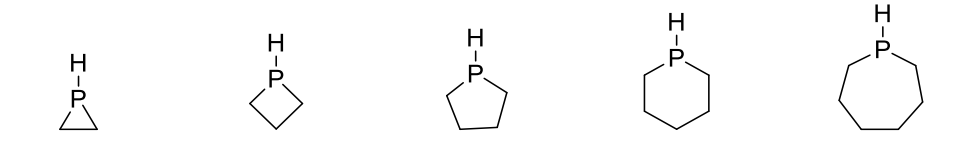

Figure 1.1: Homologous row of phosphacycles.

In the following, a short overview of these CH_2-homologous cycles will be given, starting from the larger phosphinane **VI** going to the smaller rings.

The history of phosphacycles stretches back to 1915, when Grüttner and Wiernik presented the reaction of a bifunctional Grignard reagent **VI** with $PhPCl_2$ (**VII**), leading to 1-phenyl-phosphinane (**VIII**) (see Scheme 1.1, top).[21] Shortly after, Grüttner and Krause presented the synthesis of the first phospholane **X** by a similar reaction (see Scheme 1.1, bottom).[22]

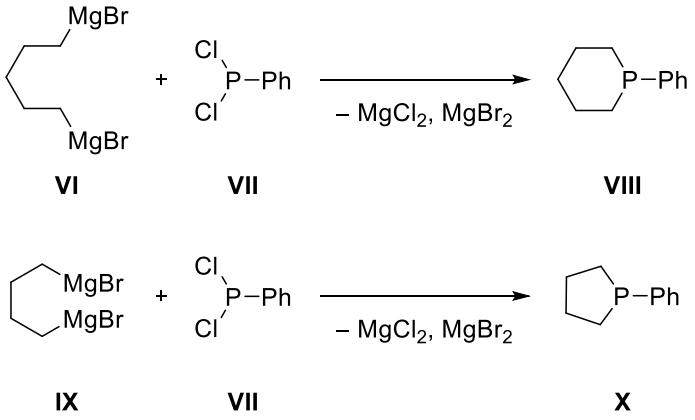

Scheme 1.1: Synthesis of phosphinane **VIII**[21] and phospholane **X**[22]

In 1953 Wittig and Geissler reported the first synthesis of a phosphole derivative. Dibenzophosphole **XII** was first obtained in a mixture as a thermal decomposition product from PPh_5 (**XI**), and was then selectively prepared from dilithium species **XII** and dichlorophenylphosphane (**VII**).[23]

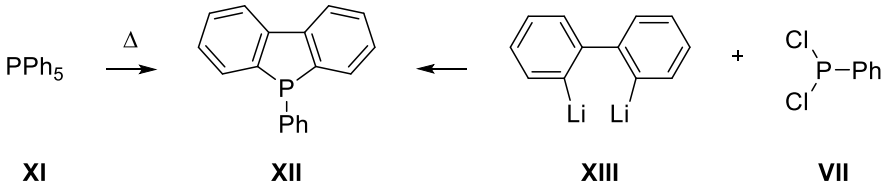

Scheme 1.2: Synthesis of tricyclic phosphole **XII**.[23]

1953 was also the year of the great breakthrough in the synthesis of five-membered phosphacyles. The so-called McCormack reaction (see Scheme 1.3) allowed for a facile synthesis of 2,5-dihydrophosphole oxides like **XVII**.[24] This kickstarted the phosphole/phospholane chemistry for the next decades.[25]

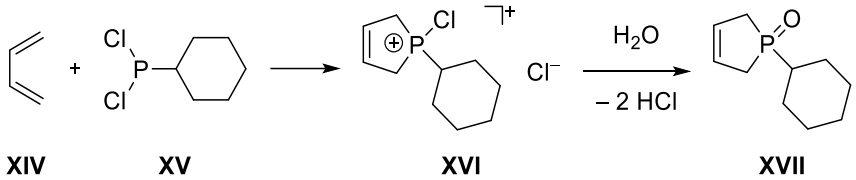

Scheme 1.3: The McCormack reaction.[24]

Later, in 1970 Quin presented the synthesis of 1-benzylphosphole **XXIV** (see Scheme 1.4). He also reported the X-ray crystal structure of **XXIV**, showing that the P-CH_2Ph bond is at an angle of 67° towards the ring plane.[25,26] This experimental evidence shows that phospholes (in contrast to furans,

thiophenes and pyrroles) are not (or only very weakly) aromatic, as the free electron pair at phosphorus is not participating in the delocalized π-system.

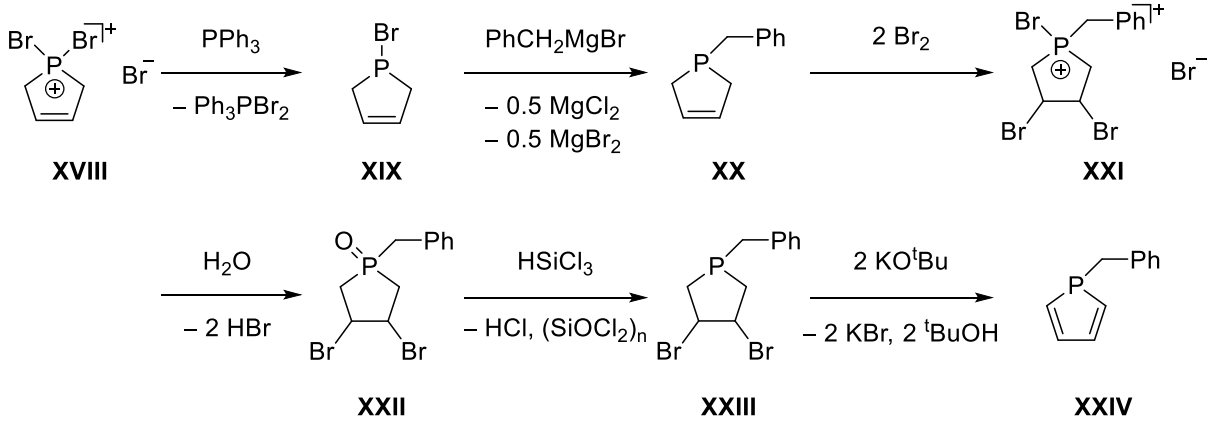

Scheme 1.4: Synthesis of 1-benzylphosphole **XXIV**.[26]

A further facilitating step was the discovery of Mathey in 1969 that the "McCormack product" **XXV** can be directly converted to the corresponding phosphole **XXVI** by addition of base (see Scheme 1.5).[27]

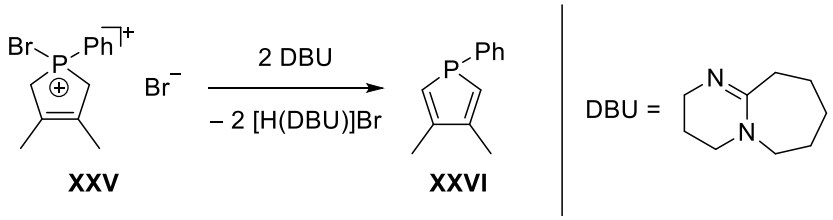

Scheme 1.5: Direct dehydrohalogenation of **XXV**.[27]

Leaving the domain of the five-membered rings, 1962 showed the first synthesis of a phosphetane *P*-oxide **XXXI** *via* the reaction of olefin **XXVII** and PCl_3 in the presence of $AlCl_3$ (see Scheme 1.6).[28] The reaction occurs over a nucleophilic attack of the olefinic double bond at phosphorus, leading to secondary carbenium **XXVIII**. **XXVIII** then undergoes a [1,2] sigmatopic methyl shift forming the more stable tertiary carbenium **XXIX**. Phosphorus now attacks the carbenium centre intramolecularly, forming the phosphetanium cation **XXX**. After hydrolysis, **XXX** yields **XXXI** as desired product.

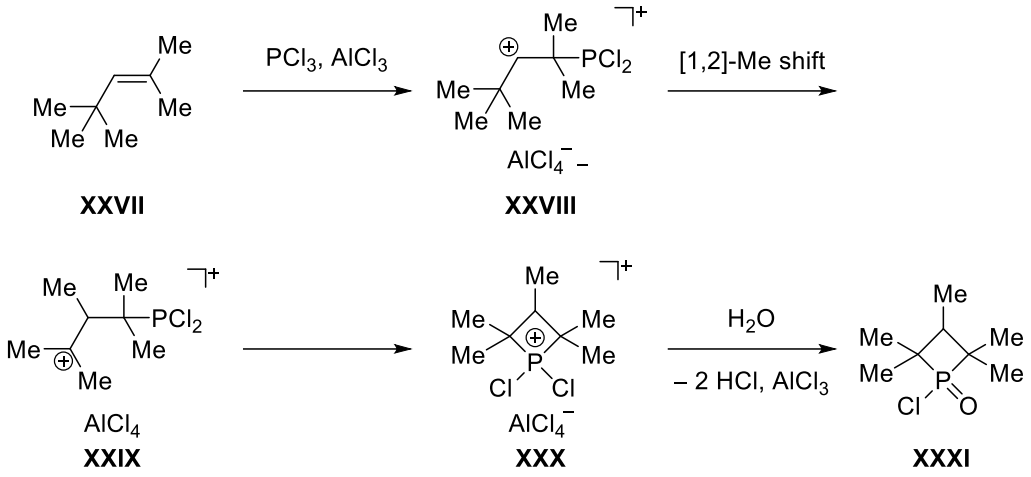

Scheme 1.6: Synthesis of phosphetane *P*-oxide **XXXI**.[28]

Shortly after in 1967 Chorvat demonstrated that phosphetane oxides can be reduced to the corresponding phosphetanes by trichlorosilane. [29]

Also in 1967, Wagner reported the synthesis of phosphirane **XXXIV** by reaction of 1,2-dichloroethane (**XXXII**) and sodium phosphanide (**XXXIII**).[30]

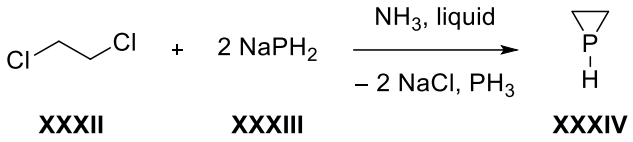

Scheme 1.7: Synthesis of phosphirane **XXXIV**.[30]

1.2.2 Small heterocycles containing both phosphorus and oxygen

Given the vast reactivity of small oxygen heterocycles and the many interesting properties of phosphorus, heterocycles containing both oxygen and phosphorus are of great synthetic interest.

1.2.2.1 Oxaphosphiranes

The smallest possible P-O-heterocycles are the three-membered oxaphosphiranes. Given that phosphorus can be either trivalent or pentavalent, both "high-coordinate" $\sigma^5\lambda^5$- **XXXV** or $\sigma^4\lambda^5$-oxaphosphiranes **XXXVI** as well as "low-coordinate" $\sigma^3\lambda^3$-oxaphosphiranes **XXXVII** are possible, as well as $\sigma^3\lambda^3\eta^1$-oxaphosphirane metal complexes **XXXVIII** (see Figure 1.2).

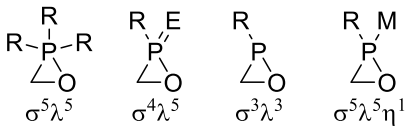

XXXV **XXXVI** **XXXVII** **XXXVIII**

Figure 1.2: The subcategories of oxaphosphiranes.

The $\sigma^3\lambda^3$-oxaphosphiranes were for the longest time a very elusive compound class, as the oxidation of a phosphaalkenes leads to the phosphaalkene oxides **XXXIX** instead to the desired oxaphosphirane **XL**.[31] Conclusions from early theoretical studies by Schöller suggest that the oxaphosphirane **XL** and the acyclic valence isomer **XXXIX** are in equilibrium, and that **XXXIX** is strongly preferred (see Scheme 1.8).[32] More recent calculations by Espinosa Ferao validate these findings. The valence isomerisation of a large number of oxaphosphiranes **XL** were calculated, showing an exothermic reaction for most cases. Only the use of electron withdrawing fluorine or trifluoromethyl groups yielded stable oxaphosphiranes **XL** (R_2, R_3 = F; R_1, R_2, R_3 = CF_3).[33]

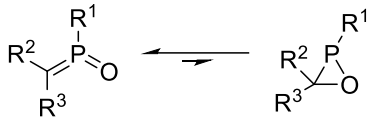

XXXIX **XL**

Scheme 1.8: Valence isomerisation of **XL**.

A possibility to obtain stable oxaphosphiranes is the involvement of the free electron pair of phosphorus in bonding, *i.e.*, by forming higher coordinate $\sigma^4\lambda^5$-oxaphosphiranes instead of $\sigma^3\lambda^3$-oxaphosphiranes. The first and only result was presented by Röschenthaler using the reaction of iminophosphane **XLI** with hexafluoroacetone **XLII** (see Scheme 1.9).[34]

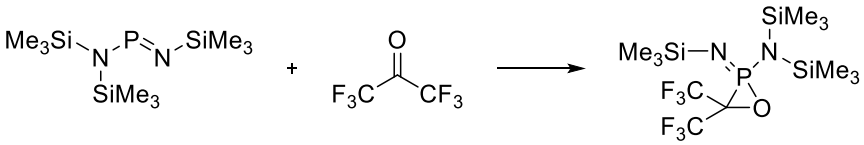

XLI **XLII** **XLIII**

Scheme 1.9: Synthesis of $\sigma^4\lambda^5$-oxaphosphirane **XLIII**.[34]

Another way to block the phosphorus lone pair is by coordinating a metal fragment, thus resulting in η^1-oxaphosphirane metal complexes. The first successful synthesis of an oxaphosphirane metal

complex **XLV** was reported by Mathey in 1990 by oxidizing a phosphaalkene tungsten complex **XLIV** with *meta*-chloroperbenzoic acid (see Scheme 1.10).[35]

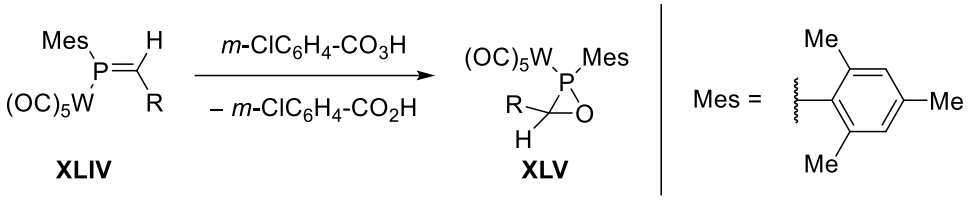

XLIV **XLV**

Scheme 1.10: Synthesis of oxaphosphirane complexes **XLV**.[35]

The synthesis of oxaphosphirane complexes could also be achieved by reaction of transient phosphinidene complexes with aldehydes, as published by Streubel in 1994. The synthesis could be achieved but was rather elaborate and yields were low. [36]

The breaktrough in the synthesis of oxaphosphirane complexes was presented by Streubel in 2007, *i.e.*, the addition of Li/Cl phosphinidenoid complexes **XLVI** to aldehydes and ketones **XLVII** (see Scheme 1.11).[37] The first publication only presented the case for R^1 = $CH(SiMe_3)$ and M = W, but in the meantime, the synthesis of chromium[38], molybdenum[38] and iron[39] complexes was published, as well as *P*-C_5Me_5[38] and *P*-CPh_3[40] compounds, and even the much smaller *P*-*tert*-butyl[41] substituent could be realized.

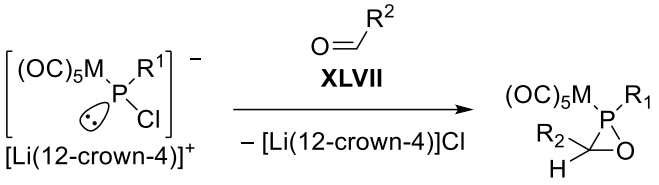

XLVI **XLVIII**

Scheme 1.11: Synthesis of oxaphosphirane complexes **LXVIII**.[37]

The newest development in oxaphosphirane chemistry was the discovery that suitable oxaphosphirane complexes could be decomplexed using ligand displacement strategies. In 2023 Streubel published the decomplexation of **IL** using a chelating ligand, yielding the first free $\sigma^3\lambda^3$-oxaphosphirane **L** (see Scheme 1.12).[42]

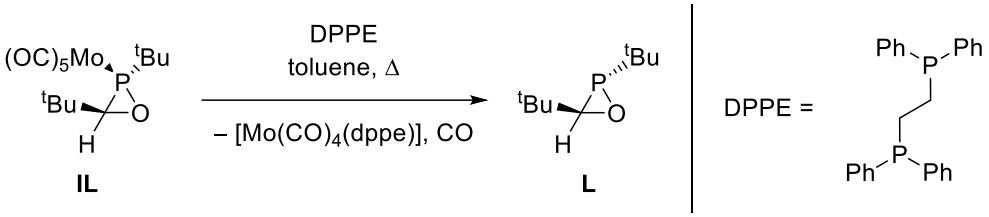

IL **L**

Scheme 1.12: Synthesis of the first free oxaphosphirane **L**.[42]

1.2.3 1,2-Oxaphosphetanes

The substance class of 1,2-oxaphosphetanes can be split into three subgroups, the pentacoordinate pentavalent $\sigma^5\lambda^5$ **LI**, the tetracoordinate pentavalent $\sigma^4\lambda^5$ **LII**, and the tricoordinate trivalent $\sigma^3\lambda^3$ **LIII** derivatives (see Figure 1.3). There is also the possibility to form complexes of the 1,2$\sigma^3\lambda^3$-oxaphosphetanes **LIII**, leading to 1,2$\sigma^3\lambda^3$-oxaphosphetane metal complexes **LIV**.

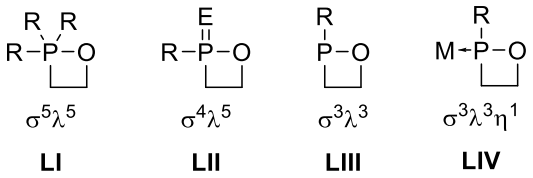

$\sigma^5\lambda^5$ $\sigma^4\lambda^5$ $\sigma^3\lambda^3$ $\sigma^3\lambda^3\eta^1$

LI **LII** **LIII** **LIV**

Figure 1.3: The subcategories of 1,2-oxaphosphetanes.

The "high-coordinate" 1,2$\sigma^5\lambda^5$-oxaphosphetanes are best known as being potential intermediates in the Wittig reaction, where they can be formed as [2+2]-cycloaddition product between a phosphorylid **LV** and a carbonyl **LVI**. These so-called "Wittig-oxaphosphetanes" **LVII** then undergo retro-[2+2]-cycloaddition to yield a phosphane oxide **LVIII** and an olefin **LIX** (see Scheme 1.13, and Chapter 1.3.1 for further information about the Wittig reaction).

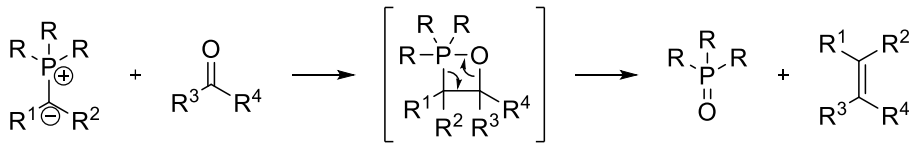

LV **LVI** **LVII** **LVIII** **LIX**

Scheme 1.13: The 1,2$\sigma^5\lambda^5$-oxaphosphetane **LVII** as intermediate of the Wittig reaction.

1,2$\sigma^5\lambda^5$-Oxaphosphetanes have also been found as intermediates in the phosphane-mediated deoyxgenative homocoupling of ketones to yield olefins (see Scheme 1.14).[43]

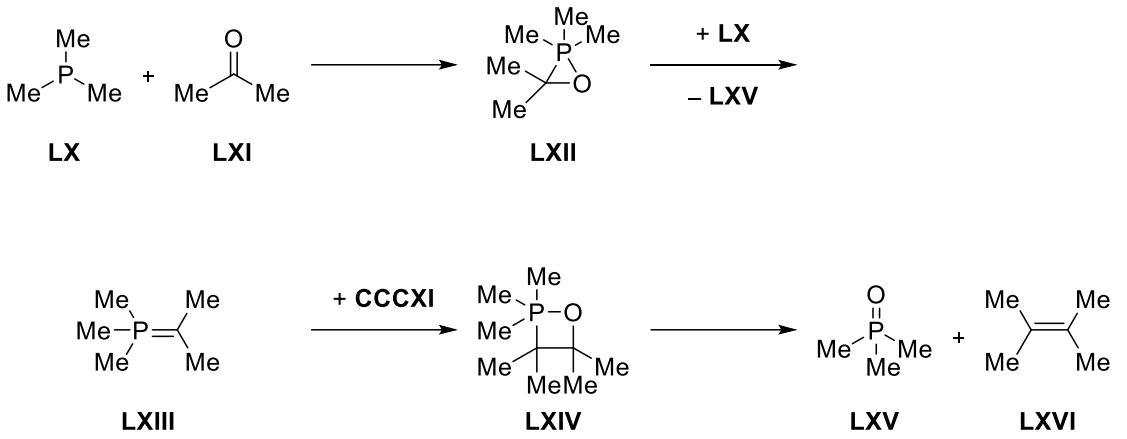

Scheme 1.14: Deoxygenative homocoupling of **LXI**.[43]

Although most 1,2$\sigma^5\lambda^5$-oxaphosphetanes are unstable under normal conditions, the synthesis of some stable derivatives were reported as early as 1967 by Matthews (see Scheme 1.15)[44,45]. At this time, it was still discussed if the first formed intermediate in the Wittig reaction was a betaine or a 1,2-oxaphosphetane. So, Matthews expected a betaine structure **LXVIII'** as product, but the experimental evidence (*e.g.* the presence of two doublet signals in the $^{31}P\{^1H\}$ NMR spectrum) strongly hinted to the cyclic structure of **LXVIII**. This was soon proved by obtaining a X-ray diffraction crystal structure.[46] There are also several other stable 1,2$\sigma^5\lambda^5$-oxaphosphetane known.[47]

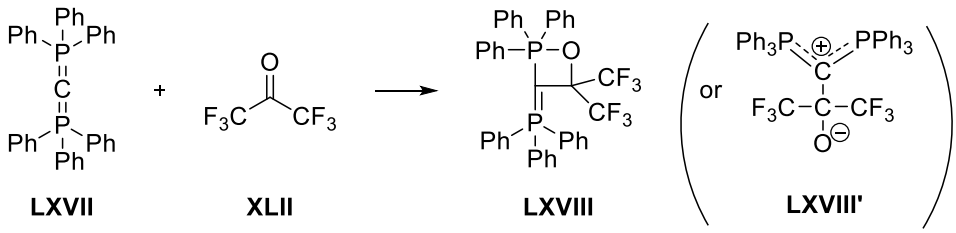

Scheme 1.15: Synthesis of stable 1,2$\sigma^5\lambda^5$-oxaphosphetane **LXVIII**.[44,45]

In the following time, it was also possible to obtain X-ray crystal structures of different 1,2$\sigma^5\lambda^5$-oxaphosphetanes (see Figure 1.4). Common features to stabilise the four-membered ring are the use of electron withdrawing groups and incorporating the phosphorus in a rigid spirocyclic system. In the case of **LXXIII**, the relative stability most likely results from a high lying transition state, and the resulting olefin would possess a highly strained cyclopropylidene group.

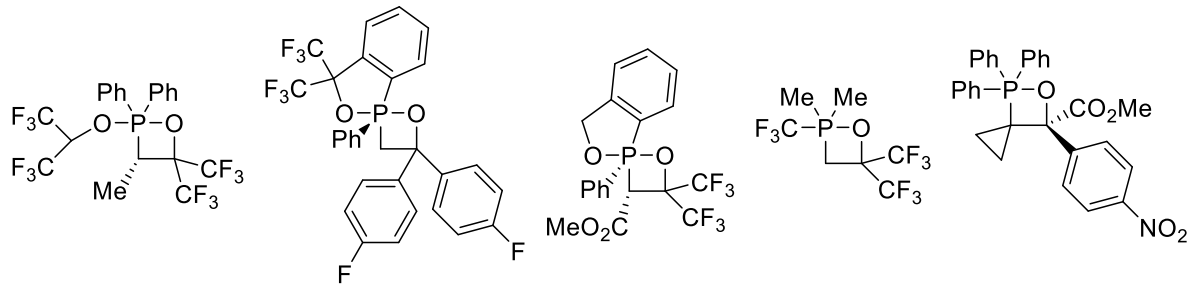

LXIX **LXX** **LXXI** **LXXII** **LXXIII**

Figure 1.4: Examples of 1,2σ^{5}λ^5-oxaphosphetanes with known crystal structure: **LXIX**[48], **LXX**[49], **LXXI**[50], **LXXII**[51], **LXXIII**[52].

In contrast, the chemistry of the "low-coordinate" 1,2σ^{3}λ^3-oxaphosphetanes was unknown for a long time. Before the work of the Streubel group, there was only one proposed derivative of a 1,2σ^{3}λ^3-oxaphosphetane. In 1991 Samuilov proposed the polycyclic structure **LXXVI** as reaction product of a 2*H*-1,2,3-diazaphosphole **LXXIV** and a cyclopentadienone **LXXV** (see Scheme 1.16).[53] However, they did not report a crystal structure, so the structure was not confirmed.

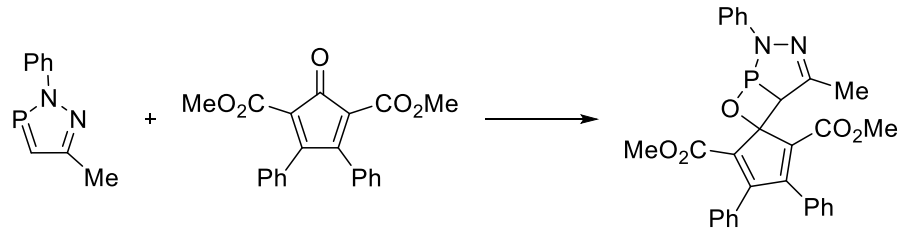

LXXIV **LXXV** **LXXVI**

Scheme 1.16: Proposed polycyclic structure **LXXVI**.[53]

The first crystal structure of a (monocyclic) 1,2σ^{3}λ^3-oxaphosphetanes would not be published until the year 2018 (*vide infra*).[54] On the quest for the 1,2σ^{3}λ^3-oxaphosphetanes, a reliable precursor was desirable.

One such suitable precursor for the synthesis of 1,2σ^{3}λ^3-oxaphosphetanes **LIII** could be their metal complexes **LIV** (see Scheme 1.17), which could generate free **LIII** by a suitable ligand exchange reaction.

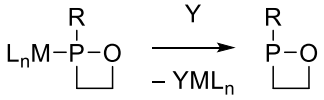

LIV **LIII**

Scheme 1.17: Decomplexation of **LIV**.

Although there were no known derivatives of **LIV** beforehand, Kyri from the Streubel group presented a synthetic route in 2014,[55] and the chemistry was further developed in the following years. [56–58] The route utilizes a Li/Cl phosphinidenoid complex **LXXVIII** as P_1-building block, that formally inserts into an epoxide derivative **LXXIX**, yielding the desired 1,2$\sigma^3\lambda^3$-oxaphosphetane complexes **LXXX** and **LXXXI** (see Scheme 1.18). It should be mentioned that in almost all cases the C^4-substituted isomer **LXXX** is observed, as the attack of **LXXVIII** proceeds from the sterically less hindered side. Only for R' = Ph the C^3-substituted isomer **LXXXI** can be observed, as the electron withdrawing effect of the aromatic ring makes the benzylic position more electrophilic. For R = $CH(SiMe_3)_2$, **LXXXI** is formed selectively, for R = CPh_3, a mixture of **LXXX** and **LXXXI** is formed.[59] Furthermore, it should be noted that while the reaction to **LXXX** and **LXXXI** is usually regioselective, they are still formed as mixture of isomers. Since the mono-substitution pattern at either C^4 or C^3 the rest R' can be either *cis* or *trans* toward the metal fragment, leading to a pair of diastereomers. In addition, in the case of R = $CH(SiMe_3)_2$, the rotation around the P-C_{exo} bond can be limited, leading to atropisomerism, leading to a total of four isomers. A mathematical reduction of isomers can be either achieved by substituting $CH(SiMe_3)_2$ for either CPh_3 or C_5Me_5 (no atropisomerism), or changing the substitution pattern at the C^4/C^3 carbon to a symmetric disubstitution or having no substitution.

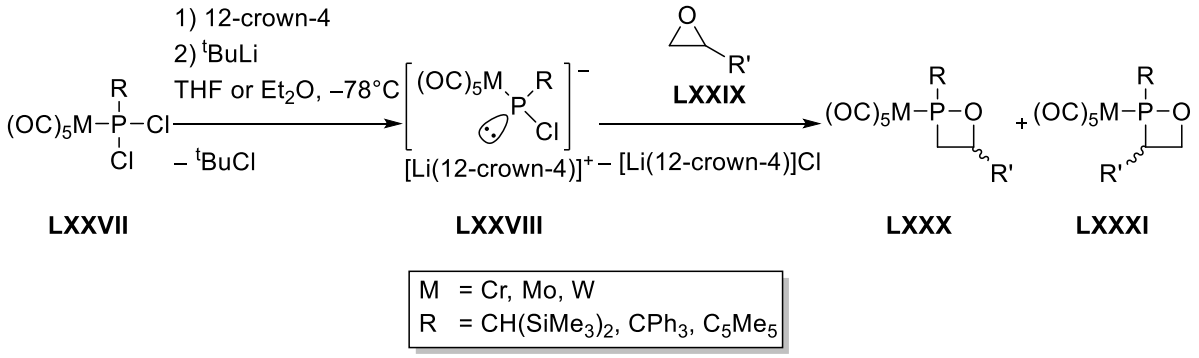

Scheme 1.18: Formal insertion of Li/Cl phosphinidenoid complex **LXXVIII** in epoxides **LXXIX**.[55–58]

The reaction of Li/Cl phosphinidenoid complex **LXXVIII** (M = W, R = $CH(SiMe_3)_2$) with the smallest possible disubstituted epoxide, 2,2-dimethyloxirane (**LXXXII**), gave not only the desired complex **LXXXIII** but also the phosphinite complex **LXXXIV** in near equal amount (ratio 47:53) (see Scheme 1.19).[56] While this did reduce the number of isomers, the formation of the unwanted product was undesirable.

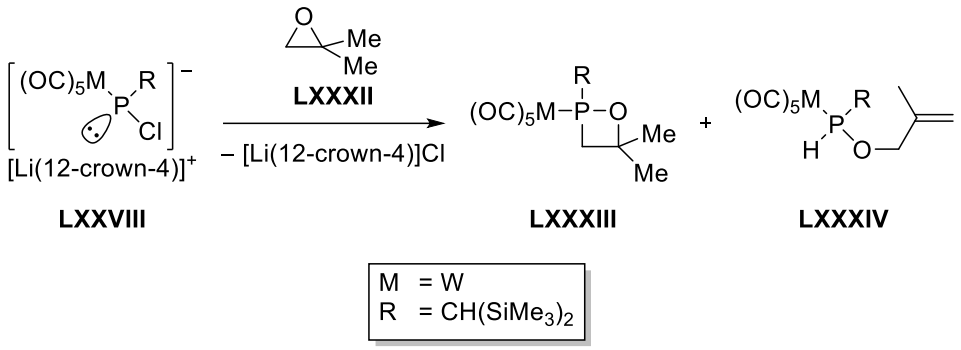

Scheme 1.19: Synthesis of 4,4-dimethyl-1,2-oxaphosphetane complex **LXXXIII**.[56]

When instead of 2,2-dimethyloxirane (**LXXXII**) the 2,2-bis(trifuoromethyl)oxirane (**LXXXV**) is used, the corresponding 4,4-disubstituted 1,2-oxaphosphirane complex **LXXXVI** is formed selectively (see Scheme 1.20). This is due to the activation of **LXXXV** *via* the electron withdrawing CF_3 groups, as bulkier substituents normally lead to a less selective reaction. As this eliminates the possibility of *cis*/*trans*-isomerism, in the case of R = $CH(Si(Me_3)_2$ the number of isomers is reduced to two, for R = CPh_3, C_5Me_5 only one isomer is obtained.[56,57]

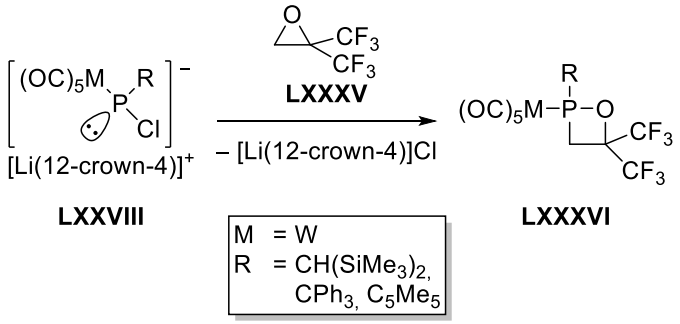

Scheme 1.20: Synthesis of 4,4-bis(trifluoromethyl)-1,2-oxaphosphetane complex **LXXXVI**.[56,57]

The synthesis of unsubstituted 1,2-oxaphosphetane complexes **LXXXIX** was not attempted *via* the above mentioned synthetic route. However, Kyri developed an alternative route, *i.e.*, Li/Cl phosphinidenoid complex **LXXVIII** formally inserted into the O-H bond of 2-iodoethanol (**LXXXVII**), leading to (2-iodoethoxy)phosphane complex **LXXXVIII**, which after deprotonation and intramolecular nucleophilic attack of phosphorus yielded the unsubstituted 1,2-oxaphosphetane complexes **LXXXIX** (see Scheme 1.21). This route is limited to R = $CH(SiMe_3)_2$, as both R = CPh_3, C_5Me_5 don't react cleanly with **LXXXVII**.[56,58]

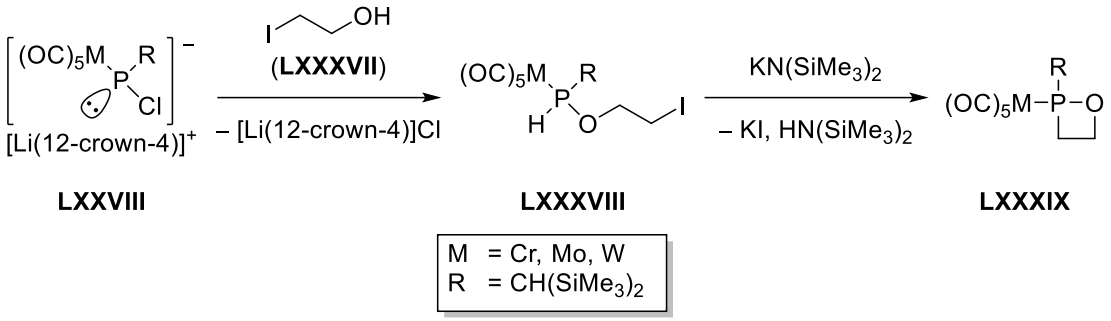

Scheme 1.21: Synthesis of unsubstituted 1,2-oxaphosphetane complexes **LXXXIX**.[56,58]

With this variability of 1,2-oxaphosphetane complexes at hand, Kyri managed to develop a ligand substitution strategy to obtain free 1,2$\sigma^3\lambda^3$-oxaphosphetanes. Therein, the chelating, bidentate diphosphino ligand **XCI** was used to drive out the 1,2-oxaphosphetane ligand of the coordination sphere of the molybdenum centre, yielding the desired free ligand **XCII** (see Scheme 1.22).[54] The use of **XCI** as chelating ligand to obtain free phosphorus ligands was already demonstrated by Mathey.[60]

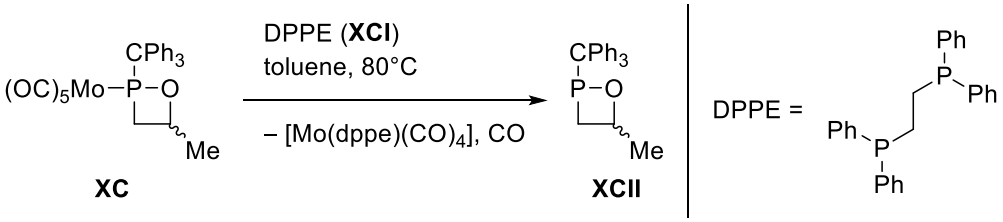

Scheme 1.22: Synthesis of first free 1,2-oxaphosphetane **XCII**.[54]

In the same publication the two first reactions of **XCII** were reported: the complexation towards gold(I) chloride and the oxidation using *o*-chloranil (see Scheme 1.23).[54]

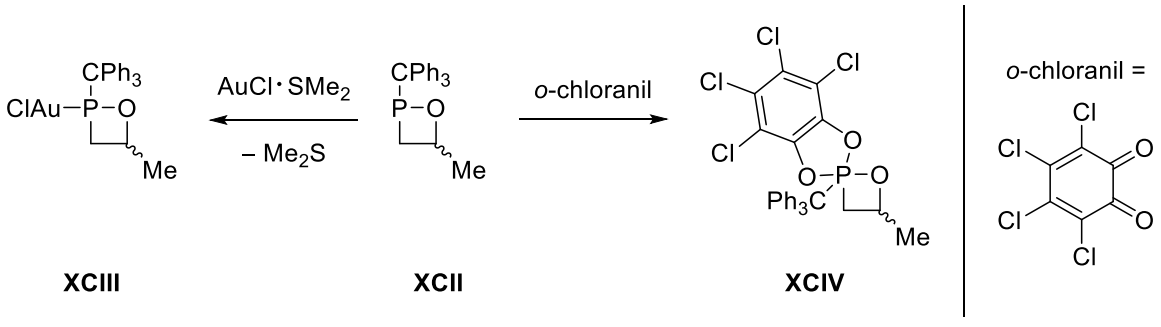

Scheme 1.23: First reported reactions of **XCII**.[54]

1.3 Selected important reactions of acyclic and cyclic organophosphorus compounds

1.3.1 Wittig reactions

The Wittig reaction was first reported back in 1953[23] and is an important reaction in organic synthesis and can be used in large, industrial scale, *e.g.* for the synthesis of vitamin A[61]. It is used to form olefins from phospha-ylids and carbonyl compounds (aldehydes, ketones). Up to now, several modifications of the Witting reaction are known and the mechanism, and thus the selectivity, of the reaction are dependent on several criteria, such as the stabilisation of the ylid, the substitution at phosphorus, the carbonyl compound and the presence of salt.

For example, the case of the non-stabilized, i.*e.* alkyl-substituted, ylids **XCV** the reaction with aldehydes **XLVII** processes *via* an early transition state **XCVIa**. **XCVIa** is in an early state of rehybridization and geometrical change, with phosphorus still in pseudo-tetrahedral environment and long bond distances. The ring geometry in the transition state is "puckered", meaning the aldehyde **XLVII** is approaching perpendicular to the ylid **XCV**.[62] As Scheme 1.24 shows, four different possibilities to form the transition state (**XCVIa-d**) exist. Of those four, only **XCVIa** minimizes both the repulsive 1,2 interaction between the ylid-C and the carbonyl-C substituents (see **XCVId**) and the repulsive 1,3 interaction between the carbonyl-C and the P substituents (see **XCVIb,c**); making **XCVIa** the most favoured transition state. **XCVIa** leads to the [2+2]-cycloaddition product 1,2$\sigma^5\lambda^5$-oxaphosphetane *cis*-**XCVII**. Then *cis*-**XCVII** reacts in a [2+2]-cycloreversion reaction to yield phosphane oxide **XCVIII** and selectively the *Z*-olefin *Z*-**IC**. The driving force of the reaction is the synthesis of the very stable phosphane oxide **XCVIII**, the release of ring strain energy, and the formation of the stable P=O and C=C double bonds. The reaction is under kinetic control by formation of the most favoured transition state **XCVIa**, leading to high *Z*-selectivity.

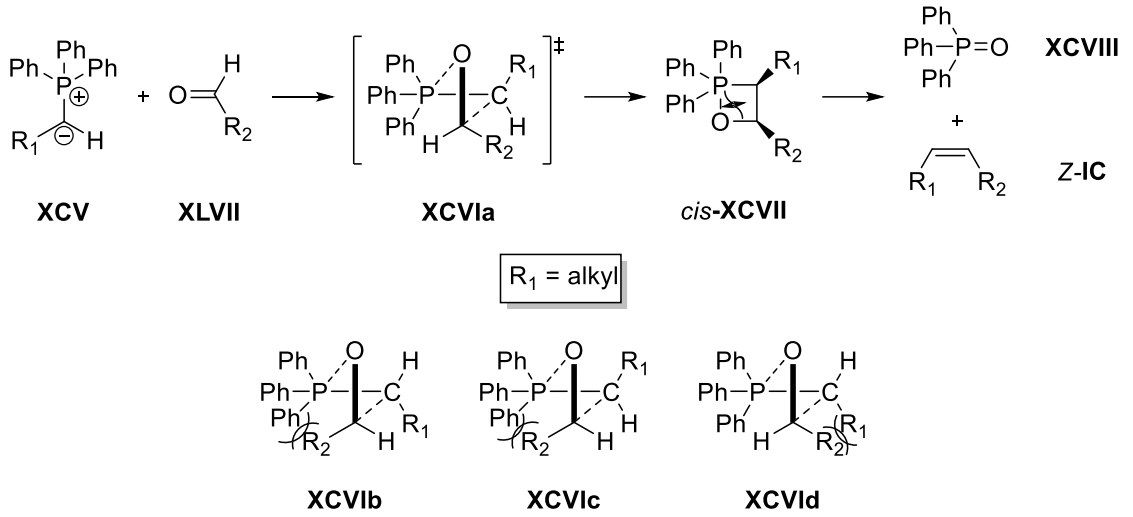

Scheme 1.24: Wittig reaction of non-stabilized ylid **XCV** and aldehyde **XLVII**.

In the case of semi-stabilized ylids **XCV** (*i.e.* R_1 = aryl) the *E*:*Z* selectivity is often low. This is because another probable transition state **C** is energetically available, concurring with **XCVIa** (see Scheme 1.25). **C** is a late transition state with proceeded rehybridization and trigonal bipyramidal geometry at phosphorus.[62] In this conformation, the minimization of repulsive 1,2 interaction leads to the [2+2]-cycloaddition product *trans*-**XCVII**, which selectively undergoes [2+2]-cycloreversion to yield *E*-**IC**.

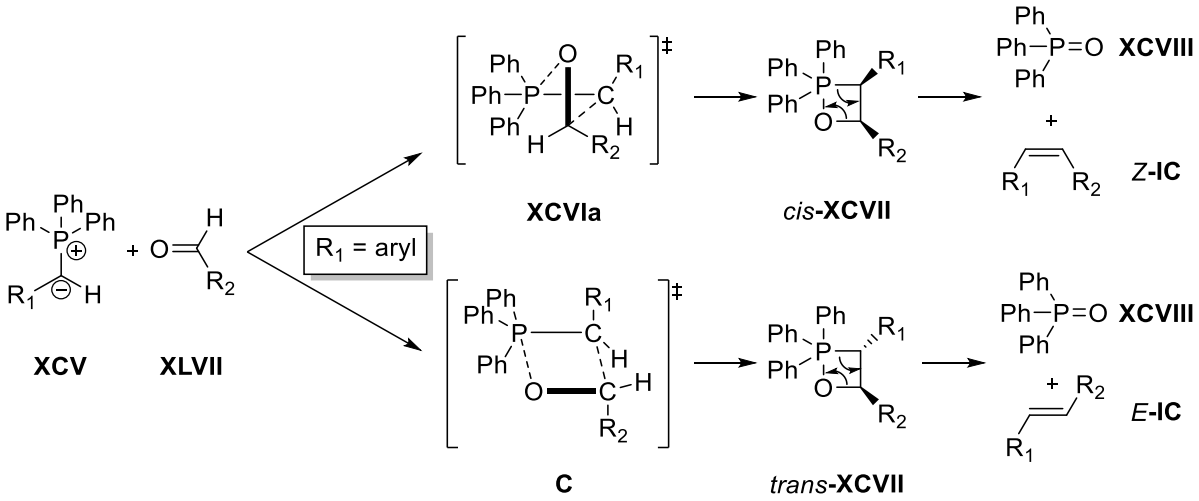

Scheme 1.25: Wittig reaction of semi-stabilized ylid **XCV** and aldehyde **XLVII**.

For the case of stabilized ylids (*i.e.* ylids bearing a carboxylate group) usually high *E*-selectivity is observed. It was found that for stabilized ylids also the dipole moments of the carbonyl groups have to be considered beyond simple steric repulsion.[62] This leads to a late transition state **CII**, similar to **C**, but here the aldehyde is puckered in a negative sense to achieve a favourable anti-parallel orientation

to the two carbonyl dipoles (depicted by blue arrows, see Scheme 1.26). Minimizing the 1,2 interaction leads to the *trans*-1,2-oxaphosphetane *trans*-**CIII** and after [2+2]-cycloreversion selectively to the *E*-olefin *E*-**CIV**.

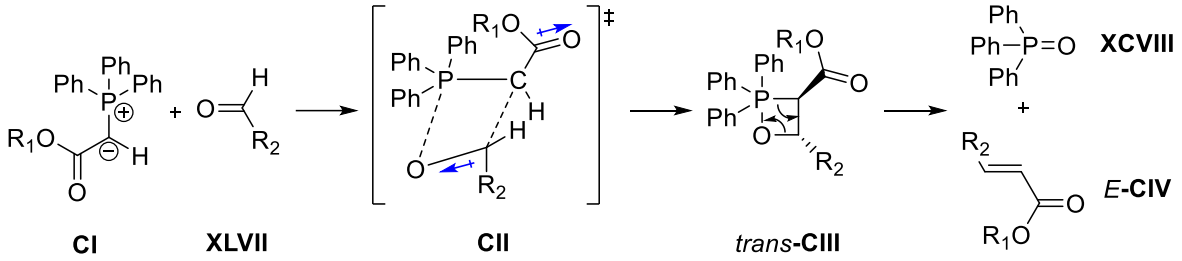

Scheme 1.26: Wittig reaction of stabilized ylid **CI** and aldehyde **XLVII**.

1.3.2 Arbuzov and Perkow reactions

The Arbuzov reaction takes place between a trivalent phosphorus compound bearing at least one OR group (*i.e.*, phosphinites $ROPR^1_2$, phosphonites $(RO)_2PR^1$, or phosphite esters $P(OR)_3$) with an alkyl halide R^2X to yield pentavalent phosphorus species (respectively: phosphane oxides $R^2P(O)R^1_2$, phosphinates $R^2P(O)R^1(OR)$, or phosphonates $R^2P(O)(OR)_2$) and a new alkyl halide RX. With this reaction, a broad variety of phosphorus compounds are hence available. The reaction mechanism (see Scheme 1.27) starts with the alkylation at phosphorus of a suitable species (*e.g.* **CV**) to form a transient phosphonium species **CVII**. The halide ion then nucleophilicly attacks the α-carbon centre of the organic rest of an OR group, forming both the new alkyl halide derivative RX **CIX** and the pentavalent phosphorus species **CVIII**.[63]

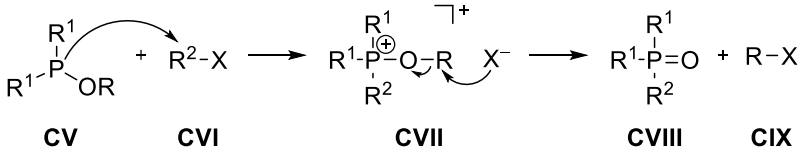

Scheme 1.27: Arbuzov reaction of a phosphinite **CV**.[63]

The reaction pattern becomes more complex in the case of heterocyclic substrates. It was shown that 1,3,2-dioxaphospholane **CX** and 1,3,2-dioxaphosphinane **CXII** don't react in an Arbuzov reaction, but only under exchange of the exocyclic substituent (see Scheme 1.28).[64]

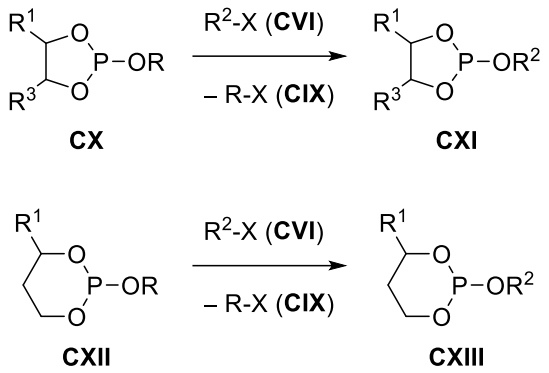

Scheme 1.28: Reaction of **CX** and **CXII** with alkyl halide **CVI**.[64]

In contrast, 1,3,2-dioxaphospholanes of type **CXIV** undergo Arbuzov reactions by cleavage of an endocyclic C-O bond, followed by cleavage of alkyl halide **CIX** and re-cyclisation to **CXVI**; while methyl-substituted 1,3,2-dioxaphosphinane **CXVII** reacts *via* cleavage of the exocyclic bond (see Scheme 1.29).[64]

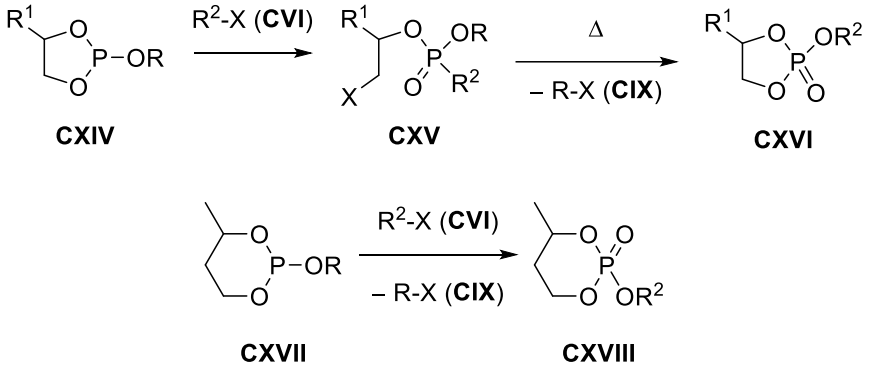

Scheme 1.29: Reaction of **CXIV** and **CXVII** with alkyl halide **CVI**.[64]

In general, 1,3,2-dioxaphospholanes react by cleavage of the exocyclic bond if the backbone is tetra-substituted (**CXIX**) and by cleavage of the endocyclic bond if the carbon backbone is unsubstituted (**CXX**). In both cases the first reaction step is the formation of the phosphonium species (**CXXI** or **CXXII**, respectively). Which bond is cleaved depends on the nucleophilic attack of the halide ion, weighing the release of ring strain (unsubstituted) versus the stabilization of positive inductive effects (tetra-substituted) (see Scheme 1.30).[65]

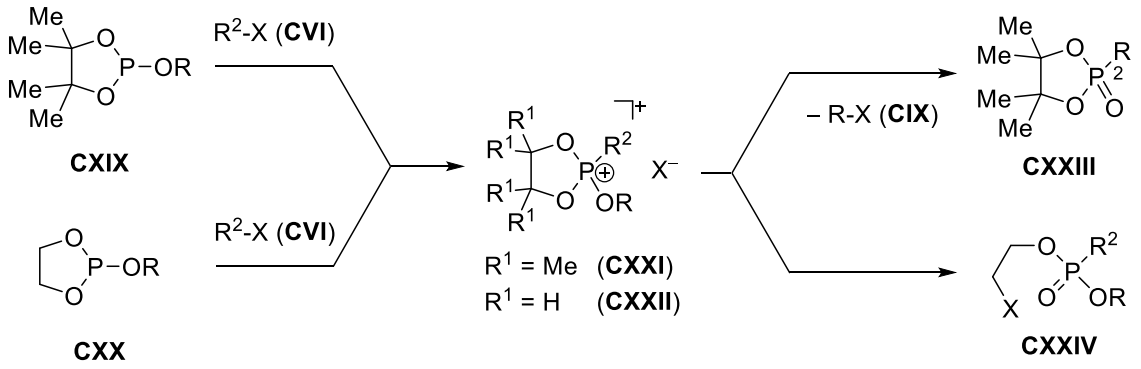

Scheme 1.30: Reaction of **CXIX** and **CXX** with alkyl halide **CVI**.[65]

If the only P-O bond of the starting material of an Arbuzov reaction is endocyclic, it is cleaved selectively. It should be mentioned that due to the cyclic nature of those intermediates, no new alkyl halide is generated. Rather, both the halide and the new rest are incorporated into the product. Mathey and Mercier used the Arbuzov reaction of 1,2-oxaphospholane **CXXV** to identify the oxidizable species by its expected follow-up product **CXXVI**.[66]

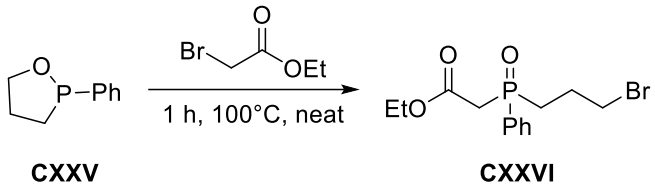

Scheme 1.31: Arbuzov reaction of 1,2-oxaphospholane **CXXV**.[66]

A similar, and in some cases competing reaction to the Arbuzov reaction is the Perkow reaction. Therein a phosphite ester **CXXVII** reacts with an α-halo ketone **CXXVIII** to form vinyl phosphate **CXXIX** and alkyl halide **CIX** (see Scheme 1.32).

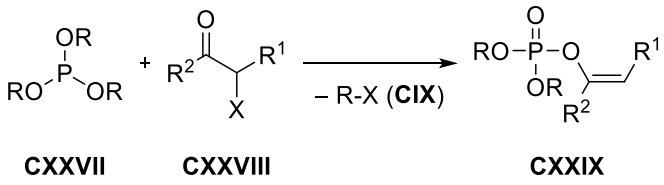

Scheme 1.32: Perkow reaction of phosphite ester **CXXVII**.[63]

The halo ketone **CXXVIII** possesses two electrophilic sites, the halo-carbon and the carbonyl-carbon. Attack of phosphorus on the halo-carbon would lead to an Arbuzov reaction. Several proposals for the mechanism of the Perkow reaction have been made in the past, but recent quantum chemical

calculations by Espinosa Ferao showed that the initial reaction step is a cheletropic reaction between phosphorus and the carbonyl function forming oxaphosphirane **CXXXII** as intermediate.[67] **CXXXII** then reacts further by cleavage of the endocyclic P-C bond, flowed by formation of the double bond and cleavage of the halide ion. The last reaction step is the (Arbuzov-like) nucleophilic attack of the halide at one of the organic rests of phosphonium **CXXXIII**, forming the vinyl phosphate **CXXXIV** and eliminating alkyl halide **CXXXV**.

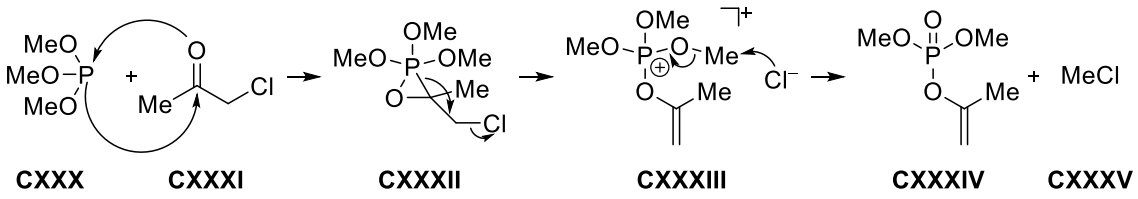

Scheme 1.33: Reaction mechanism of the Perkow reaction, calculated by Espinosa Ferao.[67]

1.3.3 Polymerisation reactions of P-containing monomers

Polymers containing phosphorus in the backbone are of great interest due to their physical and chemical properties that can't be achieved by purely organic polymers (*e.g.* flame retardancy, fluorescence, electric conductivity). While "inorganic rubber" $(NPCl_2)_n$ was one of the first discovered inorganic polymers, the explosion of research and new compounds only started during the last decades, as it lacked general procedures to incorporate phosphorus in a polymer backbone. In the following, the syntheses of phosphorus containing polymers from cyclic *P*-heterocycles will be presented.

1.3.3.1 Polyphosphazenes

The earliest and best established route to P-containing polymers relies on the thermal ring opening polymerisation of hexachloro-cyclotriphosphazene (**CXXXVI**) (see Scheme 1.34, left).[68] By now, various other routes to polyphosphazenes **CXXXVII** have been published.[69] A major improvement was the ambient temperature synthesis from $Cl_3P{=}N(SiMe_3)$ (**CXXXVIII**) with PCl_5 as initiator (see Scheme 1.34, right); the reaction pursues *via* a living cationic polymerisation.[70,71] The dichloro compound **CXXXVIIa** can easily be modified with alcoholates or amines to yield poly(dialkoxyphosphazenes) **CXXXVIIb** or poly(diaminylphosphazenes) **CXXXVIIc** (see Scheme 1.34, bottom).[70]

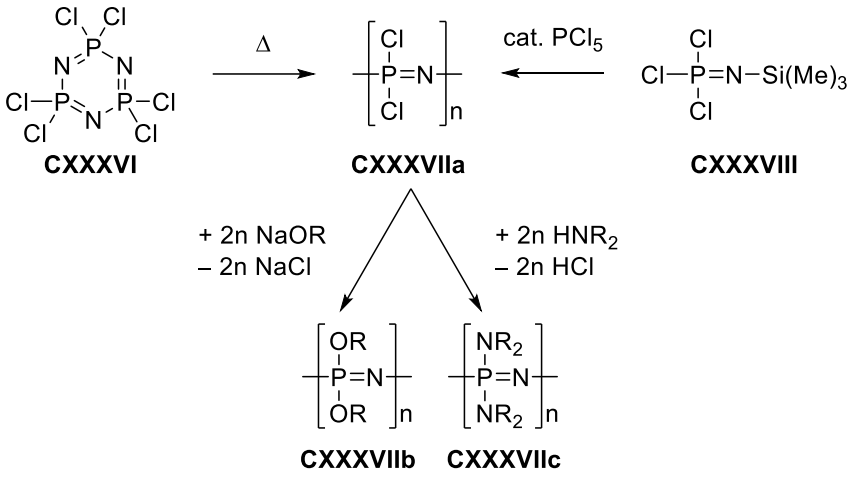

Scheme 1.34: Synthesis and functionalization of **CXXXIIa**.[68,70,71]

1.3.3.2 Poly(vinylenephosphane)s.

As the focus of this thesis is on synthesis and use of strained ring systems, only polymerisation reactions involving small *P*-heterocycles will be discussed hereafter. The first poly(vinylenephosphane) **CXLa** was synthesized by anionic ring opening polymerisation of phosphirene **CXXXIX** using *n*-butyllithium as initiator (see Scheme 1.35, top).[72] Later, another route to poly(vinylenephosphane) **CXLb** was developed *via* the reaction of *cyclo*-$(PMe)_5$ (**CXLI**) with alkyne **CXLII** in the presence of a radical starter (see Scheme 1.35, bottom).[73] The latter method produced lower molecular weight polymers in comparison (2500 g/mol versus up to 18000 g/mol).[74]

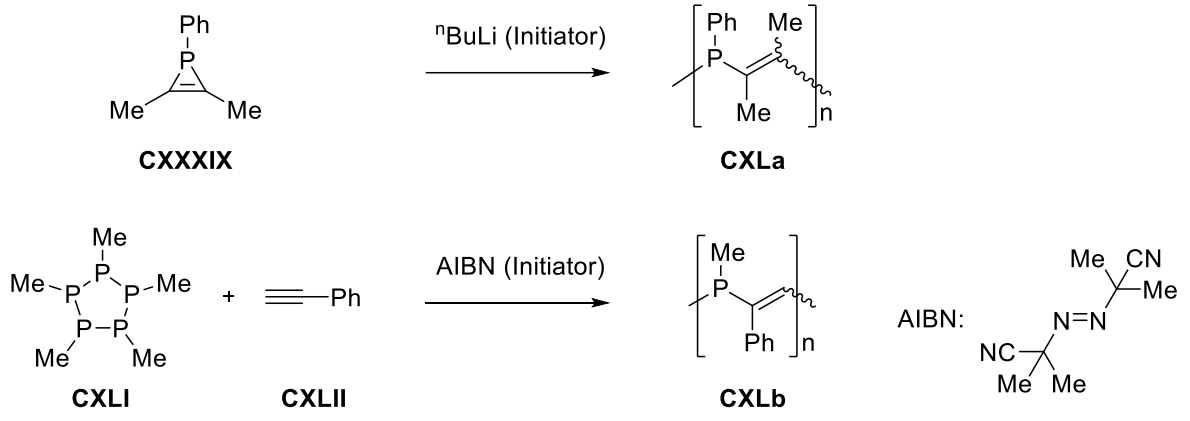

Scheme 1.35: Synthesis of poly(vinylenephosphanes) **CXLa** and **CXLb**.[72,73]

1.3.3.3 Cationic ring opening of *P*-heterocycles

In contrast to strained three-, four- and five-membered oxacycles, the polymerisation of the homologous phosphacycles (*i.e.*: phosphirane (**CXLIII**), phosphetane (**CXLIV**), phospholane (**CXLV**), see Figure 1.5) is not well investigated.

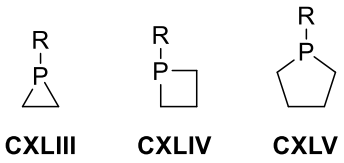

Figure 1.5: Homologous row of strained phosphacycles.

In 1994, Kobayashi reported the cationic polymerisation of aryl substituted phosphirane **CXLVI** to yield polyphosphane **CXLVII** (see Scheme 1.36).[75,76] Although quantum chemical calculations by Coote claim that the radical ring opening polymerisation of derivatives of **CXLIII** and **CXLIV** are exothermic,[77] the topic was not further investigated experimentally.

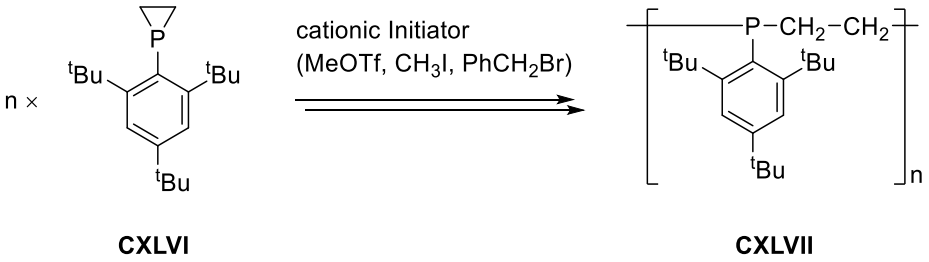

Scheme 1.36: Cationic polymerisation of phosphirane **CVIIa**.[75,76]

1.3.3.4 Polymerisation of oxygen-containing phosphorus heterocycles

The ring opening polymerisation of strained heterocycles is well studied only for strained oxygen-containing heterocycles, *i.e.* oxiranes **CXLVIII**, oxetanes **CIL**, oxolanes **CL** (see Figure 1.6).

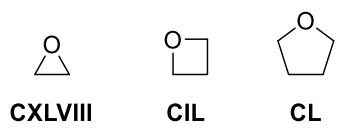

Figure 1.6: Strained oxocycles.

Oxiranes are highly interesting, as they are the precursor for two families of polymers, polyepoxides or epoxy resins ("epoxy") **CLI** and polyethyleneglycol (PEG) **CLII** (Figure 1.7).

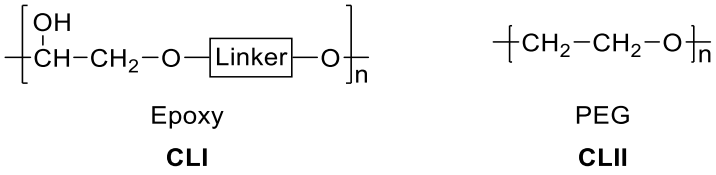

CLI **CLII**

Figure 1.7: Epoxy resin **CLI** and PEG **CLII**.

Epoxies are the reaction product of oxiranes (most often epichlorohydrin (**CLIII**) and bifunctional alcohols, acids or other compounds with acidic hydrogens (most often bisphenol A (**CLIV**)).[78] They are an important compound class for various applications,[79] but they are not the "simple" ring opening product of an oxirane (see Scheme 1.37).

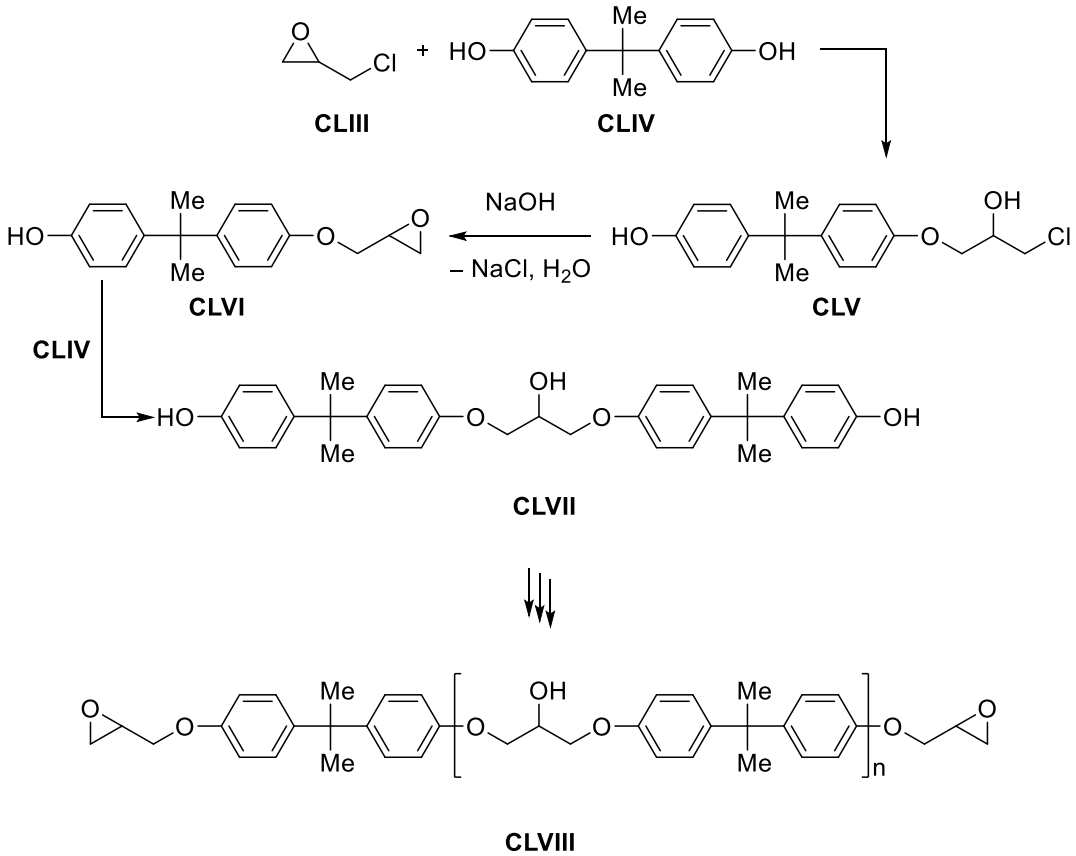

Scheme 1.37: Synthesis of bisphenol A (**CLIV**) based epoxy resin **CLVIII**.

Rather, the first reaction step is the nucleophilic attack of an alcohol function of **CLIV** at the unsubstituted carbon centre of oxirane **CLIII**, forming ring-opened compound **CLV** with vicinal chloro

and hydroxy groups. A base induced dehydrohalogenation leads to the formation of a new oxirane moiety in molecule **CLVI**. Here, another unit of **CLIV** can attack, leading to **CLVII**. Now these steps repeat to form polymer **CLVIII**.

PEGs **CLII** were known for a long time and first described by Lourenço in 1859 and shortly after independently by Wurtz.[80] While Lourenço obtained PEG **CLIIa** as a reaction product of ethylene glycol (**CLIX**) and 1,2-dibromoethane (**CLX**), Wurtz obtained PEG **CLIIb** through the cationic ring opening of ethylene oxide (**CLXI**), using water, or ethylene glycol (**CLIX**) as initiator (see Scheme 1.38). The polymerisation of ethylene oxide (**CLXI**) can be catalysed by both acids and bases. PEGs **CLII** have a broad area of application, depending on molecular weight and possible derivatisation.[81]

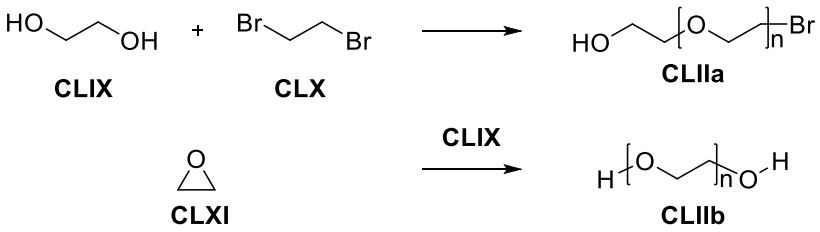

Scheme 1.38: Synthesis of PEGs after Lourenço (**CLIIa**) and Wurtz (**CLIIb**).[80]

The first polymerisation of an oxetane was reported in 1954, when **CLXII** was treated with a strong Lewis acid (*i.e.* BF_3) in the presence of trace amounts of water to yield polyoxetane **CLXIII** (see Scheme 1.39, top) in high molecular weight and as highly crystalline substance. The polymerisation of the parent oxetane **CLXIV** was presented shortly after in 1956 by a similar reaction.[82] Over a hundred different derivatives of polyoxetanes **CLXVI** have been synthesised by now, their properties dependent on their substitution.[83] The polymerisation occurs *via* a cationic ring opening polymerisation. [83]

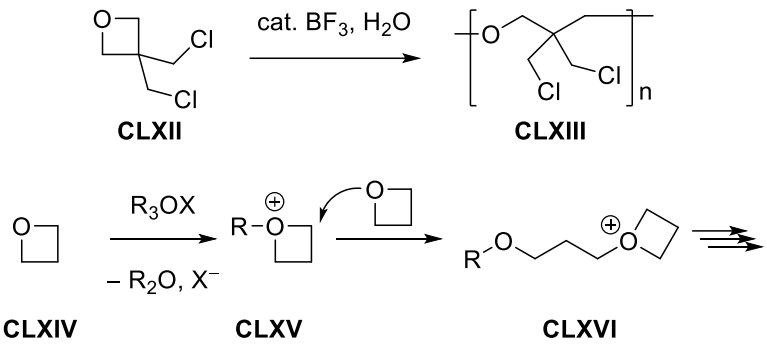

Scheme 1.39: Synthesis and propagation mechanism of polyoxetanes **CLXIII**, **CLXVI**.[82]

The parent oxolane **CLXVIII** (*i.e.* tetrahydrofuran) can also be catalysed by cationic initiators similar to **CLXIV**. But in contrast to **CLXI** and **CLXIV**, which both feature high ring strain energies, the ring strain energy of **CLXVIII** is rather small. This leads to the observation that the free energy of polymerisation of cationic ring opening of substituted derivatives of **CLXVIII** becomes positive, preventing polymerisation.[84] The polymerisation of the parent oxolane **CLXVIII** to yield polytetrahydrofuran **CLXX**was firstly reported in 1939 and further explored in the following years.[85,86]

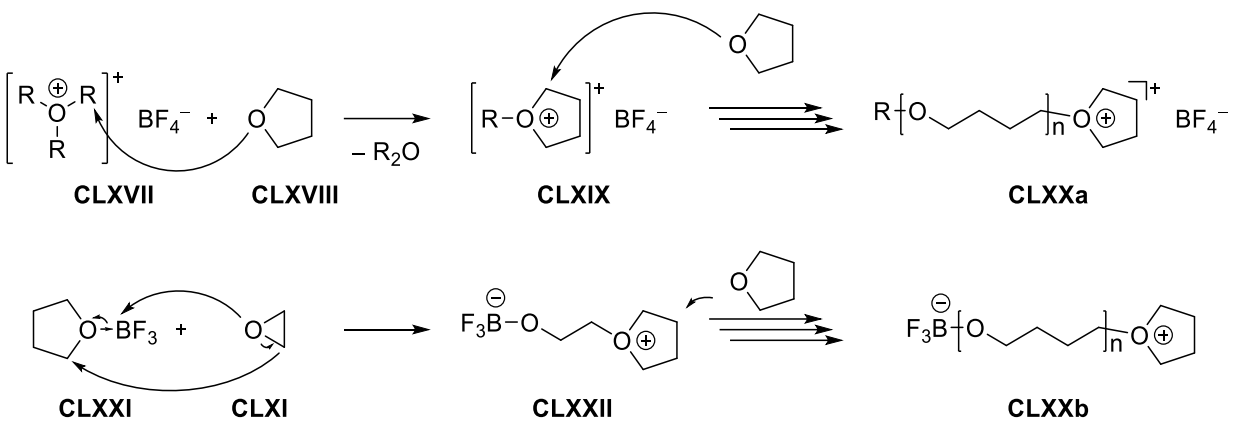

Scheme 1.40: Synthesis of polytetrahydrofuranes **CLXXa,b**.[85,86]

1.3.3.5 Polymerisation of heterocycles containing both phosphorus and oxygen

As the integration of phosphorus into polymers is still of interest, the polymerisation of various cycles containing both phosphorus and oxygen was realised. The first polymerisation of a 1,3,2-dioxaphospholane **CLXXIII** and a 1,3,2-dioxaphosphorinane **CLXXVI** were presented by Petrov in 1962 and 1960, respectively.[87] These reactions occur *via* cationic polymerisation and in an Arbuzov like reaction mechanism (see Scheme 1.41).

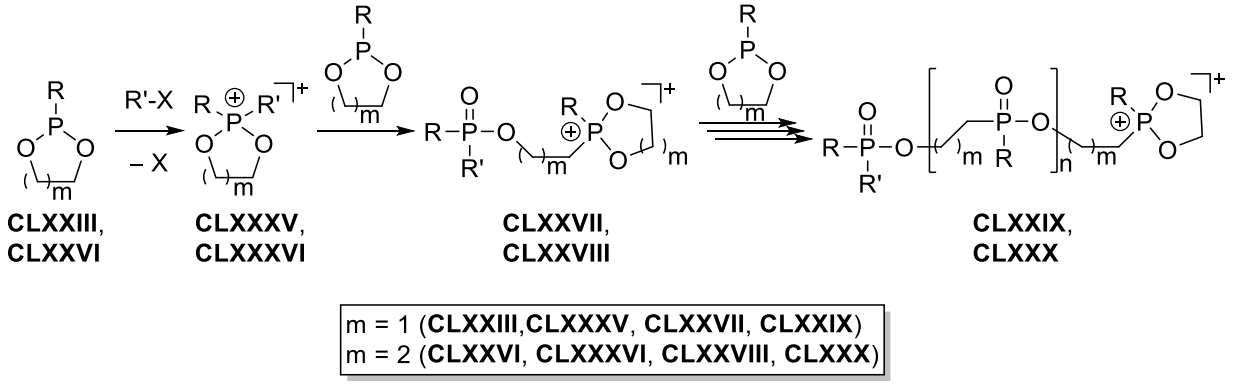

Scheme 1.41: Synthesis of phospha-cycle based polyphosphinates **CLXXIX** and **CLXXX**, respectively.[87]

In a similar manner, Saegusa presented in 1981 the polymerisation of a 1,3,6,2-trioxaphosphocane **CLXXXI** using cationic initiators (see Scheme 1.42).[88]

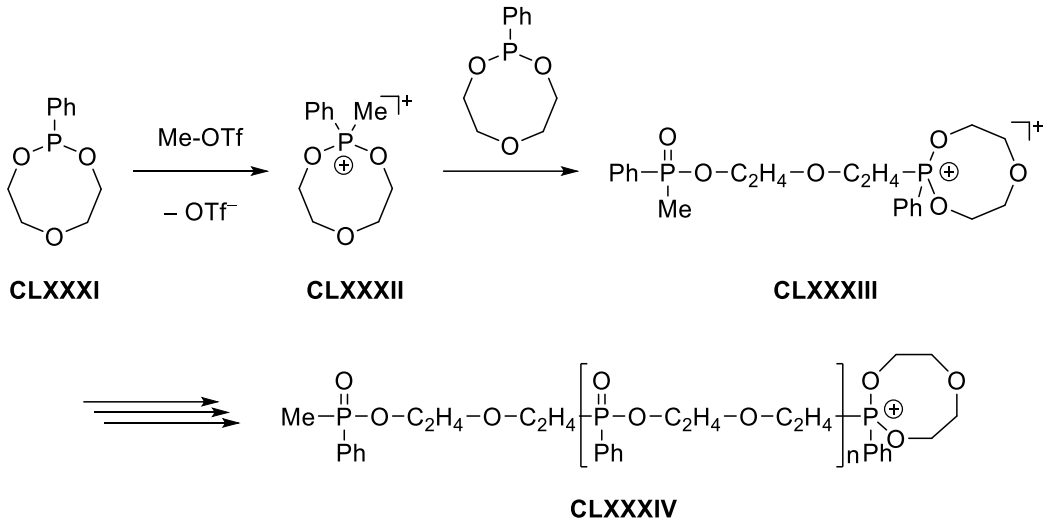

Scheme 1.42: Cationic polymerisation of **CLXXXI**.[88]

Also in 1981, Saegusa presented the cationic polymerisation of 1,2-oxaphospholane **CLXXXV**. In contrast to the previous presented cyclic compounds **CLXXIII**, **CLXXIV** and **CLXXXI**, which are cyclic phosphonites, **CLXXXV** is a cyclic phosphinite; making the resulting polymer **CLXXXVIII** a phosphane oxide (instead of a phosphinate). They also reported the reduction of **CLXXXVIII** to yield the poly(propylenephosphane) **CLXXXVIII** (see Scheme 1.43).[87]

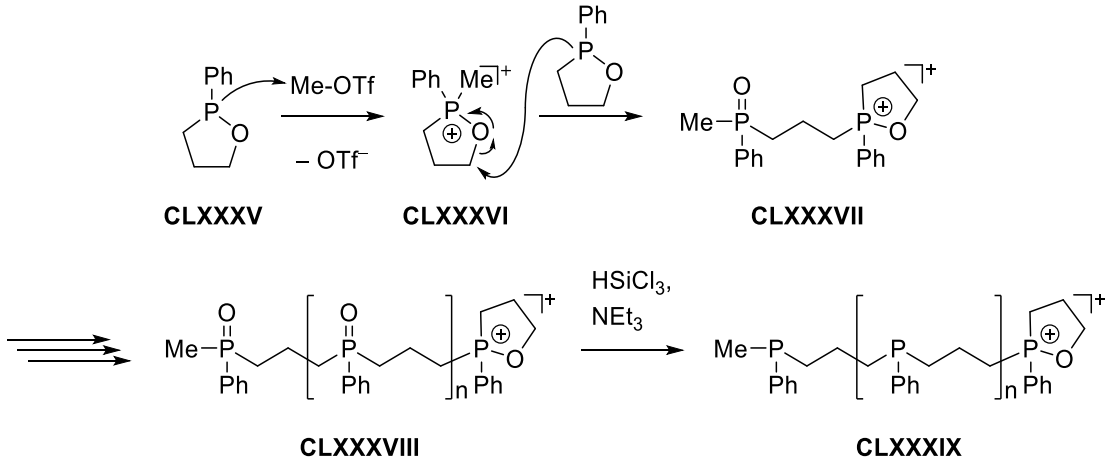

Scheme 1.43: Cationic polymerisation of 1,2-oxaphospholane **CLXXXVIII**.[87]

While the polymerisation of the five-membered 1,2-oxaphospholane was further investigated, there was no possibility to investigate the polymerisation of smaller P-O heterocycles, as the trivalent 1,2-oxaphosphetane and oxaphosphirane were unknown before the work of the Streubel group, and the

trivalent 1,3,2-dioxophosphetane is still unknown (see Chapter 1.2 for more information of phosphorus heterocycles).

2 Objective of this PhD Thesis

The aim of this PhD thesis is the synthesis and investigation of reactions of 1,2$\sigma^3\lambda^3$-oxaphosphetanes. Therefore, the main part of this work is dedicated to reactivity studies of unligated 1,2$\sigma^3\lambda^3$-oxaphosphetanes which includes:

- oxidation of the phosphorus centre
- complexation of phosphorus
- reactions with electrophiles
- cationic polymerisation
- reactions with acids
- theoretical investigation of important reaction pathways.

3 Results and Discussion

3.1 1,2$\sigma^3\lambda^3$-Oxaphosphetanes

3.1.1 Synthesis of 1,2$\sigma^3\lambda^3$-oxaphosphetanes from their metal complexes

Since 2007, Li/Cl phosphinidenoid metal complexes were powerful and versatile P_1-building blocks. The term phosphinidenoid was first coined by Yoshifuji in 1988 in analogy to carbenoids, when it was shown that the reaction of dichloro(2,4,6-tri-*tert*-butylphenyl)phosphane with magnesium did not yield a phosphinidene.[89] To obtain easier manageable P_1-building blocks, the stabilisation of phosphinidenoids *via* ligation to transition metals was desirable. The breakthrough of this chemistry happened in the group of Streubel when the first Li/Cl phosphinidenoid complex was synthesised; either by deprotonation of a suitable chloro(organo)phosphane complex or by lithium/chlorine exchange of a suitable dichloro(organo)phosphane complex.[37] The scope of the available phosphinidenoid complexes was further investigated by the Streubel group in the following years, regarding the main group metal and transition metal centre, the P-substituent as well as the trapping reagents.

As already described in Chapter 1.2.3, the use of Li/Cl phosphinidenoid complexes is a reliable way to generate 1,2-oxaphosphetane complexes. The first step of this synthetic route towards 1,2$\sigma^3\lambda^3$-oxaphosphetanes (**8**) was the generation of a suitable dichloro(organo)phosphane metal complex *via* the photolysis of the corresponding hexacarbonyl metal complex and addition to the dichloro(organo)phosphane (see Scheme 3.1). As the decomplexation only works for molybdenum complexes, the dichloro(organo)phosphane molybdenum complex **4** was chosen. Although the syntheses of the corresponding tungsten and chromium complexes are well studied and reported to deliver good yields (92% and 86%, respectively), the synthesis of the molybdenum containing complex **4** was less established and provided a significantly lower yield (30% conversion by NMR, 25% yield after column chromatography).[90] During the work of this investigation, the reaction conditions could be significantly improved to yield up to 81%, and it proved crucial to bubble a slight stream of argon through the solution during photolysis to remove carbon monoxide from the equilibrium.

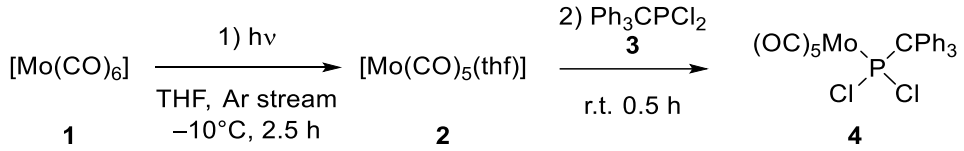

Scheme 3.1: Optimized synthesis of **4**.

As described previously, mono C^4-substituted 1,2$\sigma^3\lambda^3$-oxaphosphetane molybdenum complexes are easily accessible from the formal insertion of Li/Cl-phosphinidenoid complexes, *e.g*. **5**, into suitable epoxides.[54,56]Due to the generation of the second stereo centre at the C^4-carbon having just one substitutent, always two diastereomers were formed (*cis* and *trans* forms). These were usually not separated and, hence, led to NMR spectra hard to interpret due to overlapping signals. Therefore, it was desirable for further investigations to reduce the number of diastereomers to one. This can be achieved through the synthesis of either C^4-unsubstituted 1,2$\sigma^3\lambda^3$-oxaphosphetane molybdenum complex **7a** (from oxirane (**6a**)), or symmetrically C^4-disubstituted 1,2$\sigma^3\lambda^3$-oxaphosphetane molybdenum complex **7b** (*e.g.* from 2,2-dimethyloxirane (**6b**)) (see Scheme 3.2).

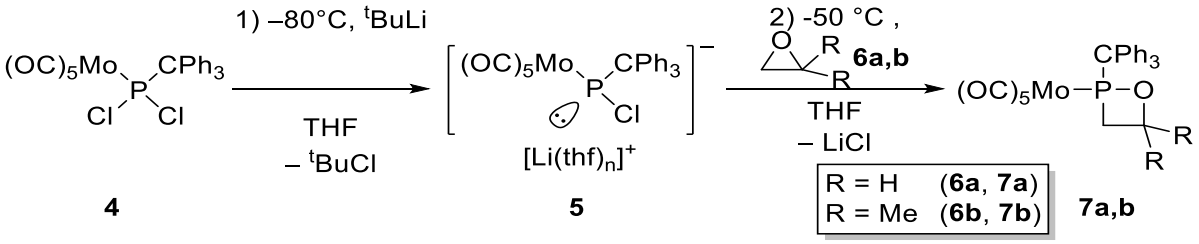

Scheme 3.2: Synthesis of non-diastereomeric 1,2$\sigma^3\lambda^3$-oxaphosphetanes **7a,b**.

The synthesis of **7a,b** used the literature protocol,[54] and the formal P_1 unit insertion from **5** into the oxiranes **6a,b** led selectively to **7a,b** which could be isolated in good yields (65% for **7a**, 77% for **7b**). Interestingly, their $^{31}P\{^1H\}$ NMR shifts differed drastically, *i.e.*, 220.6 ppm for **7a** and 184.5 ppm for **7b**. Interestingly, this was similar to the shifts of the different isomers of the C^4-methyl 1,2$\sigma^3\lambda^3$-oxaphosphetane molybdenum complex **6c,c'** (207.2 ppm for *trans*, 185.6 ppm for *cis*).[54]

As shown below (see Figure 3.1), the 1:1-diastereomeric mixture of C^4-methyl 1,2$\sigma^3\lambda^3$-oxaphosphetane complexes **6c,c'** gave rise to six independent signals in the ^{1}H-NMR spectrum (not counting aromatic hydrogen of the trityl group). Especially the four C^3-hydrogen signals showed a tendency to overlap and thus made an interpretation of the coupling constants impossible. In case of **7a** being present as enantiomers only four non-aromatic ^{1}H-NMR signals were observed. In case of **7b** the ^{1}H-NMR spectrum displayed only two doublet of doublets and two singlets, instead of formerly observed complicated dddd signals. In conclusion, this led to the interest of generating **8a**, or preferably **8b**.

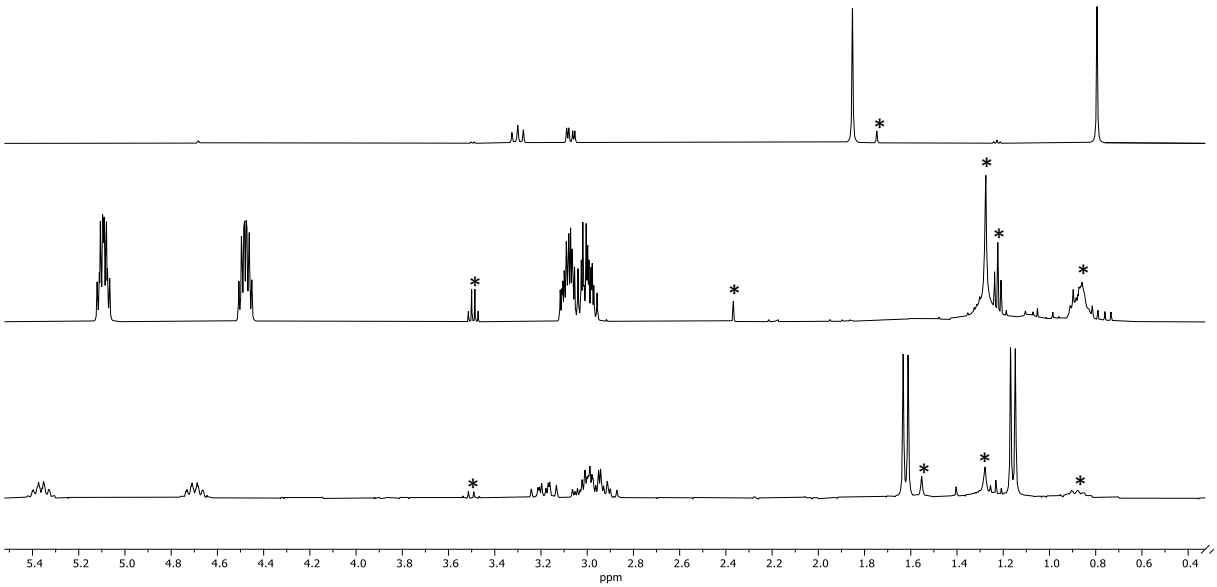

Figure 3.1: Excerpts of ^{1}H-NMR spectra of: bottom: *C*^{4}-methyl 1,2σ^{3}λ^{3}-oxaphosphetane complexes **6c,c'**, middle: *C*^{4}-unsubstituted 1,2σ^{3}λ^{3}-oxaphosphetane complex **7a**, top: *C*^{4}-dimethyl 1,2σ^{3}λ^{3}-oxaphosphetane complex **7b**. Impurities marked with *.

High resolution mass spectra were measured of **7a,b**. For **7a**, the quasi-molecule peak was detected directly (theor./exp. 557.0047/557.0041 $[M+H]^+$), while for **7b** only fragments after loss of carbon monoxide units could be detected (theor./exp. 501.0517/ 501.0517 $[M-3(CO)+H]^+$, 529.0467/ 529.0468 $[M-2(CO)+H]^+$). More interestingly, the peak corresponding to loss of the whole $Mo(CO)_5$ fragment could be detected (theor./exp. 347.1559/347.1555 $[M-Mo(CO)_5+H]^+$), which is identical to the quasi-molecule peak of the desired metal-free **8b**.

Both **7a,b** yielded single crystals suitable for X-ray diffraction studies. It was interesting that, even though the large difference between their chemical shifts implied a large electronic difference, **7a,b** both display rather similar structural features: a nearly planar ring-system and similar bond lengths and angles at phosphorus (see Table 3.1 and Figure 3.2).

Table 3.1: Selected bond lengths and angles of **7a,b** and **8a**. Bond lengths in Å, angles in °.

	P-O	P-CH_2	P-CPh_3	CH_2-P-O	CPh_3-P-O	Σ(endocyclic angles)
7a	1.661(3)	1.845(5)	1.895(5)	80.81(19)	107.48(19)	359.7 (11)
7b	1.666(4)	1.839(5)	1.896(5)	80.1(2)	107.8(2)	358.0 (12)
8a	1.670(3)	1.849(4)	1.923(5)	80.47(18)	104.29(18)	359.6 (11)

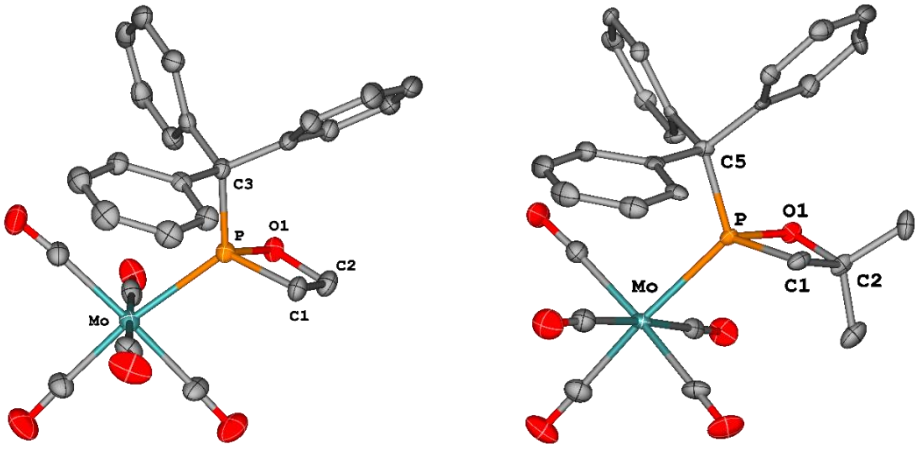

Figure 3.2: Molecular structures of **7a** (left) and **7b** (right) in the solid state.
Hydrogen atoms are omitted and the thermal ellipsoids are set at the 50% probability level.

To obtain metal-free 1,2$\sigma^3\lambda^3$-oxaphosphetanes **8a,b**, **7a** and **7b** were treated with 1,2-bis(diphenylphosphino)ethan (DPPE) (see Scheme 3.3), but the two cases had a rather different outcome. While **8a** could be obtained, using elongated reaction times,[54] and isolated in good yields (70%), **8b** was formed as intermediate ($\delta(^{31}P)$ = 161.2 ppm), which was proven by the formation of the by-product [$Mo(CO)_4$(dppe)]. **8b** started to decompose when the reaction solution was heated for longer times (see also Chapter 3.1.2). When only heated for 2 h, **8b** was observed in the $^{31}P\{^1H\}$ NMR spectrum with a signal at 161.1 ppm. The $^{31}P\{^1H\}$ NMR chemical shift of **8a,b** showed the same trend as was observed for **7a,b**: **8a** had a chemical shift of 212.1 ppm, while the isomers of *C*^{4}-methyl 1,2$\sigma^3\lambda^3$-oxaphosphetane **8c,c'** appeared at 163.7 ppm (*cis*) and 199.0 ppm (*trans*) in the spectrum.

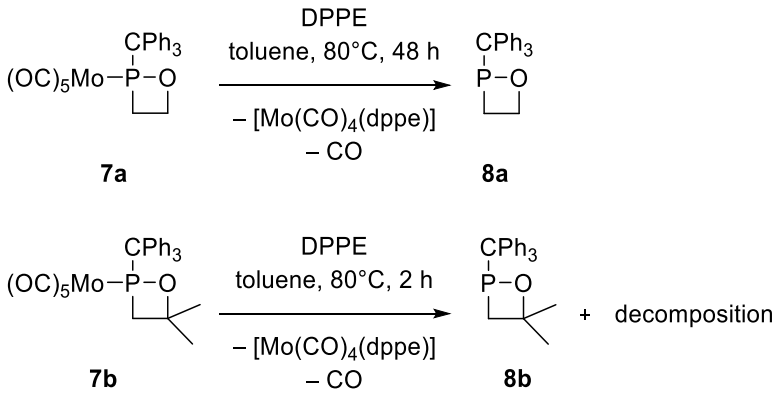

Scheme 3.3: Synthesis of 1,2$\sigma^3\lambda^3$-oxaphosphetanes **8a,b**.

8a was isolated and characterised by NMR spectroscopy and high-resolution mass spectrometry (theor./exp. 319.1246/319.1244 $[M+H]^+$). Unfortunately, **8b** could not be isolated.

Single crystals suited for X-ray diffractometry could be obtained by evaporation of solvent after extraction with *n*-pentane (see Figure 3.3 and Table 3.1).

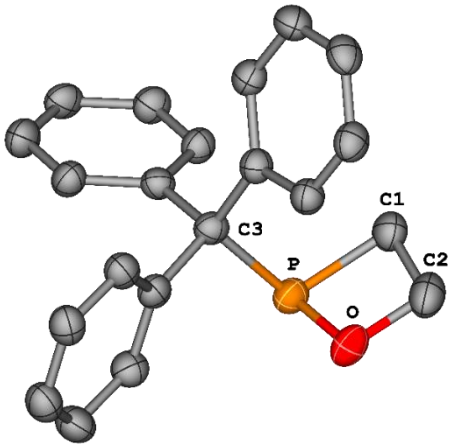

Figure 3.3: Molecular structures of **8a** in the solid state. Hydrogen atoms are omitted and the thermal ellipsoids are set at the 50% probability level.

While the work of this investigation started using the C^4-methyl 1,2$\sigma^3\lambda^3$-oxaphosphetanes **8c,c'**, it was later shifted to 1,2$\sigma^3\lambda^3$-oxaphosphetanes obtained as pair of enantiomers. Because the C^4-disubstituted **8b** was not isolated, later investigations focused on the C^4-unsubstituted derivative **8a**, but C^4-methyl substituted and known **8c,c'** were used earlier on.

3.1.2 Study on the thermal stability of C-unsubstituted and C-disubstituted 1,2$\sigma^3\lambda^3$-oxaphosphetanes

As briefly mentioned in chapter 3.1.1, **8b** possessed an unexpected thermal lability, but the C^4-methyl and C^4-unsubstituted 1,2$\sigma^3\lambda^3$-oxaphosphetanes **8c,c'** and **8a** showed no indication of thermal instability. For example, **8a** was heated in 1,2-dichlorobenzene and the reaction progress monitored by $^{31}P\{^1H\}$ NMR spectroscopy (see Figure 3.4). First, no significant change was observed in the spectra and the signal-to-noise ratio (SNR) seemed constant. But upon closer investigation, the SNR decreased by 11% from the start to the end. As this minor change might be neglectable, **8a** appears to be rather thermostable, showing no to only slight decomposition even at 155°C.

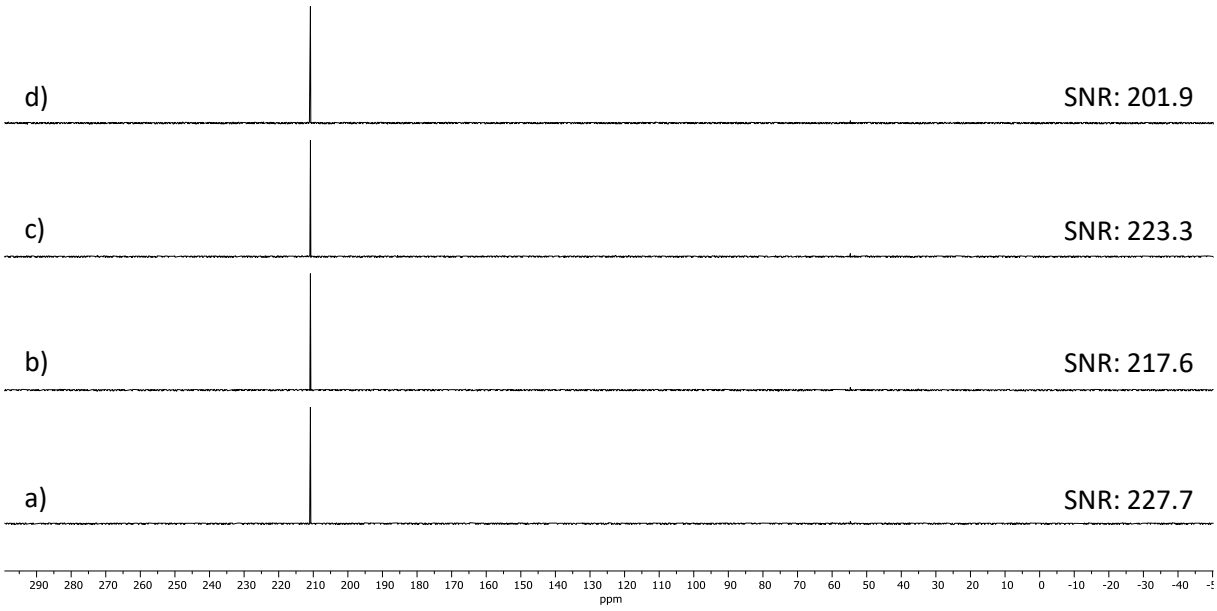

Figure 3.4: $^{31}P\{^{1}H\}$ NMR spectra of **8a** after cumulative heating, starting from bottom to top. a) 1 h at 100°C, b) 1 h at 120°C, c) 1 h at 140°C, d) 1.5 h at 155°C (oil bath limit). Signal to noise ratio (SNR) given on the right side.

While **8a** could be handled easily, **8b** appeared to be so thermolabile that it decomposes under the synthesis conditions. If subjected to the usual conditions for the formation of 1,2$\sigma^3\lambda^3$-oxaphosphetanes (*i.e.* heating at 80°C for 20-48 h), one observed complete decomposition, with only one signal for $[Mo(CO)_4(dppe)]$ ($\delta(^{31}P\{^{1}H\})$ = 56.2 ppm) present. If **7b** was heated to 60°C for 2 h, one observed the formation of **8b**. 16% of **7b** were converted to **8b** (by integration of $^{31}P\{^{1}H\}$ NMR spectrum, not accounting for possibly already decomposed species) (see Figure 3.5). After two more hours and raising temperature to 80°C, nearly full conversion (91%) was observed, and after one additional hour, **7b** could no longer be detected. Interestingly, the signal of **8b** was diminished in comparison to $[Mo(CO)_4(dppe)]$, thus the thermal decomposition had already begun. Most likely the thermal decomposition led to the formation of oligo- or polymers, which could not be detected by the NMR experiment (*cf*. Chapter 3.3.2); the residue of the reaction was not further investigated.

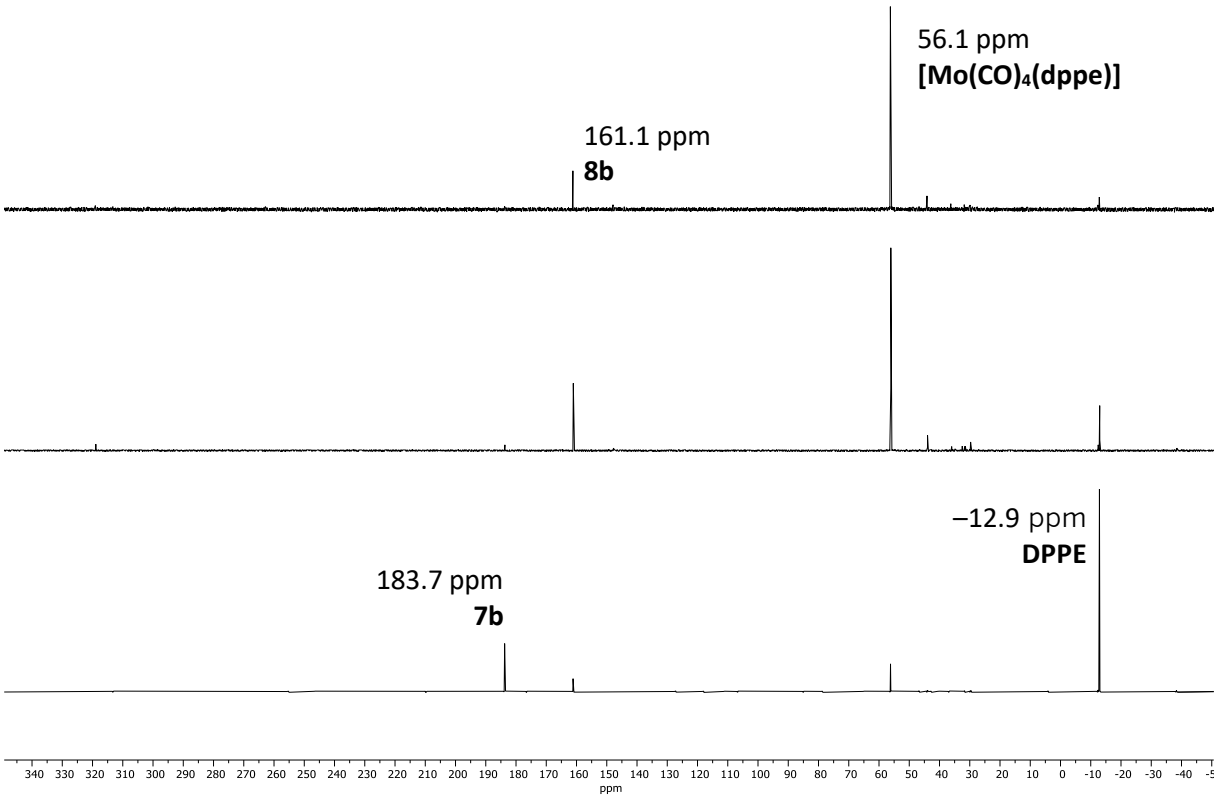

Figure 3.5: $^{31}P\{^{1}H\}$ NMR spectra of the synthesis of **8b** in the reaction solution. Bottom: After 2 h at 60°C Middle: After additional 2 h at 80°C. Top: After additional 1 h at 80°C.

3.2 P-centred reactions

3.2.1 Oxidation of phosphorus

3.2.1.1 Oxidation with oxygen-transfer reagents

As knowledge about (*P*-C substituted) 1,2$\sigma^4\lambda^5$-oxaphosphetane *P*-oxides[91,92] and *P*-sulfides[93] is scarce, and *P*-selenides and *P*-tellurides are unknown, it was desirable to study the synthesis and properties of such P(V) derivatives. In case of oxygen, a suitable oxygen transfer reagent was required. While a number of oxygen transfer reagents are established such as propylene oxide, trimethylamine N-oxide, *tert*-butylhydroperoxide, *meta*-chloroperoxybenzoic acid, and others, only iodosyl benzene (**9**) could be successfully applied here to **8a** and **8c,c'**, thus yielding the respective *P*-oxides **10a** and **10c,c'** (see Scheme 3.4).

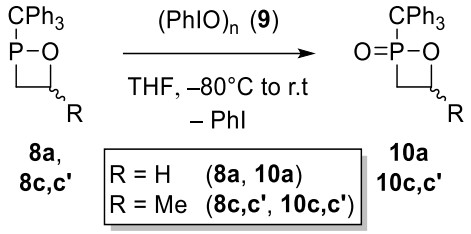

Scheme 3.4: Synthesis of 1,2$\sigma^4\lambda^5$-oxaphosphetane *P*-oxides **10a,c,c'**.

Although no crystal structure was determined, **10a,c,c'** could be characterised by NMR spectroscopy and a high resolution mass spectrometry experiments confirmed the molecular mass for the quasi-molecular ion of **10a** (m/z theor./exp. 349.1352/349.1356 $[M+H]^+$). The $^{31}P\{^1H\}$ NMR chemical shifts are 62.1 ppm and 63.5 ppm for the isomers of **10c,c'** and 70.8 ppm for **10a**. Compared to the only other 1,2-oxaphosphetane oxides with published $^{31}P\{^1H\}$ NMR shifts **10d** and **10e** (see Figure 3.6 and Table 3.2), the signals of **10a,c,c'** appear downfield-shifted.

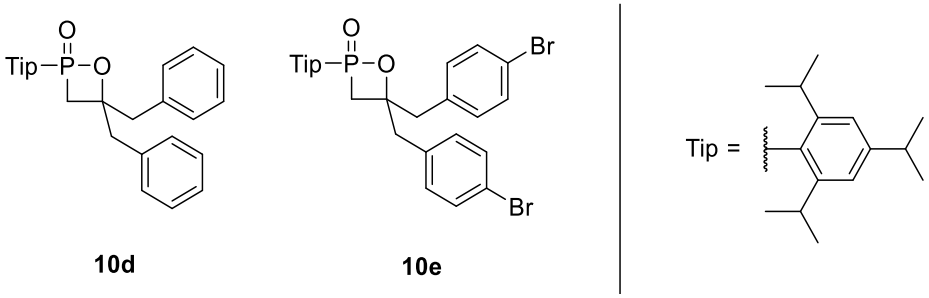

Figure 3.6: Literature known 1,2-oxaphosphetane oxides **10d,e**.[92]

Comparison showed that the geminal $^2J_{H\text{-}H}$ and the $^2J_{P\text{-}H}$ coupling constants of the non-equivalent C^3-protons of **10a** and **10d** were very similar, showing both a smaller (10.2 ppm, 10.9 ppm) and a larger (18.1 ppm, 17.9 ppm) $^2J_{P\text{-}H}$ coupling constant, respectively, and a nearly identical $^2J_{H\text{-}H}$ coupling constant (14.9 Hz (**10a**), 14.4 Hz (**10d**)). Furthermore, the $^1J_{P\text{-}C}$ and $^2J_{P\text{-}C}$ coupling constants of **10a,c,c'** and **10d,e** were in close similarity, same was true for the $^{13}C\{^1H\}$ NMR chemical shift of the C^3-carbon nucleus. The largest deviations were observed for the C^4-carbon, as was expected due to the changing number of substituents.

Table 3.2: Comparison of selected NMR values of **10a,c,c'** with the literature know 1,2-oxaphosphetane oxides **10d,e** by *Okazaki*.[92] Chemical shifts in ppm, coupling constants in Hz.

	δ(*P*)	δ(C^3) ($^1J_{P\text{-}C}$)	δ(C^4) ($^2J_{P\text{-}C}$)	δ(P-C*H*H') ($^2J_{H\text{-}H}$, $^2J_{P\text{-}H}$)	δ(P-CH*H'*) ($^2J_{H\text{-}H}$, $^2J_{P\text{-}H}$)
10a	70.8	33.4 (60.8)	62.9 (22.1)	2.65 (14.9, 10.2)	3.00 (14.9, 18.1)
10c	62.1	39.5 (60.8)	72.1 (20.2)	2.53 (m)	2.75 (14.5, 9.7)
10c'	63.5	38.9 (64.0)	74.3 (20.2)	2.56 (m)	2.96 (13.9, 16.6)
10d	48.7	43.4 (68.3)	83.4 (18.1)	2.97 (14.4, 10.9)	3.06 (14.4, 17.9)
10e	48.5	43.4 (68.3)	72.7 (18.1)	/	/

3.2.1.2 Oxidation with elemental sulfur and selenium

Where the synthesis of **10a,c,c'** required a transfer reagent, the 1,2-oxaphosphetane *P*-sulfides **11a,c,c'** and *P*-selenides **12c,c'** could be effectively synthesised using a reaction with elemental chalkogenes (see Scheme 3.5). The molecular mass of **11a,c,c'** and **12c,c'** was confirmed by detection of their quasi-molecular ion by high resolution mass spectrometry (m/z theor./exp.: **11a** 351.0967/351.0963, **11c,c'** 365.1123/365.1115, **12c,c'** 413.0568/413.0558). They were further characterised by NMR spectroscopy (see Table 3.3).

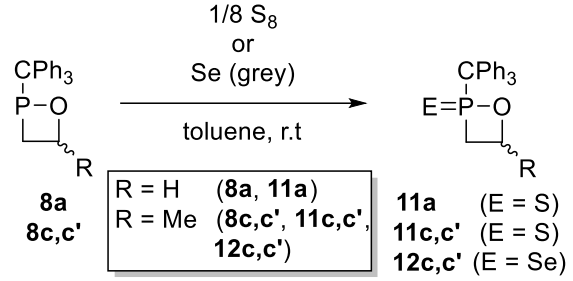

Scheme 3.5: Synthesis of 1,2-oxaphosphetane *P*-sulfides **11a,c,c'** and *P*-selenides **12c,c'**.

Table 3.3: Comparison of selected NMR values of **11a,c,c'** and **12c,c'**. Chemical shifts in ppm, coupling constants in Hz.

	δ(*P*)	δ(*C*^{3}) ($^1J_{P\text{-}C}$)	δ(*C*^{4}) ($^2J_{P\text{-}C}$)	δ(P-C*H*H') ($^2J_{H\text{-}H}$, $^2J_{P\text{-}H}$)	δ(P-CH*H'*) ($^2J_{H\text{-}H}$, $^2J_{P\text{-}H}$)
11a	129.8	38.4 (50.4)	64.9 (21.5)	2.48 (m)	2.48 (m)
11c	115.8	44.8 (51.5)	75.2 (19.49)	2.50 (m)	2.50 (m)
11c'	120.0	44.4 (49.8)	74.5 (19.9)	2.22 (14.1, 14.4)	2.72 (13.6, 11.7)
12c	115.8	45.6 (44.6)	76.1 (19.4)	2.62 (12.3, 12.3)	2.76 (13.0, 13.0)
12c'	121.5	44.6 (43.5)	76.1 (19.4)	2.42 (13.7, 15.0)	2.98 (13.8, 12.3)

As Table 3.3 shows, the $^{31}P\{^1H\}$ NMR chemical shifts of **11c,c'** and **12c,c'** were nearly identical, showcasing the similarity of sulfur and selenium. For comparison, PPh_3S and PPh_3Se have ^{31}P-NMR chemical shifts of 43.3 ppm and 35.3 ppm, respectively, differing only by 8.0 ppm.[94] **12c,c'** also showed ^{77}Se satellites in the $^{31}P\{^1H\}$ NMR spectrum ($^1J_{Se\text{-}P}$ = 839.7 Hz /845.8 Hz, respectively) and had a $^{77}Se\{^1H\}$ NMR shift of −10.7 ppm and 79.4 ppm. A difference of 90 ppm might seem significant, but the width of ^{77}Se NMR spectroscopy reaches from −1000 to 2000 ppm. Compared to literature known phosphane selenides **12d-g**[95] and the phospholane selenide **12h**[96], the $^{77}Se\{^1H\}$ shifts of the 1,2-oxaphosphetane selenides **12c,c'** were significantly downfield-shifted. This indicated a slightly weaker P=Se double bond, as Vela had shown that a stronger highfield shift correlates with higher bond dissociation energy.[95]

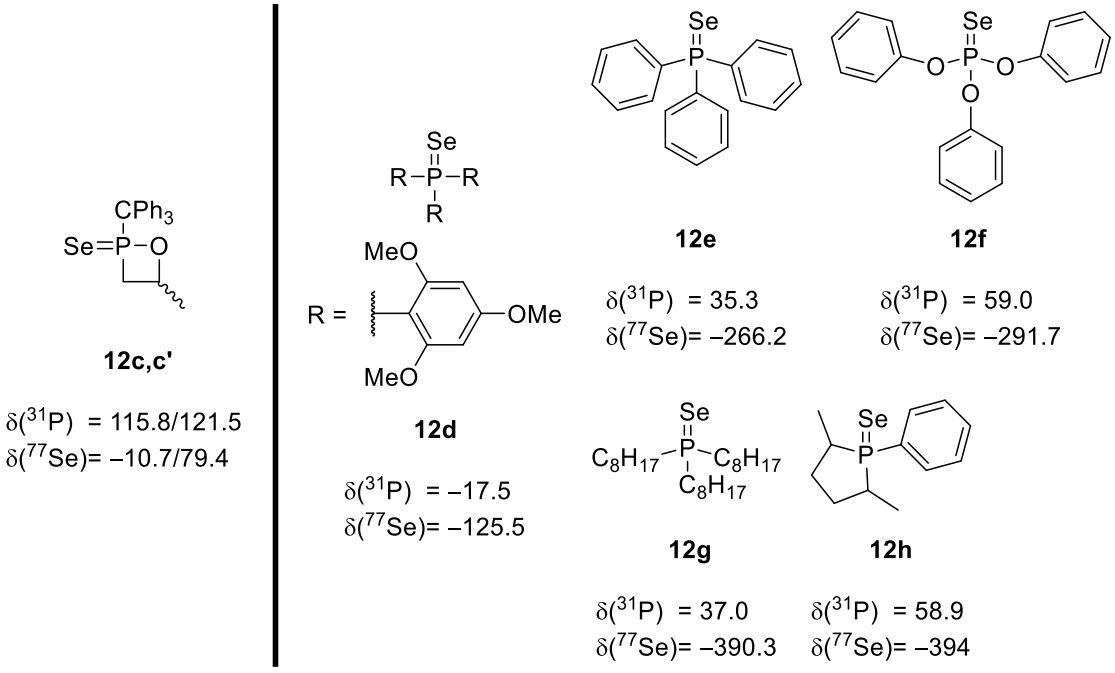

Figure 3.7: Comparison of ^{31}P and ^{77}Se NMR chemical shifts of 1,2-oxaphosphetane *P*-selenide **12c,c'** and literature known phosphane selenides **12d-g**[95] and **12h**[96].

Single crystals of **11a** suitable for X-ray diffractometry could be obtained by evaporation of the solvent from a *n*-pentane solution (see Figure 3.8). On comparison of the crystallographic data of 1,2-oxaphosphetane **8a** with its *P*-sulfide **11a** (see Table 3.4), it showed that the four-membered ring remained planar. In contrast, the endocyclic P-O and P-C bonds were shortened by 0.039 Å and 0.047 Å, respectively, whereas the exocyclic P-C bond was shortened by only 0.017 Å. A shortening of these bonds upon oxidation of phosphorus was expected, as the electron withdrawing oxygen atom ledto a positive partial charge at phosphorus, leading to higher attraction of bond electrons and thus a shorter bond distance.[97]

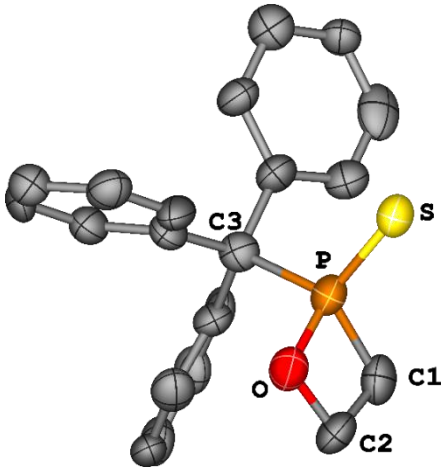

Figure 3.8: Molecular structure of **11a** in the solid state. Hydrogen atoms are omitted and the thermal ellipsoids are set at the 50% probability level.

Table 3.4: Selected bond lengths and angles of **8a** and **11a**. Bond lengths in Å, angles in °.

	P-O	P-CH_2	P-CPh_3	CH_2-P-O	CPh_3-P-O	Σ(endocyclic angles)	P=S
8a	1.670(3)	1.849(4)	1.923(5)	80.47(18)	104.29(18)	359.6 (11)	/
11a	1.631(12)	1.802(18)	1.906(15)	82.4(7)	104.7(6)	360.0(39)	1.923(6)

3.2.1.3 Attempted oxidation using elemental tellurium and tri(*n*-butyl)phosphane telluride

In analogy to the syntheses of **11c,c'** and **12c,c'**, 1,2-oxaphosphetane **8c,c'** was treated with elemental tellurium, hoping to yield 1,2-oxaphosphetane telluride **13c,c'** (see Scheme 3.6). As no conversion was observed in the $^{31}P\{^{1}H\}$ NMR spectrum of the reaction solution, it was attempted to synthesize **13c,c'** *via* a transfer reaction using tri(*n*-butyl)phosphane telluride.

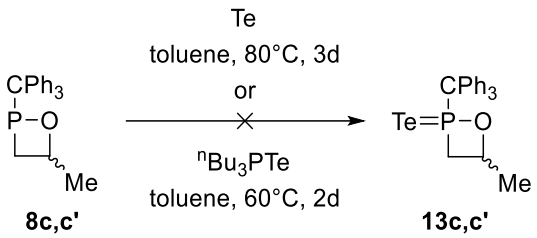

Scheme 3.6: Attempted synthesis of 1,2-oxaphosphetane telluride **13c,c'**.

But again no clean formation of **13c,c'** could be observed. In the $^{31}P\{^{1}H\}$ NMR spectrum of the reaction mixture, two signals at 42.5 ppm and 46.7 ppm were observed besides the starting material **8c,c'**. While these might be fitting for a regular phosphane telluride (see Figure 3.9), the comparison with 1,2-oxaphosphetane sulfides **11a,c,c'** and selenides **12c,c'** suggested a more highfield-shifted signal for **13c,c'**. The observed signals most likely derived from hydrolysis products of **8c,c'**.

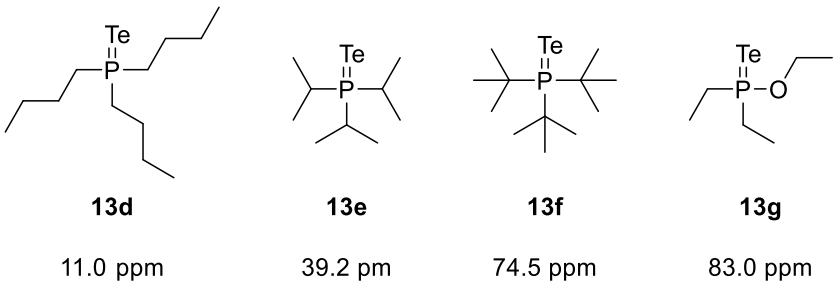

Figure 3.9: Literature known phosphane tellurides **13d-f**[98] and alkoxy-phosphane telluride **13g**[99].

3.2.2 Complexation of the P-centre with borane

Phosphane-borane complexes are of high interest during the recent decades, either as protected phosphanes or in organic synthesis.[100] To explore the possible formation of 1,2-oxaphosphetane-borane complexes, 1,2-oxaphosphetanes **8a,c,c'** were treated with the $BH_3{\cdot}SMe_2$ adduct. The reactions selectively yielded the corresponding 1,2-oxaphosphetane P-borane adducts **14a,c,c'** (see Scheme 3.7). **14a,c,c'** were both characterised with NMR spectroscopy and a crystal structure could be obtained for **14a** (see Figure 3.10).

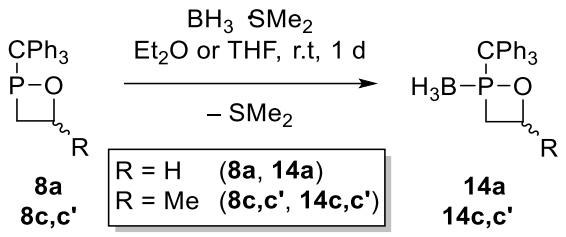

Scheme 3.7: Synthesis of 1,2-oxaphosphetane *P*-borane adducts **14a,c,c'**.

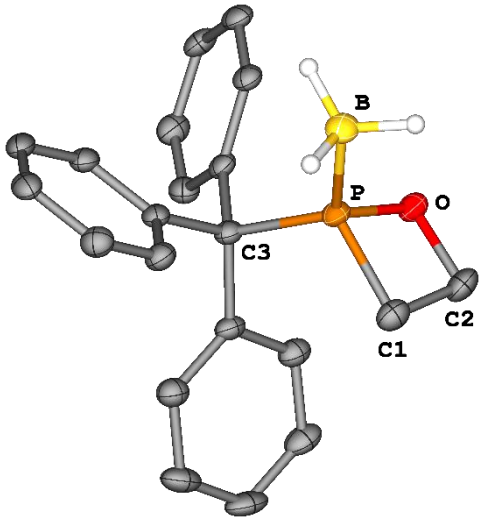

Figure 3.10: Molecular structures of **14a** in the solid state. Hydrogen atoms (except bonded to borane) are omitted and the thermal ellipsoids are set at the 50% probability level.

The structural changes from **8a** to **14a** were comparable to the changes from **8a** to **11a** (see Table 3.5): The four-membered ring remained planar, while the endocyclic P-O and P-C bonds were shortened by 0.031 Å and 0.032 Å, respectively, and the exocyclic P-C bond was shortened by 0.028 Å. This could again be explained by the higher charge density at phosphorus.

Table 3.5: Selected bond lengths and angles of **8a** and **14a**. Bond lengths in Å, angles in °.

	P-O	P-CH_2	P-CPh_3	CH_2-P-O	CPh_3-P-O	Σ(endocyclic angles)	P-BH_3
8a	1.670(3)	1.849(4)	1.923(5)	80.47(18)	104.29(18)	359.6(11)	/
14a	1.6395(15)	1.817(2)	1.895(2)	82.74(9)	106.53(8)	359.1(5)	1.907(2)

While the reaction with an adduct of the parent borane worked smoothly, this was not the case for a number of substituted boranes. For example, when **8a** was treated with triethylborane or triphenylborane no reaction was observed, and this might be explained by stereoelectronic reasons.

3.3 Arbuzov reactions of 1,2σ³λ³-oxaphosphetanes

3.3.1 Molecular Arbuzov reactions

To further investigate the reactivity of 1,2-oxaphosphetanes, it was planned to treat **8a** with alkyl halides, trying to generate 1,2σ⁴λ⁵-oxaphosphetanium derivatives **15**. These could serve as precursors for a subsequent deprotonation to yield either unsaturated rings or cyclic phosphonium ylids **16**. The ylids **16** would thus enable an entry into Wittig-like chemistry,[23,101] maybe even into catalysis[102] (see Scheme 3.8).

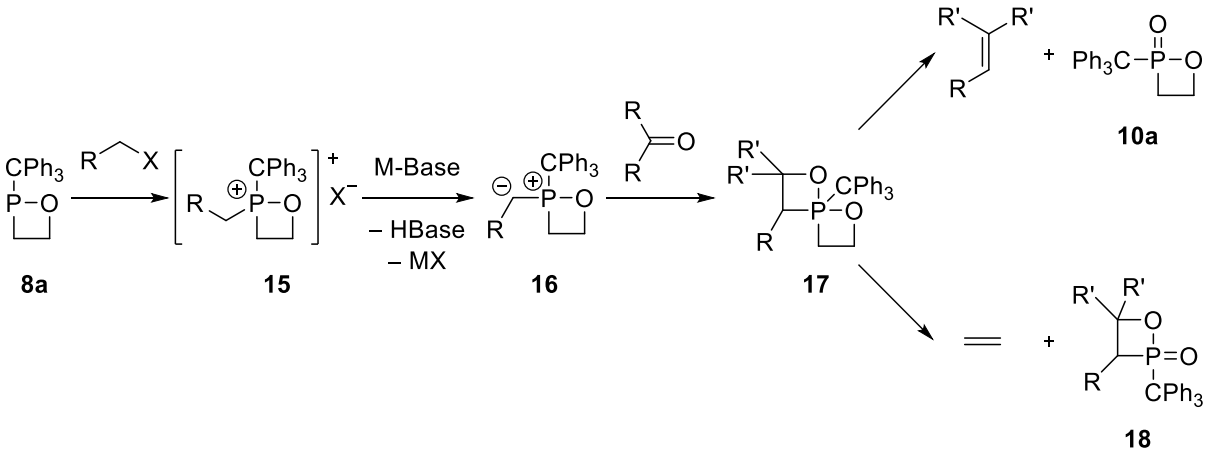

Scheme 3.8: Desired synthesis of cyclic phosphonium ylids **16**, followed by a possible Wittig reaction.

But due to the fact that **8a** possesses a direct P-O bond, **15** will not be stable in the presence of a nucleophile, *i.e.* a halide anion, and an Arbuzov reaction will occur, leading to β-haloethylorgano(trityl)phosphane oxides **19** (see Scheme 3.9).

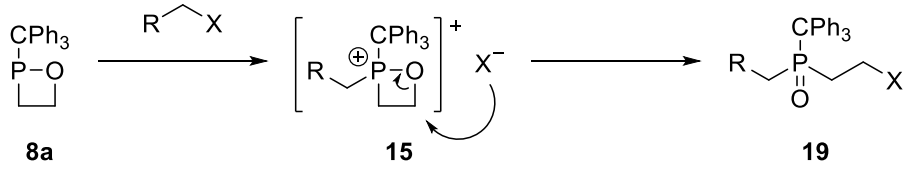

Scheme 3.9: Arbuzov reaction of **8a**, leading to phosphane oxides **19**.

To gain broader insight, **8a** was treated with various activated alkyl halides to form phosphane oxides **19a-c** (see Scheme 3.10). The reactions occurred selectively, and products **19a-c** could be isolated. The

molecular mass of **19a-c** was confirmed by detection of their quasi-molecular ion by high resolution mass spectrometry, and their constitution was characterised by NMR spectroscopy.

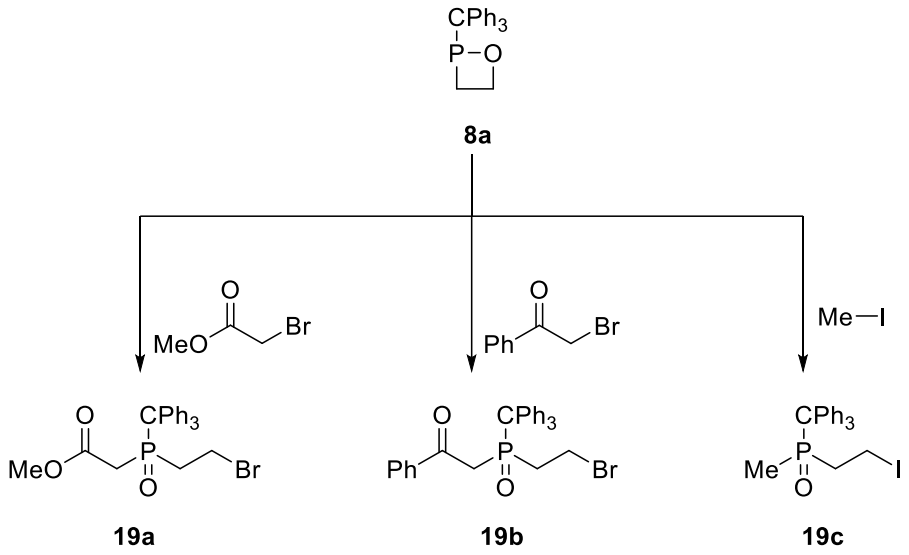

Scheme 3.10: Syntheses of phosphane oxides **19a-c**.

Apparently, the $^{31}P\{^{1}H\}$-NMR resonances of the products (see Table 3.6) were significantly highfield-shifted in comparison to the 1,2-oxaphosphetane **8a**, *i.e.*, the chemical shifts appeared in the range of 40 to 50 ppm, which was typical for phosphane oxides.[103] The $^{31}P\{^{1}H\}$ NMR chemical shift increases in the order **19a** < **19b** < **19c**. This could be explained by the shielding provided by the electron rich ester and benzoyl groups in **19a** and **19b** respectively, whereas **19c** was only subjected to a slight deshielding through the −I-inductive effect of the methyl group.

Table 3.6: Selected NMR chemical shifts in ppm of **19a-c** in comparison with **8a**.

	δ(*P*)	δ(XCH$_2$-*C*H$_2$)	δ(X*C*H$_2$)	δ(*C*H$_x$)	δ(XCH$_2$-C*H*$_2$)	δ(XC*H*$_2$)	δ(C*H*$_x$)
19a	48.4	33.8	25.3	37.6	2.43 / 2.60	3.53 / 3.53	2.48 / 3.15
19b	49.7	33.6	25.3	40.7	2.44 / 2.56	3.32 / 3.51	2.98 / 4.07
19c	53.6	35.4	−5.6	14.9	1.99 / 2.55	3.12 / 3.36	1.43
8a	212.1	24.1	74.0	/	2.29 / 2.83	4.42 / 5.05	/

Through evaporation of an *n*-pentane (**19a,b**) or DCM (**19c**) solution, suitable single crystals for X-ray diffraction studies could be obtained for all three compounds (see Figure 3.11). The observed bond lengths were within the expected range (see Table 3.7, *c.f.*: *n*-Bu$_3$PO P=O 1.494 Å, P-C 1.804 Å, C-C 1.526 Å.[104] EtBr: C-C 1.485 Å, C-Br 1.955 Å.[105] EtI: C-C 1.496 Å, C-I 2.157 Å.[105]).

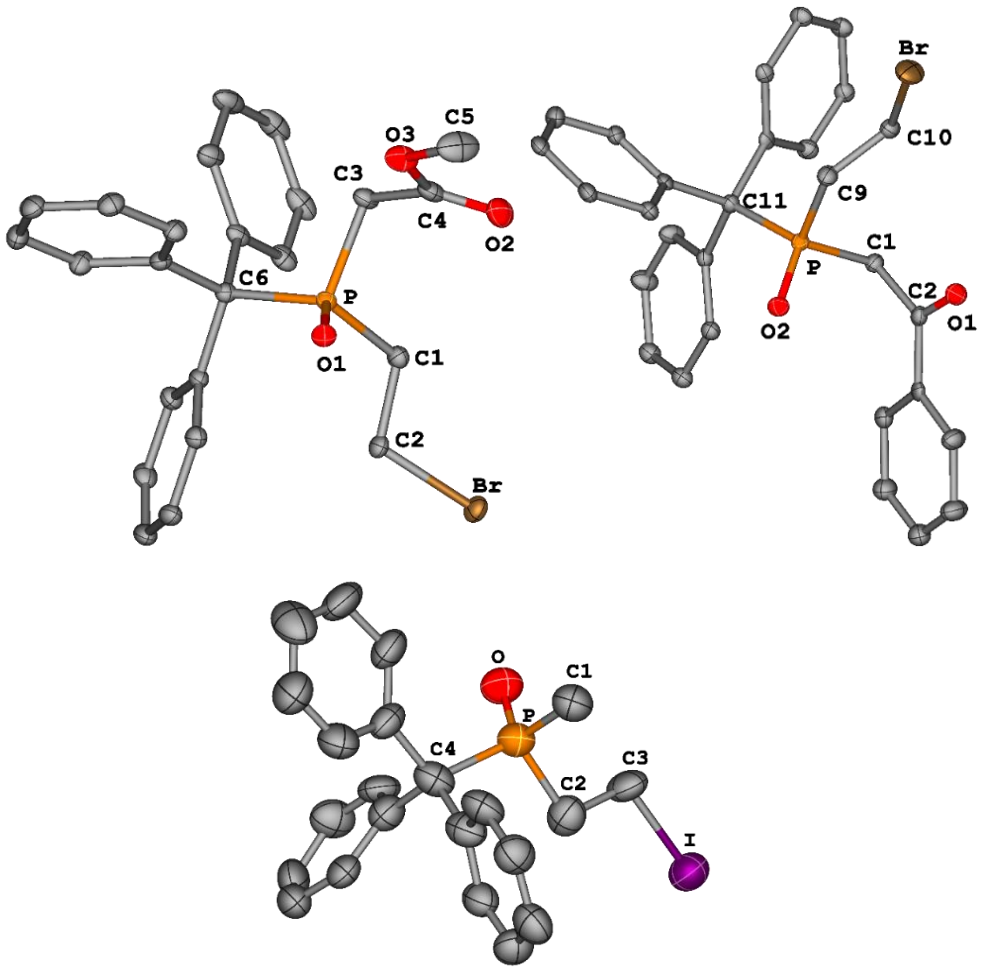

Figure 3.11: Molecular structures of **19a** (top left), **19b** (top right) and **19c** (bottom) in the solid state. Hydrogen atoms are omitted and the thermal ellipsoids are set at the 50% probability level.

Table 3.7: Selected bond lengths and angles of **19a-c**. Bond lengths in Å, angles in °.

	P=O	P-CH_2CH_2X	PCH_2-CH_2X	CH_2-X	P-CH_2R	P-CPh_3	CH_2-P-CH_2	O=P-CPh_3
19a	1.4841(10)	1.8254(14)	1.5195(19)	1.9604(13)	1.8290(14)	1.8809(14)	104.05(7)	114.89(6)
19b	1.500(6)	1.813(8)	1.510(11)	1.971(8)	1.832(8)	1.868(8)	108.8(4)	114.9(3)
19c	1.502(12)	1.852(19)	1.52(2)	2.165(15)	1.820(17)	1.899(18)	105.2(9)	115.0(8)

As mentioned in chapter 3.1, the 1,2-oxaphosphetanes were first synthesized as mixtures of diastereomers, with **8a** being the first derivative consisting of only one diastereomer. In an attempt to obtain some kind of chiral resolution by functionalization, **8a** was also reacted with a suitable enantiopure alkyl halide (−)menthyl bromoacetate **20** (see Scheme 3.11).

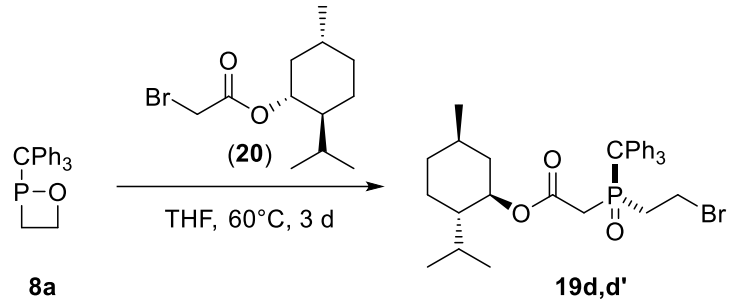

Scheme 3.11: Synthesis of diastereomeric mixture of **19d,d'**.

The reaction occurred selectively and the molecular composition of **19d,d'** was confirmed by detection of the quasi-molecular ion by high resolution mass spectrometry (m/z theor./exp.: 595.1971/595.1969 $[M+H]^+$). In the $^{31}P\{^1H\}$-NMR spectrum, two products at 48.0 ppm and 48.4 ppm in 1:1 ratio were observed. This diastereomeric mixture was further analysed with ^1H and $^{13}C\{^1H\}$ NMR-spectroscopy. The very small shift difference both in the $^{31}P\{^1H\}$-NMR spectrum ($\Delta\delta(^{31}P)$= 0.4 ppm) as well as in the $^{13}C\{^1H\}$-NMR spectrum ($\Delta\delta(^{13}C)$= 0.0–0.2 ppm) indicated the presence of two very similar diastereomers. All signals could be assigned by 2D-NMR spectra (HMBC, HSQC), but due to too low resolution (and near equal isomeric ratio after purification), it was not possible to assign the signals to the isomers. In the ^1H NMR spectrum, a multitude of very similar, nearly isochorus multiplets made the determination of coupling constants impossible in most cases (see Figure 3.12). In theory, the separation of the diastereomers of **19d,d'** should now be possible, followed by crystallisation of the separated enantiopure diastereomers, enabling the determination of absolute configuration. However, due to small scales of the experiment, no column chromatographic purification was attempted and **19d,d'** was only isolated as diastereomeric mixture.

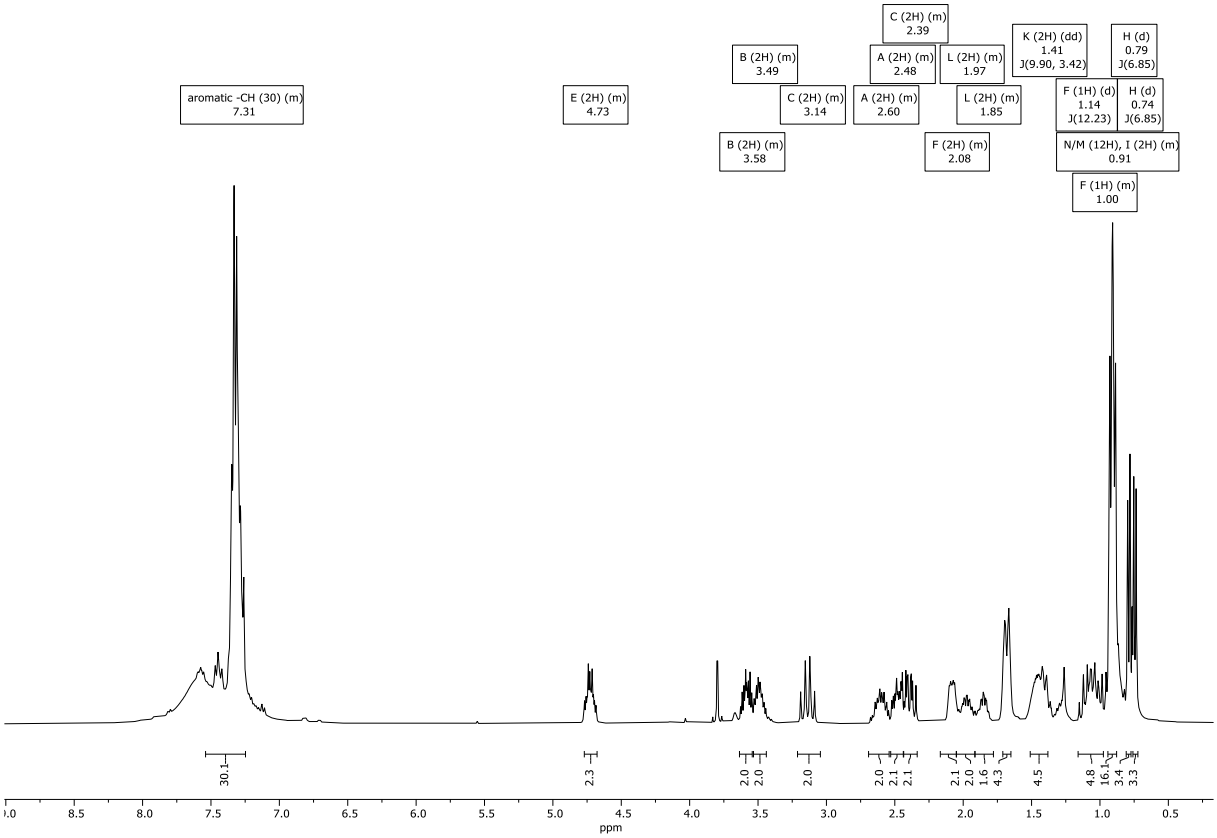

Figure 3.12: ^{1}H NMR spectrum of **19d,d'**.

3.3.2 Oligomer formation through Arbuzov-type reactions

The original aim of the reactions with alkyl halides was not the synthesis of Arbuzov-products, but rather the generation of 1,2-oxaphosphetanium cation-containing compounds. Therefore it was attempted to react **8a** with less nucleophilic reagents, and methyl triflate was chosen because triflate acts more as weakly coordinating anion compared to halides.[106] When **8a** was treated with one equivalent of methyl triflate at −80°C and warmed up to ambient temperature, no sharp signals could be observed in the ^{31}P{^{1}H} NMR spectrum. The first assumption was that poly- or oligomers **22^{n}** (n denotes the amount of monomeric 1,2-oxaphosphetane unit are incorporated in the oligomer) had formed (see Scheme 3.12).

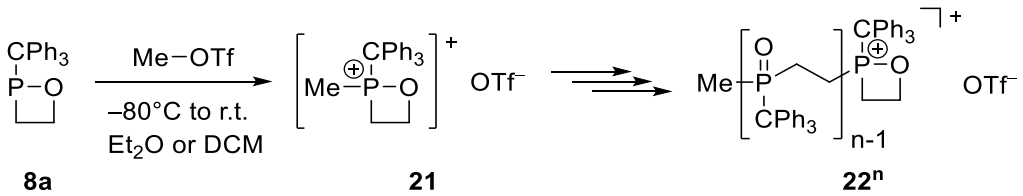

Scheme 3.12: Synthesis of phosphorus-containing oligomer **22^{n}**.

After removal of the solvent, a MALDI mass spectrum was recorded (see Figure 3.13) which proved the hypothesis of oligomer formation *via* the existence of equidistant mass peaks with a difference of m/z = 318.12. This difference corresponded to the exact mass of one 1,2-oxaphosphetane unit **8a**. The highest mass oligomer was observed at 3196.3 m/z, corresponding to $\mathbf{22^{10}}$. All oligomers from $\mathbf{22^2}$ to $\mathbf{22^{10}}$ could be observed but the spectrum showed a strong preference for the dimer $\mathbf{22^2}$, which was not surprising given the equimolar amount of methyl triflate.

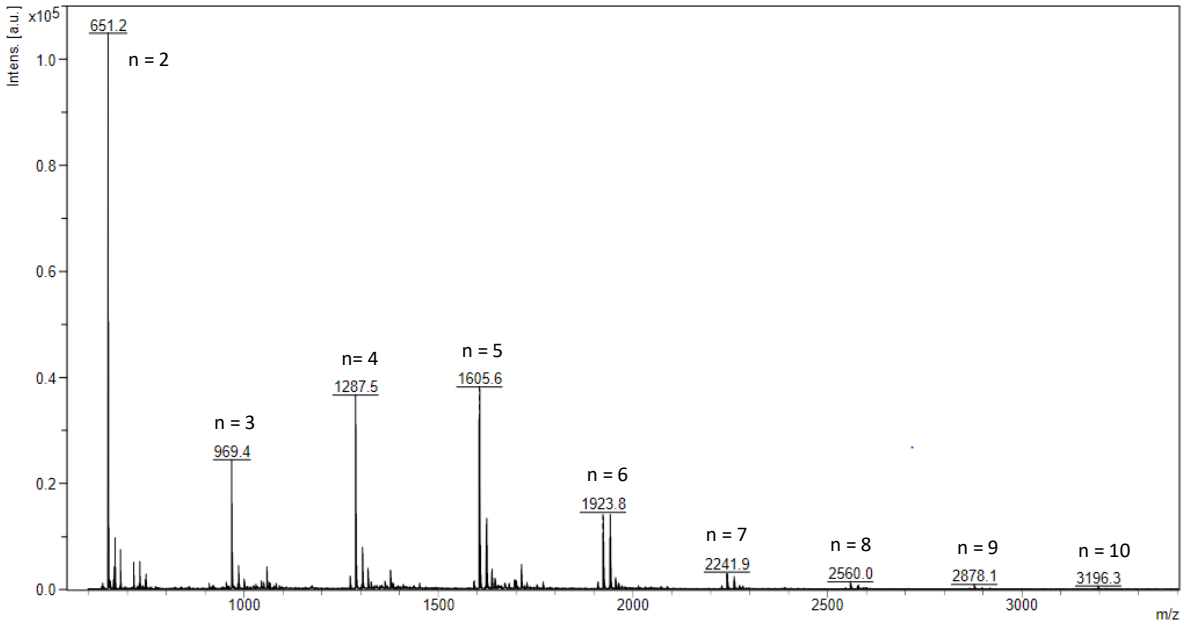

Figure 3.13: MALDI mass spectrum of oligomers $\mathbf{22^n}$, DCTB as matrix.

To further investigate the oligomer formation, a series of experiments were performed with varying concentrations of **8a** and equivalents of methyl triflate. Also, the solvent was changed from Et_2O to DCM to raise the solubility, both of the starting material as well as of the growing oligomer chain.

In the first series of experiments, varying equivalents of metyl triflate were added to a constant amount of **8a** in a defined volume of solvent. Although the pentamer $\mathbf{22^5}$ is the preferred product in all cases, the relative distribution of $\mathbf{22^n}$ shows clearly that a substoichiometric amount of methyl triflate leads to a preferred formation of heavier oligomers $\mathbf{22^{6\text{-}9}}$ (see Figure 3.14, left). It is also observed that the reaction showed a preference for the dimer $\mathbf{22^2}$ if 0.5 equivalents of methyl triflate were used, which corresponded to the stoichiometry of the dimer $\mathbf{22^2}$. Still, the pentamer $\mathbf{22^5}$ stayed the preferred product and no selective formation of the dimer $\mathbf{22^2}$ could be observed. In a second series, the solvent volume and ratio of **8a** to methyl triflate (1 eq) was kept constant, while the concentration of **8a** in the solvent varied. As expected, a higher concentration led to a preferred formation of heavier oligomers $\mathbf{22^{6\text{-}10}}$ (see Figure 3.14, right). For a concentration of 1 mol/L, the preferred product was the pentamer

22^{5}, with a significantly higher content of heavier oligomers **22**$^{6\text{-}10}$ formed. For a concentration of 0.2 mol/L, **27**^{5} was still the main product, but with significantly less of heavier oligomers **22**$^{6\text{-}10}$, and a strong preference for the dimer **22**^{2}, as second most abundant oligomer. In the case of 0.04 mol/L, the situation changed drastically, with the dimer **22**^{2} being the main product and a drastic drop of abundancy for all other oligomers. Interestingly, the second most abundant product was still the pentamer **22**^{5}, showing no preference for the other lighter oligomers **22**$^{3\text{-}4}$.

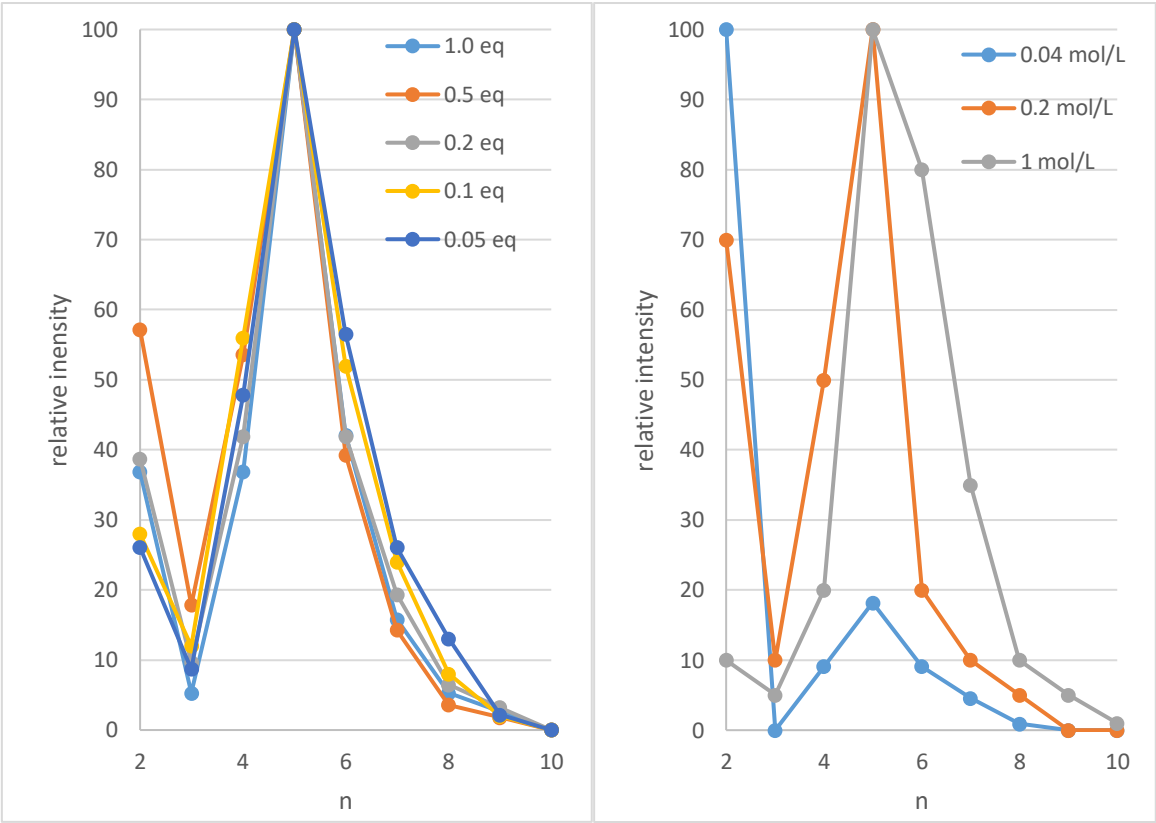

Figure 3.14: Relative distribution of individual oligomers of **22**^{n}, normalized to the most abundant oligomer. Left: Constant concentration of **8a** with changing equivalents of methyl triflate. Right: Constant, equimolar amount of methyl triflate with changing concentration of **8a** in the solvent.

For a last set of experiments, the influence of the equivalents of used methyl triflate with a relative high concentration of **8a** was examined. The concentration had two limiting factors, the solubility of **8a** in DCM at low temperature and the amount of **8a** one synthesis cycle provided so only a small volume of solvent was used. This last series started with a concentration of 0.5 mol/L with a volume of 0.5 mL. While **8a** was completely soluble at ambient temperature, it precipitated at −80°C, so another 0.5 mL DCM were added, leading to a concentration of 0.25 mol/L. The distribution of oligomers of **22**^{n} showed a strong similarity to the first series (see Figure 3.15). The substoichiometric equivalents of methyl triflate (0.25 eq, 0.1 eq, 0.05 eq) showed a clear preference for the heavier oligomers **22**$^{6\text{-}10}$,

whereas an equimolar amount of methyl triflate prefers the lighter oligomers **22**$^{2\text{-}4}$. For both these cases the main product is still the pentamer **22**^{5}. The only exception from the observed trend was again the case of 0.5 eq of methyl triflate, showing a strong preference for the dimer **22**^{2} and making it the main product, reducing the pentamer **22**^{5} to a relative abundancy of 50%. Interestingly, the use of 0.25 equivalents methyl triflate didn't show an observable preference for the stoichiometric product tetramer **22**^{4} but formed preferably the pentamer **22**^{5} and then the heavier oligomers **22**$^{6\text{-}10}$.

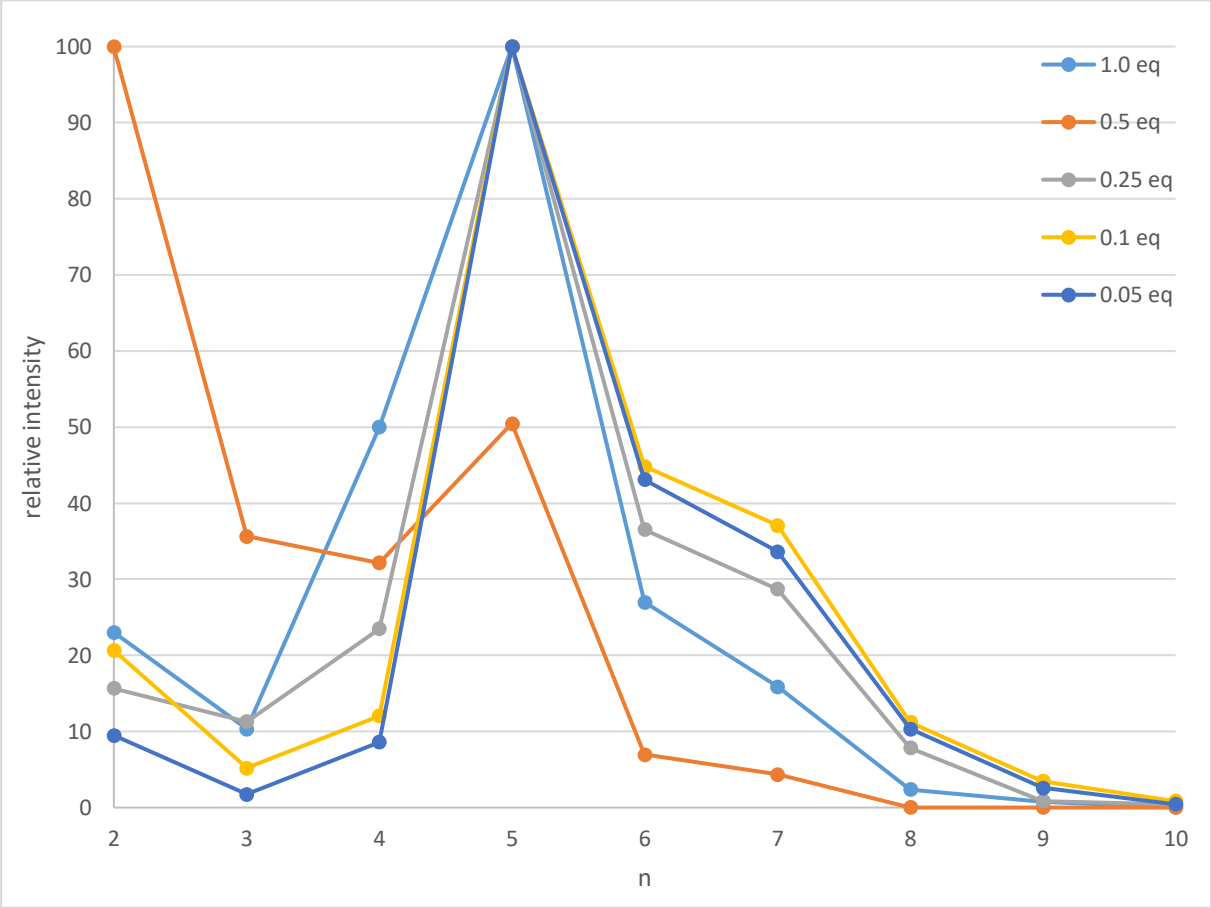

Figure 3.15: Relative distribution of individual oligomers of **22**^{n}, normalized to the most abundant oligomer. Concentration of **8a** fixed at 0.25 mol/L.

To investigate the mechanism of the oligomerisation reaction, variable low temperature $^{31}P\{^{1}H\}$ NMR spectra were recorded from −80°C to 40°C (see Figure 3.16). From −80°C to −50°C the signal of the starting material **8a** was visible at 212.2 ppm, vanishing when reaching −40°C. Already at −80°C, small signals at 54.8 ppm and 130.4 started to appear. These signals became more intense until reaching −30°C, with broad signals forming directly next to them. Upon further warming these signals diminished with no sharp signal observable at 40°C.

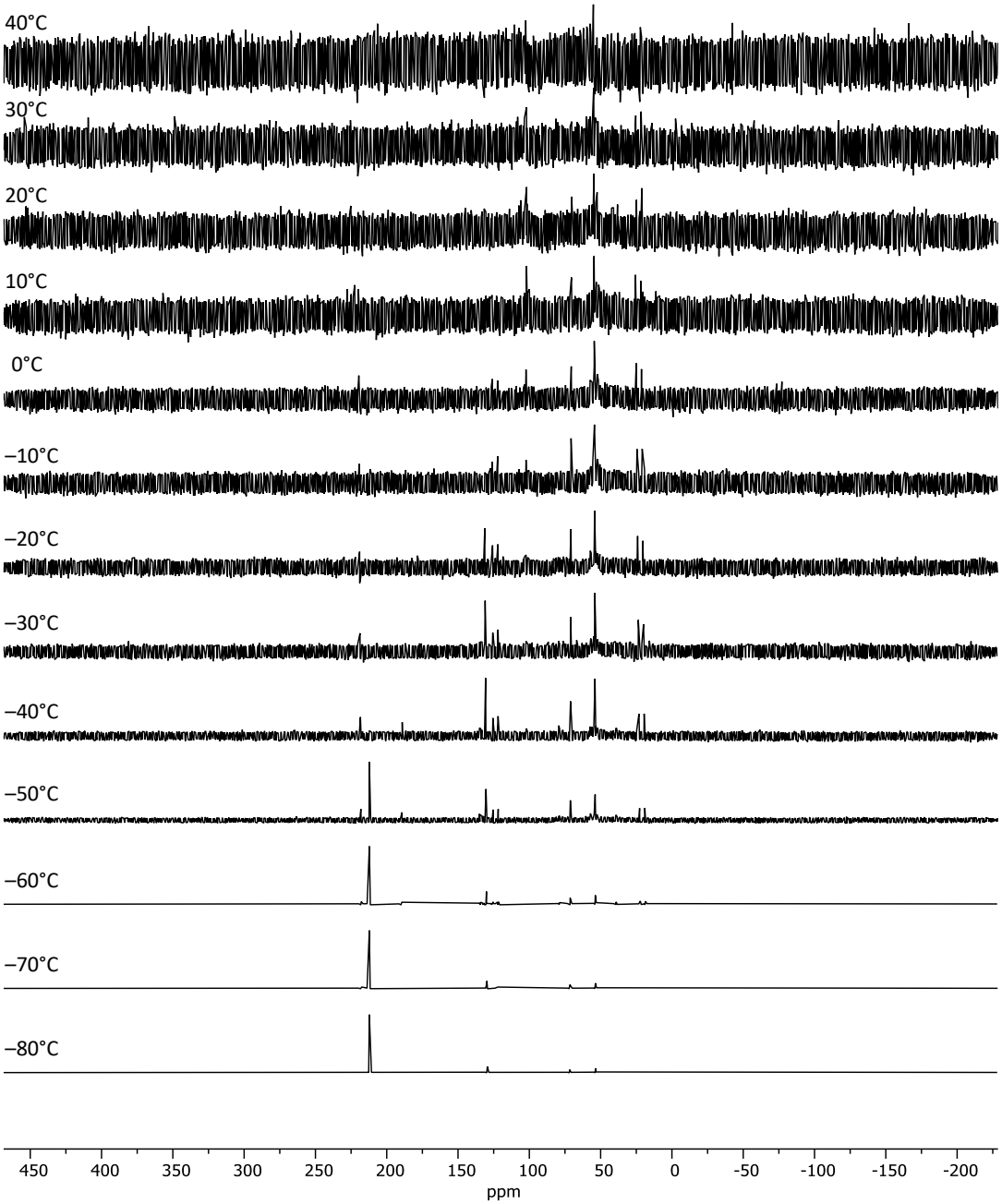

Figure 3.16: Variable temperature $^{31}P\{^{1}H\}$ NMR spectra of the reaction of **8a** with methyl triflate.

In the following, the $^{31}P\{^{1}H\}$ NMR spectrum at −50°C was shown (see Figure 3.17) and shall be discussed further. While the 1,2-oxaphosphetanes were unknown for a long time and thus no comparable, experimental values were available, the poly- or oligomerisation of the 1,2-oxaphospholanes has been investigated in the past. Saegusa has reported on the reaction of 2-phenyl-1,2-oxaphospholane **23** with methyl triflate, showing a series of broad signals in the $^{31}P\{^{1}H\}$ NMR spectrum, hinting to polymerisation (see Figure 3.18, top row).[107] Saegusa observed the first methylated 1,2-

oxaphospholanium species **24** at 101 ppm, slightly highfield-shifted in comparison to the starting material **23** at 109 ppm. The shift difference of over 100 ppm between the four-membered O,P-cycle **8a** and the five-membered O,P-cycle **23** emphasised the different electronic situation in the regarding ring systems.[54] Also, the oligomerisation of **8a** already takes place at −60°C, whereas **23** has to be heated to 70°C to show polymerisation. Upon reaching this temperature, Saegusa observed two new signals at 34 ppm and 38 ppm, which he attributed to the methylated, ring opened terminal end of the emerging polymer **25** and the ring opened middle unit of the polymer (bearing another opened unit at phosphorus) **26**.

Additionally, the chemical shifts of model compounds **27** and **28** were computed by Espinosa Ferao using quantum chemical calculations (see Figure 3.18).[108] For the *P*-dimethyl 1,2-oxaphosphonium **27** a shift of 151.1 ppm was calculated. For the trimer **28**, a chemical shift of 156.0 ppm was calculated for the cyclic propagating end. For the phosphorus nucleus of the terminal, ring opened end 39.3 ppm was calculated with the nuclei of the middle unit at 40.7 ppm.

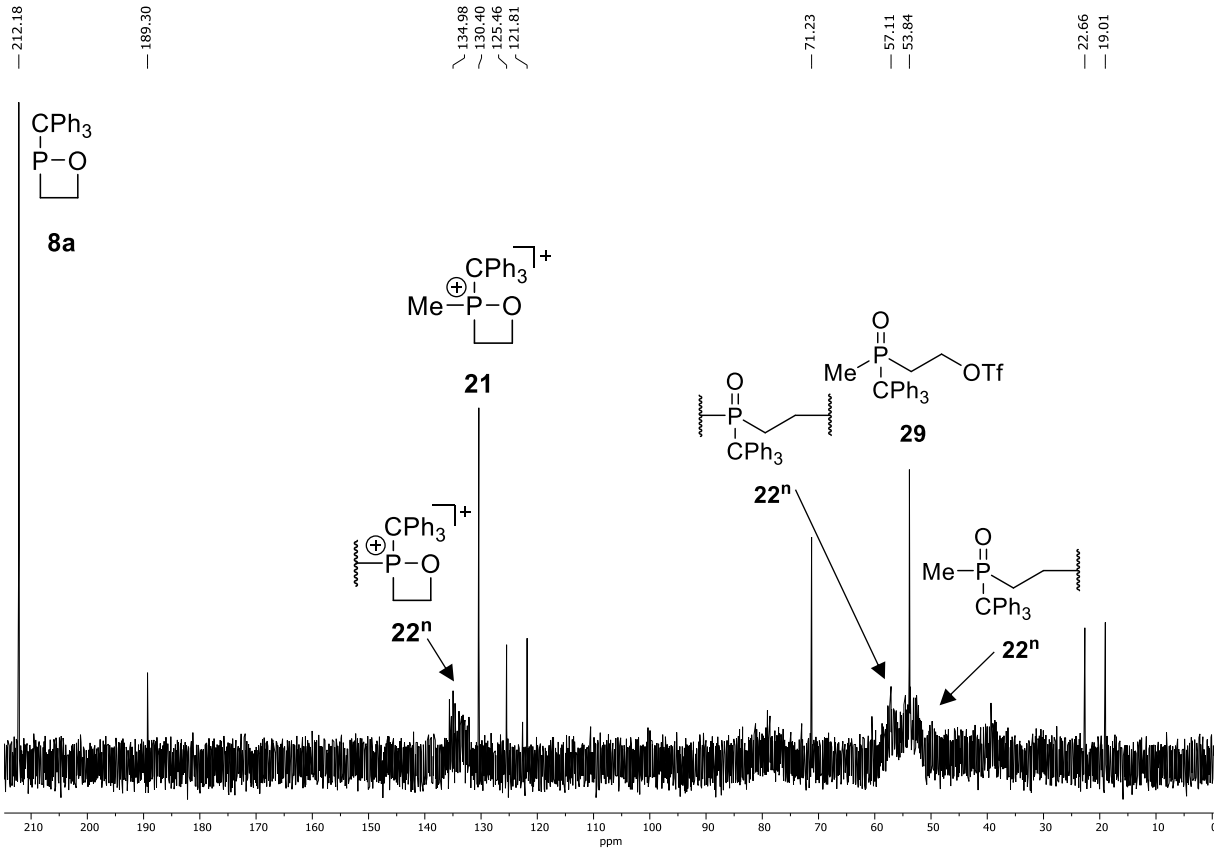

Figure 3.17: $^{31}P\{^{1}H\}$ NMR spectra of the reaction of **8a** with methyl triflate at −50°C.

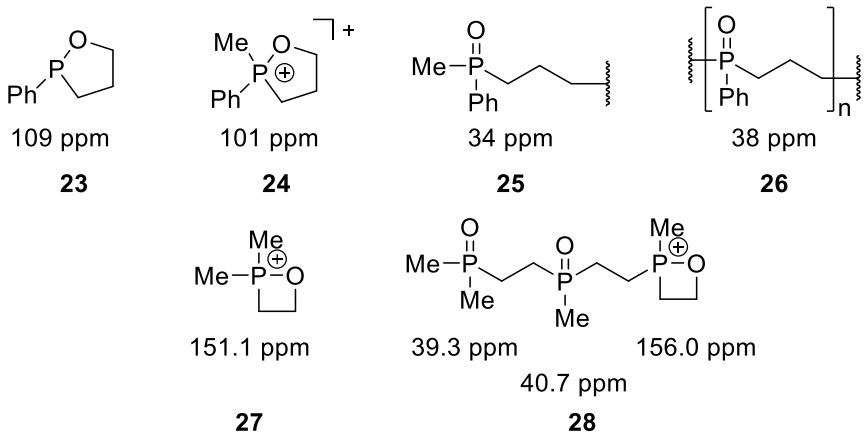

Figure 3.18: Lewis formulae and $^{31}P\{^{1}H\}$ NMR chemical shifts for comparison. Top row: experimental values of 1,2-oxaphospholane derivatives by Saegusa.[107] Bottom row: Calculated shift values of model 1,2-oxaphosphetane, at NMR(GIAO)/$CPCM_{DCM}$/PBEO/def2-TZVP, geometries optimized at $CPCM_{DCM}$/PBEh-3c level of theory by Espinosa Ferao.[108]

Taking all this information into account, the experimentally obtained signals were interpreted as folows: The sharp signal at 130.4 ppm was tentatively assigned to the *P*-methylated 1,2-oxaphosphetanium **21**, due to the similarity with the calculated model **27** and the slight similarity with methylated 1,2-oxaphospholanium **23**. The broad signal around 134 ppm was assigned to the cyclic, propagating end of oligomers **22^{n}**, as the signals did not only become broader due to the increasing size, but also due to the number of overlaying signals of the varying, individual oligomers of **22^{n}**. The sharp signal at 53.8 ppm was assigned to the possible ring opened part, the regular Arbuzov product **29**, based on the extreme similarity with the methyl iodine Arbuzov product **19c**. The broad signals around 53 ppm and 57 ppm were assigned to the oligomers **22^{n}**, the slightly highfield-shifted signal group was assigned to the terminal end, whereas the more downfield-shifted signal group is assigned to the middle units. The chemical shift fitted well with the calculated values, and the shift difference of 4 ppm fitted very well to the difference of the 1,2-oxaphospholane derivatives **25** and **26**.

While it was not yet possible to generate long-chained, high mass polymers suitable for application, this work provided the first insight into the possible polymerisation of 1,2-oxaphosphetane **8a** and an entry point for further research towards novel inorganic polymers and co-polymers with flame retardant properties.

3.3.3 The Perkow reaction in competition to the Arbuzov reaction

Lesser known than the Arbuzov reaction is the Perkow reaction, in which a trialkyl phosphite ester reacts with an α-haloketone. The α-haloketone possesses two electrophilic moieties, the α-halo-carbon and the carbonyl-carbon. While an attack of the phosphite ester at the α-halo-carbon would lead to the formation of a phosphonate (the Arbuzov product), the nucleophilic attack of phosphorus at the carbonyl-carbon leads to the formation of a vinyl phosphate (the Perkow product). As the 1,2-oxaphosphetane **8a** possessed an internal P-O bond, it should also be able to undergo Perkow reactions, and Perkow and Arbuzov reactions should be considered as competing reactions. In fact, one possibility for a Perkow reaction was already reported in chapter 3.3.1; **8a** was reacted with methyl bromoacetate, which possesses a carbonyl function and thus could in theory react in a Perkow reaction, although only the selective formation of the Arbuzov product **19a** was observed. This didn't seem unusual, as here the carbonyl-group was part of a mesomerically stabilized carboxylate group. This was further supported by quantum chemical computations, performed by Espinosa Ferao, which showed that the highest occupied molecular orbital (HOMO) of the model 2-methyl-1,2-oxaphosphetane **8e** was at phosphorus. But the lowest occupied molecular orbital (LUMO) of methyl bromoacetate was not the π*(C=O) orbital but rather the σ*(C-Br) orbital (see Figure 3.19). For comparison, the frontier orbitals of chloroacetone were also computed. Here the situation is inverted, with the π*(C=O) orbital as the LUMO and the σ*(C-Cl) as LUMO-1. To further investigate the possibility to form a Perkow product, **8a** was reacted with chloro- and bromoacetone (see Scheme 3.13).

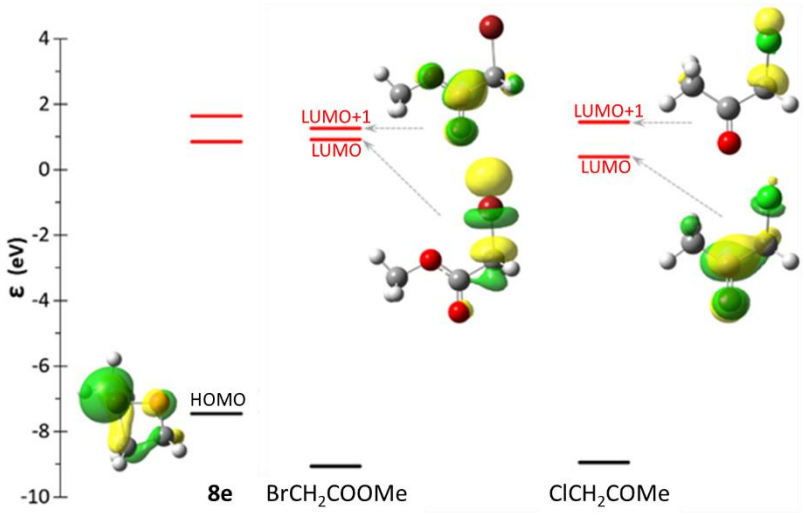

Figure 3.19: Computed (CPCMTHF/PWPB95-D3/def2-QZVPP//CPCMTHF/PBEh-3c) frontier orbitals of **8e**, methyl bromoacetate and chloroacetate, by Espinosa Ferao.[108,109]

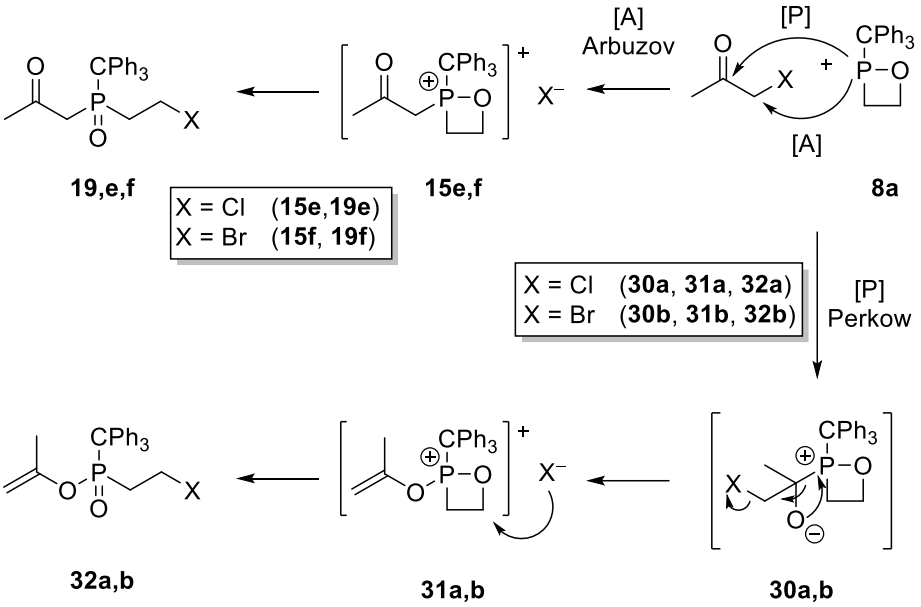

Scheme 3.13: Reaction of 1,2-oxaphosphetane **8a** with chloro-and bromoacetone, showing the two possible product classes: Arbuzov products **19e,f** and Perkow products **32a,b**.

In addition to the frontier orbital energies, the Gibbs energy profile for the reaction of **8e** with chloroacetone was computed (see Figure 3.20), showing both the Arbuzov (blue) and the Perkow (red) pathway. The calculations showed that for the model case, the Perkow product **32c** was the kinetically preferred product, as the highest transition state was by 6.68 kcal/mol lower than the highest transition state of the Arbuzov product **19g**. In contrast, the Arbuzov product **19g** was the thermodynamically preferred product, as the final product was by 1.85 kcal/mol lower in energy than the Perkow product **32c**. The calculations also showed that the first intermediate in the Perkow pathway was not generated by nucleophilic attack of phosphorus on the carbonyl-carbon, but rather by a chelotropic cycloaddition of the phosphorus lone pair to the π*(C=O) molecular orbital of the chloroacetone, affording a spiro-oxaphosphirane intermediate **33c** (see Scheme 3.14).

Experimentally, it turned out that both chloro- and bromoacetone are rather unreactive towards **8a**. The reaction with bromoacetone was complete after stirring for 7 d at ambient temperature. A product with a $^{31}P\{^{1}H\}$ NMR chemical shift of 48.5 ppm was formed selectively. As this shift was nearly identical to that of the Arbuzov product **19a** (48.4 ppm), it was assumed that ambient temperature was favouring the thermodynamic product **19f** instead of the kinetic Perkow product **32b**. This was later confirmed by single crystal X-ray diffraction (see Figure 3.21). **19f** was characterised by NMR spectroscopy and high-resolution mass spectrometry. The structural parameters as well as the chemical shifts of **19f** are similar to those of **19a-c** (discussed in Chapter 3.3.1). The $^{13}C\{^{1}H\}$-NMR chemical shifts of the α-carbonyl-CH_2 group in **19a** (37.6 ppm), **19b** (40.7 ppm) and **19f** (45.3 ppm) highlighted the influence of changing electron rich substituents for less electron rich ones, going from a highfield shift to a deshielded downfield shift.

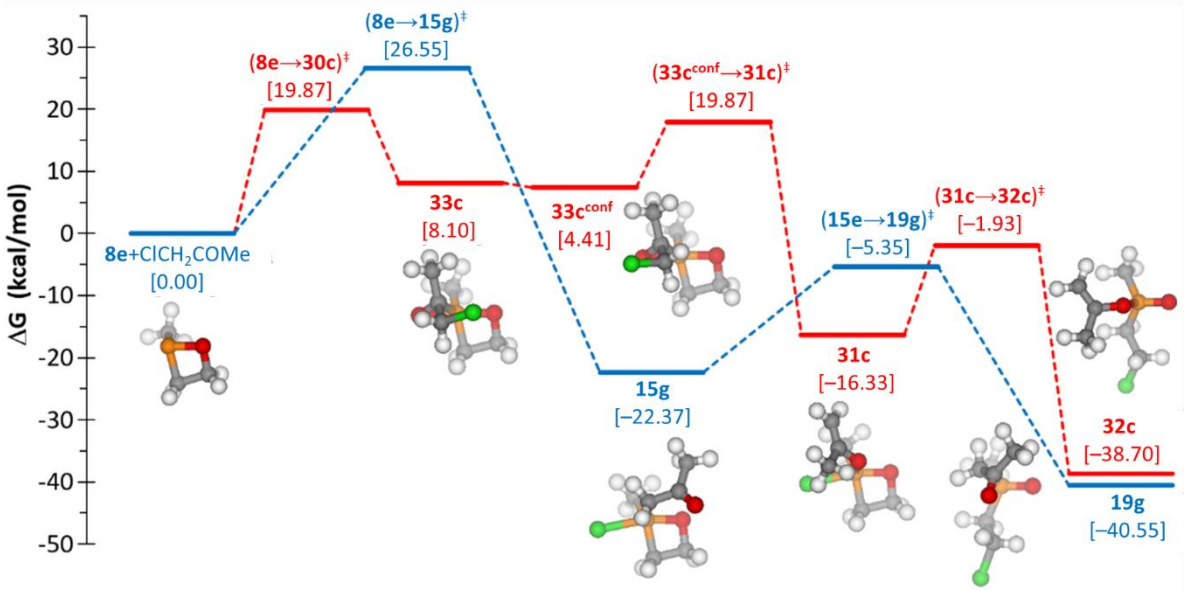

Figure 3.20: Computed ($CPCM_{THF}$/PWPB95-D3/def2-QZVPP//$CPCM_{THF}$/PBEh-3c) Gibbs energy profile for the reaction of **8e** with chloroacetone, by Espinosa Ferao.[108]

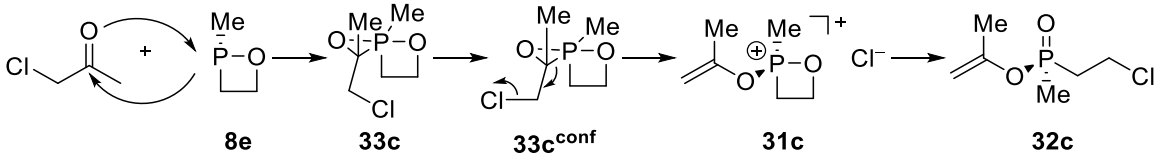

Scheme 3.14: Calculated reaction pathway of **8e** with chloroacetone, yielding Perkow product **32c**.

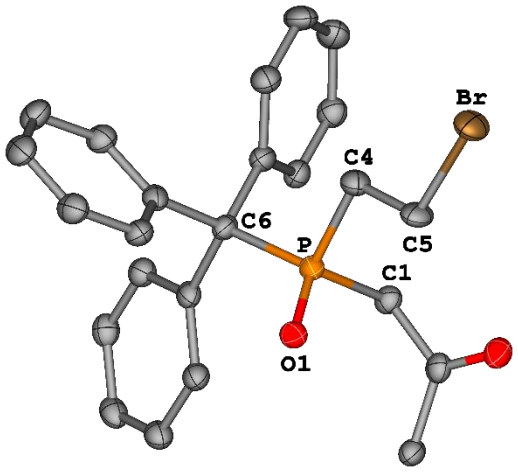

Figure 3.21: Molecular structures of **19f** in the solid state. Hydrogen atoms are omitted and the thermal ellipsoids are set at the 50% probability level. Selected bond lengths in Å and angles °: P=O1 1.488(3), P−C4 1.823(4), C4-C5 1.518(5), P−C1 1.960(3), P−C6 1.960(3), C4−P−C1 106.16(17) and O1−P−C6 116.91(15).

When chloroacetone as substrate was investigated, the situation turned out to be more complicated. When **8a** was stirred in the presence of chloroacetone for one day, the $^{31}P\{^{1}H\}$ NMR spectrum showed the formation of side products at 25.4 ppm, 42.2 ppm and 67.3 ppm, all of them only with a low signal intensity (the signal at 55.6 ppm was identified as $[Mo(CO)_4(dppe)]$). These signals vanished in the ^{31}P NMR proton-coupled spectrum, giving rise to a small signal at 150.7 ppm (see Figure 3.22).

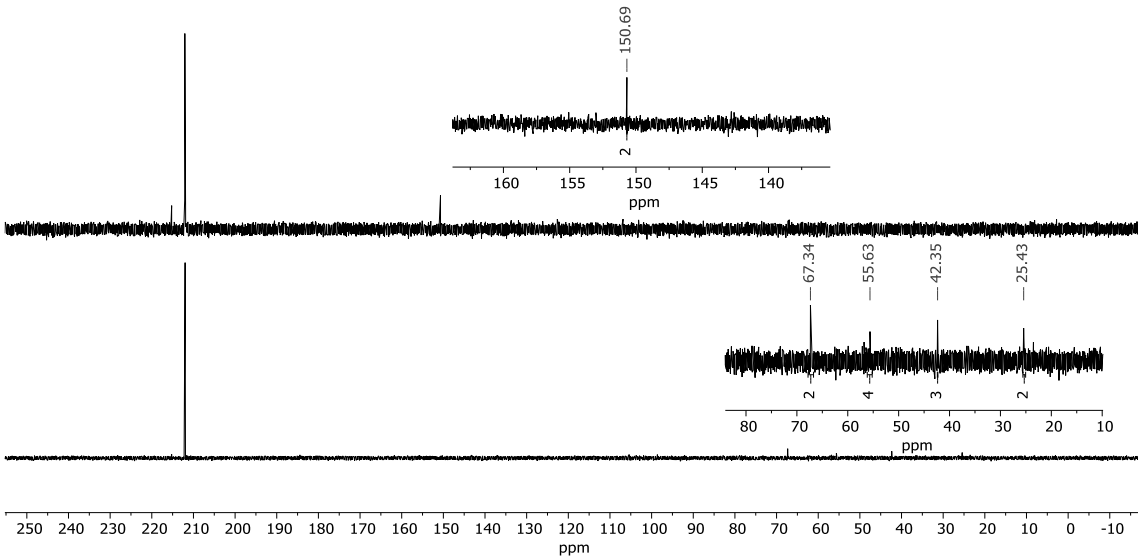

Figure 3.22: NMR spectra of the reaction of **8a** with chloroacetone at room temperature.

Bottom: $^{31}P\{^{1}H\}$ NMR spectrum, Top: ^{31}P NMR spectrum.

If the reaction was repeated for prolonged times at higher temperature, *i.e.* 50–70°C, two main signals were observed: a singlet at 46.7 ppm and a singlet at 115.1 ppm. Due to its similarity to the signals of **19a** (48.4 ppm) and **19f** (48.5 ppm), the signal at 46.7 ppm was assigned to the thermodynamic Arbuzov product **19e**. The signal at 115.1 ppm could be the desired Perkow product **32a**, but it was difficult to find suitable O-vinyl phosphinates for comparison, and compared with common *O*-alkyl phosphinates (*e.g.* ethyl di-*tert*-butylphosphinate, $\delta(^{31}P)$= 64.3 ppm)[110], the signal appeared too far downfield-shifted, making this assignment unlikely. The shift was similar to that of *P*-methyl 1,2-oxaphosphonium triflate **21** (130.4 ppm), but it was highly unlikely that this corresponded to the intermediate 1,2-oxaphosphetanium chloride **15e**, as the triflate compound **21** could only be observed at low temperatures, while bearing the less nucleophilic anion. Further heating led to vanishing of the signal at 115.1 ppm, and gave raise to various minor signals (*i.e.* 37.1 ppm, 41.1 ppm, 45.2 ppm, 49.2 ppm, 51.7 ppm). This shows that the product at 115.2 ppm either decomposed at higher temperature, or is in equilibrium with **19a** (or the unidentified side products). No further products could be identified.

The different behaviour of chloro- and bromoacetone towards **8a** was rationalised as follows: The Arbuzov reaction occurred *via* an S_N2 mechanism, with the nucleophilic attack of phosphorus at the α-carbon. Since bromide was a better leaving group than chloride, the reaction with bromoacetone occurred at lower temperature, *i.e.* ambient temperature. In contrast, the Perkow reaction started either with the nucleophilic attack of phosphorus at the carbonyl-carbon or the cheletropic addition to the carbonyl-double bond. In both cases the leaving group ability of the halogen had no immediate influence, but rather the higher −I-effect and lesser steric bulk of chlorine.[111] Thus, the Perkow reaction was more likely to occur for chloroacetone than bromoacetone, while the Arbuzov reaction is hindered.

3.4 Arbuzov-like reactions with halogens and related compounds

3.4.1 Reactions with halogens

To further test the scope of the reactivity of 1,2-oxaphosphetanes their ability to act as precursors for functionalized phosphane oxides was probed. Therefore, 1,2-oxaphosphetane **8a** was treated with various halogens, *i.e.* Cl_2, Br_2, I_2, as one would expect first the formation of a halophosphonium halide, but cyclic halophosphoranes are expected to be less stable[112], followed by attack of the halide at the C^4-carbon (due to the direct P-O bond) to form halo(2-haloethyl)phosphane oxides **34a-c** (see Scheme 3.15).

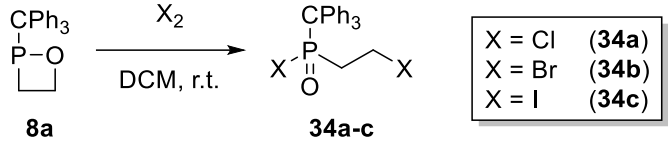

Scheme 3.15: Synthesis of halo(2-haloethyl)phosphane oxides **34a-c**.

The reactions with elemental bromine and chlorine yielded selectively **34b** and **34c** in an Arbuzov-like manner (*vide infra*). Despite this, the synthesis of the P-chloro derivative **34a** was problematic, somehow, and will be discussed later in this chapter. The molecular composition of **34b** was proven by detection of quasi-molecular ion peaks by high resolution mass spectrometry (m/z theor./exp. 4495.9859/495.9856 $[M+NH_4]^+$, 500.9413/ 500.9410 $[M+Na]^+$). The $^{31}P\{^1H\}$ NMR chemical shifts of **34b** and **34c** appeared at 71.1 ppm and 62.1 ppm, respectively, with **34c** being slightly downfield-shifted. This was expected due to the higher electron density and polarizability of iodine (*cf.*: $Ph_2P(O)Br$: $\delta(^{31}P)$ = 38.7 ppm, $Ph_2P(O)I$: $\delta(^{31}P)$ = 27.1 ppm)[113]. Comparison of the $^{13}C\{^1H\}$ NMR data of **34b,c** (see Table 3.8) with those of the β-bromine substituted phosphane oxides **19a,b** and the β-iodine substituted phosphane oxide **19c** (see Table 3.6) showed that the X*C*H_2-carbon chemical shift remained very similar, while replacement of the alkyl substituent at phosphorus through a halide led to a downfield shift of the P-CH_2 carbon. This effect was more prominent for **34c** than **34b**, and could again be explained by the higher electron density and polarizability of iodine.

Table 3.8: Selected NMR chemical shifts in ppm of **34b,c**.

	δ(*P*)	δ(P-*C*H$_2$)	δ(X*C*H$_2$)	δ(P-C*H*$_2$)	δ(XC*H*$_2$)
34b	71.1	40.9	24.1	2.61 / 2.86	3.59 / 3.68
34c	62.1	44.4	−5.8	2.70 / 2.89	3.41 / 3.41

Through slow evaporation of the solvent, suitable single crystals for X-ray diffraction studies could be obtained for **34b,c** (see Figure 3.23). The structural parameters all were within the expected ranges (see Table 3.9, *c.f.*: *n*-Bu$_3$PO: P=O 1.494 Å, P-C 1.804 Å, C-C 1.526 Å.[104] EtBr: C-C 1.485 Å, C-Br 1.955 Å.[105] EtI: C-C 1.496 Å, C-I 2.157 Å.[105] *t*-Bu$_2$P(O)Br: P-Br 2.24 Å.[114] *t*-Bu$_2$P(Se)I: P-I 2.45 Å.[115]).

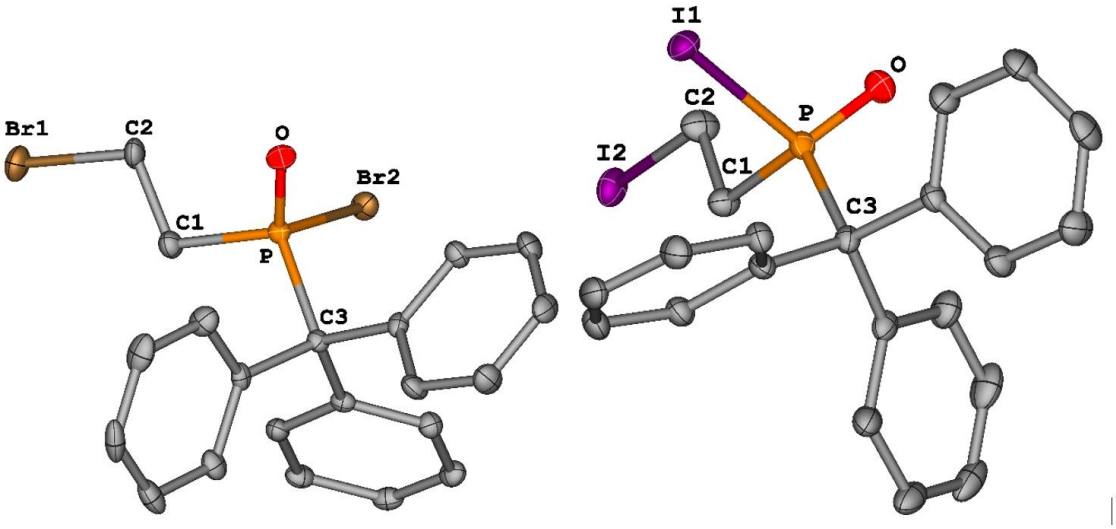

Figure 3.23: Molecular structures of **34b** (left) and **34c** (right) in the solid state. Hydrogen atoms are omitted and the thermal ellipsoids are set at the 50% probability level.

Table 3.9: Selected bond lengths and angles of **34b,c**. Bond lengths in Å, angles in °.

	P=O	P-CH$_2$	CH$_2$-CH$_2$	CH$_2$-X	P-X	P-CPh$_3$	X-P-CH$_2$	O=P-CPh$_3$
34b	1.4761(15)	1.824(2)	1.515(3)	1.962(2)	2.2191(6)	1.890(2)	101.65(7)	114.19(9)
34c	1.480(2)	1.840(2)	1.516(4)	2.157(3)	2.4565(6)	1.898(2)	100.92(8)	114.04(11)

The reaction with iodine was also investigated by quantum chemical calculations by Espinosa Ferao for the model 1,2-oxaphosphetane **8e**. The Gibbs energy profile of the reaction (see Figure 3.24) showed that after polarization of iodine the reaction occurred *via* two 1,2-oxaphosphetanium species **35e** and **35e'** (see Scheme 3.16), the latter possessing a pnictogen bond ($d_{P\cdots I}$ = 3.040 Å; compare to $d_{P\text{-}I}$ =

2.404 Å in the same molecule). Overall, the reaction proceeded very similar to the calculated reaction of **8e** with chloroacetone, yielding **19g** (see Chapter 3.3.3, Figure 3.20). **19g** and **34e** also have very similar ΔG values, −40.55 kcal/mol and −39.93 kcal/mol, respectively.

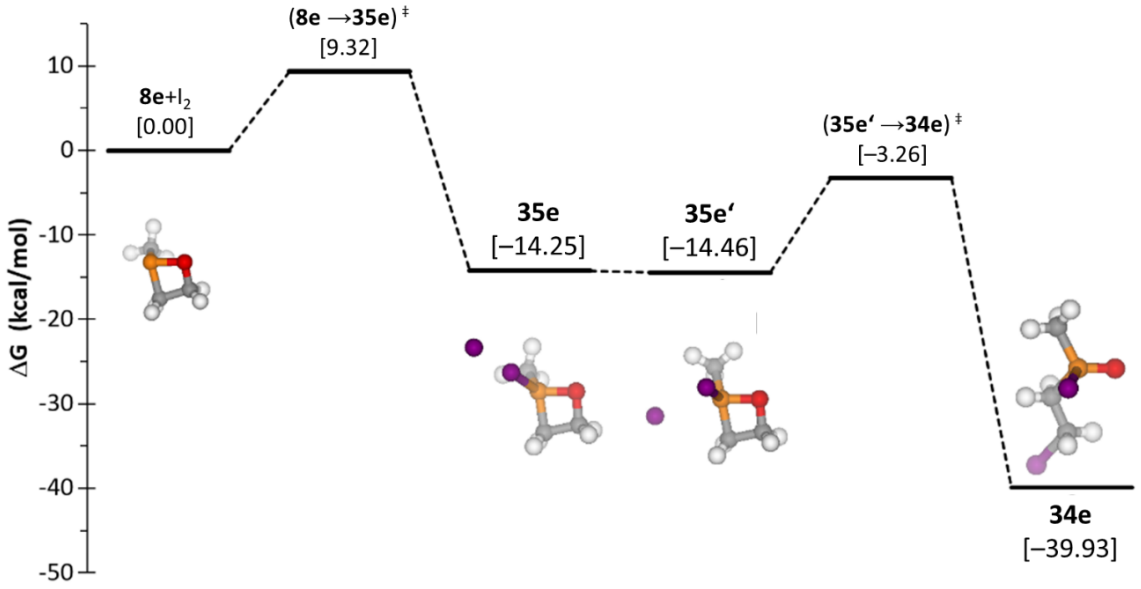

Figure 3.24: Computed (CPCMTHF/PWPB95-D3/def2-QZVPP//CPCMTHF/PBEh-3c) Gibbs energy profile for the reaction of **8e** with iodine by Espinosa Ferao.[108]

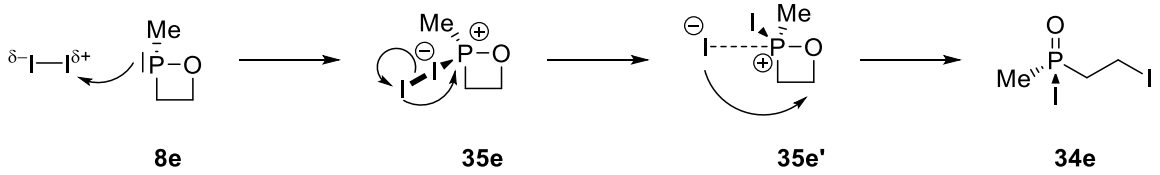

Scheme 3.16: Reaction scheme of model 1,2-oxaphosphetane **8e** with iodine.

Additionally, the isosurfaces of the electrostatic potential of some structures were calculated by Brehm (see Figure 3.25). The isosurface of **8a** displayed a raised electron density at phosphorus due to the lone pair and the surface of dibromine showcases the σ-hole, *i.e.* a partial positive charge, along the bond axis. The following depiction shows the transition state [**8a**→**35b**]‡ as an interaction of the lone pair and the σ-hole. The last depiction shows the 1,2-oxaphosphetanium cation of **35b**, displaying greater differences in electrostatic potential, likely due to the positive charge at phosphorus.

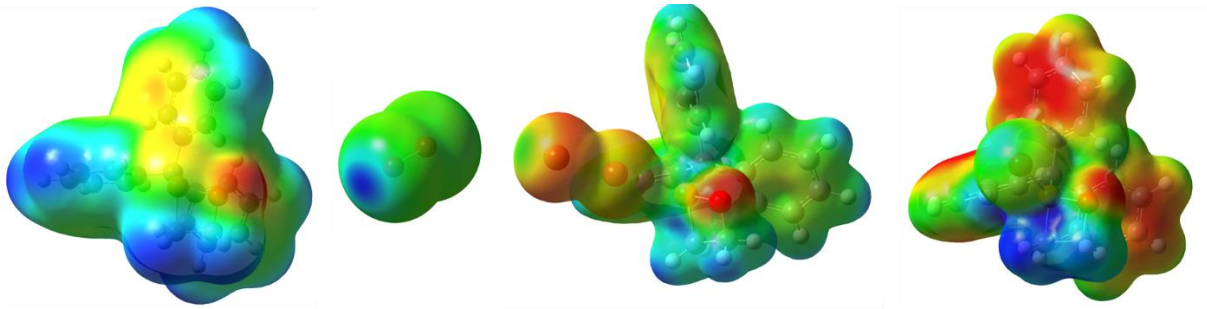

Figure 3.25: Isosurfaces of the electrostatic potential of, from left to right: 1,2.-oxaphosphetane **8a**, dibromine, the transition state [**8a**→**35b**]‡, intermediate **35b**; calculated at the PW6B95-D3BJ/def2-QZVP(CPCM(DCM))//TPSS-D3BJ/def2-TZVP(CPCM(DCM)) level of theory by Brehm.[116]

In contrast to the synthesis of **34b,c**, the reaction of **8a** with chlorine gas did not lead to an isolable product. As it was a possible source of error, it should be mentioned that the chlorine gas was freshly prepared by dropping concentrated hydrochloric acid on solid potassium permanganate. The generated chlorine gas was first led through demineralised water and over phosphorus pentoxide, to remove traces of hydrogen chloride and water. The chlorine was then bubbled through a solution of **8a**. The reaction seemed promising at first, with the selective generation of one main signal at 70.4 ppm in the $^{31}P\{^{1}H\}$ NMR spectrum, which was very similar to the chemical shift of **35b**, leading to the assignment of this shift to the desired product **34a**. It showed that either after stirring for extended periods or after removing of solvent, partial decomposition occurred, leading to signals in the $^{31}P\{^{1}H\}$ NMR spectrum at 150.4 ppm, 41.2 ppm, 40.3 ppm, 38.0 ppm and 37.0 ppm (see Figure 3.26). The shift of the latter four signals might suggest a phosphane oxide like structure. The hydrolysis of **8a** as a side product could be excluded, as none of the signals displayed a $^{1}J_{P\text{-}H}$ coupling and the hydrolysis product of **8a** had a chemical shift of 46.7 ppm (see Chapter 3.5.3). The hydrolysis of **34a** was also unlikely, as no similar side products could be observed for **34b,c** even after handling under atmospheric conditions. Probably, either the excess of chlorine gas or traces of hydrogen chloride led to the formation of these side products, and the nature of which could not be further clarified.

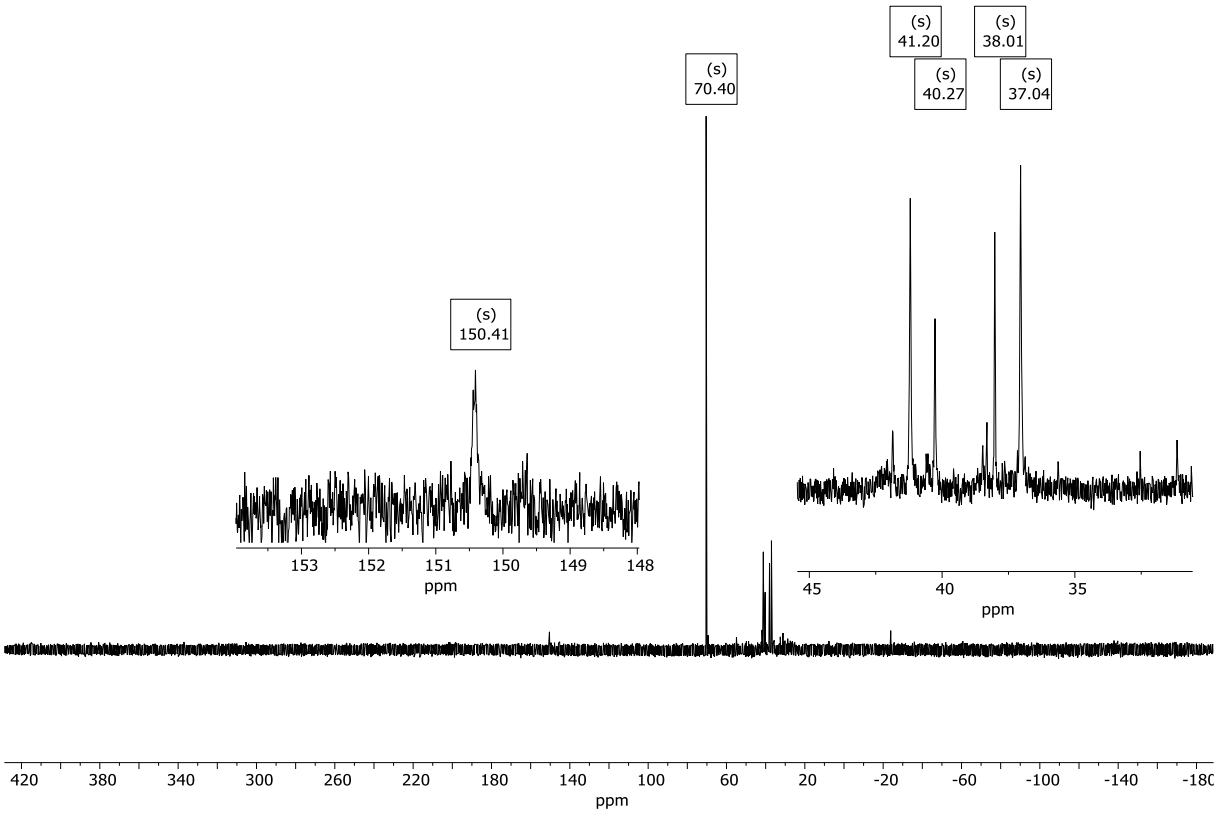

Figure 3.26: $^{31}P\{^{1}H\}$ NMR spectrum of reaction of **8a** with chlorine gas, in $CDCl_3$.

3.4.2 Reaction with inter- and pseudo-halogens

As the former chapter showed, the 1,2-oxaphosphetane **8a** readily reacted with halogens leading to halo(haloethyl)phosphane oxides **34a-c**. To further explore this reactivity and to see how it is influenced by polar bonds, **8a** was also reacted with an interhalogen such as iodine monochloride and a pseudo-halogen, *i.e.*, cyanogen bromide.

For the reaction of **8a** with iodine monochloride, two possible isomers could be formed: **36a**, bearing iodine at phosphorus and chlorine at the former C^4-carbon, or **36b**, with chlorine at phosphorus and iodine at carbon (see Scheme 3.17).

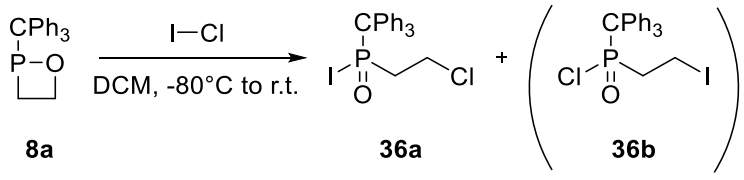

Scheme 3.17: Reaction of **8a** with iodine monochloride.

As the calculations for the reaction with iodine showed, the first step was the nucleophilic attack of phosphorus. As iodine monochloride was polarized due to different electronegativities the nucleophilic attack at the partially positively charged iodine was preferred, which should selectively lead to formation of product **36a**. In the $^{31}P\{^{1}H\}$ NMR spectrum, at first only one signal at 62.2 ppm was observed. This shift was nearly identical to that of *P*-iodide compound **34c**, whereas the signal of *P*-chloride derivative **34a** was around 10 ppm downfield-shifted. This strongly hinted to the selective formation of **36a**. Unfortunately, **36a** appeared to decompose after evaporation of solvent, leaving a nearly empty $^{31}P\{^{1}H\}$ NMR spectrum in the measuring area of −190 ppm to 430 ppm. The solid residue was investigated with mass spectrometry, but no molecular or oligomeric compound could be identified.

The reaction of **8a** with cyanogen bromide should behave similar. As bromine is more electronegative than carbon, the nucleophilic attack of phosphorus should happen at carbon, yielding **37a** as main product, with the *P*-Br species **37b** as possible side product (see Scheme 3.18).

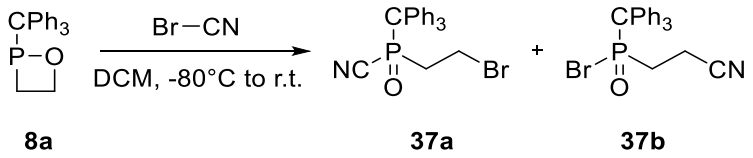

Scheme 3.18: Reaction of **8a** with cyanogen bromide.

Interestingly, two main signals were observed in the $^{31}P\{^{1}H\}$ NMR spectrum of the reaction at 34.2 ppm and 71.3 ppm in a ratio of 25:75 (see Figure 3.27). As the *P*-Br derivative **34b** has a near identical shift (71.1 ppm), the signal at 71.3 ppm was assigned to **37b**. The signal at 34.2 ppm was assigned to the *P*-CN product **37a**; as reference, a shift of 40.5 ppm was reported for methyl(phenyl)phosphinic cyanide.[117] While neither **37a** or **37b** could be isolated, it showed an interesting contrast compared to the reaction with iodine monochloride, where only one product, **36a**, is observed. For **36a**, the explanation is straight forward, the difference of electronegativities could be calculated as $\Delta\chi_{ClI} = \chi_{Cl} - \chi_{I} = 0.50$ (with $\chi_{Cl} = 3.16$ and $\chi_{I} = 2.66$)[118], showing a weak polarization towards chlorine and thus a positive partial charge of iodine, making it the electrophile. For **37a,b**, the case was more complicated. If the generic value for the electronegativity was used, a value of $\Delta\chi_{BrC} = \chi_{Br} - \chi_{C} = 0.41$ (with $\chi_{Br} = 2.96$ and $\chi_{C} = 2.55$)[118] was obtained. Although the $\Delta\chi$ value was lower than for ICl, it still indicated a positive partial charge at carbon, somehow contradicting the outcome of the experiment. As the electronegativity is dependent on the hybridisation of an atom, and the carbon in cyanogen bromide is sp hybridised, the use of the proper sp-electronegativity gave the following:

$\Delta\chi_{BrC(sp)} = \chi_{Br} - \chi_{C(sp)} = -0.14$ (with $\chi_{C(sp)} = 3.1$)[119]. This now indicated a weak polarisation towards carbon, making bromine the electrophile, which is in accordance with the experimental results. These calculations should be treated with care, as the influence of the triple bonded nitrogen was not considered, as no $\chi_{N(sp)}$ value could be found. Another aspect that should be considered was the hard and soft acids and bases theory (HSAB).[120] Phosphorus as a third period element was a rather soft base and would react preferably with a soft base. Bromine as a fourth period element was soft, whereas carbon was hard, especially in a nitrile where the electron density is polarized away from carbon. These two approaches explain why **37b** was the preferred product.

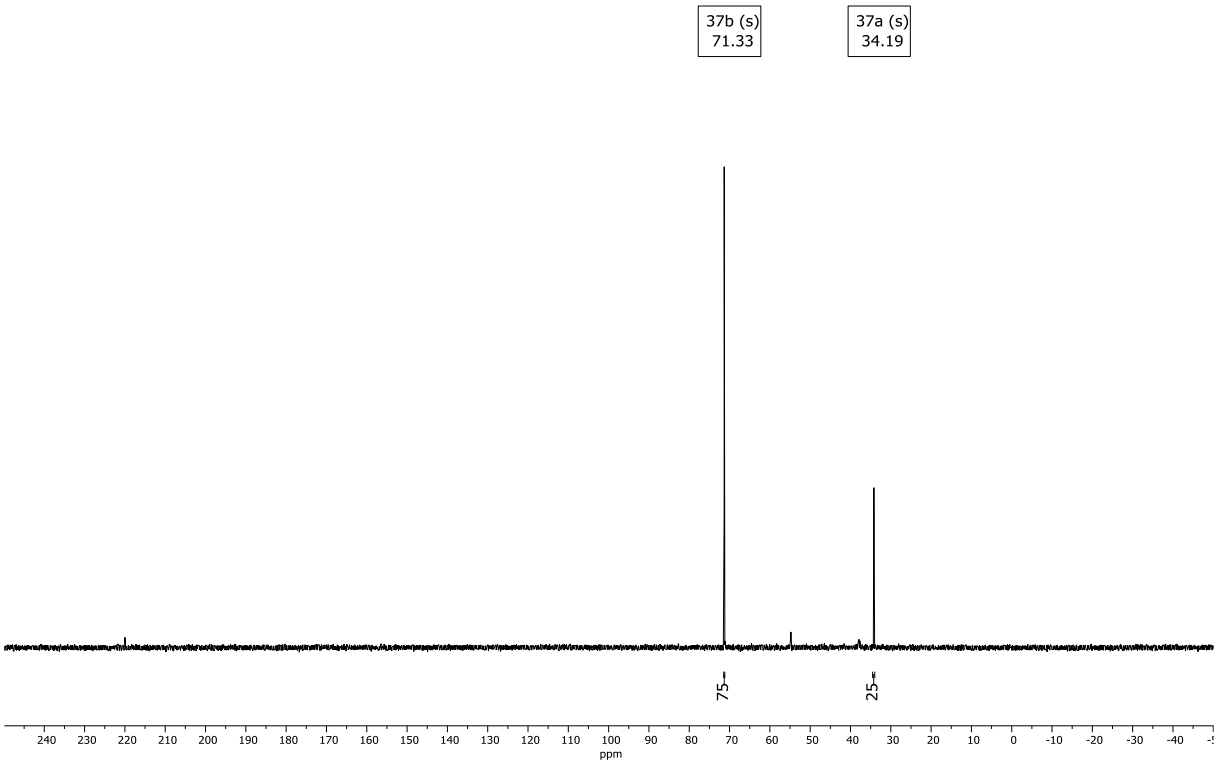

Figure 3.27: $^{31}P\{^{1}H\}$ NMR spectrum of the reaction of **8a** with cyanogen bromide.

3.5 Ring opening reactions with Brønsted acids

3.5.1 Acidolysis with acetic acid and hydrochloric acid

As shown in chapter 3.3, the 1,2-oxaphosphetane **8a** reacted with carbon electrophiles at the phosphorus centre. But in theory, **8a** possesses a second nucleophilic centre, namely the ring oxygen atom. To further investigate on the selectivity of these two nucleophilic sites, **8a** was reacted with common Brønsted acids, *i.e.,* acetic acid and hydrochloric acid. While one might have assumed a selective reaction, up to four main products (**39a**-**41a** for the reaction with HOAc, **39b**-**41b** for HCl) were observed in both cases (see Scheme 3.19). As it was not possible to separate these, the identification of the products proved to be very difficult.

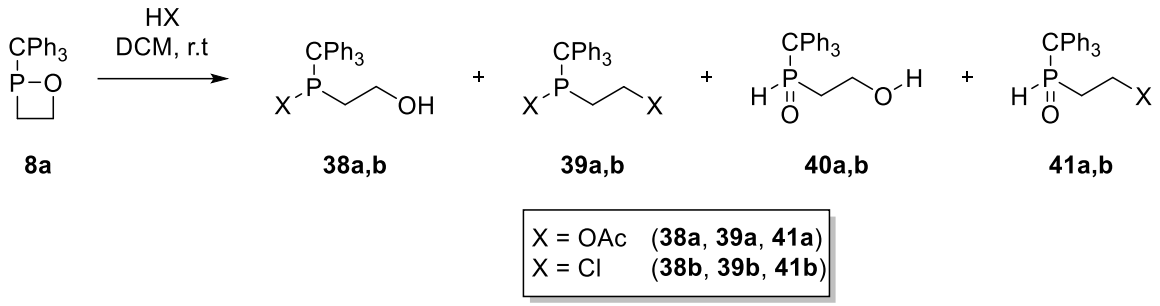

Scheme 3.19: Reaction of **8a** with acetic acid or hydrochloric acid.

The ^{31}P NMR spectra gave some first insights. For the reaction with acetic acid (see Figure 3.28), the spectrum showed two downfield-shifted signals at 127.2 ppm (**38a**) and 123.0 ppm (**39a**), as well as two more highfield-shifted signals at 45.8 ppm (**40a**) and 41.9 ppm (**41a**). The latter both showed a large $^{1}J_{P\text{-}H}$ coupling of 485.4 Hz and 483.0 Hz, respectively. Likely, two different classes of compounds were observed. Due to the close similarity in shift with the Arbuzov products **19a-f**, it is very likely that the highfield products **40a** and **41a** were also phosphane oxides (bearing one hydrogen directly at phosphorus).

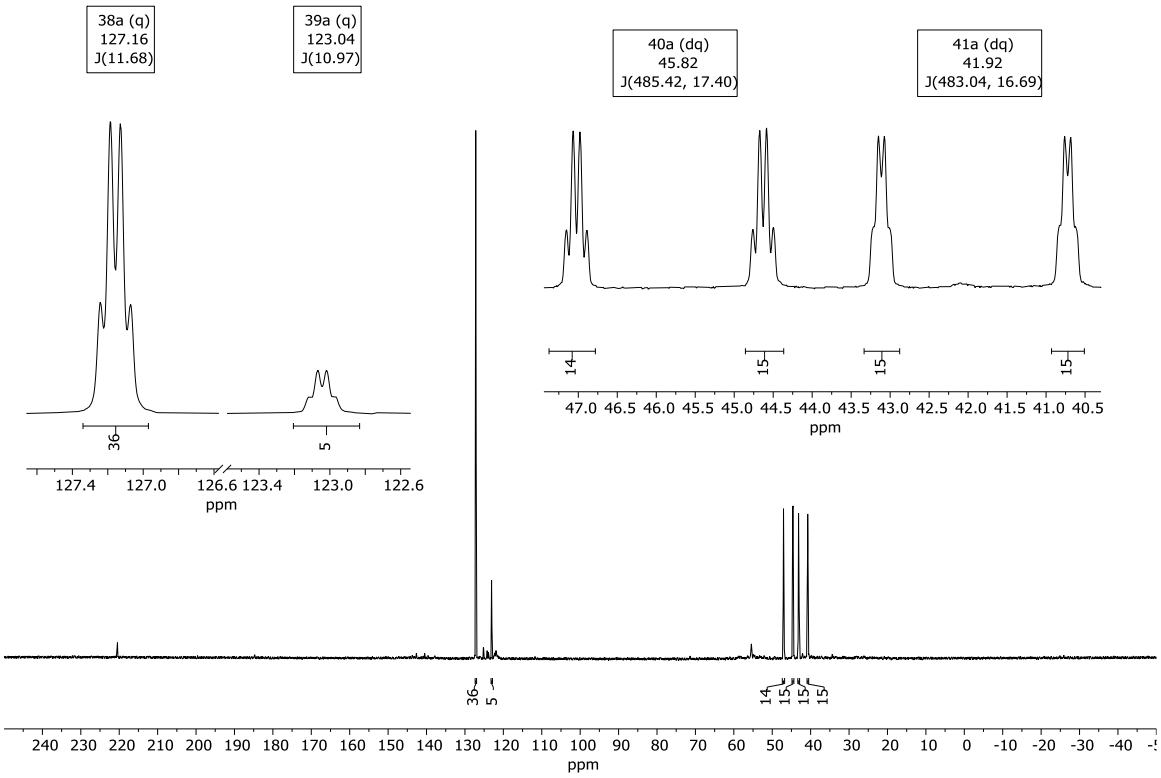

Figure 3.28: ^{31}P NMR spectrum of the reaction of **8a** with acetic acid.

The $^{31}P\{^{1}H\}$ and ^{31}P NMR spectra of the reaction with hydrochloric acid gave further insights (see Figure 3.1). The two highfield products were very similar to the reaction with acetic acids, with shifts of 46.8 ppm for **40b** and 40.7 ppm for **41b**, and $^{1}J_{P\text{-}H}$ coupling constants of 481.6 Hz and 479.7 Hz respectively. The downfield products **38b** and **39b** appeared slightly highfield-shifted, appearing at 112.0 ppm and 109.4 ppm, respectively. More importantly, the signals of both **38b** and **39b** showed a shoulder in roughly a 3:1 ration, that was minimally highfield-shifted by 0.03 ppm (**38b**) or 0.04 ppm (**39b**). This strongly hinted to a secondary isotropic effect due to a direct bond of phosphorus to the different chlorine isotopes ^{35}Cl and ^{37}Cl.[121]

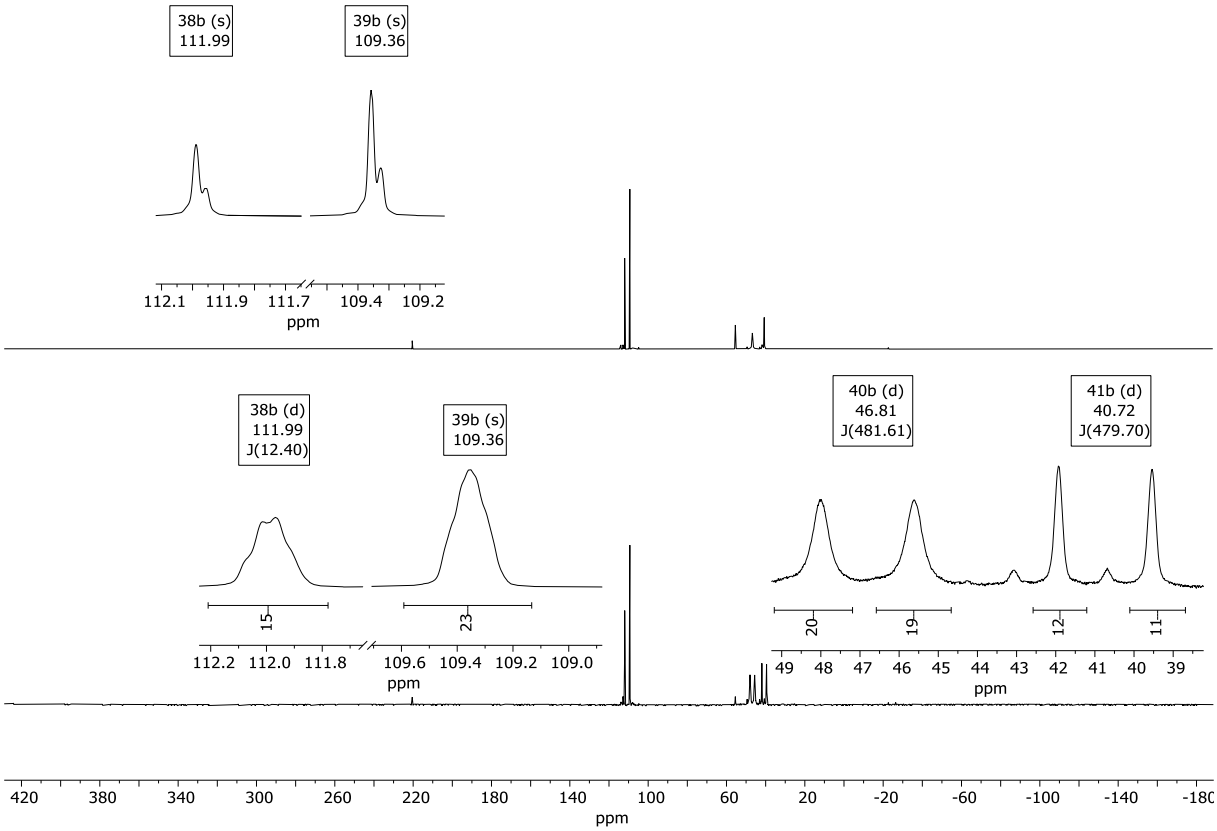

Figure 3.29: NMR spectra of the reaction of **8a** with HCl, top: $^{31}P\{^{1}H\}$ NMR, bottom: ^{31}P NMR.

The signals having the "chlorine-37 shoulder" therefore were identified clearly as **38b** and **39b**, as P-Cl compounds. Assuming similar reaction pathways, it was concluded that **38a** and **39a** have a P-OAc moiety. Comparison with literature known compounds showed that the chemical shift of **38a,b** and **39a,b** are within a reasonable shift range of related compounds (see Figure 3.30).

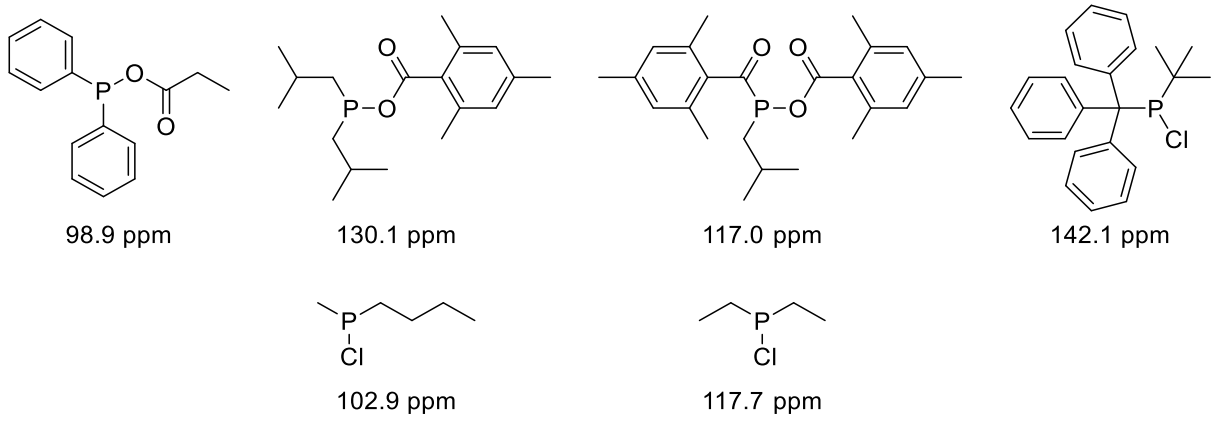

Figure 3.30: Literature known *P*-carboxyl[122][123] and *P*-chloro[124][125] compounds and their $^{31}P\{^{1}H\}$ NMR chemical shifts.

As two sets of rather similar signals were observed, the corresponding compounds should be similar. The most simple modification of **38a,b** would be a substitution of the OH-group with the corresponding acid anion. Combined with the information that **40a,b** and **41a,b** most likely bore a PH(O) motif, the following proposition for the products were made (see Figure 3.31):

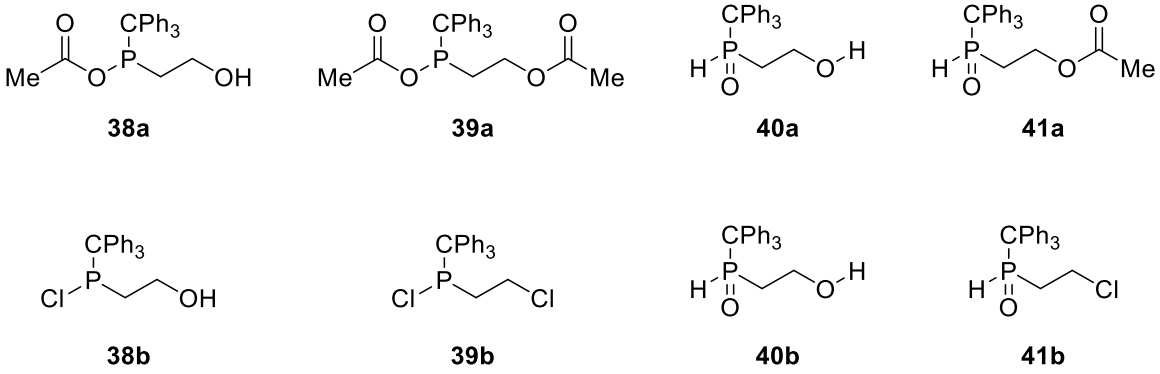

Figure 3.31: Proposed structures of compound **38a,b**-**41a,b**.

To obtain further insight into the identity of these products and the related mechanisms, the possible reactivities of model 1,2-oxaphosphetane **8e** towards acetic acid and hydrochloric acid were explored with quantum chemical calculations by Brehm using a *P*-Me model system instead of the *P*-CPh_3 substituent.[116] In the following it was assumed that protonation of phosphorus or oxygen occurs without a transition state, as the proton has very low steric demand and requires nearly no change of geometry.

At first, the relative energies of the phosphorus- or oxygen-protonated 1,2oxaphosphetane **8e** were calculated for the reaction with acetic acid (see Scheme 3.20). It showed that the O-protonated intermediate **42c** was very high in energy, 44.8 kcal/mol, so that its formation is unlikely. The P-protonated intermediate **43c** was 24.8 kcal/mol up in energy and might have been formed, but it couldn't form the observed downfield products. So, further investigations were performed.

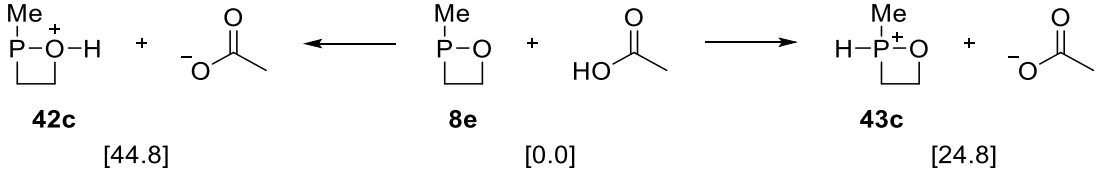

Scheme 3.20: Calculated protonation of **8e** with acetic acid, ΔG values in kcal/mol, calculated at the PW6B95-D3BJ/def2-QZVP(CPCM(DCM))//TPSS-D3BJ/def2-TZVP(CPCM(DCM)) level of theory by Brehm.[116]

Then, the assumption of a “naked” proton attacking either phosphorus or oxygen was abandoned, and a 1:1 adduct of a molecule of acetic acid coordinated to phosphorus or oxygen was assumed, forming complexes **44c** and **45c**, followed by the nucleophilic attack of an acetate ion either at the C^4-carbon or at phosphorus was taken into account (see Scheme 3.21). The acetic acid complexes were low in energy, with ΔG values of only 6.1 kcal/mol for the κ-oxygen complex **44c** and 7.7 kcal/mol for the κ-phosphorus complex **45c**. While this seemed promising, the Arbuzov-like ring opening *via* nucleophilic attack at the C^4-carbon was still significantly hindered with high energy transition states of 34.8 kcal/mol (**46c**, κ-O) or 38.8 kcal/mol (**47c**, κ-P). In contrast, the attack of the acetate at phosphorus occurred barrierless, leading slightly endergonically to *P*-acetate compound **38c**.

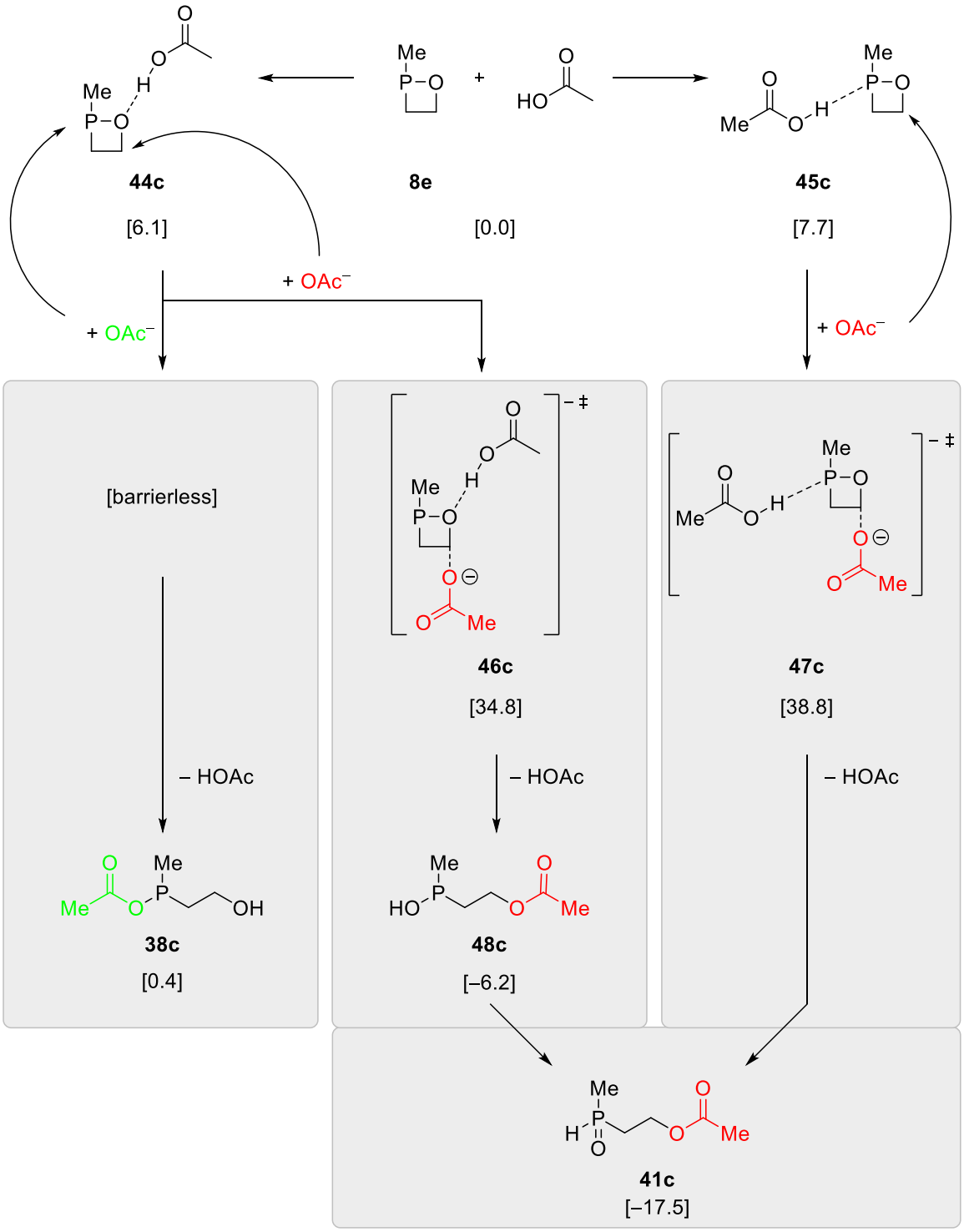

Scheme 3.21: Formation of acetic acid complexes **44c** and **45c**, and following reactions, ΔG values in kcal/mol, calculated at the PW6B95-D3BJ/def2-QZVP(CPCM(DCM))//TPSS-D3BJ/def2-TZVP(CPCM(DCM)) level of theory by Brehm.[116]

Now, as a plausible route for the generation of one of the four observed products was derived (excluding the attack on the C^4-carbon as the transition states are too high in energy), the question arose if **38c** was able to react with itself, transferring one acetate unit from *P*-OAc to *C*-OH, forming the diacetyl product **39c** and the formal hydrolysis product **40c** (see Scheme 3.22). As the reaction was

strongly exergonic by −18.4 kcal/mol and the tetrahedron-intermediate **49c** only 6.0 kcal/mol up in energy, this appeared to be a viable route for the generation of **39c** and **40c**.

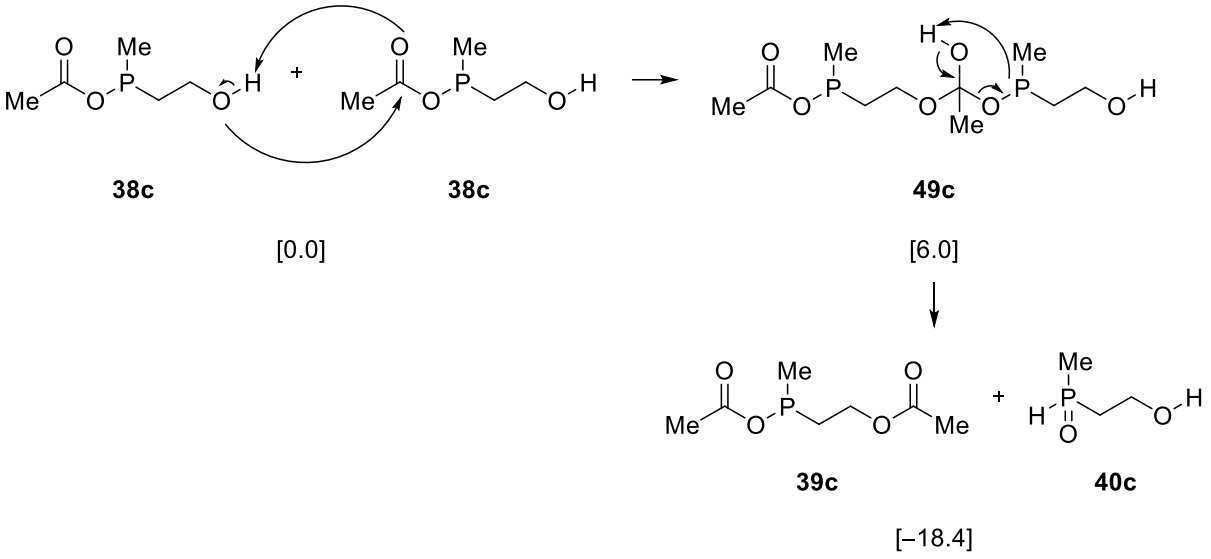

Scheme 3.22: Formation of **39c** and **40c**, ΔG values in kcal/mol, calculated at the PW6B95-D3BJ/def2-QZVP(CPCM(DCM))//TPSS-D3BJ/def2-TZVP(CPCM(DCM)) level of theory by Brehm.[116]

What was still missing was the generation of the *C*-OAc phosphane oxide **41c**, which should be accessible by the reaction of **38c** with **39c**, transferring the *P*-OAc acetate unit of **39c** to the *C*-OH unit of **38c**, transforming **38c** into **39c** and **39c** into **41c** (see Scheme 3.23).

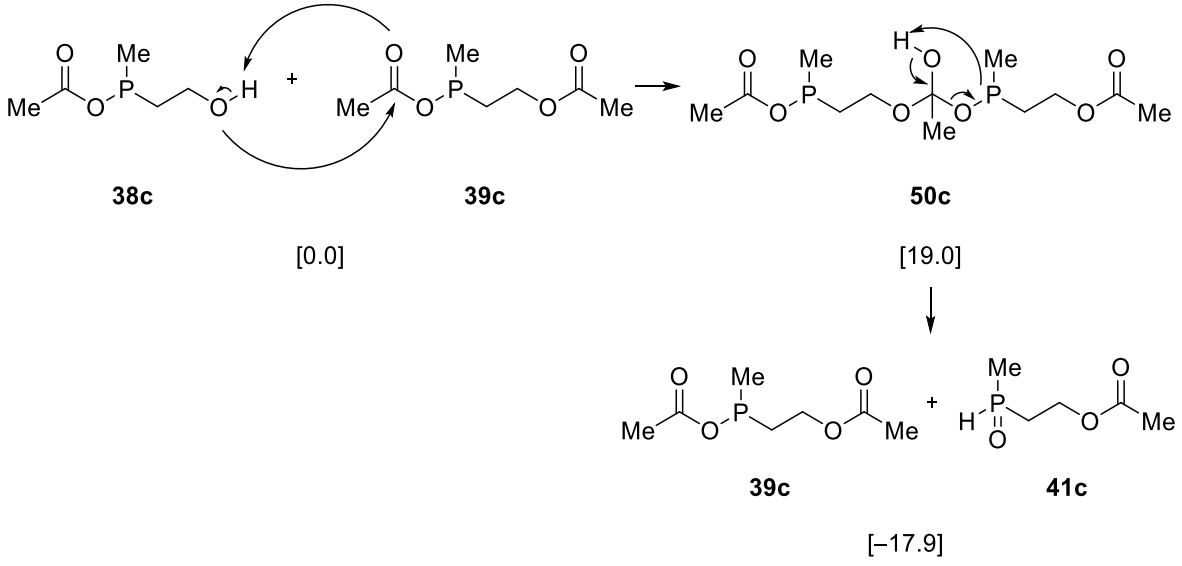

Scheme 3.23: Formation of **39c** and **41c**, ΔG values in kcal/mol, calculated at the PW6B95-D3BJ/def2-QZVP(CPCM(DCM))//TPSS-D3BJ/def2-TZVP(CPCM(DCM)) level of theory by Brehm.[116]

Although the intermediate **50c** was significantly higher in energy with 19.0 kcal/mol, the overall reaction was still strongly exergonic with −17.9 kcal/mol, and thus shows a plausible way to generate **41c**. To find an explanation for the significant energy difference between the intermediates **49c** and **50c**, their Laplacians of the electron density were calculated (see Figure 3.32). Both Laplacians show a P···H-O bond path with a bond critical point, hinting to the presence hydrogen bridge stabilizing the intermediate. As a bond path could be found for both **49c** and **50c**, no reason for the difference could be identified.

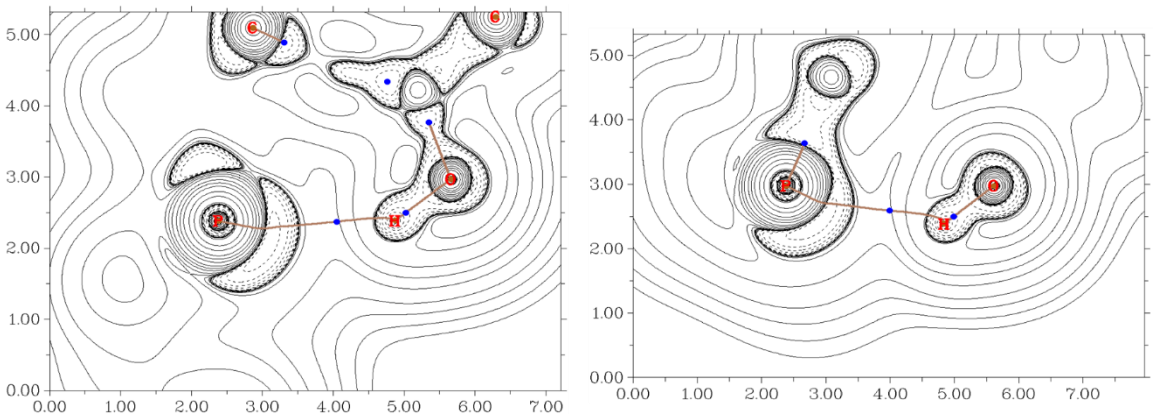

Figure 3.32: Laplacian of the electron density of **49c** (left) and **50c** (right), calculated at PW6B95-D3BJ/def2-QZVP(CPCM(DCM))//TPSS-D3BJ/def2-TZVP(CPCM(DCM)) level of theory by Brehm.[116]

While the structure of the products of the reaction of **8a** with acetic acid could not be determined with certainty, the comparison of their ^{31}P NMR chemical shifts with literature and the performed calculations strongly suggested the proposed structures for **38a-41a**. Furthermore, mass spectrometry experiments were performed on the product mixtures, showing peaks at m/z 379.145 (isomers [**38a**+H]$^+$ or [**41a**+H]$^+$) and m/z 337.135 ([**40a**+H]$^+$); high resolution mass spectrometry experiments showing the quasi-molecular peak of **38a**/**41a**(m/z theor./exp. 379.1458/379.1450 [M+H]$^+$).

Now when going (theoretically) from the acetic acid case to hydrochloric acid while keeping the reaction conditions constant, the outcome showed that the O- and P-protonated intermediates **42d** and **43d** were by around 10 kcal/mol lower in energy compared to the analogous acetate species **42c** and **42d** (see Scheme 3.24). While **42d** was still too high in energy (35.0 kcal/mol) so that the reaction pathway seemed unlikely, **43d** was low enough in energy (15.1 kcla/mol) to further persecute this pathway. After a low energy transition state (**51d**, 11.1 kcal/mol), the *C*-chlorine phosphane oxide product **41d** was formed exergonically (−22.6 kcal/mol).

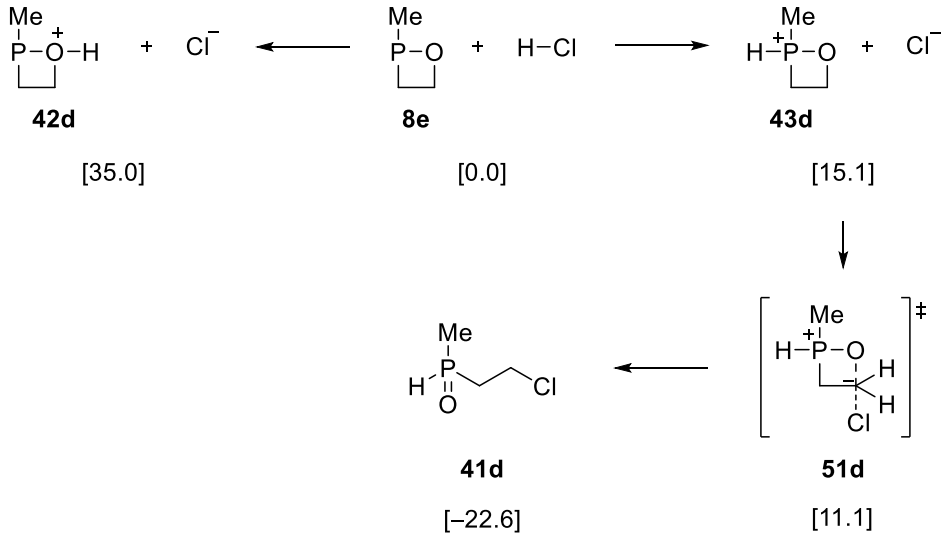

Scheme 3.24: Protonation of **8e** with hydrochloric acid and follow up reactions, ΔG values in kcal/mol, calculated at the PW6B95-D3BJ/def2-QZVP(CPCM(DCM))//TPSS-D3BJ/def2-TZVP(CPCM(DCM)) level of theory by Brehm.[116]

To further lower the barriers, the generation of κ-O and κ-P H-Cl complexes were also considered (see Scheme 3.25). The formation of the κ-O H-Cl complex **44d** occurred slightly endergonic (4.5 kcal/mol). The attack of chloride at phosphorus now was barrierless and led to the formation of **38d**, which was exergonic by −18.2 kcal/mol. Alternatively, the nucleophilic attack at the C^4-carbon led to the low energy transition state **46d** (10.4 kcal/mol), which reacted firstly to hydroxylphosphane **48d** (−12.4 kcal/mol), which then tautomerized to phosphane oxide **41d** (−22.6 kcal/mol). The attack of chloride on the slightly endergonic κ-P H-Cl complex **45d** (0.7 kcal/mol) also led to phosphane oxide **41d** over a very low energy transition state **47d** (3.3 kcal/mol).

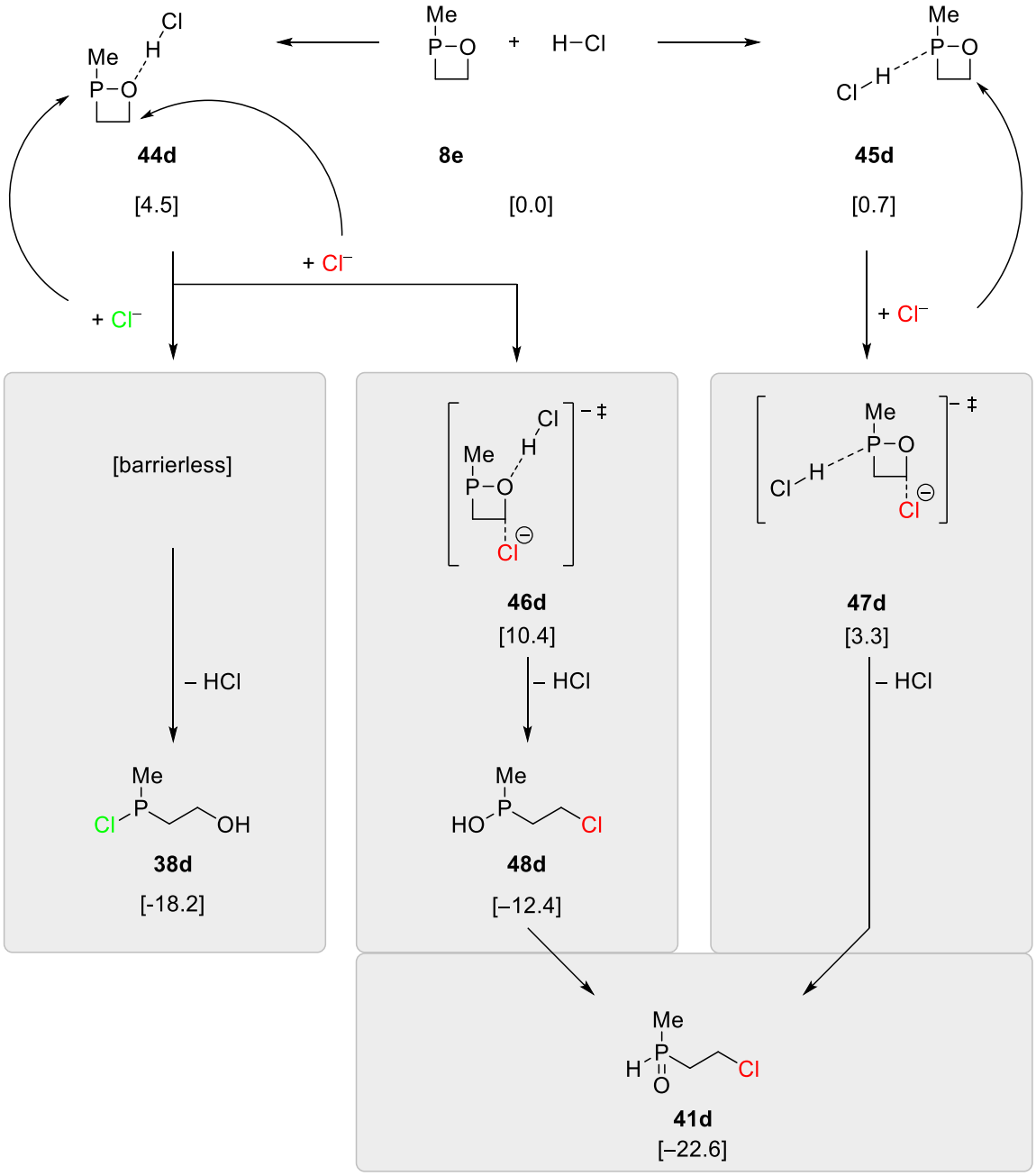

Scheme 3.25: Formation of hydrochloric acid complexes **44d** and **45d**, and following reactions, ΔG values in kcal/mol, calculated at the PW6B95-D3BJ/def2-QZVP(CPCM(DCM))//TPSS-D3BJ/def2-TZVP(CPCM(DCM)) level of theory by Brehm.[116]

In conclusion, two (**38d** and **41d**) of the four expected products were reasonably explained from the reaction of the H-Cl complexes **44d** and **45d**. The missing products **39d** and **40d** could have been formed by the reaction of two equivalents of **38d**. But this seemed to be unlikely as no fitting tetrahedral intermediate could be formed here due to the lack of a carbonyl group (*cf*. **49c**, **50c**). More likely, **39d** and **40d** were formed through reaction of **38d** with either hydrochloric acid or water (see Scheme 3.26). Both reactions showed to be weakly exergonic, thus completing the set of pathways to explain all four NMR product signals.

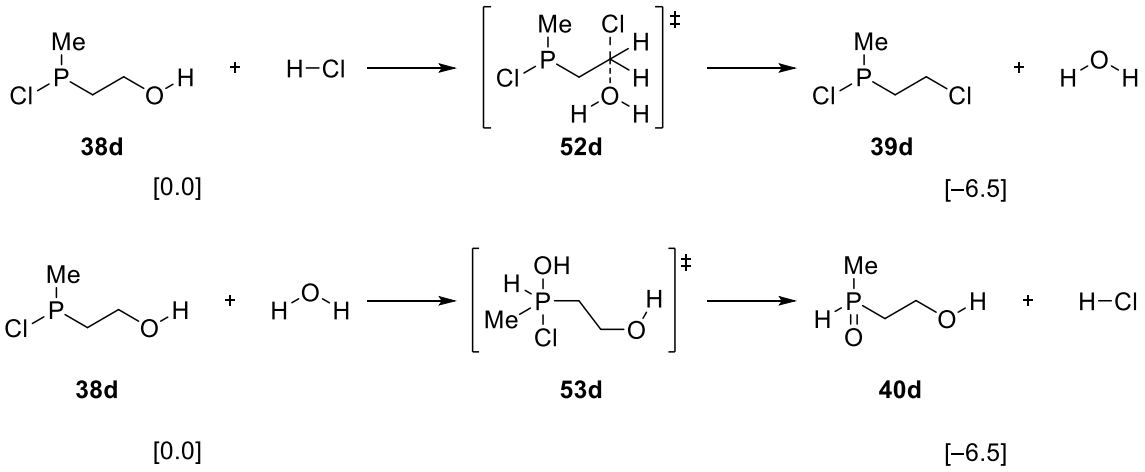

Scheme 3.26: Possible formation of **39d** and **40d**, ΔG values in kcal/mol, calculated at the PW6B95-D3BJ/def2-QZVP(CPCM(DCM))//TPSS-D3BJ/def2-TZVP(CPCM(DCM)) level of theory by Brehm.[116]

3.5.2 Complexation of Acidolysis products

As the chemical composition of **38ab**-**41a,b** wasn't clear in the beginning, it was attempted to trap the primary reaction products by coordinating the lone pair of phosphorus to a metal centre, thus preventing the formation of further products. A precursor for the pentacarbonyltungsten(0) fragment was chosen, as the expected tungsten-phosphorus bond would offer further NMR information (see Scheme 3.27).

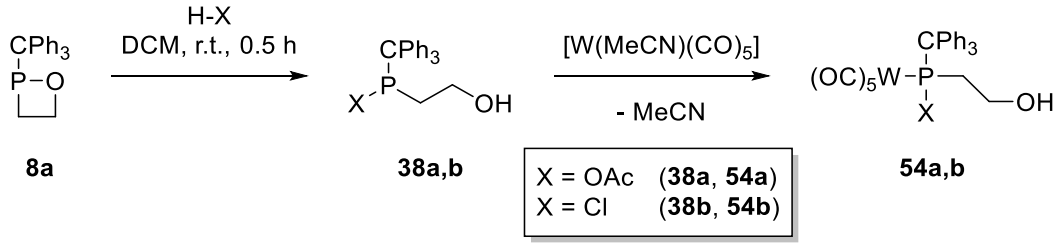

Scheme 3.27: Synthesis of tungsten complexes **54a,b**.

While the intermediately formed **38a,b** reacted with the pentacarbonyltungsten(0) fragment and formed the tungsten complexes **54a,b** (see Scheme 3.27), still various side products could be observed (see Figure 3.33). This could not be prevented, as **38a,b** needed time to form before adding the tungsten fragment, and while **38a,b** was not formed quantitively yet, it partially already decomposed to yield **39a,b**-**41a,b**. Following the results from the theoretical calculations, the main products were assigned to **54a,b**. Both signals showed a clear $^{1}J_{W\text{-}P}$ coupling constant in the $^{31}P\{^{1}H\}$ NMR spectrum (130.1 ppm, 287.5 Hz for **54a**, 123.2 ppm, 274.1 Hz for **54b**). For both **54a,b** HRMS spectra were

measured and their quasi-molecular ions were detected (m/z theor./exp.: 701.0575/701.0572 $[M-H]^-$ (**54a**), 677.0122/677.0117 $[M-H]^-$ (**54b**)). Remarkably, both quasi-molecular ions were formed by deprotonation, not protonation; hinting to the presence of an acidic proton, like an OH-group. All of this was in accordance with tentative assignment to **54a,b**, featuring a primary alcohol.

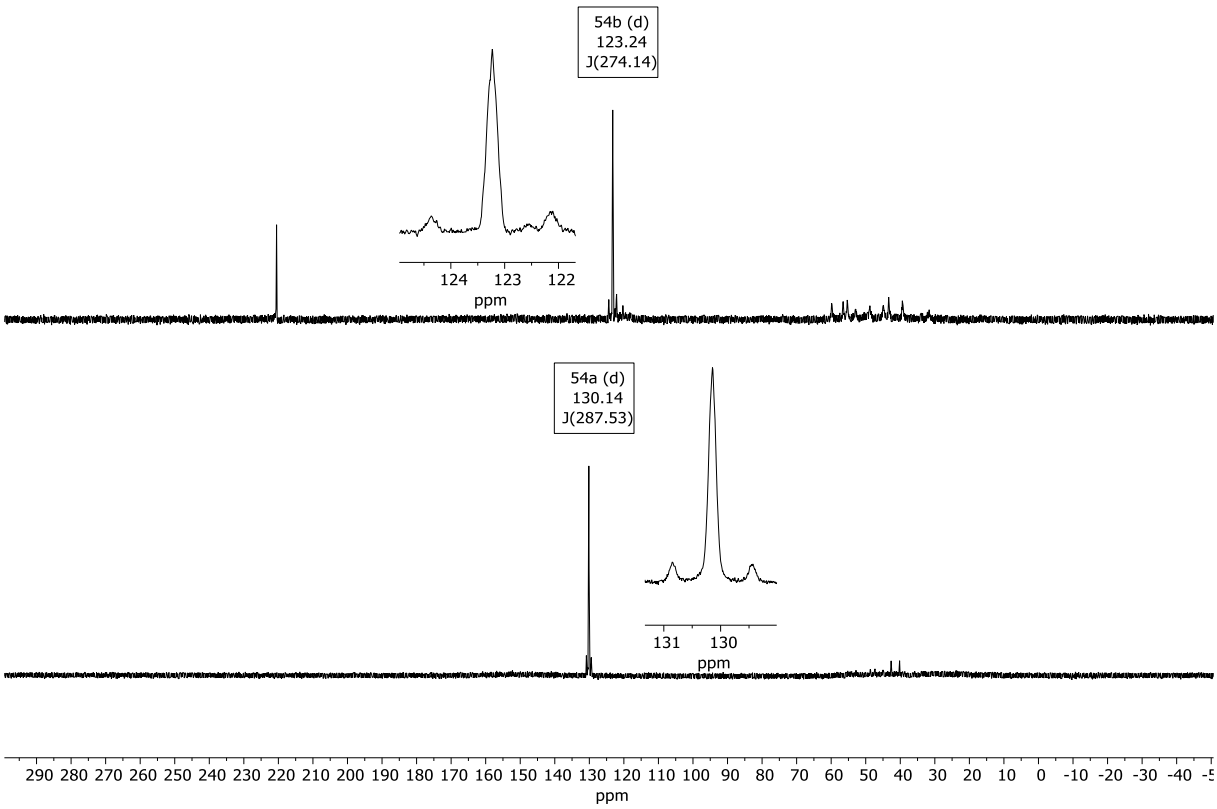

Figure 3.33: $^{31}P\{^1H\}$ NMR spectra of the reaction of **8a** with acetic acid (bottom) and hydrochloric acid (top), followed by complexation towards a tungsten fragment.

The obtained shifts of **54a,b** fitted well to literature known compounds (see Figure 3.34), although it should be noted that no suitable P-acetate complex could be found for comparison.

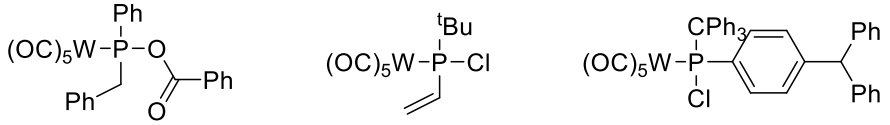

Figure 3.34: Literature known P-carboxyl[126] and P-Cl[127][128] compounds.

While no pure sample of **54a,b** could be obtained (when performing column chromatography on **54a**, the compound remained on the stationary phase), a single crystal suitable for X-ray diffraction experiments could be obtained from a reaction mixture of **54a** (see Figure 3.35). Surprisingly, the

measured structure was not the expected structure of the *P*-acetate complex **54a**, but that of a P-OH complex **55a**.

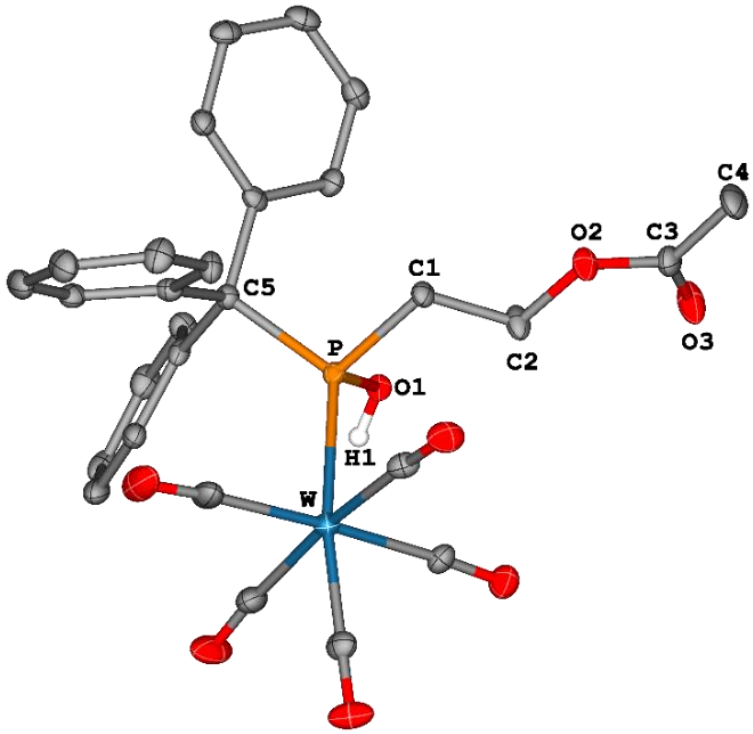

Figure 3.35: Molecular structures of **55a** in the solid state. Hydrogen atoms are omitted and the thermal ellipsoids are set at the 50% probability level. Selected bond lengths in Å and angles °: P–O1 1.614(3), P–C1 1.857(4), C1-C2 1.515(6), P–C5 1.940(4), P–W 2.5458(11), C2–O2 1.465(5), C1–P–C5 105.81(19) and O1–P–W 112.09(12).

This could easily be rationalized, as the side product of the reaction **41a** was a secondary phosphane oxide and this exists in an equilibrium with its tautomer, the hydroxyphosphane **48a**. While normally, the equilibrium is strongly on the side of the oxide form, it is known that the equilibrium can be shifted towards the hydroxyl form by the presence of metal fragments to form complexes (see Scheme 3.28).[129]

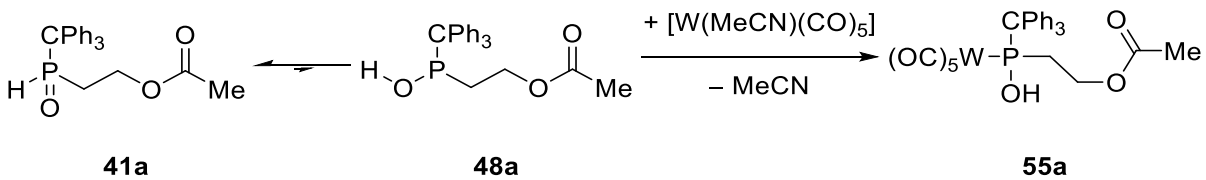

41a **48a** **55a**

Scheme 3.28: Possible mechanism for the generation of **55a**.

Thus, the obtained crystal structure **55a** was explained simply by picking a crystal of the "wrong" minor product, maybe because **55a** crystalized more easily or rapidly than **54a**. Interestingly, the unit cell of

55a showed hydrogen bonding between the P-OH hydrogen and the C=O oxygen of the carboxyl group (see Figure 3.36). The OH···O distance in **55a** was determined to be 1.823 Å, indicating a moderately strong hydrogen bond.[130]

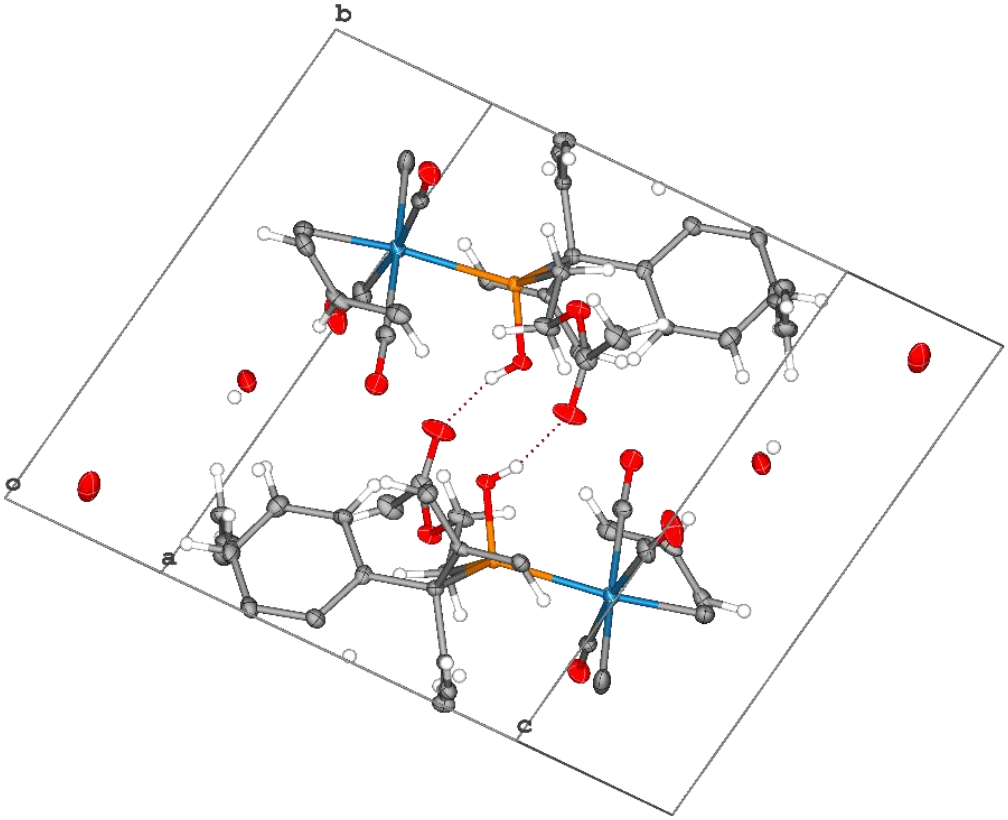

Figure 3.36: Unit cell of **55a** in the solid state. Thermal ellipsoids are set at the 50% probability level.

In conclusion, while it was not yet possible to isolate **54a,b**, the complexation towards a metal fragment appeared to be a suitable method to reduce the amount of formed side products as shown in the $^{31}P\{^{1}H\}$ NMR spectra (see Figure 3.33).

3.5.3 Hydrolysis

As it was shown that **8a** readily reacted with Brønsted acids, it was also attempted to react **8a** with the ampholyte water (see Scheme 3.29). The reaction selectively formed one product with a ^{31}P NMR chemical shift of 46.7 ppm, which was in similarity with the phosphane oxides **19a-f**, and a large $^{1}J_{P\text{-}H}$ coupling constant of 479.7 Hz. This strongly supported the phosphane oxide structure **40a**. The trivalent *P*-hydroxy structural motif of **56a** was not observed due to fast tautomerization. The

molecular composition was proven by detection of the quasi-molecular ion peak by high-resolution mass spectrometry (m/z theor./exp. 337.1352/337.1350 $[M+H]^+$).

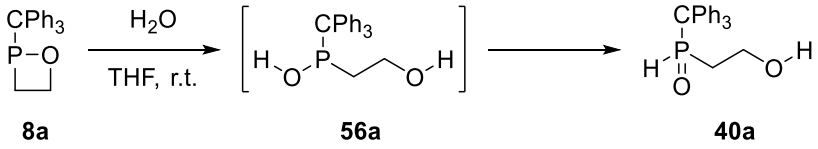

8a **56a** **40a**

Scheme 3.29: Hydrolysis of **8a**.

The hydrolysis of **8a** was also investigated by quantum chemical computations performed by Espinosa Ferao for the model compound **8e**.[108] The computed Gibbs energy profile showed that the initial step is not the protonation of the ring oxygen, but a nucleophilic attack of the water oxygen at the σ-hole (areas of positively charged electrostatic potential on otherwise negatively charged atoms)[131] on phosphorus, followed by a proton transfer involving five molecules of water in total. The hydrolysis needed to overcome a moderately high energy barrier of 33.37 kcal/mol and is exergonic by −14.04 kcal/mol (see Figure 3.37). **56e** then tautomerized to the more stable **40e** (ΔG = −27.22 kcal/mol); this occurred through a moderate barrier ($\Delta\Delta G^{\ddagger}$ = 28.70 kcal/mol) and required two molecules of water, as the use of only one or none molecule water led to much higher barriers ($\Delta\Delta G^{\ddagger}$ = 36.36 kcal/mol and $\Delta\Delta G^{\ddagger}$ = 49.55 kcal/mol, respectively).

The calculations also showed that the reaction of **8e** with water could be catalysed by addition of a Brønsted acid (see Figure 3.37). Triflic acid was chosen for the model. In the acid-catalysed reaction, the first step was the near barrierless protonation of phosphorus, leading to 1,2-oxaphosphetanium salt **57e** (ΔG = −12.78 kcal/mol). The enhanced electrophilicity and ring strain allowed for easy attack of water at the C^4-carbon, forming the oxonium intermediate **58e** that lost triflic acid to form the final product **40e**^{i}, which showed an inverted geometry at phosphorus in contrast to the neutral mechanism.

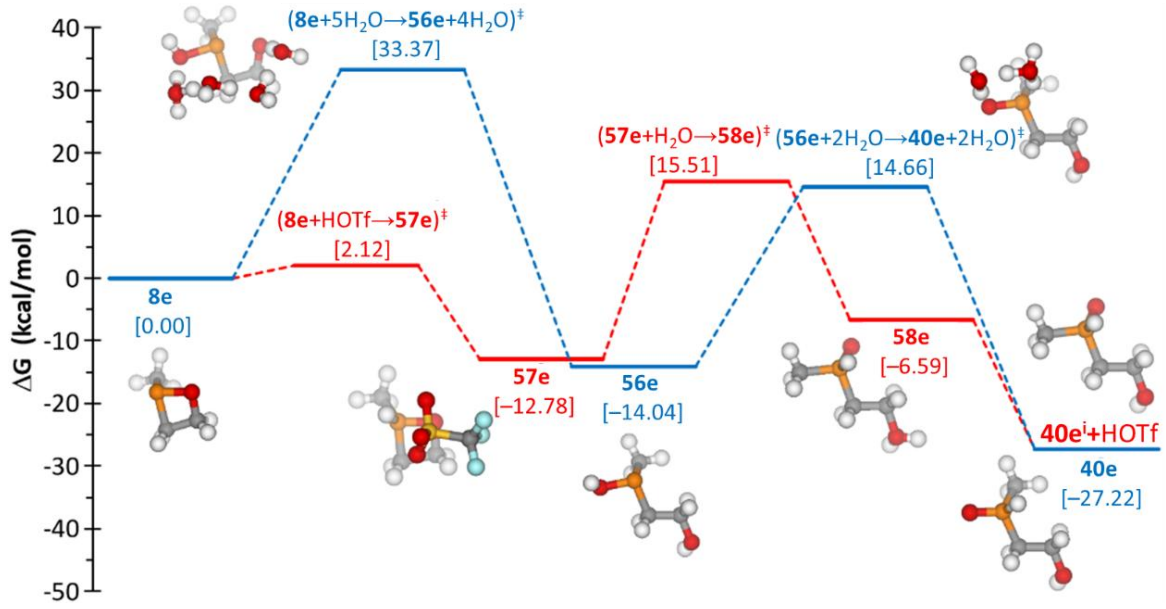

Figure 3.37: Computed Gibbs energy profile for the neutral (blue) and acid-catalysed (red) hydrolysis of **8e**, computed at $CPCM_{H2O}$/PWPB95-D3/def2-QZVPP//$CPCM_{H2O}$/PBEh-3c by Espinosa Ferao.[108]

To experimentally investigate the theoretical results, **8a** was reacted with water in the presence of *para*-toluene sulfonic acid (see Scheme 3.30).

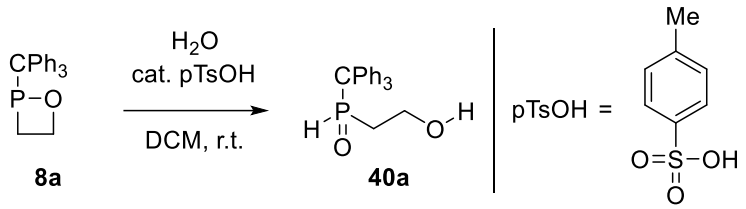

Scheme 3.30: Acid-catalysed hydrolysis of **8a**.

The acid-catalysed reaction was complete within 2 h, while in contrast the reaction under neutral conditions was only completed to 80% after one day of reaction time. These results agreed well with the calculations.

4 Summary

While examples of 1,2$\sigma^5\lambda^5$-oxaphosphetanes were known and have been investigated for a long time, the 1,2$\sigma^3\lambda^3$-oxaphosphetanes having a lower coordinated phosphorus centre became available only recently. Since very few was known about "free" 1,2$\sigma^3\lambda^3$-oxaphosphetanes, it was of high interest to investigate their synthesis and reactivity, especially as they could serve as interesting entry point for phosphorus-containing new functional molecules and/or polymers.

In order to create a solid platform for a broad investigation it was required to improve the synthetic protocol. The yield for the photolytic synthesis of molybdenum complex **4** could be increased from 25% to 81%. A further breakthrough was the synthesis of the *C*-unsubstituted 1,2-oxaphosphetane **8a** which led to better interpretable ^{1}H and ^{13}C{^{1}H} NMR spectra, finally. The isolation of the desirable *C*^{4}-dimethyl 1,2-oxaphosphetane **8b** could not be achieved due to thermal decomposition at elevated temperatures and, hence, only its molybdenum complex **7b** could be isolated.

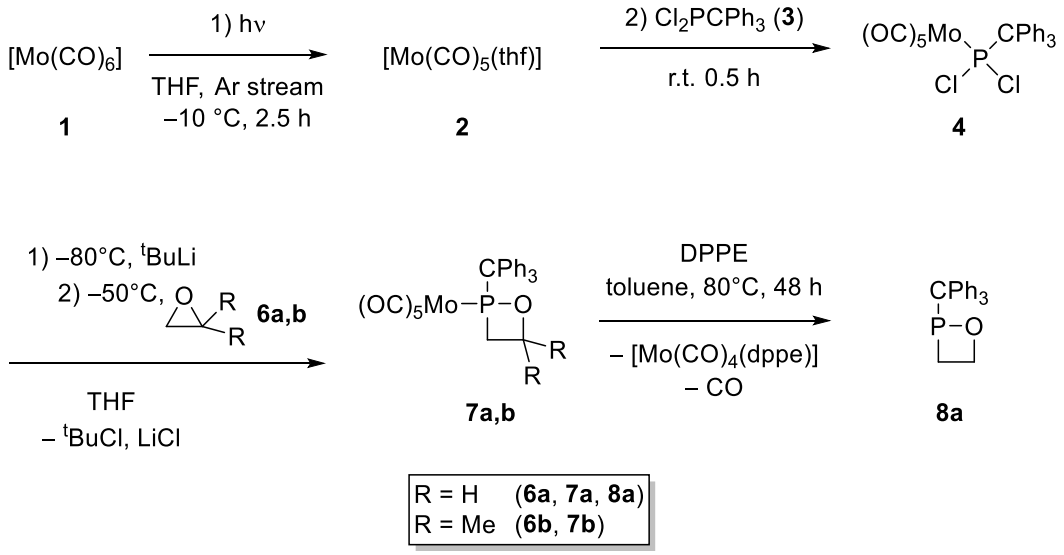

Scheme 4.1: Overview on starting material synthesis.

In chapters 3.2-3.5, the reactivity of 1,2-oxaphosphetanes **8a,c,c'** was explored. This is divided into three main research lines: oxidation or complexation of the phosphorus centre (chapter 3.2), Arbuzov and similar reactions (chapters 3.3 and 3.4), and reactions with Brønstedt acids (chapter 3.5).

In chapter 3.2, the phosphorus centre could be oxidised by elemental chalcogens or transfer reagents (see Scheme 4.2) and a crystal structure for the 1,2-oxaphosphetane sulfide **11a** was obtained. Also the first examples of 1,2-oxaphosphetane borane complexes **14a,c,c'** were isolated and a crystal structure of complex **14a** was obtained. The 1,2-oxaphosphetane oxides **10c,c'**, the 1,2-oxaphosphetane sulfides **11a** and **11c,c'**, and the oxaphosphetane selenides **12c,c'** were isolated and characterised by NMR spectroscopy and HRMS spectrometry. The 1,2-oxaphosphetane oxide **10a**, and the 1,2-oxaphosphetane borane complexes **10a** and **10c,c'** were also synthesised but only investigated by NMR spectroscopy. The synthesis of 1,2-oxaphosphetane tellurides **13c,c'** was not possible by employing either elemental tellurium or tri-*n*-butylphosphane telluride.

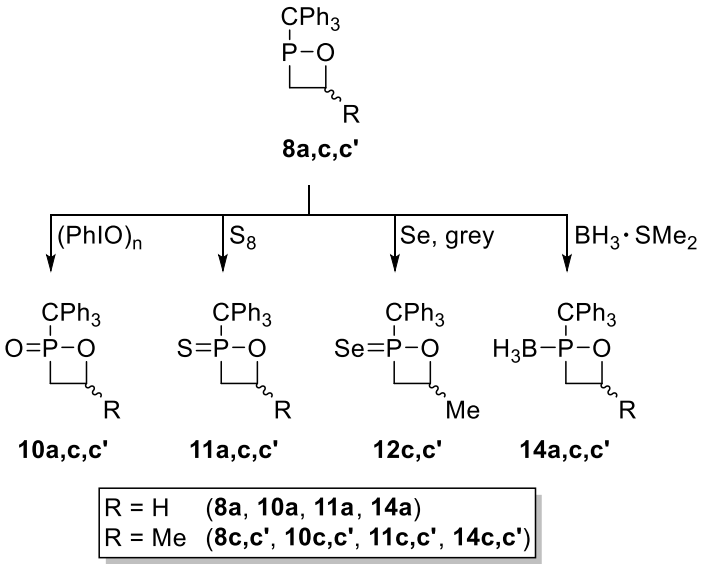

Scheme 4.2: Overview of successful synthesis of *P*-chalcogenides and κP-borane complexes.

In chapter 3.3, a series of Arbuzov reactions was performed using 1,2-oxaphosphetane **8a** and activated alkyl halides were required to achieve fast and clean reactions. Given the cyclic nature of **8a**, the Arbuzov reaction yielded products incorporating both the alkylated phosphorus centre and the halide function, and three β-haloethylphosphane oxides **19a-c** (see Scheme 4.3) could be isolated. They were characterised by NMR spectroscopy and HRMS spectrometry, further, X-ray diffraction experiments could be performed on all three compounds to obtain their structure in the solid state.

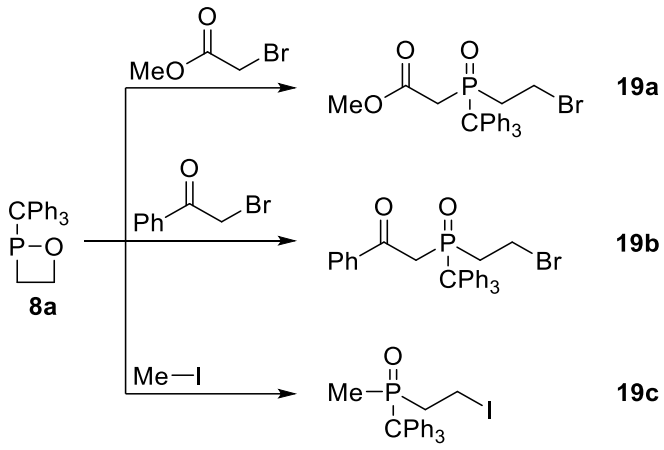

Scheme 4.3: Arbuzov reactions of **8a**.

8a was also reacted with (−)menthyl bromoacetate, leading to the compounds **19d** and **19d'** (see Scheme 4.4). Unfortunately, the mixture of **19d,d'** could not be separated but the compounds were characterised by NMR spectroscopy and HRMS spectrometry.

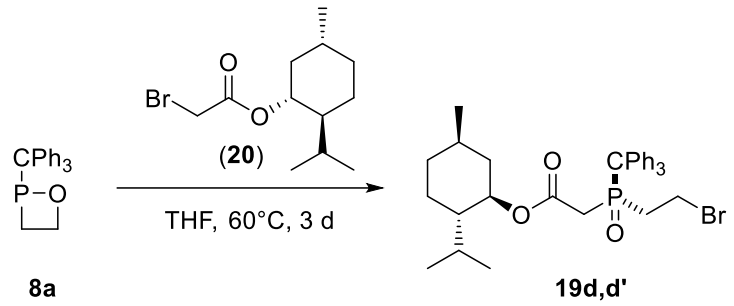

Scheme 4.4: Synthesis of **19d,d'**.

After the synthesis of functional monomers, based on P-alkylation as primary step, the synthesis of oligo- or polymers was investigated. Oligomer mixtures containing up to 10 units of **8a** could be synthesised by treating a solution of 1,2-oxaphosphetane **8a** with methyl triflate (see Scheme 4.5). The oligomers $\mathbf{22^n}$ were detected by MALDI mass spectrometry for n = 2-10. Experimental series showed that a high concentration of **8a** and substoichiometric amount of methyl triflate prefer heavier oligomers, with a clear preference for the pentamer $\mathbf{22^5}$ for most cases. The reaction was investigated by quantum chemical computations performed by Espinosa Ferao and by VT-NMR studies. In comparison to known literature and calculated NMR shifts, a signal observed at low temperatures at 130.4 ppm was tentatively attributed to the transient 1,2-oxaphosphetanium salt **21**.

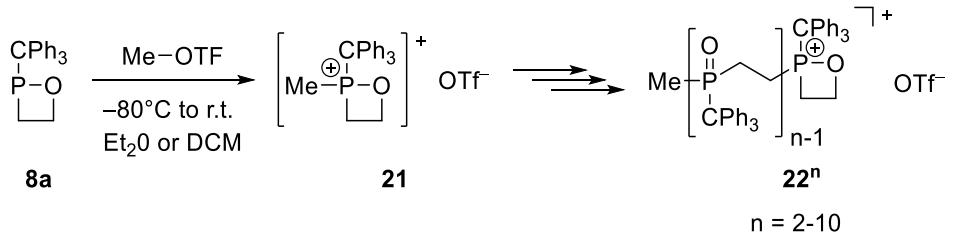

Scheme 4.5: Synthesis of oligomers **22ⁿ**.

After obtaining promising results with Arbuzov reactions, the possibility to perform Perkow reactions was explored, too. Quantum chemical calculations suggested that 1,2-oxaphosphetanes should undergo Perkow reactions with chloroacetone. But the experiments showed a different result (see Scheme 4.6). Reaction of **8a** with bromoacetone showed slow, but selective formation of the Arbuzov product **19f**, favouring the thermodynamic over the kinetic product at ambient temperature. **19f** was isolated and characterised by NMR spectroscopy and HRMS spectrometry; the structure of **19f** in solid state could be obtained by X-ray diffraction studies. Almost no reaction was observed at ambient temperature for chloroacetone. At higher temperatures (50°C–70°C), two main signals at 46.7 ppm and 115.1 ppm were observed. While the signal at 46.7 ppm could be safely assigned to the thermodynamic Arbuzov product **19e**, no safe assignment for 115.1 ppm could be made. **19e** was characterised by NMR spectroscopy and HRMS spectrometry.

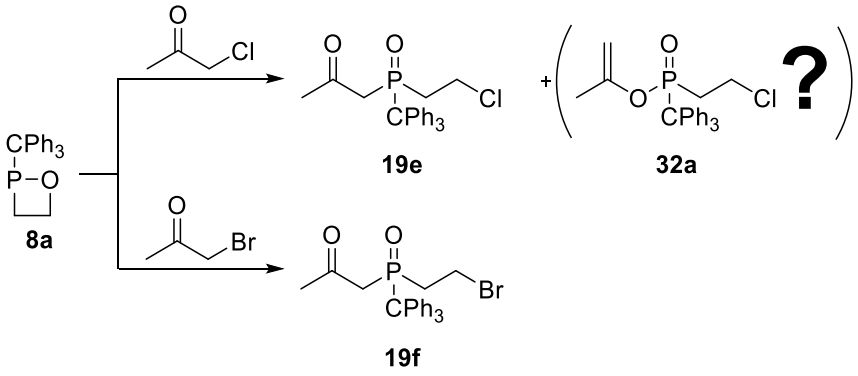

Scheme 4.6: Attempted Perkow reactions of **8a**.

In chapter 3.4, the scope of the investigation was broadened and small inorganic molecules, namely halogens (chlorine, bromine, iodine), an interhalogen (iodine monochloride), and a pseudo-halogen (cyanogen bromide) were tested.

The reactions of **8a** with bromine and iodine were highly selective and yielded the halo(2-haloethyl)phosphane oxides **34b,c**. **34b,c** (see Scheme 4.7) which were characterised by NMR

spectroscopy and HRMS spectrometry, and single crystals suitable for X-ray diffraction studies were obtained. In the reaction with chlorine, the desired product **34a** could only be observed in the $^{31}P\{^{1}H\}$ NMR spectrum, but it decomposed rapidly before any purification could be performed. The reaction was also investigated by quantum chemical calculations performed by Espinosa Ferao, showing that reaction of model 1,2-oxaphosphetane **8e** with iodine occurs over an Arbuzov-like mechanism, starting with the nucleophilic attack of phosphorus on the easy to polarize iodine.

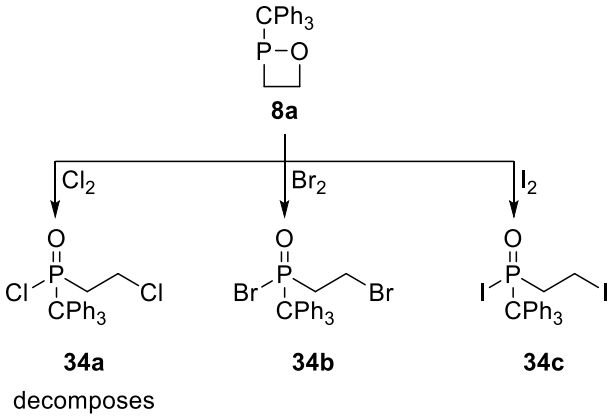

Scheme 4.7: Reaction of **8a** with halogens.

The reaction of **8a** with iodine monochloride could a priori deliver two products, the *P*-iodine isomer **36a** and the *P*-chlorine isomer **36b** (see Scheme 4.8). The $^{31}P\{^{1}H\}$ NMR spectrum showed only one signal at 62.2 ppm, which was attributed to **36a**, due to close similarity with *P*-iodine compound **34c**. This was expected, as the first reaction step is (in analogy for the calculated reaction pathway for iodine) assumed to be the nucleophilic attack of phosphorus on the partially positively charged iodine atom. Upon removable of the solvent, the product signal vanished in the $^{31}P\{^{1}H\}$ NMR spectrum and no identifiable product could be observed in a mass spectrometric experiment; thus, no further characterisation was possible. The reaction with cyanogen bromide yielded two isomers, the *P*-nitrile isomer **37a** and the *P*-bromine isomer **37b** (see Scheme 4.7) which were observed in the $^{31}P\{^{1}H\}$ NMR spectrum at 34.2 ppm (25%) and 71.3 ppm (75%). Due to the close similarity with **34b**, the signal at 71.3 ppm was assigned to **37b**, being the main product, and the signal at 34.2 ppm to **37a**. This outcome can be rationalized by calculating the difference of electronegativities $\Delta\chi_{Br\text{-}C(sp)} = -0.14$, showing bromine as less electronegative and thus the preferred atom for the nucleophilic attack. The isomers could not be separated and, hence, no further characterisation was achieved.

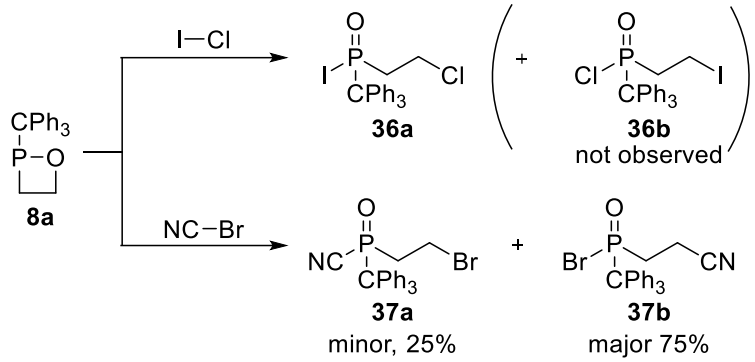

Scheme 4.8: Reaction of **8a** with ICl and (CN)Br.

The last chapter (3.5) of this thesis was focused on reactions with Brønstedt acids. **8a** was treated with acetic acid or hydrochloric acid. In both cases, four main signals were observed, *i.e.* **38a,b**-**41a,b** (see Scheme 1.12). Through a combination of $^{31}P\{^{1}H\}$ NMR spectroscopic data and quantum chemical computations performed by Brehm, structure proposals were made for all products and a feasible reaction pathway constructed.

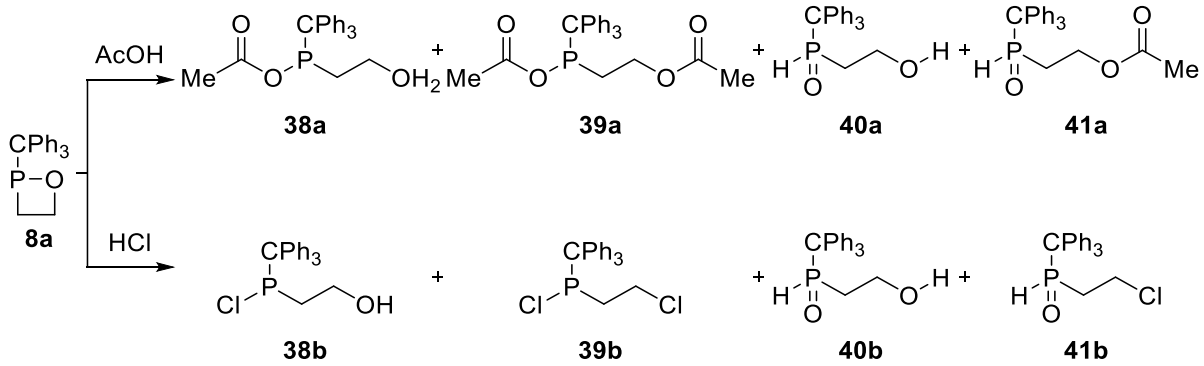

Scheme 4.9: Reaction of **8a** with acetic acid and hydrochloric acid.

In an attempt to reduce the number of products, a reactive tungsten metal fragment was added to the reaction mixtures of **38a**-**41a** and **38b**-**38b** (see Scheme 4.10) which resulted in only one major signal in each case, and the $^{31}P\{^{1}H\}$ NMR signals of the products **54a** and **54b** were assigned in comparison with literature known compounds. Their molecular composition was proven by HRMS spectrometry but they could not be isolated in pure form as the formation of side products could not be suppressed completely. However, a single crystal suitable for X-ray diffraction experiments could be obtained from the reaction mixture containing **54a**. Surprisingly, it turned out that the determined structure was not that of the *P*-OAc anhydride complex **54a** but that of *P*-OH containing acid complex **55b**.

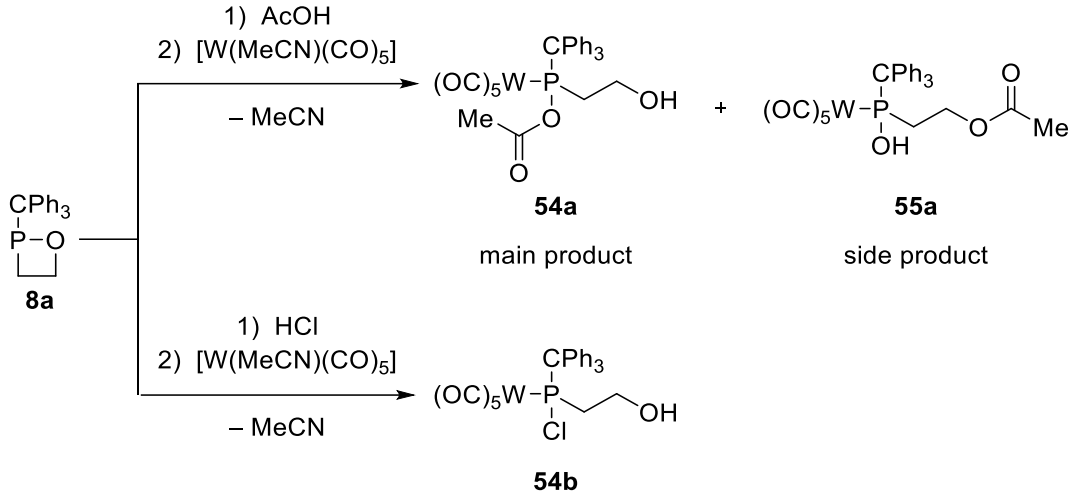

Scheme 4.10: Synthesis of metal complexes **54a**+**55a** and **54b**.

Also in chapter 3.5, the hydrolysis of **8a** was investigated experimentally (see Scheme 4.11) following quantum chemical calculations by Espinosa Ferao, and these results suggested that the hydrolysis could be catalysed by the addition of a strong acid. This was experimentally proven by addition of a catalytic amount of *p*-toluene sulfonic acid, leading to a drastic reduction of reaction time from several days to a few hours. The hydrolysis product **40a** was characterised by NMR spectroscopy and HRMS spectrometry.

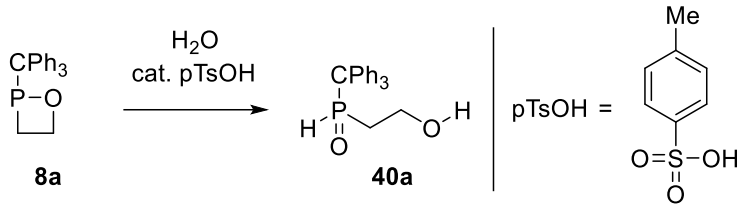

Scheme 4.11: Hydrolysis of **8a**.

5 Experimental Part

5.1 General Part

All reactions were performed under dried and deoxygenated argon atmosphere using Schlenk or glovebox techniques. The used argon (>99.998 %) was purified by a system of three columns (deoxygenation by a BTS copper catalyst (BASF PuriStar® R3-15S) at ca. 100°C, removing moisture with silica gel, phosphorus pentoxide desiccant with indicator (Sicapent®) and calcium chloride). Glassware, spatulae, cannulae and filter papers were dried in a compartment dryer at 110 °C for at least one hour. Prior to use, the glassware was heated with a heat gun (up to 550°C) under active vacuum (<0.02 mbar) and filled with argon three times. Sterile syringes were purged with argon three times before use. The solvents were dried by standard procedures[132] by refluxing over proper desiccants under an argon atmosphere (*n*-pentane, petroleum ether 40/65 and toluene over sodium wire (Ø = 2 mm); diethyl ether stabilized with 3,5-di-*tert*-butyl-4-hydroxytoluene (BHT) and tetrahydrofuran over benzophenone and sodium wire, dichloromethane over calcium hydride) for several days and distilled before use. Alternatively, diethyl ether and toluene were dried using a MBRAUN SPS-800 solvent purification system. For filtrations, Schlenk frits or stainless steel cannulae (Ø = 1 mm and 2 mm) with Whatmann® Cytiva grade 595 cellulose filter paper or for finer residues Whatman® glass microfiber filters (grade GF/B) were used. After use, devices made of stainless steel were cleaned with diluted hydrochloric acid, demineralised water and acetone. Glassware was cleaned by storage in a concentrated solution of potassium hydroxide in isopropanol for at least two days and in diluted hydrochloric acid for several hours. Afterwards, the glassware was washed with tap water and soap, followed by demineralised water, acetone and petroleum ether 40/65. All joints were greased with OKS 1112 grease or with PTFE paste (Carl Roth). Low temperatures (<0°C to −100°C) were achieved using an ethanol bath and liquid nitrogen.

5.2 Analytical Methods

5.2.1 Melting Point Determination

Melting points were measured using a Toledo *MPmeter* device or a Büchi melting point determination device according to Dr. Tottoli. The samples were prepared in a glass capillary (Ø = 0.1 mm) and heated quickly (ca. 5 K/min) for a rough determination of the melting point or decomposition temperature. Afterwards, a heating rate of approximately 2 K/min was used until the sample melted or decomposed. No internal or external temperature corrections were performed.

5.2.2 Nuclear magnetic resonance (NMR) spectroscopy

NMR spectra were recorded on a Bruker Avance I 300 MHz, Bruker Avance I 400 MHz, Bruker Avance I 500 MHz or Bruker Avance III HD Ascend 500 MHz spectrometer at the NMR department of the University of Bonn and subsequently analysed by the program Mestrenova 14.2. The calibration of the ^{1}H and ^{13}C NMR spectra was done *via* the solvent residual signals relative to tetramethylsilane (<1 % in $CDCl_3$) ($CDCl_3$: $\delta(^{1}H)$ = 7.26 ppm and $\delta(^{13}C)$ = 77.16 ppm, C_6D_6: $\delta(^{1}H)$ = 7.16 ppm and $\delta(^{13}C)$ = 128.06 ppm).[133] ^{31}P NMR spectra were measured relative to 85 % H_3PO_4 in water as external reference by using the ^{2}H frequency of the deuterated solvent (lock frequency) and the frequency ratio value $\Xi(^{31}P)$ = 40.480742% as recommended by IUPAC, ^{11}B NMR spectra relative to $BF_3{\cdot}OEt_2$ in $CDCl_3$ using the ^{2}H frequency of the deuterated solvent (lock frequency) and the frequency ratio value $\Xi(^{11}B)$ = 32.083974%, ^{77}Se NMR spectra relative to Me_2Se using the ^{2}H frequency of the deuterated solvent (lock frequency) and the frequency ratio value $\Xi(^{77}Se)$ = 19.071513%.[134] All lock frequencies were calibrated internally against the ^{1}H signals of solutions of tetramethylsilane with a volume fraction of $\Phi \leq 1\%$ in the corresponding deuterated solvent. Deuterated solvents were stored over 10 w% molecular sieve (4 Å) for min. 2 days before usage. The chemical shift (δ) is given in parts per million (ppm) and the coupling constant ($^{n}J_{X\text{-}Y}$) in Hertz (Hz) as absolute values neglecting the sign where n is the number of bonds between the coupling nuclei X and Y. For assigning the multiplicity following abbreviations were used: s = singlet, d = doublet, dd = doublet of doublets, ddd = doublet of doublets of doublets, dddd = doublet of doublets of doublets of doublets, dq = doublet of quartets, m = multiplet and br = broad. For ^{1}H NMR spectra additionally the number of nuclei is given according which is determined *via* integration. For complex NMR spectra, the ^{1}H and ^{13}C NMR signals of compounds were

assigned by a combination of 1D- and 2D-experiments (COSY, HMQC, HMBC). All measurements were performed at ambient temperature (298 K) if not stated otherwise.

5.2.3 Mass Spectrometry

Mass spectra using liquid injection field desorption ionization (LIFDI) were recorded on a Thermo Finnigan MAT 90 sector field instrument equipped with a LIFDI ion source (Linden CMS). The samples were dissolved in dichloromethane. Electrospray ionization (ESI) and atmospheric pressure chemical ionization (APCI) measurements were performed on a Thermo Fisher Scientific Orbitrap XL spectrometer with an HPLC autosampler using acetonitrile or dichloromethane as solvents. Matrix-assisted laser desorption/ionization (MALDI) were recorded on a Bruker Daltonik MALDI ultrafleXtreme TOF/TOF. Only selected data are given for detected ions. The peaks are given in mass-to-charge ratio (m/z) while only the isotopomer with the highest relative abundance is represented. Additionally, the relative intensities of the peaks are given in parentheses and the proposed molecule fragments in square brackets. High resolution mass spectra (HRMS) that were obtained using ESI or APCI were recorded in a single measurement and, hence, no standard deviations for ESI/APCI HRMS were obtained.

5.2.4 Infrared (IR) spectroscopy

ATR-IR spectra of solids were recorded in the spectral range of 4000–400 cm^{-1} on a Bruker Alpha FTIR spectrometer with a single-reflection ATR measurement attachment (Platinum-ATR Diamond) or a Shimadzu IRSpirit FTIR spectrometer with a single-reflection ATR measurement attachment (QATR-S) in a glovebox at ambient temperature. Alternativly, stable samples could be measured on a Thermo Nicolet 380 under air at ambient temperature. For apodization the Happ-Genzel function was used. All analyses were performed using the programs *EZ OMNIC 7.3* from *Fisher Scientific*, *OPUS* from *Bruker* or *LabSolutions IR 2.26* from *Shimadzu*. The intensities of the bands are marked as very strong (vs), strong (s), medium (m) or weak (w). Only selected wavenumbers of the absorption bands are given using reciprocal centimeters (cm^{-1}).

5.2.5 Single crystal X-ray diffraction

Single crystal X-ray diffraction analyses were performed on a Bruker X8-KappaApex II diffractometer, a Bruker D8 Venture diffractometer, a STOE IPDS-2T diffractometer or a STOE STADIVARI

diffractometer, equipped with a low-temperature device (Bruker Kryoflex, Oxford Cryostream 700 series or Oxford Cryostream 800 series) at 100(2) K, 123(2) K or 180(2) K by using graphite monochromated Mo-Kα radiation (λ = 0.71073 Å) or Cu-Kα radiation (λ = 1.54186 Å). Intensities were measured by fine-slicing ϕ and ω scans and corrected background, polarization and Lorentz effects. A semi-empirical absorption correction was applied for the data sets following Blessing's method.[135] The structure was solved by direct methods and refined anisotropically by the least-squares procedure implemented in ShelX program system.[136] All non-hydrogen atoms were refined anisotropically. The hydrogen atoms were included isotropically refined using a riding model at the bound carbon atoms. The quality of the crystals was evaluated by the X-ray diffraction service within the chemical institutes of the University of Bonn with an in-house grading: A = solving and refinement without any (identifiable) errors (excellent structure), B = only marginal problems during refinement (very good structure), C = small problems during refinement (good structure), D = significant problems during refinement (moderate structure), E = not for precise discussions, only structural motive confirmed, F = structural motive vague, 1 = found structure was identical with the beforehand proposed structure, 2 = found structure was close to the beforehand proposed structure, 3 = found structure contained motives of the beforehand proposed structure, 4 = found structure was not related to the beforehand proposed structure. The program *Olex2 1.5*[137] of *OlexSys* was used for analyses and the ellipsoid representations of the molecular structures with the probability level set to 50 %. Detailed crystallographic data including bond lengths and bond angles as well as the refinement parameters of the respective compounds can be found in the appendix.

5.3 Chemicals used

The following list includes all commercially available used chemicals.

Chemical	Producer
acetic acid	VWR
Acetone	Fluka
aluminum oxide 90 active neutral (70–230 mesh ASTM)	Merck
Benzene	Riedel-de Haën
benzene-d6	Aldrich
1,2-bis(diphe+C9:E35nylphosphino)ethane	TCI
borane dimethylsulfide	Aldrich
Bromine	Aldrich
2-bromoacetic acid	Fluka
2-bromoacetophenone	Alfa Aesar
calcium chloride	Sigma-Aldrich
Chloroacetone	Fisher Scientific
Chloroform	Alfa Aesar
chloroform-d1	Deutero
cyanogen bromide	Riedel-de Haën
Dichloromethane	Fisher Scientific
Diethylether	VWR
2,2-dimethyloxirane	ThermoFisher
ethylene oxide solution (2.5-3.3 M in THF)	Merck
hydrochloric acid, 37%	VWR
hydrochloric acid solution (2M in Et2O)	Acros
Iodine	Grüssing
iodine monochloride	Fluka
Iodomethane	Fischer, Merck
iodosobenzene diacetate	Merck
(−)menthol	Fluka
methyl triflate	Mercl, Fluorochem
methyl 2-bromoacetate	Alfa Aesar
molybdenum hexacarbonyl	Alfa, Acros

n-pentane	Fisher Scientific
para-toluene sulfonic acid hydrate	Riedel-de Haën
petrol ether 40/65	Julius Hoesch
phosphorus pentoxide	J. T. Baker
phosphorus trichloride	Acros
potassium permanganate	Aldrich
Selenium	Aldrich
sodium carbonate	Riedel-de Haën
sodium hydroxide	VWR
sodium phosphinate monohydrate	Alfa Aesar
sodium sulfite	ABCR
Sulfur	Merck
sulfuric acid	Merck
Tellurium	Aldrich
tert-butyllithium solution (1.6 M in n-pentane)	Aldrich
Tetrahydrofurane	Fisher Scientific
Toluene	VWR
Triphenylmethanole	TCI
tri-n-butylphosphane	Alfa Aesar

The following chemicals were prepared according to literature:

Chemical
bromoacetone[138]
dichloro(triphenylmethyl)phosphane[139]
iodosylbenzene[140]
(−)menthyl bromoacetate[141]
tri-*n*-butylphosphane telluride[142]

The chemical acetonitrile(pentacarbonyl)tungsten(0) was provided by Dr. Philipp Brehm.

5.4 Waste Disposal

The disposal of laboratory chemical waste was performed according to the Hazardous Substances Ordinance (Gefahrstoffverordnung) (GefStoffV). Solvents, solids, column waste, heavy metal waste and syringes were separated from each other and collected in designed containers before disposing. Remaining reactive compounds or their residues were neutralized and/or quenched before disposal. The waste was submitted to the department 4.2 *Arbeits- und Umweltschutz* of the University of Bonn.

5.5 Syntheses and characterisations

5.5.1 Synthesis of dichloro(organo)phosphane complexes and 1,2σ³λ³-oxaphosphetane complexes

5.5.1.1 Synthesis of [pentacarbonyl{dichloro(triphenylmethyl)phosphane-κ*P*}molybdenum(0)] (**4**)

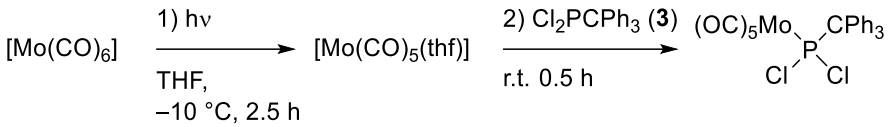

1 **2** **4**

Synthesis: 5.27 g (20.00 mmol, 1.33 eq) of $Mo(CO)_6$ (**1**) was dissolved in 420 mL of THF in a 500 mL photolysis reactor, the solution was flushed with argon and cooled to −10 °C. The solution was then irradiated using a Hg-lamp (200-280 nm, 150 W) for a period of 2.5 h and, after removal of the cooling, the solution was stirred for 15 min. Then the solution was transferred to a flask containing 5.18 g (15 mmol, 01 eq) **3**. After stirring for 30 min, the solvent was removed *in vacuo* (0.02 mbar).

Purification: The crude product was purified *via* column chromatography (h = 10 cm, d = 5 cm, r.t., Et_2O, Al_2O_3). After this, to regain unreacted $Mo(CO)_6$, the crude product was sublimed (50 °C, 0.05 mbar, 3.5 h). A second sublimation was carried out to remove $HCPh_3$ (100°C, 0.05 mbar, 2.0 h). The product was obtained as beige to grey powder.

Yield: 7.0552 g, 12.12 mmol, 81% (Lit:25%)[90].

^{1}H NMR (300.1 MHz, 298 K, $CDCl_3$): δ (ppm) = 7.36 (m, 9H, *meta/para*-C*H*), 7.42 (m, 6H, *ortho*-C*H*).

^{31}P{^{1}H} NMR (121.5 MHz, 298 K, $CDCl_3$): δ (ppm) = 201.5 (s).

5.5.1.2 Synthesis of [pentacarbonyl{-2-(triphenylmethyl)-1,2-oxaphosphetane-κ*P*}molybdenum(0)] (**7a**)

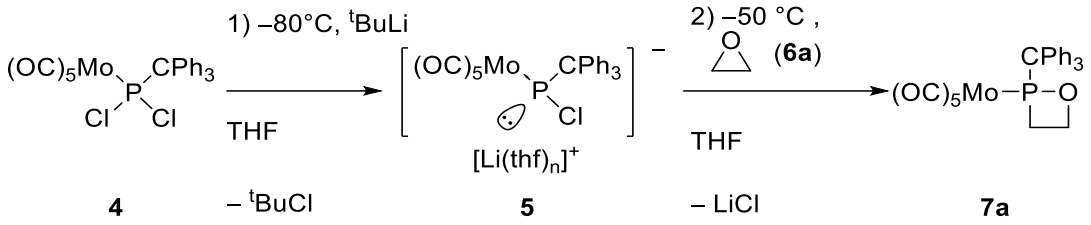

Synthesis: 2.433 g (4.19 mmol, 1 eq) **4** was dissolved in 60 mL of dried THF and cooled to −80°C. 3.14 mL (5.02 mmol, 1.2 eq) of a *tert*-butyllithium solution (1.6 M in n-pentane) was slowly added. The solution was kept stirring while slowly warming up. Upon reaching −50°C, 4.0 mL (10 mmol, 2.4 eq) ethylene oxide (**6a**) solution (2.5-3.3 M in THF) was added. The solution was further kept stirring while slowly warming up to ambient temperature. After reaching room temperature, all volatiles were removed in vacuo (0.02 mbar).

Purification: The crude product was purified by filtration with 300 mL of Et_2O over Al_2O_3 (h = 10 cm, d = 3 cm, r.t.) and removal of the solvent in vacuo (0.02 mbar). The crude product was further washed with *n*-pentane (four times 10 mL) at −60°C. After removal of the solvent in vacuo (0.02 mbar) the product was obtained as a white solid.

Reaction cipher: FLG-313 (05p5a021.21)

Molecular formula: $C_{26}H_{19}MoO_6P$

Molecular weight: 554.36 g/mol

Yield: 1.5085 g, 2.72 mmol, 65%.

MS (APCI) m/z (%): 243.117 (14) $[CPh_3]^+$, 319.124 (26) $[M-(Mo(CO)_5)+H]^+$, 388.999 (100) $[Mo-P(CPh_3)OH]^+$, 557.005 (10) $[M+H]^+$.

HRMS (APCI): theor./exp. 557.0047/557.0041 $[M+H]^+$.

^{1}H NMR (500 MHz, 298 K, $CDCl_3$): δ (ppm) = 3.00 (dddd, 1H, $^{2}J_{H\text{-}H}$ = 13.1 Hz, $^{2}J_{P\text{-}H}$ = 10.4 Hz, $^{3}J_{H\text{-}H}$ = 10.3 Hz, $^{3}J_{H\text{-}H}$ = 7.1 Hz, -PCH_2), 3.09 (dddd, 1H, $^{2}J_{H\text{-}H}$ = 14.1 Hz, $^{3}J_{H\text{-}H}$ = 8.5 Hz, $^{3}J_{H\text{-}H}$ = 5.6 Hz, $^{2}J_{P\text{-}H}$ = 3.8 Hz, -PCH_2), 4.48 (dddd, 1H, $^{3}J_{H\text{-}H}$ = 10.5 Hz, $^{2}J_{H\text{-}H}$ = 7.0 Hz, $^{3}J_{P\text{-}H}$ = 5.5 Hz, $^{3}J_{H\text{-}H}$ = 5.5 Hz, -OCH_2), 5.09 (dddd, 1H, $^{3}J_{H\text{-}H}$ = 8.5 Hz, $^{3}J_{H\text{-}H}$ = 7.0 Hz, $^{2}J_{H\text{-}H}$ = 7.0 Hz, $^{3}J_{P\text{-}H}$ = 4.7 Hz, -OCH_2), 7.37 (m, 15H, -CH).

^{1}H{^{31}P} NMR (500 MHz, 298 K, $CDCl_3$): δ (ppm) = 3.00 (ddd, 1H, $^{2}J_{H\text{-}H}$ = 13.6 Hz, $^{3}J_{H\text{-}H}$ = 10.3 Hz, $^{3}J_{H\text{-}H}$ = 7.0 Hz, -PCH_2), 3.09 (ddd, 1H, $^{2}J_{H\text{-}H}$ = 14.1 Hz, $^{3}J_{H\text{-}H}$ = 8.5 Hz, $^{3}J_{H\text{-}H}$ = 5.7 Hz, -PCH_2), 4.48 (dddd, 1H, $^{3}J_{H\text{-}H}$ = 10.3 Hz, $^{2}J_{H\text{-}H}$ = 7.0 Hz, $^{3}J_{H\text{-}H}$ = 5.6 Hz, -OCH_2), 5.09 (ddd, 1H, $^{3}J_{H\text{-}H}$ = 8.6 Hz, $^{3}J_{H\text{-}H}$ = 7.0 Hz, $^{2}J_{H\text{-}H}$ = 7.0 Hz, -OCH_2), 7.36 (m, 15H, -C*H*).

^{13}C NMR (126 MHz, 298 K, $CDCl_3$): δ (ppm) = 33.9 (d, $^{1}J_{P\text{-}C}$= 22.6 Hz, -P*C*H_2), 67.7 (d, $^{1}J_{P\text{-}C}$ = 9.3 Hz, -*C*Ph_3), 71.6 (d, $^{2}J_{P\text{-}C}$ = 13.4 Hz, -O*C*H_2), 127.7 (s_{br}, para-*C*H), 128.7 (s, meta-*C*H), 130.6 (s_{br}, ortho-*C*H), 141.3 (s_{br}, ipso-*C*), 204.7 (d, $^{2}J_{P\text{-}C}$= 9.3 Hz, cis-*C*O), 210.5 (d, $^{2}J_{P\text{-}C}$= 32.4 Hz, trans-*C*O).

^{31}P{^{1}H} NMR (202 MHz, 298 K, $CDCl_3$): δ (ppm)= 220.6 (s).

Single crystal measurement: FLG-359, good structure (B1), GSTR768, GXraymo_6902f

5.5.1.3 Synthesis of [pentacarbonyl{-4,4-dimethyl2-(triphenylmethyl)-1,2-oxaphosphetane-κ*P*}molybdenum(0)] (**7b**)

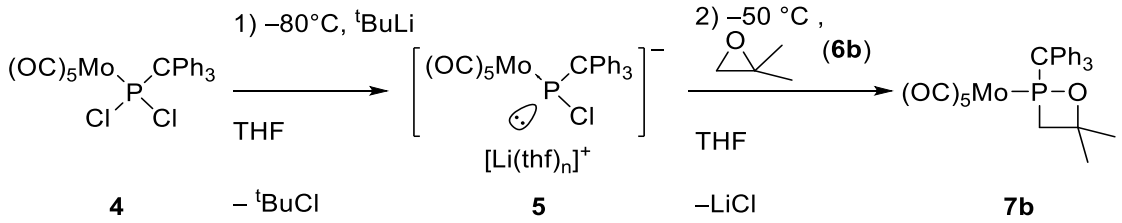

Synthesis: 2.96 g (5.09 mmol, 1 eq) **4** was dissolved in 60 mL of dried THF and cooled to −80°C. 3.82 mL (6.11 mmol, 1.2 eq) of a *tert*-butyllithium solution (1.6 M in n-pentane) was slowly added. The solution was kept stirring while slowly warming up. Upon reaching −50°C, 1.35 mL (15.3 mmol, 3 eq) 2,2-dimethyloxirane (**6b**) was added. The solution was further kept stirring while slowly warming up to ambient temperature. After reaching room temperature, all volatiles were removed *in vacuo* (0.02 mbar).

Purification: The crude product was purified by filtration with 300 mL of Et_2O over Al_2O_3 (h = 10 cm, d = 3 cm, r.t.) and removal of the solvent *in vacuo* (0.02 mbar). The crude product was further washed with *n*-pentane (three times 15 mL at −80°C, once with 5 mL at −30°C). After removal of the solvent in vacuo (0.02 mbar) the product was obtained as a white solid.

Reaction cipher: FLG-513 (FLG230814p5a004)

Molecular formula: $C_{28}H_{23}MoO_6P$

Molecular weight: 582.41 g/mol

Yield: 2.29 g, 3.9 mmol, 77%.

MS (APCI) m/z (%): 243.117 (100) $[CPh_3]^+$, 291.092 (35) $[HOPCPh_3]^+$, 347.155 (25) $[M\text{-}Mo(CO)_5+H]^+$, 388.997 (5) $[MoPh_3CPO+H]^+$, 444.987 (10) $[M\text{-}5(CO)+H]^+$, 472.982 (5) $[M\text{-}4(CO)+H]^+$, 501.049 (5) $[M\text{-}3(CO)+H]^+$, 529.044 (5) $[M\text{-}2(CO)+H]^+$

HRMS (APCI): theor./exp. 347.1559/347.1555 $[M\text{-}Mo(CO)5+H]^+$, 501.0517/ 501.0517 $[M\text{-}3(CO)+H]^+$, 529.0467/ 529.0468 $[M\text{-}2(CO)+H]^+$.

^{1}H NMR (500 MHz, 298 K, $CDCl_3$): δ (ppm) = 0.79 (s, 3H, -C*H*$_3$), 1.85 (s, 3H, -C*H*$_3$), 3.07 (dd, 1H, $^2J_{H\text{-}H}$ = 13.0 Hz, $^2J_{P\text{-}H}$ = 4.6 Hz, -C*H*$_2$), 3.30 (dd, 1H, $^2J_{H\text{-}H}$ = 13.1 Hz, $^2J_{P\text{-}H}$ = 11.7 Hz, -C*H*$_2$), 7.30 (t, 3H, $^3J_{H\text{-}H}$ = 7.8 Hz, para-CH), 7.36 (dd, 6H, $^3J_{H\text{-}H}$ = 7.6 Hz, $^3J_{H\text{-}H}$ = 7.6 Hz, meta-CH), 7.46 (d, 6H, $^3J_{H\text{-}H}$ = 7.6 Hz, ortho-CH).

^{13}C NMR (126 MHz, 298 K, $CDCl_3$): δ (ppm) = 31.5 (s, -*C*H$_3$), 32.2 (d, $^3J_{P\text{-}C}$ = 1.6 Hz,-*C*H$_3$), 44.6 (d, $^1J_{P\text{-}C}$ = 16.6 Hz, -*C*H$_2$), 67.6 (d, $^1J_{P\text{-}C}$ = 10.9 Hz, -*C*Ph$_3$), 88.2 (d, $^2J_{P\text{-}C}$ = 10.9 Hz, -*C*Me$_2$), 127.7 (s, para-*C*H), 128.4 (s, meta-*C*H), 131.8 (d, $^3J_{P\text{-}C}$ = 7.1 Hz, ortho-*C*H), 140.9 (s_{br}, ipso-*C*), 204.9 (d, $^2J_{P\text{-}C}$= 9.3 Hz, cis-*C*O), 210.3 (d, $^2J_{P\text{-}C}$= 32.4 Hz, trans-*C*O).

^{31}P{^{1}H} NMR (202 MHz, 298 K, $CDCl_3$): δ (ppm)= 184.5 (s).

^{31}P NMR (202 MHz, 298 K, $CDCl_3$): δ (ppm)= 184.5 (d, $^2J_{P\text{-}H}$= 16.2 Hz).

Single crystal measurement: FLG-308, good structure (BC1), GSTR755, GXraymo_6850_0m0

5.5.2 Synthesis of unligated 1,2σ³λ³-oxaphosphetanes

5.5.2.1 Synthesis of 2-(triphenylmethyl)-1,2-oxaphosphetane (**8a**)

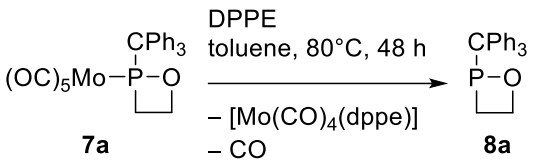

Synthesis: 3.2409 g (5.85 mmol, 1 eq) **7a** and 2.2827 g (5.73 mmol, 0.98 eq) 1,2-bis(diphenylphosphino)ethane (DPPE) were dissolved in 60 mL toluene and heated to 80 °C for 48 h. Full conversion was proven by ^{31}P NMR measurement. All volatiles were removed *in vacuo* (0.02 mbar).

Purification: The product was obtained after extraction with *n*-pentane (six times 20 mL, ambient temperature) as yellow solid.

Yield: 1.289 g, 4.08 mmol, 70%.

Molecular formula: $C_{21}H_{19}OP$

Molecular weight: 318.36 g/mol

Reaction cipher: FLG-502 (FLG230810pa007)

MS (APCI) m/z (%) = 243.117 (100) $[CPh_3]^+$, 319.125 (2) $[M+H]^+$, 335.120 (24) $[M+O+H]^+$.

HRMS (APCI): theor./exp. 319.1246/319.1244 $[M+H]^+$.

^{1}H NMR (500 MHz, 298 K, $CDCl_3$): δ (ppm) = 2.29 (dddd, 1H, $^2J_{H\text{-}H}$ = 13.3 Hz, $^3J_{H\text{-}H}$ = 10.3 Hz, $^3J_{H\text{-}H}$ = 6.7 Hz, $^2J_{P\text{-}H}$ = 3.2 Hz,-PCH_2), 2.83 (dddd, 1H, $^2J_{P\text{-}H}$ = 21.4 Hz, $^2J_{H\text{-}H}$ = 12.8 Hz, $^3J_{H\text{-}H}$ = 8.7 Hz, $^3J_{H\text{-}H}$ = 6.1 Hz,-PCH_2), 4.42 (dddd, 1H, $^3J_{H\text{-}H}$ = 10.5 Hz, $^2J_{H\text{-}H}$ = 7.1 Hz, $^3J_{H\text{-}H}$ = 5.9 Hz, $^3J_{P\text{-}H}$ = 0.9 Hz,-OCH_2), 5.05 (dddd, 1H, $^3J_{H\text{-}H}$ = 8.7 Hz, $^2J_{H\text{-}H}$ = 7.0 Hz, $^3J_{H\text{-}H}$ = 6.9 Hz, $^3J_{P\text{-}H}$ = 1.8 Hz,-OCH_2), 7.28 (m, 9H, -C*H*), 7.34 (m, 6H, -C*H*).

^{13}C NMR (126 MHz, 298 K, $CDCl_3$): δ (ppm) = 24.1 (d, $^1J_{P-C}$ = 24.1 Hz, -P*C*H$_2$), 63.4 (d, $^1J_{P-C}$ = 50.1 Hz, -*C*Ph$_3$), 74.0 (d, $^2J_{P-C}$ = 3.3 Hz, -O*C*H), 126.8 (s, *para*-*C*H), 128.5 (s, *meta*-*C*H), 129.8 (d, $^3J_{P-C}$ = 9.5 Hz, *ortho*-*C*H), 143.1 (d, $^2J_{P-C}$ = 8.5 Hz, *ipso*-*C*).

^{31}P{^{1}H} NMR (202 MHz, 298 K, $CDCl_3$): δ (ppm) = 212.1 (s).

^{31}P NMR (202 MHz, 298 K, $CDCl_3$): δ (ppm) = 212.1 (d, $^2J_{P-H}$ = 21.5 Hz)

Single crystal measurement: FLG-326, very good structure (B1), GSTR746, GXray6808

5.5.2.2 Attempted synthesis of 4,4-dimenthyl-2-(triphenylmethyl)-1,2-oxaphosphetane (**8b**)

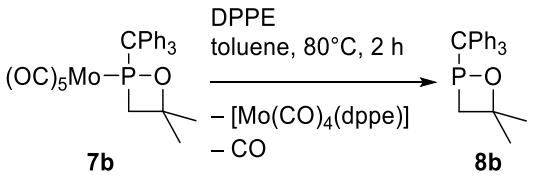

Synthesis: 116.5 mg (0.2 mmol, 1 eq) **7b** and 79.7 mg (0.2 mmol, 1 eq) 1,2-bis(diphenyl-phosphino)ethane (DPPE) were dissolved in 15 mL toluene and heated to 80 °C for 2 h. The formation of **8b** can be observed in the ^{31}P{^{1}H}-NMR spectrum. Further heating leads to decomposition. The product **8b** could not be isolated.

Reaction cipher: FLG-305 (02m3a001.22)

Molecular formula: $C_{23}H_{23}OP$

Molecular weight: 346.41 g/mol

^{31}P{^{1}H} NMR (121 MHz, 298 K, toluene): δ (ppm) = 161.2 (s).

5.5.3 Synthesis of 1,2-oxaphosphetane chalcogenides and complexes

5.5.3.1 Synthesis of 2-(triphenylmethyl)-1,2-oxaphosphetane *P*-oxide (**10a**)

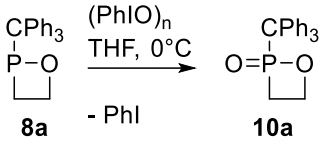

Synthesis: 159.2 mg **8a** were dissolved in 5 mL THF and cooled to −50 °C. 121 .0 mg (0.55 mmol, 1.1 eq) iodosylbenzene ($(PhIO)_n$) were added to the cooled solution. The reaction mixture was stirred and allowed to warm to room temperature for 2 d. After that, all volatiles were removed *in vacuo* (0.02 mbar).

Purification: The crude product was washed first twice with 5 mL Et_2O, then twice with 5 mL *n*-pentane. After removal of all volatiles *in vacuo* (0.02 mbar), the product was obtained as white solid.

Reaction cipher: FLG-520 (FLG230824pa042)

Molecular formula: $C_{21}H_{19}O_2P$

Molecular weight: 334.35 g/mol

Yield: 57.7 mg, 0.17 mmol, 35%.

^{1}H NMR (500 MHz, 298 K, $CDCl_3$): δ (ppm) = 2.65 (dddd, 1H, $^2J_{H\text{-}H}$ = 14.9 Hz, $^2J_{P\text{-}H}$ = 10.2 Hz, $^3J_{H\text{-}H}$ = 9.0 Hz, $^3J_{H\text{-}H}$ = 6.0 Hz,-PCH_2), 3.00 (dddd, 1H, $^2J_{P\text{-}H}$ = 18.1 Hz, $^2J_{H\text{-}H}$ = 14.9 Hz, $^3J_{H\text{-}H}$ = 9.0 Hz, $^3J_{H\text{-}H}$ = 5.9 Hz,-PCH_2), 4.01 (dddd, 1H, $^3J_{P\text{-}H}$ = 15.0 Hz, $^3J_{H\text{-}H}$ = 9.0 Hz, $^3J_{H\text{-}H}$ = 6.0 Hz, $^2J_{H\text{-}H}$ = 6.0 Hz,-OCH_2), 4.38 (dddd, 1H, $^3J_{P\text{-}H}$ = 10.0 Hz, $^3J_{H\text{-}H}$ = 8.9 Hz, $^3J_{H\text{-}H}$ = 6.0 Hz, $^2J_{H\text{-}H}$ = 6.0 Hz,-OCH_2), 7.13−7.39 (m_{br}, 15H, -C*H*).

^{1}H{^{31}P} NMR (500 MHz, 298 K, $CDCl_3$): δ (ppm) = 2.65 (ddd, 1H, $^2J_{H\text{-}H}$ = 14.7 Hz, $^3J_{H\text{-}H}$ = 9.0 Hz, $^3J_{H\text{-}H}$ = 5.9 Hz,-PCH_2), 3.00 (ddd, 1H, $^2J_{H\text{-}H}$ = 14.8 Hz, $^3J_{H\text{-}H}$ = 9.1 Hz, $^3J_{H\text{-}H}$ = 5.9 Hz,-PCH_2), 4.01 (ddd, 1H, $^3J_{H\text{-}H}$ = 9.0 Hz, $^3J_{H\text{-}H}$ = 5.9 Hz, $^2J_{H\text{-}H}$ = 5.9 Hz,-OCH_2), 4.38 (ddd, 1H, $^3J_{H\text{-}H}$ = 9.1 Hz, $^3J_{H\text{-}H}$ = 6.0 Hz, $^2J_{H\text{-}H}$ = 6.0 Hz,-OCH_2), 7.13−7.39 (m_{br}, 15H, -C*H*).

^{13}C NMR (126 MHz, 298 K, $CDCl_3$): δ (ppm) = 33.4 (d, $^1J_{P-C}$ = 60.8 Hz, -P*C*H$_2$), 62.9 (d, $^2J_{P-C}$ = 22.1 Hz, -O*C*H$_2$), 77.4 (*,-*C*Ph$_3$), 127.8 (d, $^5J_{P-C}$ = 1.9 Hz, *para*-*C*H), 128.7 (d, $^4J_{P-C}$ = 1.6 Hz, *meta*-*C*H), 129.8 (d, $^3J_{P-C}$ = 6.5 Hz, *ortho*-*C*H), 140.3 (s, *ipso*-*C*).

*: Overlaps with the solvent signal of $CDCl_3$ (δ=77.2, t), only visible as slight shoulder, second peak of expected doublet signals totally obscured.

^{31}P{^{1}H} NMR (202 MHz, 298 K, $CDCl_3$): δ (ppm) = 70.8 (s).

^{31}P NMR (202 MHz, 298 K, $CDCl_3$): δ (ppm) = 70.8 (m).

5.5.3.2 Synthesis of 4-methyl-2-(triphenylmethyl)-1,2-oxaphosphetane *P*-oxide (**10c,c'**)

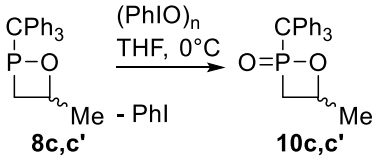

Synthesis: 166.2 mg **8c,c'** (0.5 mmol, 1 eq) were dissolved in 15 mL THF and cooled to 0°C. 132.0 mg (0.6 mmol, 1.2 eq) iodosylbenzene ((PhIO)$_n$) were added to the cooled solution. The reaction mixture was stirred at 0°C for 28 h. After that, all volatiles were removed *in vacuo* (0.02 mbar) at 0°C.

Purification: The crude product was washed at 0°C; first twice with a mixture of 5 mL *n*-pentane and 1 mL Et_2O, then twice with 5 mL pure *n*-pentane. After removal of solvent *in vacuo* (0.02 mbar) at 0 °C, the product was obtained as white solid.

Reaction cipher: FLG-341 (13p5a023.22)

Molecular formula: $C_{22}H_{21}O_2P$

Molecular weight: 348.38 g/mol

Yield: 86.3 mg, 0.25 mmol, 50%.

Ratio (Isomer 1: Isomer 2) = 66:34.

MS (ESI+) m/z (%) : 243.1 (100) $[CPh_3]^+$, 349.1 (25) $[M+H]^+$, 371.1 (8) $[M+Na]^+$.

HRMS (APCI) : theor./exp. 349.1352/349.1356 $[M+H]^+$.

^{1}H NMR (500 MHz, 298 K, $CDCl_3$): δ (ppm) = (**Isomer 1**) 1.52 (d, 3H, $^3J_{H-H}$= 6.2 Hz, -C*H*$_3$), 2.53 (m, 1H, -C*H*$_2$), 2.75 (ddd, 1H, $^2J_{H-H}$= 14.5 Hz, $^2J_{P-H}$= 9.7 Hz, $^3J_{H-H}$= 7.8 Hz, -C*H*$_2$), 4.25 (m, 1H, -C*H*), 7.28−7.42 (m, 15H, -C*H*); (**Isomer 2**) 1.14 (d, 3H, $^3J_{H-H}$= 6.3 Hz, -C*H*$_3$), 2.56 (m, 1H, -C*H*$_2$), 2.96 (ddd, 1H, $^2J_{P-H}$= 16.6 Hz, $^2J_{H-H}$= 13.9 Hz, $^3J_{H-H}$= 6.8 Hz, -C*H*$_2$), 5.04 (m, 1H, -C*H*), 7.28−7.42 (m, 15H, -C*H*).

^{1}H{^{31}P} NMR (500 MHz, 298 K, $CDCl_3$): δ (ppm) = (**Isomer 1**) 1.52 (d, 3H, $^3J_{H-H}$= 6.1 Hz, -C*H*$_3$), 2.53 (dd, 1H, $^2J_{H-H}$= 14.5 Hz, $^3J_{H-H}$= 2.0 Hz, -C*H*$_2$), 2.75 (dd, 1H, $^2J_{H-H}$= 14.5 Hz, $^3J_{H-H}$= 7.8 Hz, -C*H*$_2$), 4.25 (dq, 1H, $^3J_{H-H}$= 7.9 Hz, $^3J_{H-H}$= 6.1 Hz -C*H*), 7.28−7.42 (m, 15H, -C*H*); (**Isomer 2**) 1.14 (d, 3H, $^3J_{H-H}$= 6.3 Hz, -C*H*$_3$), 2.56 (dd, 1H, $^2J_{H-H}$= 14.3 Hz, $^3J_{H-H}$= 5.2 Hz, -C*H*$_2$), 2.96 (dd, 1H, $^2J_{H-H}$= 13.9 Hz, $^3J_{H-H}$= 6.8 Hz, -C*H*$_2$), 5.04 (m, 1H, -C*H*), 7.28-7.42 (m, 15H, −C*H*).

^{13}C NMR (126 MHz, 298 K, $CDCl_3$): δ (ppm) = (**Isomer 1**) 24.7 (d, $^3J_{P-C}$= 4.1 Hz, -*C*H$_3$), 39.5 (d, $^1J_{P-C}$= 60.8 Hz, -*C*H$_2$), 65.6 (d, $^1J_{P-C}$= 73.3 Hz, -*C*Ph$_3$), 72.1 (d, $^2J_{P-C}$= 20.2 Hz, -*C*H), 127.7 (d, $^5J_{P-C}$= 2.2 Hz, *para*-*C*H), 128.6 (d, $^4J_{P-C}$= 1.4 Hz, *meta*-*C*H), 130.6 (d, $^3J_{P-C}$= 6.6 Hz, *ortho*-*C*H), 140.5 (d, $^2J_{P-C}$= 3.0 Hz, *ipso*-*C*); (**Isomer 2**) 21.2 (d, $^3J_{C-H}$= 13.1 Hz, -*C*H$_3$), 38.9 (d, $^1J_{P-C}$= 64.0 Hz, -*C*H$_2$), 66.2 (d, $^1J_{P-C}$= 71,9 Hz, -*C*Ph$_3$), 74.3 (d, $^2J_{P-C}$= 20.2 Hz, -*C*H), 127.7 (d, $^5J_{P-C}$= 2.2 Hz, *para*-*C*H), 128.5 (d, $^4J_{P-C}$= 1.4 Hz, *meta*-*C*H), 131.1 (d, $^3J_{P-C}$= 6.3 Hz, *ortho*-*C*H), 140.3 (d, $^2J_{P-C}$= 3.0 Hz, *ipso*-*C*).

^{31}P{^{1}H} NMR (202 MHz, 298 K, $CDCl_3$): δ (ppm) = (**Isomer 1**) 62.1; (**Isomer 2**) 63.5.

5.5.3.3 Synthesis of 2-(triphenylmethyl)-1,2-oxaphosphetane P-sulfide (**11a**)

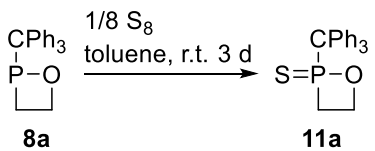

8a **11a**

Synthesis: 0.1592 g (0.5 mmol, 1eq) **8a** were dissolved in 5 mL toluene. To that, 16.0 mg S_8 (0.61 mmol, 1 eq) were added. The reaction was stirred for 3 d. After that, the solvent was removed *in vacuo* (0.02 mbar).

Purification: The crude product was washed at r.t; first thrice with 3 mL Et_2O, then twice with 3 mL *n*-pentane. After removal of solvent *in vacuo* (0.02 mbar), the product was obtained as yellow solid.

Reaction cipher: FLG-399 (39p5a023.22)

Molecular formula: $C_{21}H_{19}OPS$

Molecular weight: 350.42 g/mol

Yield: 70.6 mg, 0.20 mmol, 40%.

MS (APCI) m/z (%) : 243.117 (100) $[CPh_3]^+$, 351.096 (3) $[M+H]^{+\cdot}$.

HRMS (ESI+): theor./exp. 351.0967/351.0963 $[M+H]^+$.

^{1}H NMR (500 MHz, 298 K, C_6D_6): δ (ppm) = 2.48 (m, 2H, -PC*H*$_2$), 3.55 (m, 1H, -OC*H*$_2$), 3.92 (m, 1H,-OC*H*$_2$), 7.03 (m, 9H, -C*H*), 7.59 (d_{br}, 6H, $^3J_{H\text{-}H}$ = 7.7 Hz, -C*H*).

^{1}H{^{31}P} NMR (500 MHz, 298 K, C_6D_6): δ (ppm) = 2.48 (m, 2H, -PC*H*$_2$), 3.55 (m, 1H, -OC*H*$_2$), 3.92 (m, 1H, -OC*H*$_2$), 7.03 (m, 9H, -C*H*), 7.59 (d_{br}, 6H, $^3J_{H\text{-}H}$ = 7.7 Hz, -C*H*).

^{13}C NMR (126 MHz, 298 K, C_6D_6): δ (ppm) = 38.4 (d, $^1J_{P\text{-}C}$ = 50.4 Hz, -P*C*H$_2$), 64.9 (d, $^2J_{P\text{-}C}$ = 21.5 Hz, -O*C*H$_2$), 70.03 (d, $^1J_{P\text{-}C}$ = 46.6 Hz, -*C*Ph$_3$), 127.6 (d, $^5J_{P\text{-}C}$ = 2.5 Hz, *para*-*C*H), 128.4 (s, *meta*-*C*H), 131.3 (d, $^3J_{P\text{-}C}$ = 6.8 Hz, *ortho*-*C*H), 141.8 (d, $^2J_{P\text{-}C}$ = 1.6 Hz, *ipso*-*C*).

^{31}P{^{1}H} NMR (202 MHz, 298 K, C_6D_6): δ (ppm) = 129.8 (s).

^{31}P NMR (202 MHz, 298 K, C_6D_6): δ (ppm) = 129.8 (m).

Single crystal measurement: FLG-399, bad structure (DE1), GSTR785, GXray7060

5.5.3.4 Synthesis of 4-methyl-2-(triphenylmethyl)-1,2-oxaphosphetane *P*-sulfide (**11c,c'**)

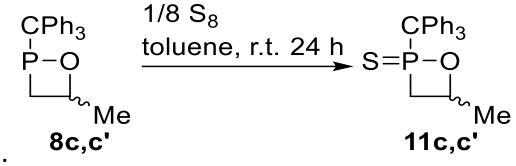

Synthesis: 0.2028 mg (0,61 mmol, 1eq) **8c,c'** were dissolved in 3 mL toluene. To that, 19.6 mg S_8 (0.61 mmol, 1 eq) were transferred with 5 times 3 mL toluene. The reaction was stirred for 24h. After that, the solvent was removed *in vacuo* (0.02 mbar).

Purification: To help remove further traces of solvent, 10 mL of n-pentane were added. After removal of solvent *in vacuo* (0.02 mbar), the product was obtained as brown solid.

Reaction cipher: FLG-333 (Original data lost with old hard drive, data taken from ESI for "1,2$\sigma^3\lambda^3$-Oxaphosphetanes and Their P-Chalcogenides—A Combined Experimental and Theoretical Study", Molecules, DOI: 10.3390/molecules27103345)

Molecular formula: $C_{22}H_{21}OPS$

Molecular weight: 364.44 g/mol

Ratio (Isomer 1: Isomer 2) = 40:60.

MS (ESI+) m/z (%) : 243.1 (100) $[CPh_3]^+$, 365.1 (5) $[M+H]^+$, 387.1 (7) $[M+Na]^+$.

HRMS (ESI+): theor./exp. 365.1123/365.1115 $[M+H]^+$.

^{1}H NMR (500 MHz, 298 K, C_6D_6): δ (ppm) = (**Isomer 1**) 0.75 (d, 3H, $^3J_{H-H}$= 6.2 Hz, -C*H*$_3$), 2.50 (m, 2H, -C*H*$_2$), 4.78 (m, 1H, -C*H*), 7.05 (m, 9H, *meta*/*para*-C*H*), 7.62 (m, 6H, *ortho*-C*H*); (**Isomer 2**) 1.21 (d, 3H, $^3J_{H-H}$= 6.1 Hz, -C*H*$_3$), 2.22 (ddd, 1H, $^2J_{P-H}$= 14.4 Hz, $^2J_{H-H}$= 14.4 Hz, $^3J_{H-H}$= 4.9 Hz, -C*H*$_2$), 2.72 (ddd, 1H, $^2J_{H-H}$= 13.6 Hz, $^2J_{P-H}$= 11.7 Hz, $^3J_{H-H}$= 8.3 Hz, -C*H*$_2$), 4.05 (m, 1H, -C*H*), 7.05 (m, 9H, *meta*/*para*-C*H*), 7.62 (m, 6H, *ortho*-C*H*).

^{13}C NMR (126 MHz, 298 K, C_6D_6): δ (ppm) = (**Isomer 1**) 21.4 (d, $^3J_{P-C}$= 13.5 Hz, -*C*H$_3$), 44.8 (d, $^1J_{P-C}$= 51.5 Hz, -*C*H$_2$), 70.4 (d, $^1J_{P-C}$= 46.0 Hz, -*C*Ph$_3$), 75.2 (d, $^2J_{P-C}$= 19.4 Hz, -*C*H), 127.6 (d, $^5J_{P-C}$= 2.1 Hz, *para*-*C*H), 128.3 (d, $^4J_{P-C}$= 1.1 Hz, *meta*-*C*H), 131.9 (d, $^3J_{P-C}$= 6.9 Hz, *ortho*-*C*H), 141.6 (d, $^2J_{P-C}$= 1.4 Hz, *ipso*-*C*); (**Isomer 2**) 24.7 (d, $^3J_{C-H}$= 3.3 Hz, -*C*H$_3$), 44.4 (d, $^1J_{P-C}$= 49.8 Hz, -*C*H$_2$) , 69.8 (d, $^1J_{P-C}$= 47.8 Hz, -*C*Ph$_3$), 74.5 (d, $^2J_{P-C}$= 19.9 Hz, -*C*H), 127.6 (d, $^5J_{P-C}$= 2.1 Hz, *para*-*C*H), 128.3 (d, $^4J_{P-C}$= 1.0 Hz, *meta*-*C*H), 131.4 (d, $^3J_{P-C}$= 6.7 Hz, *ortho*-*C*H), 141.9 (d, $^2J_{P-C}$= 1.4 Hz, *ipso*-*C*).

^{31}P{^{1}H} NMR (202 MHz, 298 K, C_6D_6): δ (ppm) = (**Isomer 1**) 115.8; (**Isomer 2**) 120.0.

5.5.3.5 Synthesis of 4-methyl-2-(triphenylmethyl)-1,2-oxaphosphetane *P*-selenide (**12c,c'**)

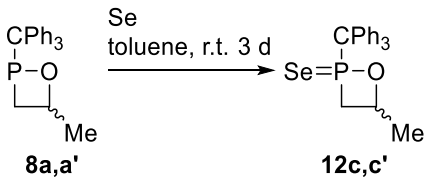

Synthesis: 40.0 mg (0.5 mmol, 1 eq) selenium were placed in a Schlenk-tube. 167.0 mg (0.5 mmol, 1 eq) **8c,c'** were transferred to the selenium with five times 2 mL toluene. The reaction was stirred for 3 d.

Purification: The reaction solution was filtrated to remove remaining selenium metal. After removal of solvent *in vacuo* (0.02 mbar), the product was obtained as yellow solid.

Reaction cipher: FLG-334 (Original data lost with old hard drive, data taken from ESI for "1,2$\sigma^3\lambda^3$-Oxaphosphetanes and Their P-Chalcogenides—A Combined Experimental and Theoretical Study", Molecules, DOI: 10.3390/molecules27103345)

Molecular formula: $C_{22}H_{21}OPSe$

Molecular weight: 411.35 g/mol

Ratio (Isomer 1: Isomer 2) = 30:70.

MS (LIFDI) m/z (%) : 243.1 (70) $[CPh_3]^+$, 412.1 (10) $[M]^{+\cdot}$.

HRMS (ESI+): theor./exp. 413.0568/413.0558 $[M+H]^+$.

^{1}H NMR (500 MHz, 298 K, C_6D_6): δ (ppm) = (**Isomer 1**) 0.75 (d, 3H, $^3J_{H-H}$= 6.3 Hz, -C*H*$_3$), 2.62 (ddd, 1H, $^2J_{P-H}$= 12.3 Hz, $^2J_{H-H}$= 12.3 Hz, $^3J_{H-H}$= 6.4 Hz, -C*H*$_2$), 2.74 (ddd, 1H, $^2J_{P-H}$= 13.0 Hz, $^2J_{H-H}$= 13.0 Hz, $^3J_{H-H}$= 8.2 Hz, -C*H*$_2$), 4.89 (m, 1H, -C*H*), 7.05 (m, 9H, *meta*/*para*-C*H*), 7.63 (m, 6H, *ortho*-C*H*); (**Isomer 2**) 1.27 (d, 3H, $^3J_{H-H}$= 6.2 Hz, -C*H*$_3$), 2.42 (ddd, 1H, $^2J_{P-H}$= 15.0 Hz, $^2J_{H-H}$= 13.7 Hz, $^3J_{H-H}$= 5.1 Hz, -C*H*$_2$), 2.98 (ddd, 1H, $^2J_{H-H}$= 13.8 Hz, $^2J_{P-H}$= 12.3 Hz, $^3J_{H-H}$= 8.3 Hz, -C*H*$_2$), 4.26 (m, 1H, -C*H*), 7.05 (m, 9H, *meta*/*para*-C*H*), 7.63 (m, 6H, *ortho*-C*H*).

^{13}C NMR (126 MHz, 298 K, C_6D_6): δ (ppm) = (**Isomer 1**) 21.7 (d, $^3J_{P-C}$= 12.7 Hz, -*C*H$_3$), 45.6 (d, $^1J_{P-C}$= 44.6 Hz, -*C*H$_2$), 70.4 (d, $^1J_{P-C}$= 33.4 Hz, -*C*Ph$_3$), 76.1 (d, $^2J_{P-C}$= 19.4 Hz, -*C*H), 127.7 (d, $^5J_{P-C}$= 2.2 Hz, *para*-*C*H), 128.3 (d, $^4J_{P-C}$= 1.2 Hz, *meta*-*C*H), 131.8 (d, $^3J_{P-C}$= 7.0 Hz, *ortho*-*C*H), 141.3 (d, $^2J_{P-C}$= 0.5 Hz, *ipso*-*C*); (**Isomer 2**) 24.8 (d, $^3J_{C-H}$= 3.1 Hz, -*C*H$_3$), 44.6 (d, $^1J_{P-C}$= 43.5 Hz, -*C*H$_2$), 69.8 (d, $^1J_{P-C}$= 35.4 Hz, -*C*Ph$_3$), 76.1 (d, $^2J_{P-C}$= 19.4 Hz, -*C*H), 127.7 (d, $^5J_{P-C}$= 2.1 Hz, *para*-*C*H), 128.3 (d, $^4J_{P-C}$= 1.1 Hz, *meta*-*C*H), 131.3 (d, $^3J_{P-C}$= 6.9 Hz, *ortho*-*C*H), 146.7 (d, $^2J_{P-C}$= 0.5 Hz, *ipso*-*C*).

^{31}P{^{1}H} NMR (202 MHz, 298 K, C_6D_6): δ (ppm) = (**Isomer 1**) 115.8 (s_{sat}, $^1J_{Se-P}$= 839.7 Hz); (**Isomer 2**) 121.5 (s_{sat}, $^1J_{Se-P}$= 846.4 Hz).

^{77}Se{^{1}H} NMR (95 MHz, 298 K, C_6D_6): δ (ppm) = (**Isomer 1**) −10.7 (d_t, $^1J_{Se-P}$= 839.8 Hz); (**Isomer 2**) 79.4 (d, $^1J_{Se-P}$= 845.8 Hz).

5.5.3.6 Attempted synthesis of 4-methyl-2-(triphenylmethyl)-1,2-oxaphosphetane *P*-telluride (**13c,c'**)

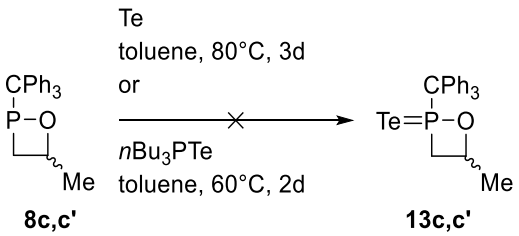

Synthesis: 0.0667 g (0.2 mmol, 1 eq) **8c,c'** and 0.0255 g (0.36 mmol, 1.8 eq) tellurium were added to a Schlenk-tube and 3 mL toluene were added. The reaction was stirred for 3 d. After that, the solvent was removed *in vacuo* (0.02 mbar). After stirring at 80°C for 3 d, no reaction was observed.

Reaction cipher: FLG-124 (Original data lost with old hard drive)

or

Synthesis: 0.0667 g (0.2 mmol, 1eq) **8c,c'** and 0.0660 g (0.2 mmol, 1. eq) tri-*n*-butylphosphane telluride were added to a Schlenk-tube and 5 mL toluene were added. After stirring at 60°C for 2 d, only partial hydrolysis could be observed.

Reaction cipher: FLG-154 (32m3a050.20)

5.5.3.7 Synthesis of 2-(triphenylmethyl)-1,2-oxaphosphetane P-borane (**14a**)

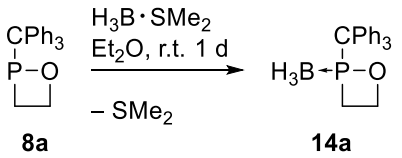

8a **14a**

Synthesis: 0.0955 g (0.3 mmol, 1 eq) **8a** were dissolved in Et_2O. 0.03 mL (0.3 mmol, 1.0 eq) $H_3B{\cdot}SMe_2$ were added. The reaction was stirred for 1 d, followed by removal of all volatiles *in vacuo* (0.02 mbar).

Purification: The crude product was washed at room temperature, twice with a mixture of 2.5 mL Et_2O and 2.5 mL *n*-pentane, and once with 5 mL pure *n*-pentane. After removal of all volatiles *in vacuo* (0.02 mbar), the product was obtained as off-white solid.

Reaction cipher: FLG-363 (18p5a053.22)

Molecular formula: $C_{21}H_{22}BOP$

Molecular weight: 332.19 g/mol

Yield: 48.9 mg, 0.15 mmol, 50%.

IR (ATR Diamond, selected data): $\tilde{\nu}$ (cm^{-1}) = 2341 (w, ν(B-H)), 2377 (w, ν(B-H)), 2423 (w, ν(B-H)), 2855 (w, ν(C-H)), 2927 (w, ν(C-H)), 3060 (w, ν(C-H)).

^{1}H NMR (500 MHz, 298 K, $CDCl_3$): δ (ppm) = 1.07 (s_{br}, 3H, -BH_3), 2.72 (dddd, 1H, $^{2}J_{H-H}$= 13.4 Hz, $^{2}J_{P-H}$= 11.4 Hz, $^{3}J_{H-H}$= 10.1 Hz, $^{3}J_{H-H}$= 6.7 Hz, -PCH_2), 2.98 (dddd, 1H, $^{2}J_{H-H}$= 12.0 Hz, $^{3}J_{H-H}$= 5.7 Hz, $^{3}J_{H-H}$= 5.7 Hz, $^{2}J_{P-H}$= 2.9 Hz, -PCH_2), 4.54 (dddd, 1H, $^{3}J_{H-H}$= 10.0 Hz, $^{3}J_{P-H}$= 6.6 Hz, $^{2}J_{H-H}$= 6.6 Hz, $^{3}J_{H-H}$= 6.6 Hz, -OCH_2), 4.98 (dddd, 1H, $^{3}J_{P-H}$= 8.6 Hz, $^{2}J_{H-H}$= 6.6 Hz, $^{3}J_{H-H}$= 6.6 Hz, $^{3}J_{H-H}$= 6.6 Hz, -OCH_2), 7.30−7.39 (m, 15H, -C*H*).

^{1}H{^{31}P} NMR (500 MHz, 298 K, $CDCl_3$): δ (ppm) = 1.06 (s_{br}, 3H, -BH_3), 2.72 (ddd, 1H, $^{2}J_{H-H}$= 13.5 Hz, $^{3}J_{H-H}$= 10.1 Hz, $^{3}J_{H-H}$= 6.7 Hz, -PCH_2), 2.98 (ddd, 1H, $^{2}J_{H-H}$= 13.9 Hz, $^{3}J_{H-H}$= 7.3 Hz, $^{3}J_{H-H}$= 7.3 Hz, -PCH_2), 4.54 (ddd, 1H, $^{3}J_{H-H}$= 11.7 Hz, $^{2}J_{H-H}$= 6.1 Hz, $^{3}J_{H-H}$= 6.1 Hz, -OCH_2), 4.98 (ddd, 1H, $^{2}J_{H-H}$= 7.1 Hz, $^{3}J_{H-H}$= 7.1 Hz, $^{3}J_{H-H}$= 7.1 Hz, -OCH_2), 7.30−7.39 (m, 15H, -C*H*).

^{13}C NMR (126 MHz, 298 K, $CDCl_3$): δ (ppm) = 27.9 (d, $^{1}J_{P-C}$= 33.5 Hz, -P*C*H_2), 64.2 (d, $^{1}J_{P-C}$= 6.8 Hz, -*C*Ph_3), 71.1 (d, $^{2}J_{P-C}$= 16.1 Hz, -O*C*H_2), 127.8 (d, $^{5}J_{P-C}$= 1.9 Hz, *para*-*C*H), 128.6 (s, *meta*-*C*H), 130.2 (d, $^{3}J_{P-C}$= 6.0 Hz, *ortho*-*C*H), 140.0 (s, *ipso*-*C*).

^{31}P{^{1}H} NMR (202 MHz, 298 K, $CDCl_3$): δ (ppm) = 182.7 (d, $^{1}J_{P-B}$= 40.5 Hz).

^{31}P NMR (202 MHz, 298 K, $CDCl_3$): δ (ppm) = 182.7 (s_{br}).

^{11}B{^{1}H} NMR (160 MHz, 298 K, $CDCl_3$): δ (ppm) = −32.9 (s_{br}).

Single crystal measurement: FLG-363, very good structure (A1), GSTR769, GXraycu_6906f

5.5.3.8 Synthesis of 4-methyl-2-(triphenylmethyl)-1,2-oxaphosphetane borane (**14c,c'**)

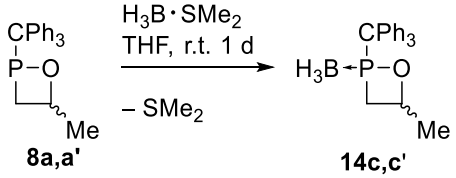

Synthesis: 0.3324 g (1.0 mmol, 1 eq) **8a** were dissolved in 10 mL THF. 0.09 mL (1.0 mmol, 1.0 eq) $H_3B{\cdot}SMe_2$ were added. The reaction was stirred for 1 d, followed by removal of all volatiles *in vacuo* (0.02 mbar)

Purification: The crude product was washed at room temperature three times with 10 mL *n*-pentane. After removal of all volatiles *in vacuo* (0.02 mbar), the product was obtained as off-white solid.

Yield: 192.1 mg, 0.55 mmol, 55%.

Molecular formula: $C_{22}H_{24}BOP$

Molecular weight: 346.22 g/mol

Reaction cipher: FLG-251 (24p5a048.21)

Ratio (Isomer 1: Isomer 2) = 19:81.

^{1}H NMR (500 MHz, 298 K, $CDCl_3$): δ (ppm) = (**Isomer 1**) 1.06 (s_{br}, 3H, -B*H*$_3$), 1.29 (d, 3H, $^{3}J_{H\text{-}H}$= 6.3 Hz, -C*H*$_3$), 2.59 (ddd, 1H, $^{2}J_{P\text{-}H}$= 13.4 Hz, $^{2}J_{H\text{-}H}$= 13.4 Hz, $^{3}J_{H\text{-}H}$= 8.2 Hz, -C*H*$_2$), 2.89 (ddd, 1H, $^{3}J_{H\text{-}H}$= 13.0 Hz, $^{3}J_{H\text{-}H}$= 6.5 Hz, $^{2}J_{P\text{-}H}$= 2.7 Hz, -C*H*$_2$), 5.27 (m, 1H, -OC*H*), 7.30−7.39 (m, 15H, -C*H*); (**Isomer 2**) 0.84 (s_{br}, 3H, -B*H*$_3$) 1.64 (d, 3H, $^{3}J_{H\text{-}H}$= 6.3 Hz, -C*H*$_3$), 2.66 (ddd, 1H, $^{2}J_{H\text{-}H}$= 13.3 Hz, $^{3}J_{H\text{-}H}$= 5.5 Hz, $^{2}J_{P\text{-}H}$= 3.5 Hz, -C*H*$_2$), 2.82 (ddd, 1H, $^{2}J_{H\text{-}H}$= 13.2 Hz, $^{2}J_{P\text{-}H}$= 13.0 Hz, $^{3}J_{H\text{-}H}$= 8.7 Hz, -C*H*$_2$), 4.83 (m, 1H, -OC*H*), 7.30−7.39 (m, 15H, -C*H*).

^{13}C NMR (126 MHz, 298 K, $CDCl_3$): δ (ppm) = (**Isomer 1**) 23.6 (d, $^{3}J_{P\text{-}C}$= 5.2 Hz, -*C*H$_3$), 36.2 (d, $^{1}J_{P\text{-}C}$= 30.3 Hz, -*C*H$_2$), 64.3 (d, $^{1}J_{P\text{-}C}$= 5.5 Hz, -*C*Ph$_3$), 79.0 (d, $^{2}J_{P\text{-}C}$= 15.0 Hz, -*C*H), 127.9 (d, $^{5}J_{P\text{-}C}$= 1.9 Hz, *para*-*C*H), 128.6 (s, *meta*-*C*H), 130.8 (d, $^{3}J_{P\text{-}C}$= 6.3 Hz, *ortho*-*C*H), 139.8 (s, *ipso*-*C*); (**Isomer 2**) 24.8 (d, $^{3}J_{C\text{-}H}$= 3.8 Hz, -*C*H$_3$), 34.4 (d, $^{1}J_{P\text{-}C}$= 32.7 Hz, -*C*H$_2$) , 63.8 (d, $^{1}J_{P\text{-}C}$= 7.9 Hz, -*C*Ph$_3$), 81.2 (d, $^{2}J_{P\text{-}C}$= 15.2 Hz, -*C*H), 127.8 (d, $^{5}J_{P\text{-}C}$= 1.9 Hz, *para*-*C*H), 128.6 (s, *meta*-*C*H), 130.4 (d, $^{3}J_{P\text{-}C}$= 6.3 Hz, *ortho*-*C*H), 140.4 (s, *ipso*-*C*).

^{31}P{^{1}H} NMR (202 MHz, 298 K, $CDCl_3$): δ (ppm) = (**Isomer 1**) 153.4 (s_{br}); (**Isomer 2**) 169.4 (s_{br}).

^{31}P NMR (202 MHz, 298 K, $CDCl_3$): δ (ppm) = (**Isomer 1**) 153.4 (s_{br}); (**Isomer 2**) 169.4 (s_{br}).

^{11}B{^{1}H} NMR (160 MHz, 298 K, $CDCl_3$): δ (ppm) = (**Isomer 1**) −34.5 (s_{br}); (**Isomer 2**) −32.0 (s_{br}).

5.5.4 Synthesis of Arbuzov-products and oligomers

5.5.4.1 Synthesis of 2-bromoethyl(2-methoxy-2-oxoethyl)(triphenylmethyl)phosphane oxide (**19a**)

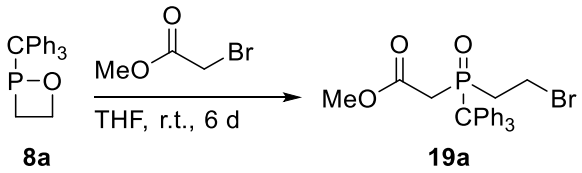

8a **19a**

Synthesis: 111.4 mg (0.35 mmol, 1 eq) **8a** were dissolved in 10 mL THF, and 0.21 mL (2.24 mmol, 1 eq) methyl 2-bromoacetate were added at room temperature. The reaction was stirred for 6 d. All volatiles were removed *in vacuo* (0.02 mbar).

Purification: 5 mL Et_2O and 5 mL *n*-pentane were added. The gooey crude product was scratched in presence of the solvents. After evaporation of solvents in vacuo (0.02 mbar), the crude product was obtained as a white powder. The crude product was washed with *n*-pentane (five times 5 mL) at ambient temperature. After drying, the product was obtained as white powder.

Reaction cipher: FLG-327 (09p5a031.22)

Molecular formula: $C_{24}H_{24}BrO_3P$

Molecular weight: 471.33 g/mol

Yield: 69.7 mg, 0.15 mmol, 42%.

MS (ESI+) m/z (%) : 243.116 (100) $[CPh_3]^+$, 471.071 (30) $[M+H]^+$, 493.052 (21) $[M+Na]^+$.

HRMS (APCI): theor./exp. 471.0719/471.0708 $[M+H]^+$.

^{1}H NMR (500 MHz, 298 K, $CDCl_3$): δ (ppm) = 2.43 (m, 1H, $BrCH_2$-CH_2), 2.48 (dd, 1H, $^2J_{H-H}$= 13.9 Hz, $^2J_{P-H}$= 10.4 Hz, -C(O)-CH_2), 2.60 (dddd, 1H, $^2J_{H-H}$= 14.7 Hz, $^2J_{P-H}$= 12.3 Hz, $^3J_{H-H}$= 12.3 Hz, $^3J_{H-H}$= 5.3 Hz, $BrCH_2$-

CH_2), 3.15 (dd, 1H, $^2J_{P\text{-}H}$= 14.4 Hz, $^2J_{H\text{-}H}$= 14.4 Hz, -C(O)-CH_2), 3.53 (m, 2H, -CH_2Br), 3.70 (s, 3H, -CH_3), 7.33 (m, 10H, -C*H*), 7.57 (s_{br}, 5H, - C*H*).

^{1}H{^{31}P} NMR (500 MHz, 298 K, $CDCl_3$): δ (ppm) = 2.43 (m, 1H, $BrCH_2$-CH_2), 2.48 (d, 1H, $^2J_{H\text{-}H}$= 13.9 Hz, -C(O)-CH_2), 2.60 (ddd, 1H, $^2J_{H\text{-}H}$= 14.7 Hz, $^3J_{H\text{-}H}$= 12.7 Hz, $^3J_{H\text{-}H}$= 5.4 Hz, $BrCH_2$-CH_2), 3.15 (d, 1H, $^2J_{H\text{-}H}$= 13.9 Hz, -C(O)-CH_2), 3.53 (m, 2H, -CH_2Br), 3.70 (s, 3H, -CH_3), 7.33 (m, 10H, -C*H*), 7.57 (s_{br}, 5H, -C*H*).

^{13}C NMR (126 MHz, 298 K, $CDCl_3$): δ (ppm) = 25.3 (s, -*C*H_2Br), 33.8 (d, $^1J_{P\text{-}C}$= 58.0 Hz, $BrCH_2$-*C*H_2), 37.6 (d, $^1J_{P\text{-}C}$= 54.0 Hz, -C(O)-*C*H_2), 52.8 (s, -*C*H_3), 63.6 (d, $^1J_{P\text{-}C}$= 60.8 Hz, -*C*Ph_3), 127.8 (s, *para*-*C*H), 128.8 (s, *meta*-*C*H), 130.5 (s, *ortho*-*C*H), 141.0 (s_{br}, *ipso*-*C*), 167.1 (d, $^2J_{P\text{-}C}$= 5.18 Hz, -*C*(O)).

^{31}P{^{1}H} NMR (202 MHz, 298 K, $CDCl_3$): δ (ppm)= 48.4 (s).

Single crystal measurement: FLG-327, excellent structure (AA1), GSTR752, GXraymo_6825f

5.5.4.2 Synthesis of 2-bromoethyl (2-oxo-2-phenylethyl)(triphenylmethyl)phosphane oxide (**19b**)

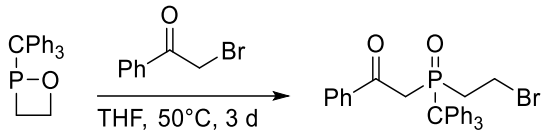

8a **19b**

Synthesis: 159.2 mg (0.5 mmol) **8a** were dissolved in 10 mL THF. 99.5 mg (0.5 mmol, 1 eq) of 2-bromoacetophenone were added at room temperature. The reaction was heated to 50°C and stirred for 3 d. All volatiles were removed *in vacuo* (0.02 mbar).

Purification: The crude product was washed at −80°C once with 10 mL *n*-pentane and thrice with a mixture of 5 mL *n*-Pentane and 2 mL Et_2O. After evaporation of all volatile components and drying *in vacuo* (0.02 mbar) the product was obtained as white powder.

Reaction cipher: FLG-350 (13p5a024.22)

Molecular formula: $C_{29}H_{26}BrO_2P$

Molecular weight: 517.40 g/mol

Yield: 136.4 mg, 0.27 mmol, 53%.

Melting Point: 157°C.

MS (ESI+) m/z (%) : 243.117 (100) $[CPh_3]^+$, 437.166 (52) $[M\text{-}Br]^+$, 519.091 (13) $[M+H]^{+}$*.

HRMS (APCI): theor./exp. 517.0927/517.0928 $[M+H]^+$.

*: program labelled ^{81}Br containing isotopomer instead of the ^{79}Br containing one.

IR (ATR Diamond, selected data): $\tilde{\nu}$ (cm^{-1}) = 1174 (m, ν(P=O), 1275 (s, ν(C-Br)),1672 (s, ν(C=O)).

^{1}H NMR (500 MHz, 298 K, $CDCl_3$): δ (ppm) = 2.44 (dddd, 1H, $^2J_{H\text{-}H}$= 14.6 Hz, $^3J_{H\text{-}H}$= 12.4 Hz, $^2J_{P\text{-}H}$= 9.3 Hz, $^3J_{H\text{-}H}$= 5.1 Hz, $BrCH_2$-CH_2), 2.56 (m, 1H, $BrCH_2$-CH_2), 2.98 (dd, 1H, $^2J_{H\text{-}H}$= 13.3 Hz, $^2J_{P\text{-}H}$= 11.1 Hz, -C(O)-CH_2), 3.32 (dddd, 1H, $^3J_{H\text{-}H}$= 12.7 Hz, $^2J_{H\text{-}H}$= 10.0 Hz, $^2J_{P\text{-}H}$= 4.9 Hz, $^3J_{H\text{-}H}$= 4.9 Hz, -CH_2Br), 3.51 (dddd, 1H, $^3J_{H\text{-}H}$= 12.4 Hz, $^2J_{H\text{-}H}$= 10.2 Hz, $^2J_{P\text{-}H}$= 5.1 Hz, $^3J_{H\text{-}H}$= 5.1 Hz, -CH_2Br), 4.07 (dd, 1H, $^2J_{P\text{-}H}$= 16.2 Hz, $^2J_{H\text{-}H}$= 13.3 Hz, -C(O)-CH_2), 7.33 (m, 10H, -CPh_2C*H*), 7.46 (t, 2H, $^3J_{H\text{-}H}$= 7.8 Hz, *meta*-C*H*), 7.58 (t, 1H, $^3J_{H\text{-}H}$= 7.4 Hz, *para*-C*H*), 7.62 (s_{br}, 5H, -CPh_2C*H*), 7.90 (d, 2H, $^3J_{H\text{-}H}$= 7.1 Hz, *ortho*-C*H*).

^{1}H{^{31}P} NMR (500 MHz, 298 K, $CDCl_3$): δ (ppm) = 2.44 (ddd, 1H, $^2J_{H\text{-}H}$= 14.8 Hz, $^3J_{H\text{-}H}$= 12.4 Hz, $^3J_{H\text{-}H}$= 5.1 Hz, $BrCH_2$-CH_2), 2.56 (ddd, 1H, $^2J_{H\text{-}H}$= 11.3 Hz, $^3J_{H\text{-}H}$= 11.3 Hz, $^3J_{H\text{-}H}$= 6.4 Hz, $BrCH_2$-CH_2), 2.98 (d, 1H, $^2J_{H\text{-}H}$= 13.3 Hz, -C(O)-CH_2), 3.32 (ddd, 1H, $^2J_{H\text{-}H}$= 11.5 Hz, $^3J_{H\text{-}H}$= 10.2 Hz, $^3J_{H\text{-}H}$= 5.1 Hz, -CH_2Br), 3.51 (ddd, 1H, $^3J_{H\text{-}H}$= 12.4 Hz, $^2J_{H\text{-}H}$= 12.4 Hz, $^3J_{H\text{-}H}$= 5.0 Hz, -CH_2Br), 4.07 (d, 1H, $^2J_{H\text{-}H}$= 13.3 Hz, -C(O)-CH_2), 7.33 (m, 10H, -CPh_2C*H*), 7.46 (t, 2H, $^3J_{H\text{-}H}$= 7.8 Hz, *meta*-C*H*), 7.58 (t, 1H, $^3J_{H\text{-}H}$= 7.4 Hz, *para*-C*H*), 7.62 (s_{br}, 5H, -CPh_2C*H*), 7.90 (d, 2H, $^3J_{H\text{-}H}$= 7.8 Hz, *ortho*-C*H*).

^{13}C NMR (126 MHz, 298 K, $CDCl_3$): δ (ppm) = 25.3 (s, -*C*H_2Br), 33.6 (d, $^1J_{P\text{-}C}$= 56.7 Hz, $BrCH_2$-*C*H_2), 40.7 (d, $^1J_{P\text{-}C}$= 51.5 Hz, -C(O)-*C*H_2), 64.0 (d, $^1J_{P\text{-}C}$= 59.1 Hz, -*C*Ph_3), 127.7 (s_{br}, *para*-*C*H), 128.7 (s_{br}, *meta*-*C*H), 128.8 (s, *meta*-*C*H), 129.3 (s, *ortho*-*C*H) 130.6 (s_{br}, *ortho*-*C*H), 133.9 (s, *para*-*C*H), 137.4 (s, -C(O)-*ipso*-*C*), 141.6 (s_{br}, Ph_3-*ipso*-*C*), 194.3 (d, $^2J_{P\text{-}C}$= 5.7, -*C*(O)).

^{31}P{^{1}H} NMR (202 MHz, 298 K, $CDCl_3$): δ (ppm)= 49.7 (s).

Single crystal measurement: FLG-350, good structure (BC1), GSTR760, GXraymo_6861f

5.5.4.3 Synthesis of 2-iodoethyl(methyl)triphenylmethyl)phosphane oxide (**19c**)

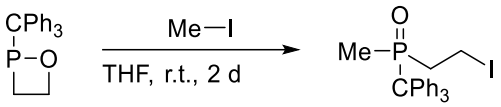

8a **19c**

Synthesis: 159.2 mg (0.5 mmol, 1 eq) **8a** were dissolved in 10 mL THF. 1.41 mL (0.5 mmol, 1 eq) iodomethane solution (0.3545 M in THF) were added at room temperature. The reaction was heated to 50°C and stirred for 2 d. All volatiles were removed *in vacuo* (0.02 mbar).

Purification: The crude product was washed four times with 10 mL *n*-pentane at −70°C. After evaporation of all volatile components and drying *in vacuo* (0.02 mbar) the product was obtained as white powder.

Reaction cipher: FLG-352 (14p5a018.22)

Molecular formula: $C_{22}H_{22}IOP$

Molecular weight: 460.30 g/mol

Yield: 93.8 mg, 0.29 mmol, 57%.

Melting Point: 149°C.

MS (APCI) m/z (%): 243.117 (100) $[CPh_3]^+$, 333.138 (2) $[M\text{-}I]^+$, 461.052 (35) $[M+H]^+$, 483.034 (5) $[M+Na]^+$.

HRMS (APCI): theor./exp. 461.0526/461.0526 $[M+H]^+$.

IR (ATR Diamond, selected data): $\tilde{\nu}$ (cm^{-1}) = 1142, (vs, ν(P=O)), 2870 (s, ν(C-H)). 2989 (s, ν(C-H)).

^{1}H NMR (500 MHz, 298 K, $CDCl_3$): δ (ppm) = 1.43 (d, 3H, $^{2}J_{P\text{-}H}$= 11.8 Hz, -C*H*$_3$) 1.99 (dddd, 1H, $^{2}J_{H\text{-}H}$= 14.8 Hz, $^{3}J_{H\text{-}H}$= 12.4 Hz, $^{2}J_{P\text{-}H}$= 7.1 Hz, $^{3}J_{H\text{-}H}$= 5.3 Hz, ICH_2-C*H*$_2$), 2.55 (dddd, 1H, $^{2}J_{P\text{-}H}$= 13.7 Hz, $^{2}J_{H\text{-}H}$= 13.1 Hz, $^{3}J_{H\text{-}H}$= 13.1 Hz, $^{3}J_{H\text{-}H}$= 4.9 Hz, ICH_2-C*H*$_2$), 3.12 (dddd, 1H, $^{3}J_{H\text{-}H}$= 12.7 Hz, $^{2}J_{P\text{-}H}$= 9.9 Hz, $^{3}J_{H\text{-}H}$= 5.5 Hz, $^{3}J_{P\text{-}H}$= 5.5 Hz, -C*H*$_2$I), 3.36 (dddd, 1H, $^{3}J_{H\text{-}H}$= 12.3, $^{2}J_{H\text{-}H}$= 9.9 Hz, $^{3}J_{P\text{-}H}$= 7.4, $^{3}J_{H\text{-}H}$= 4.8 Hz, -C*H*$_2$I), 7.30 (m, 10H, -C*H*), 7.56 (s_{br}, 5H, -C*H*).

^{1}H{^{31}P} NMR (500 MHz, 298 K, $CDCl_3$): δ (ppm) = 1.43 (s, 3H, -C*H*$_3$), 1.99 (m, 1H, ICH_2-C*H*$_2$), 2.55 (m, 1H, ICH_2-C*H*$_2$), 3.12 (m, 1H, -C*H*$_2$I), 3.36 (m, 1H, -C*H*$_2$I), 7.30 (m, 10H, -C*H*), 7.56 (s_{br}, 5H, -C*H*).

^{13}C NMR (126 MHz, 298 K, $CDCl_3$): δ (ppm) = −5.6 (d, $^{2}J_{P\text{-}C}$= 3.3 Hz, -*C*H_2I), 14.9 (d, $^{1}J_{P\text{-}C}$= 67.0 Hz, -*C*H_3), 35.4 (d, $^{1}J_{P\text{-}C}$= 57.2 Hz, ICH_2-*C*H_2), 62.9 (d, $^{1}J_{P\text{-}C}$= 59.7, -*C*Ph_3), 127.4 (s, *para*-*C*H), 128.5 (s, *meta*-*C*H), 130.6 (s, *meta*-*C*H), 142.0 (s_{br}, *ipso*-*C*).

^{31}P{^{1}H} NMR (202 MHz, 298 K, $CDCl_3$): δ (ppm)= 53.6 (s).

Single crystal measurement: FLG-352, moderate structure (DE1), GSTR830, GXray7821_1

5.5.4.4 Synthesis of 2-bromoethyl(2-(−)menthyl-2-oxoethyl)(triphenylmethyl)phosphane oxide (**19d**)

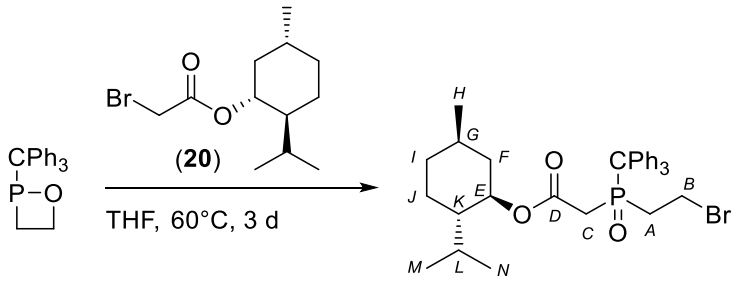

8a **19d,d'**

Synthesis: 127.3 mg (0.4 mmol, 1 eq) **8a** were dissolved in 5 mL THF. 332 mg (1.2 mmol, 3 eq) (−)menthyl bromoacetate were added. The reaction was stirred at 70°C for 3 d. All volatiles were removed *in vacuo* (0.02 mbar).

Purification: The crude product was purified by washing at −50°C with first 10 mL Et_2O, a mixture of 10 mL Et_2O and 10 mL *n*-pentane, and lastly 10 mL of pure *n*-pentane. The product could be obtained as off-white solid.

Reaction cipher: FLG-478 (FLG230621t4a007, FLG230621c5a022)

Molecular formula: $C_{33}H_{40}BrO_3P$

Molecular weight: 595.56 g/mol

Yield: 77.4 mg (0.13 mmol, 32%)

MS (APCI) m/z (%): 243.116 (100) $[CPh_3]^+$, 515.276 (7) $[M\text{-}Br]^+$, 595.196 (9) $[M+H]^+$.

HRMS (APCI): theor./exp. 595.1971/595.1969 $[M+H]^+$.

Ratio: 48:52.

Comment: The NMR spectra were recorded using a mixture of diastereomers which are very similar and in nearly identical ratio. With this information, it was not possible to assign signals to one isomer or the other. In the following, each atom will be assigned two shifts, one for each isomer

^{1}H NMR (400 MHz, 298 K, $CDCl_3$): δ (ppm) = 0.74 (d, 3H, $^3J_{H\text{-}H}$= 6.9 Hz, *H*-C*H*$_3$), 0.78 (d, 3H, $^3J_{H\text{-}H}$= 6.9 Hz, *H*-C*H*$_3$), 0.91 (m, 14H, *N/M*-C*H*$_3$ and *I*-C*H*$_2$), 1.00 (m, 1H, *F*-C*H*$_2$), 1.06 (m,2H, *J*-C*H*$_2$), 1.14 (m, 1H, *F*-C*H*$_2$), 1.41 (m, 2H, *K*-C*H*), 1.46 (m, 2H, *G*-C*H*), 1.68 (m, 4H, *I*-C*H*$_2$ and *J*-C*H*$_2$), 1.85 (m, 2H, *L*-C*H*), 1.97 (m, 2H, *L*-C*H*), 2.08 (m, 2H, *F*-C*H*$_2$), 2.39 (m, 2H, *C*-C*H*$_2$), 2.48 (m, 2H, *A*-C*H*$_2$), 2.60 (m, 2H, *A*-C*H*$_2$), 3.14 (m, 2H, *C*-C*H*$_2$), 3.49 (m, 2H, *B*-C*H*$_2$), 3.58 (m, 2H, *B*-C*H*$_2$), 4.73 (m, 2H, *E*-C*H*), 7.23-7.95 (m, 30H, aromatic -C*H*).

^{13}C NMR (126 MHz, 298 K, $CDCl_3$): δ (ppm) = 16.1 (s, *H*-CH_3), 16f.3 (s, *H*-CH_3), 20.8 (s, *M*-CH_3), 20.9 (s, *M*-CH_3), 22.0 (s, *N*-CH_3), 22.0 (s, *N*-CH_3), 23.2 (s, *J*-CH_2), 23.4 (s, *J*-CH_2), 25.3 (s, *B*-CH_2), 25.4 (s, *B*-CH_2), 26.1 (s, *L*-CH), 26.2 (s, *L*-CH), 31.5 (s, g-CH), 31.5 (s, g-CH), 34.1 (d, $^1J_{P\text{-}C}$= 57.5 Hz, *A*-CH_2), 34.2 (s, *I*-CH_2), 34.2 (s, *I*-CH_2), 34.3 (d, $^1J_{P\text{-}C}$= 57.8 Hz, *A*-CH_2), 38.1 (d, $^1J_{P\text{-}C}$= 53.4 Hz, *C*-CH_2), 38.2 (d, $^1J_{P\text{-}C}$= 54.2 Hz, *C*-CH_2), 40.7 (s, *F*-CH_2), 46.9 (s, *K*-CH_2), 47.0 (s, *K*-CH_2), 63.6 (d, $^1J_{P\text{-}C}$= 60.2 Hz, -CPh_3), 63.7 (d, $^1J_{P\text{-}C}$= 60.5 Hz, -CPh_3), 76.2 (s, *E*-CH), 76.4 (s, *E*-CH), 127.6 (s, *para*-CH), 128.7 (s, *meta*-CH), 130.4 (s, *ortho*-CH), 141.9 (s_{br}, *ipso*-*C*), 166.0 (d, $^2J_{P\text{-}C}$= 5.2 Hz, *D*-*C*), 166.4 (d, $^2J_{P\text{-}C}$= 5.5 Hz, *D*-*C*).

^{31}P{^{1}H} NMR (202 MHz, 298 K, $CDCl_3$): δ (ppm)= 48.0 (s), 48.4 (s).

5.5.4.5 Synthesis of methylated oligo-(2-triphenylmethyl-1,2-oxaphosphetane) triflate **22^n**

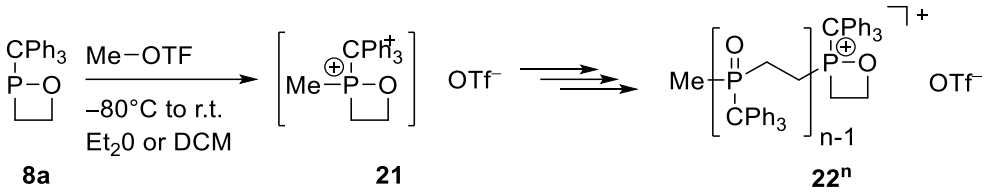

8a **21** **22^n**

Synthesis: 63.7 mg (0.2 mmol, 1 eq) **8a** were dissolved in 5 mL DCM, the solution was cooled to −80°C. 0.02 mL (0.2 mmol, 1 eq) methyl triflate were added. After warming up to ambient temperature, all volatiles were evaporated *in vacuo* (0.02 mbar)

Purification: The crude product was washed with Et_2O (three times 5 mL) at ambient temperature. The oligomers of **27^n** were obtained as pale-yellow solid.

5.5.4.6 Synthesis of 2-chloroethyl(2-oxopropyl)(triphenylmethyl)phosphane oxide (**19e**)

8a **19e**

Synthesis: 111.4 mg (0.35 mmol, 1 eq) **8a** were dissolved in 3 mL THF. 0.09 mL (1.05 mmol, 3 eq) chloroacetone were added at room temperature. The reaction was stirred at heated to 70°C for 7 d. All volatiles were removed *in vacuo* (0.02 mbar).

Purification: The crude product was suspended in a mixture of 5 mL Et_2O and 5 mL *n*-pentane, then the residue was thoroughly scratched and all volatiles were removed *in vacuo* (0.02 mbar). The crude product was then washed at −80°C thrice with 5 mL Et_2O. All volatile components were evaporated *in vacuo* (0.02 mbar). Unfortunately, the product was impure and the measured ^{1}H- and ^{13}C{1H}-NMR spectra could not be evaluated.

Reaction cipher: FLG-471 (FLG230530m3a009)

Molecular formula: $C_{24}H_{24}ClO_2P$

Molecular weight: 410,88 g/mol

MS (APCI) m/z (%): 243.116 (100) $[CPh_3]^+$, 375.150 (33) $[M\text{-}Cl]^+$, 411.126 (9) $[M+H]^+$.

HRMS (APCI): theor./exp. 411.1275/411.1272 $[M+H]^+$.

$^{31}P\{^1H\}$ NMR (202 MHz, 298 K, $CDCl_3$): δ (ppm)= 47.9 (s).

^{31}P NMR (202 MHz, 298 K, $CDCl_3$): δ (ppm)= 47.9 (s_{br}).

5.5.4.7 Synthesis of 2-bromoethyl(2-oxopropyl)(triphenylmethyl)phosphane oxide (**19f**)

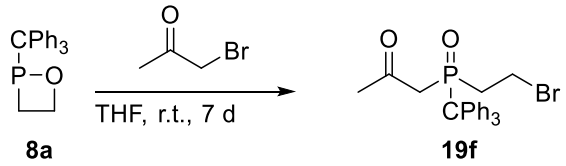

8a **19f**

Synthesis: 159.2 mg (0.5 mmol, 1 eq) **8a** were dissolved in 15 mL THF. 0.13 mL (1.5 mmol, 3 eq) bromoacetone were added at room temperature. The reaction was stirred for 7 d. All volatiles were removed *in vacuo* (0.02 mbar).

Purification: The crude product was washed at ambient temperature twice with a mixture of 5 mL Et_2O and 5 mL *n*-pentane, and once with 5 mL pure *n*-pentane. After evaporation of all volatile components and drying *in vacuo* (0.02 mbar) the product was obtained as white powder.

Reaction cipher: FLG-457 (FLG230426p5a019)

Molecular formula: $C_{24}H_{24}BrO_2P$

Molecular weight: 455.33 g/mol

Yield: 30.8 mg, 0.03 mmol, 6%.

Melting Point: 116°C.

MS (APCI) m/z (%) : 243.117 (100) $[CPh_3]^+$, 375.151 (13) $[M\text{-}Br]^+$, 455.077 (13) $[M+H]^+$.

HRMS (APCI): theor./exp. 455.0770/455.0769 $[M+H]^+$.

IR (ATR Diamond, selected data): $\tilde{\nu}$ (cm^{-1}) = 1708 (m, ν(C=O)), 2854 (w, ν(C-H)), 2923 (w, ν(C-H)), 2960 (w, ν(C-H)), 3056 (w, ν(C-H)).

^{1}H NMR (500 MHz, 298 K, $CDCl_3$): δ (ppm) = 2.27 (m, 1H, $BrCH_2$-C*H*$_2$), 2.33 (s, 3H, -C*H*$_3$), 2.50 (m, 1H, $BrCH_2$-C*H*$_2$), 2.50 (m, 1H, -C(O)-C*H*$_2$), 3.37 (m, 1H, -C*H*$_2$Br), 3.42 (m, 1H, -C(O)-C*H*$_2$), 3.48 (m, 1H, -C*H*$_2$Br), 7.32 (m, 10H, -C*H*), 7.58 (m, 5H, -C*H*).

^{13}C NMR (126 MHz, 298 K, $CDCl_3$): δ (ppm) = 24.8 (s, -*C*H_2Br), 33.3 (s, -*C*H_3), 33.9 (d, $^1J_{P\text{-}C}$= 57.2 Hz, CH_2Br-*C*H_2), 45.3 (d, $^1J_{P\text{-}C}$= 50.1 Hz, -C(O)-*C*H_2), 63.6 (d, $^1J_{P\text{-}C}$= 59.6 Hz, -*C*Ph_3), 127.8 (s_{br}, *para*-*C*H), 128.8 (s_{br}, *meta*-*C*H), 130.4 (s, *ortho*-*C*H), 141.3 (s_{br}, -*C*Ph_3), 202.6 (d, $^2J_{P\text{-}C}$= 5.2 Hz, -*C*(O)).

^{31}P{^{1}H} NMR (202 MHz, 298 K, $CDCl_3$): δ (ppm)= 48.5 (s).

Single crystal measurement: FLG-457, very good structure (AB1), GSTR813, GXray7409

5.5.5 Synthesis of ring-opened products with halogens, pseudo- and interhalogens

5.5.5.1 Attempted synthesis of chloro(2-chloroethyl)(triphenylmethyl)phosphane oxide (**34a**)

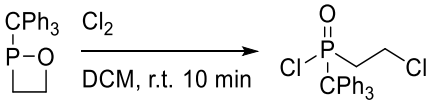

8a **34a**

Synthesis: The chlorine gas was freshly prepared by dropping 5 mL concentrated hydrochloric acid on 0.35 g potassium permanganate. The generated gas was first led through a gas washing bottle filled

with demineralized water and then through a short drying tower (l=10 cm) filled with phosphorus pentoxide, before being led into the reaction vessel. In the vessel, 0.159 g (0.3 mmol, 1 eq) **8a** were dissolved in 20 mL DCM. After bubbling trough, the reaction mixture, the gas was led through a gas washing bottle filled with aqueous sodium sulfite solution. After the chlorine gas development stopped (5 min), the apparatus was flushed with argon for another 5 min. During the course of the reaction, the reaction solution turned form pale yellow to orange. All volatiles were removed *in vacuo* (0.02 mbar).

Purification: Purification was attempted by washing with three times 10 mL *n*-pentane at room temperature and removal of all volatiles *in vacuo* (0.02 mbar). The compound starts decomposing during work up and no suitable spectra for further analytics could be measured.

Reaction cipher: FLG-498 (FLG230720p5a044)

Molecular formula: $C_{21}H_{19}Cl_2OP$

Molecular weight: 389.26 g/mol

$^{31}P\{^{1}H\}$ NMR (202 MHz, 298 K, $CDCl_3$): δ (ppm) = 70.4 (s).

5.5.5.2 Synthesis of bromo(2-bromoethyl)(triphenylmethyl)phosphane oxide (**34b**)

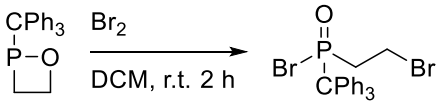

8a **34b**

Synthesis: 0.0955 g (0.3 mmol, 1 eq) **8a** were dissolved in 2 mL DCM. 0.015 mL bromine (0.3 mmol, 1 eq) were dissolved in 2 mL DCM and added slowly to the first solution until the pale-yellow solution lastingly turned brown. The reaction was stirred for 2 h, followed by removal of all volatiles *in vacuo* (0.02 mbar).

Purification: The product was obtained as off-white solid after washing with three times 10 mL *n*-pentane at room temperature.

Reaction cipher: FLG-479 (FLG230622p5a003)

Molecular formula: $C_{21}H_{19}Br_2OP$

Molecular weight: 478.16 g/mol

Yield: 54.7 mg, 0.11 mmol, 38%.

Melting Point: 218°C.

MS (ESI+) m/z (%) : 243.117 (100) $[CPh_3]^+$, 335.119 (40) $[M-2Br+O+H]^+$, 357.101 (25) $[M-2Br+O+Na]^+$, 495.986 (2) $[M+NH_4]^+$, 500.9409 (<2) $[M+Na]^+$.

HRMS (ESI+): theor./exp. 495.9859/495.9856 $[M+NH_4]^+$, 500.9413/500.9410 $[M+Na]^+$.

^{1}H NMR (500 MHz, 298 K, $CDCl_3$): δ (ppm) = 2.61 (m, 1H, -PC*H*$_2$), 2.86 (m, 1H, -PC*H*$_2$), 3.59 (m, 1H, -BrC*H*$_2$), 3.68 (m, 1H, -BrC*H*$_2$), 7.36 (m, 10H, -C*H*), 7.46 (s_{br}, 5H, -C*H*).

^{1}H{^{31}P} NMR (500 MHz, 298 K, $CDCl_3$): δ (ppm) = 2.61 (m, 1H, -PC*H*$_2$), 2.86 (m, 1H, -PC*H*$_2$), 3.59 (m, 1H, -BrC*H*$_2$), 3.68 (m, 1H, -BrC*H*$_2$), 7.36 (m, 10H, -C*H*), 7.46 (s_{br}, 5H, -C*H*).

^{13}C NMR (126 MHz, 298 K, $CDCl_3$): δ (ppm) = 24.1 (d, $^2J_{P-C}$= 2.2 Hz, -Br*C*H$_2$), 40.9 (d, $^1J_{P-C}$= 54.8 Hz, -P*C*H$_2$), 69.8 (d, $^1J_{P-C}$= 57.2 Hz, -*C*Ph$_3$), 128.2 (s, *para*-*C*H), 128.6 (s, *meta*-*C*H), 130.9 (s, *ortho*-*C*H), 139.8 (s_{br}, *ipso*-*C*).

^{31}P{^{1}H} NMR (202 MHz, 298 K, $CDCl_3$): δ (ppm) = 71.1 (s).

^{31}P NMR (202 MHz, 298 K, $CDCl_3$): δ (ppm) = 71.1 (s_{br}).

Single crystal measurement: FLG-479, excellent structure (AA1), GSTR820, GXraymo_7603f

5.5.5.3 Synthesis of iodo(2-iodoethyl)(triphenylmethyl)phosphane oxide (**34c**)

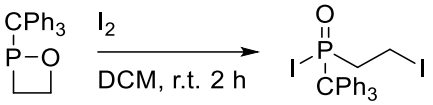

8a **34c**

Synthesis: 0.0955 g (0.3 mmol, 1 eq) **8a** were dissolved in 2 mL DCM. 0.080 g iodine (0.31 mmol, 1.05 eq) were dissolved in 7 mL DCM and added slowly to the first solution until the pale-yellow solution lastingly turned dark yellow. The reaction was stirred for 2 h, followed by removal of all volatiles *in vacuo* (0.02 mbar).

Purification: The product was obtained as off-white solid after washing with three times 10 mL *n*-pentane at room temperature.

Reaction cipher: FLG-501 (FLG230728p5a059)

Molecular formula: $C_{21}H_{19}I_2OP$

Molecular weight: 572.16 g/mol

Yield: 61.3 mg, 0.11 mmol, 36%.

Melting Point: 104°C.

^{1}H NMR (500 MHz, 298 K, $CDCl_3$): δ (ppm) = 2.70 (dddd, 1H, $^2J_{H\text{-}H}$= 14.4 Hz, $^3J_{H\text{-}H}$= 12.8 Hz, $^2J_{P\text{-}H}$= 5.2 Hz, $^3J_{H\text{-}H}$= 5.2 Hz, -PCH_2), 2.89 (dddd, 1H, $^2J_{H\text{-}H}$= 14.4 Hz, $^3J_{H\text{-}H}$= 12.5 Hz, $^2J_{P\text{-}H}$= 7.6 Hz, $^3J_{H\text{-}H}$= 4.9 Hz, -PCH_2), 3.41(*, m, 2H, -ICH_2), 7.36 (m, 10H, -C*H*), 7.46 (s_{br}, 5H, -C*H*).
*: The two protons are not magnetically equivalent, the signals of the diastereotopic protons overlap.

^{1}H{^{31}P} NMR (500 MHz, 298 K, $CDCl_3$): δ (ppm) = 2.70 (ddd, 1H, $^2J_{H\text{-}H}$= 14.6 Hz, $^3J_{H\text{-}H}$= 13.5 Hz, $^3J_{H\text{-}H}$= 6.2 Hz, -PCH_2), 2.89 (ddd, 1H, $^2J_{H\text{-}H}$= 13.4Hz, $^3J_{H\text{-}H}$= 12.7 Hz, $^3J_{H\text{-}H}$= 4.2 Hz, -PCH_2), 3.41(*, m, 2H, -ICH_2), 7.36 (m, 10H, -C*H*), 7.46 (s_{br}, 5H, -C*H*).
*: The two protons are not magnetically equivalent, the signals of the diastereotopic protons overlap.

^{13}C NMR (126 MHz, 298 K, $CDCl_3$): δ (ppm) = −5.8 (d, $^2J_{P\text{-}C}$= 5.2 Hz, -I*C*H_2), 44.4 (d, $^1J_{P\text{-}C}$= 41.4 Hz, -P*C*H_2), 69.6 (d, $^1J_{P\text{-}C}$= 45.2 Hz, -*C*Ph_3), 128.3 (s_{br}, *para*-*C*H), 128.7 (s_{br}, *meta*-*C*H), 131.0 (s_{br}, *ortho*-*C*H), 139.8 (s_{br}, *ipso*-*C*).

^{31}P{^{1}H} NMR (202 MHz, 298 K, $CDCl_3$): δ (ppm) = 62.1 (s).

^{31}P NMR (202 MHz, 298 K, $CDCl_3$): δ (ppm) = 62.1 (s_{br}).

Single crystal measurement: FLG-508, excellent structure (A1), GSTR822, GXraymo_7684f

5.5.5.4 Attempted synthesis of (2-chloroethyl)iodo(triphenylmethyl)phosphane oxide (**36a**)

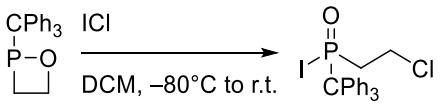

8a **36a**

Synthesis: 0.1114 g (0.35 mmol, 1 eq) **8a** were dissolved in 4 mL DCM. ≈70 mg iodine monochloride (0.42 mmol, 1.2 eq) were dissolved in 3 mL DCM. Both solutions were cooled to −80°C. The iodine monochloride solution was added dropwise to the reaction solution, until a lasting colour change occurred (pale-yellow to orange). As the compound tends to decompose, no further analytics could be performed.

Reaction cipher: FLG-503 (FLG230801m3a029)

Molecular formula: $C_{21}H_{19}ClIOP$

Molecular weight: 480.71 g/mol

^{31}P{^{1}H} NMR (121 MHz, 298 K, DCM): δ (ppm) = 62.2 (s).

^{31}P NMR (121 MHz, 298 K, DCM): δ (ppm) = 62.2 (s_{br}).

5.5.5.5 Attempted synthesis of 2-bromoethylcyano(triphenylmethyl)phosphane oxide (**37a**) and/or bromo(2-cyanoethyl)(triphenylmethyl)phosphane oxide (**37b**)

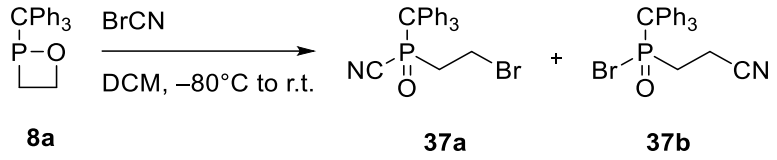

Synthesis: 0.1114 g (0.35 mmol, 1 eq) **8a** were dissolved in 3 mL DCM. 0.037 g cyanogen bromide (0.35 mmol, 1 eq) were dissolved in 2 mL DCM. Both solutions were cooled to −80°C. The cyanogen bromide solution was added to the reaction solution. The reaction yields two products which were not further isolated.

Reaction cipher: FLG-507 (FLG230804m3a030)

Molecular formula: $C_{22}H_{19}BrNOP$

Molecular weight: 424.28 g/mol

Ratio (**37a**:**37b**)= 25:75

$^{31}P\{^{1}H\}$ NMR (121 MHz, 298 K, DCM): δ (ppm) = (**37a**) 34.2 (s), (**37b**) 71.3 (s).

5.5.6 Ring opening reactions with acids

5.5.6.1 Synthesis of acetic (2-hydroxyethyl)(triphenylmethyl)phosphinous anhydride (**38a**) and its side products

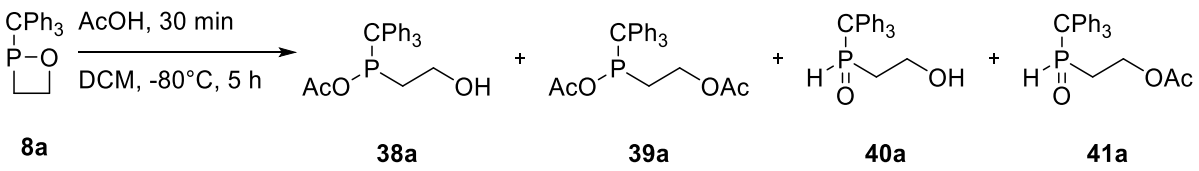

Synthesis: 0.159 mg (0.5 mmol, 1 eq) **8a** were dissolved in 5 mL DCM in a finger Schlenk. The solution was cooled to −80°C. 0.04 mL (0.7 mmol, 1.3 eq) of acetic acid was added and the reaction mixture was stirred for 2.5 h. As the NMR spectrum indicated that the conversion was incomplete, another 0.04 mL of acetic acid were added and stirred for another 2.5 h. The crude product was obtained as a mixture of products after removal of all volatiles *in vacuo* (0.02 mbar).

Purification: 5 ml Et_2O were added to the crude product. The mixture was scratched and evaporated *in vacuo* (0.02 mbar) to remove traces of acetic acid. This was repeated once. The crude product was than washed with 3 mL Et_2O and 10m mL *n*-pentane at −80°C. After removal of all volatiles *in vacuo* (0.02 mbar), the crude product was still present as mixture of the desired main product and its side products.

Reaction cipher: FLG-519 (FLG230821m3a048)

Molecular formula: $C_{23}H_{23}O_3P$

Molecular weight: 378.41 g/mol

Ration (**38a**:**39a**:**40a**:**41a**): 31:7:53:8.

MS (APCI) m/z (%) : 243.116 (100) $[CPh_3]^+$, 337.135 (12) $[M\text{-}H_2CCO+H]^+$, 379.145 (12) $[M+H]^+$.

HRMS (APCI): theor./exp. 379.1458/379.1450 $[M+H]^+$.

$^{31}P\{^1H\}$ NMR (121 MHz, 298 K, DCM): δ (ppm) = 127.2 (s).

^{31}P NMR (121 MHz, 298 K, DCM): δ (ppm) = 127.2 (q, $^xJ_{P\text{-}H}$ 12.6 Hz).

5.5.6.2 Synthesis of chloro(2-hydroxyethyl)(triphenylmethyl)phosphane (**38b**) and its side products

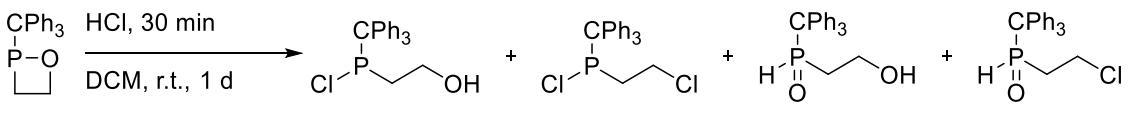

8a **38b** **39b** **40b** **41b**

Synthesis: 0.159 mg (0.5 mmol, 1 eq) **8a** were dissolved in 5 mL DCM in a finger Schlenk. 0.5 mL (1.0 mmol, 2 eq) hydrogen chloride solution (2M in Et_2O) was added and the reaction mixture was stirred for 1 d. The crude product was obtained as a mixture of side products after removal of all volatiles *in vacuo* (0.02 mbar).

Purification: The crude product was washed three times with 5 mL Et_2O −80°C. After removal of all volatiles *in vacuo* (0.02 mbar), the crude product was still present as mixture of the desired main product and its side products.

Reaction cipher: FLG-489 (FLG230712m3a037)

Molecular formula: $C_{21}H_{20}ClOP$

Molecular weight: 354.81 g/mol

Ration (**38b**:**39b**:**40b**:**41b**): 9:2:69:20.

MS (APCI) m/z (%) : 243.116 (100) $[CPh_3]^+$, 319.124 (3) $[M\text{-}Cl]^+$, 337.135 (18) $[M+H_2O\text{-}Cl]^+$, 355.101 (4) $[M+H]^+$.

HRMS (APCI): theor./exp. 355.1013/355.1007 $[M+H]^+$.

$^{31}P\{^1H\}$ NMR (121 MHz, 298 K, DCM): δ (ppm) = 111.0 (s).

^{31}P NMR (121 MHz, 298 K, DCM): (ppm) = 111.0 (s_{br}).

5.5.6.3 Synthesis of [pentacarbonyl{acetic (2-hydroxyethyl)(triphenylmethyl)phosphinous anhydride -κP}tungsten(0)] (**54a**) and [pentacarbonyl{2-((hydroxy(triphenylmethyl)phosphino)ethyl-acetate-κP}tungsten(0)] **55a**

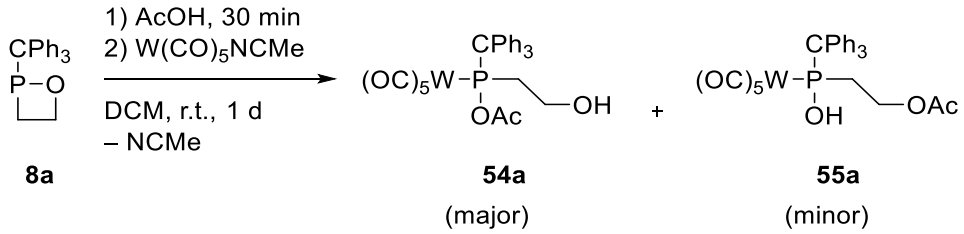

8a **54a** (major) **55a** (minor)

Synthesis: 0.159 mg (0.5 mmol, 1 eq) **8a** were dissolved in 5 mL DCM. 0.03 mL (0.5 mmol, 1 eq) acetic acid was added and the reaction mixture was stirred for 30 min. After that, 0.1825 mg (0.5 mmol, 1 eq) acetonitrile (pentacarbonyl)tungsten(0) were added and the reaction mixture stirred overnight. After removal of all volatiles *in vacuo* (0.02 mbar), the crude product mixture was obtained as dark-green solid.

Molecular formula: $C_{28}H_{23}O_8PW$

Molecular weight: 702.30 g/mol

Reaction cipher: FLG-549, FLG-542 (FLG231122p5a041)

MS (ESI−) m/z (%) : 302.9052 (100) $[C_2O_4PW]^-$, 645.0674 (10) $[M\text{-}2CO\text{-}H]^-$, 701.0575 (15) $[M\text{-}H]^-$.

HRMS (ESI−): theor./exp. 699.0540/699.0544 $[M\text{-}H]^-$.

$^{31}P\{^1H\}$ NMR (202 MHz, 298 K, $CDCl_3$): δ (ppm) = 130.1 (s_{sat}, $^1J_{W\text{-}P}$= 287.5 Hz).

^{31}P NMR (202 MHz, 298 K, $CDCl_3$): δ (ppm) = 130.1 ($s_{br,sat}$, $^1J_{W\text{-}P}$= 287.5 Hz).

Single crystal measurement: Minor side product **55a**: FLG-549, good structure (C3), GSTR834 GXraymo_7934f_pl

5.5.6.4 Synthesis of [pentacarbonyl{chloro(2-hydroxyethyl)(triphenylmethyl)phosphane -κP}tungsten(0)] (**54b**)

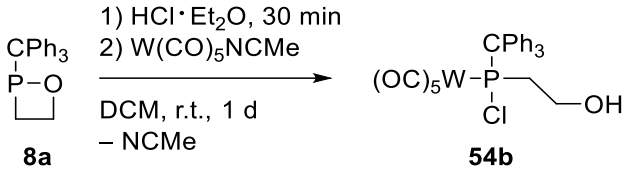

Synthesis: 0.159 mg (0.5 mmol, 1 eq) **8a** were dissolved in 5 mL DCM. 0.25 mL (0.5 mmol, 1 eq) hydrogen chloride solution (2 M in Et_2O) was added and the reaction mixture was stirred for 30 min. After that, 0.1825 mg (0.5 mmol, 1 eq) acetonitrile (pentacarbonyl)tungsten(0) were added and the reaction mixture stirred overnight. After removal of all volatiles *in vacuo* (0.02 mbar), the crude product was obtained as green sticky solid.

Molecular formula: $C_{26}H_{20}ClO_6PW$

Molecular weight: 678.70 g/mol

Reaction cipher: FLG-550 (FLG231201m3a003)

MS (ESI−) m/z (%): 302.907 (100) $[C_2O_4PW]^-$, 565.001 (3) $[M\text{-}4CO\text{-}H]^-$, 677.018 (10) $[M\text{-}H]^-$.

HRMS (ESI−): theor./exp. 675.0098/675.0104 $[M\text{-}H]^-$.

$^{31}P\{^1H\}$ NMR (121 MHz, 298 K, $CDCl_3$): δ (ppm) = 123.2 (s_{sat}, $^1J_{W\text{-}P}$= 272.9 Hz).

^{31}P NMR (121 MHz, 298 K, $CDCl_3$): δ (ppm) = 123.2 (s_{sat}, $^1J_{W\text{-}P}$= 274.1 Hz).

5.5.6.5 Synthesis of (2-hydroxyethyl)(triphenylmethyl)phosphane oxide (**40a**)

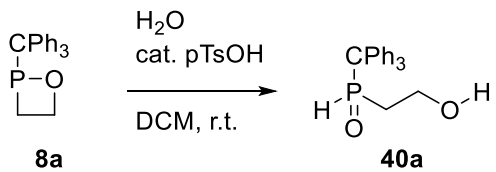

Synthesis: 0.159 g (0.5 mmol, 1 eq) **8a** were dissolved in 5 mL DCM. 0.02 mL H_2O (1 mmol, 2 eq) and then 3.5 mg (0.02 mmol, 0.04 eq) *p*-toluene sulfonic acid were added to the solution. The solution turned turbid on addition of the acid. The reaction was stirred for 2 h, followed by removal of all volatiles *in vacuo* (0.02 mbar).

Purification: The product was obtained as white solid after washing with three times 5 mL *n*-pentane at room temperature.

Reaction cipher: FLG-486 (FLG230711p5a028)

Molecular formula: $C_{21}H_{21}O_2P$

Molecular weight: 336.37 g/mol

Yield: 86.4 mg, 0.26 mmol, 51%.

MS (APCI) m/z (%) : 165.070 (6) $[CPh_2\text{-}H]^-$, 183.081 (53) $[Ph_2COH]^+$, 243.117 (100) $[CPh_3]^+$, 337.135 (13) $[M+H]^+$, 355.101 (4) $[M+H_2O+H]^+$.

HRMS (APCI): theor./exp. 337.1352/337.1350 $[M+H]^+$.

IR (ATR Diamond, selected data): $\tilde{\nu}$ (cm^{-1}) = 1016 (s, ν(C-O)), 2364 (w, ν(P-H)), 2925 (w, ν(C-H)), 2962 (w, ν(C-H)), 3024 (w, ν(C-H)), 3058 (w, ν(C-H)), 3323 (w_{br}, ν(O-H)).

^{1}H NMR (500 MHz, 298 K, $CDCl_3$): δ (ppm) = 1.51 (m, 1H, -PC*H*$_2$), 2.07 (m, 1H, -PC*H*$_2$), 3.92 (m, 2H, -OC*H*$_2$), 4.63 (s, 1H, -O*H*), 7.36 (m, 15H, -C*H*), 7.39 (dd, 2H, $^1J_{P\text{-}H}$= 480.6 Hz, $^3J_{H\text{-}H}$= 7.8 Hz, -C*H*).

^{13}C NMR (126 MHz, 298 K, $CDCl_3$): δ (ppm) = 29.6 (d, $^1J_{P\text{-}C}$= 65.1 Hz, -P*C*H$_2$), 57.5 (d, $^2J_{P\text{-}C}$= 5.5 Hz, -O*C*H$_2$), 61.0 (d, $^1J_{P\text{-}C}$= 61.0 Hz, -*C*Ph$_3$), 127.8 (d, $^5J_{P\text{-}C}$= 2.2 Hz, *para*-*C*H), 128.8 (s, *meta*-*C*H), 130.2 (d, $^3J_{P\text{-}C}$= 6.5 Hz, *ortho*-*C*H), 140.7 (s, *ipso*-*C*).

^{31}P{^{1}H} NMR (202 MHz, 298 K, $CDCl_3$): δ (ppm) = 46.7 (s).

^{31}P NMR (202 MHz, 298 K, $CDCl_3$): δ (ppm) = 46.7 (dq, $^1J_{P\text{-}H}$= 479.7 Hz, $^xJ_{P\text{-}H}$= 16.9 Hz).

6 References

[1] W. M. Haynes, D. R. Lide, T. J. Bruno, *CRC Handbook of Chemistry and Physics*, CRC Press, **2016**.
[2] A. S. Wagh, *Chemically bonded phosphate ceramics : twenty-first century materials with diverse applications*, Elsevier, **2016**.
[3] R. B. Martin, *MSF* **1998**, *293*, 5.
[4] R. J. P. Williams, *J. Chem. Soc., Dalton Trans.* **1991**, 539.
[5] B. Alberts, *Molecular biology of the cell*, CRC Press, an imprint of Garland Science, Boca Raton, FL, **2016**.
[6] a) H. Beyer, W. Walter, *Lehrbuch der organischen Chemie*, Hirzel, Stuttgart, Leipzig, **1998**; b) F. Horn, F. Blaeschke, K. Trugenberger, M. Gröll, C. Polzer, K. Lechner, J. M. Anderson, *Biochemie des Menschen*. *Das Lehrbuch für das Medizinstudium*, Georg Thieme Verlag, Stuttgart, New York, **2021**.
[7] J. R. Knowles, *Annu. Rev. Biochem.* **1980**, *49*, 877.
[8] G. W. Leibniz, *Miscnea Berol. Soc. Sci.* **1710**, 91.
[9] M. F. Crass, *J. Chem. Educ.* **1941**, *18*, 316.
[10] *Toxicity of military smokes and obscurants*, National Academy Press, Washington, D.C., **1999**.
[11] B. Crowell, *America's Munitions 1917-1918*, Washington Government Printing Office, **1919**.
[12] S. Hörold in *Polymer Green Flame Retardants*, Elsevier, **2014**, pp. 221–254.
[13] L. E. Lampila, *Ann. N. Y. Acad. Sci.* **2013**, *1301*, 37.
[14] a) R. Mason, D. W. Meek, *Angew. Chem. Int. Ed. Engl.* **1978**, *17*, 183; b) B. Bogdanović, B. Henc, A. Lösler, B. Meister, H. Pauling, G. Wilke, *Angew. Chem. Int. Ed. Engl.* **1973**, *12*, 954.
[15] C. Xie, A. J. Smaligo, X.-R. Song, O. Kwon, *ACS central science* **2021**, *7*, 536.
[16] R. S. Meena (Ed.) *Springer eBooks Earth and Environmental Science*, Springer Singapore, Imprint: Springer, Singapore, **2020**.
[17] R. Herbst-Irmer, X. Wang, L. Haberstock, I. Köhne, R. Oswald, J. Behler, D. Stalke, *IUCrJ* **2023**, *10*, 766.
[18] H. Bock, H. Mueller, *Inorg. Chem.* **1984**, *23*, 4365.
[19] N. N. Greenwood, A. Earnshaw, *Chemistry of the elements*, Recording for the Blind & Dyslexic, Princeton, N.J., **2004**.
[20] *Nomenclature of inorganic chemistry*. *IUPAC recommendations 2005*, Royal Society of Chemistry, Cambridge, **2005**.
[21] G. Grüttner, M. Wiernik, *Ber. Dtsch. Chem. Ges.* **1915**, *48*, 1473.
[22] G. Grüttner, E. Krause, *Ber. Dtsch. Chem. Ges.* **1916**, *49*, 437.
[23] G. Wittig, G. Geissler, *Justus Liebigs Ann. Chem.* **1953**, *580*, 44.
[24] W. B. McCormack, US Patent 2663737, **1953**.
[25] F. Mathey, *Phosphorus-Carbon Heterocyclic Chemistry*, Elsevier Science Limited, **2001**.
[26] P. Coggon, J. F. Engel, A. T. McPhail, L. D. Quin, *J. Am. Chem. Soc.* **1970**, *92*, 5779.
[27] F. Mathey, *C. R. Acad. Sci. Ser. C* **1969**, *269*, 1066.
[28] E. Jungermann, J. J. McBride, R. Clutter, A. Mais, *J. Org. Chem.* **1962**, *27*, 606.
[29] S. E. Cremer, R. J. Chorvat, *J. Org. Chem.* **1967**, *32*, 4066.
[30] R. I. Wagner, L. D. Freeman, H. Goldwhite, D. G. Rowsell, *J. Am. Chem. Soc.* **1967**, *89*, 1102.
[31] a) T. A. van der Knaap, T. C. Klebach, R. Lourens, M. Vos, F. Bickelhaupt, *J. Am. Chem. Soc.* **1983**, *105*, 4026; b) R. Appel, F. Knoch, H. Kunze, *Angew. Chem. Int. Ed. Engl.* **1984**, *23*, 157.
[32] M. Regitz, O. J. Scherer (Eds.) *Multiple bonds and low coordination in phosphorus chemistry*, Thieme, Stuttgart, **1990**.
[33] A. Espinosa Ferao, R. Streubel, *Eur. J. Inorg. Chem.* **2017**, *2017*, 2707.
[34] G.-V. Röschenthaler, K. Sauerbrey, R. Schmutzler, *Chem. Ber.* **1978**, *111*, 3105.
[35] S. Bauer, A. Marinetti, L. Ricard, F. Mathey, *Angew. Chem. Int. Ed. Engl.* **1990**, *29*, 1166.
[36] R. Streubel, A. Kusenberg, J. Jeske, P. G. Jones, *Angew. Chem. Int. Ed. Engl.* **1994**, *33*, 2427.

[37] A. Özbolat, G. von Frantzius, J. M. Pérez, M. Nieger, R. Streubel, *Angew. Chem. Int. Ed.* **2007**, *46*, 9327.
[38] C. Albrecht, M. Bode, J. M. Pérez, J. Daniels, G. Schnakenburg, R. Streubel, *Dalton Trans.* **2011**, *40*, 2654.
[39] R. Streubel, N. Volk, G. Schnakenburg, A. García Alcaraz, A. Espinosa Ferao, *Eur. J. Inorg. Chem.* **2021**, *2021*, 252.
[40] V. Nesterov, G. Schnakenburg, A. Espinosa, R. Streubel, *Inorg. Chem.* **2012**, *51*, 12343.
[41] J. Fassbender, G. Schnakenburg, A. Espinosa Ferao, R. Streubel, *Dalton Trans.* **2018**, *47*, 9347.
[42] J. Faßbender, N. Volk, A. García Alcaraz, S. Balasubramaniam, A. Espinosa Ferao, R. Streubel, *Chem. Commun.* **2023**, *59*, 1285.
[43] A. Espinosa Ferao, *Inorg. Chem.* **2018**, *57*, 8058.
[44] G. H. Birum, C. N. Matthews, *Chem. Commun.* **1967**, *8*, 137.
[45] G. H. Birum, C. N. Matthews, *J. Org. Chem.* **1967**, *32*, 3554.
[46] G. Chioccola, J. J. Daly, *J. Chem. Soc., A* **1968**, 568.
[47] a) F. Ramirez, C. P. Smith, J. F. Pilot, *J. Am. Chem. Soc.* **1968**, *90*, 6726; b) H. J. Bestmann, K. Roth, E. Wilhelm, R. Böhme, H. Burzlaff, *Angew. Chem. Int. Ed. Engl.* **1979**, *18*, 876; c) R. W. Saalfrank, W. Paul, H. Liebenow, *Angew. Chem. Int. Ed. Engl.* **1980**, *19*, 713.
[48] Mazhar-ul-Haque, C. N. Caughlan, F. Ramirez, J. F. Pilot, C. P. Smith, *J. Am. Chem. Soc.* **1971**, *93*, 5229.
[49] T. Kawashima, K. Kato, R. Okazaki, *J. Am. Chem. Soc.* **1992**, *114*, 4008.
[50] T. Kawashima, K. Kato, R. Okazaki, *Angew. Chem. Int. Ed. Engl.* **1993**, *32*, 869.
[51] U. Dieckbreder, E. Lork, G.-V. Röschenthaler, A. A. Kolomeitsev, *Heteroat. Chem.* **1996**, *7*, 281.
[52] M. Hamaguchi, Y. Iyama, E. Mochizuki, T. Oshima, *Tetrahedron Lett.* **2005**, *46*, 8949.
[53] E. N. Dianova, E. Y. Zabotina, I. Z. Akhmethkhaova, Samuilov Y.D., *Zh. Obs. Khim.* **1991**, 1063.
[54] A. W. Kyri, F. Gleim, A. García Alcaraz, G. Schnakenburg, A. Espinosa Ferao, R. Streubel, *Chem. Commun.* **2018**, *54*, 7123.
[55] A. W. Kyri, V. Nesterov, G. Schnakenburg, R. Streubel, *Angew. Chem. Int. Ed. Engl.* **2014**, *53*, 10809.
[56] A. W. Kyri, *Dissertation*, Rheinische Friedrich-Wilhelms-Universität Bonn, Bonn, **2017**.
[57] A. W. Kyri, G. Schnakenburg, R. Streubel, *Organometallics* **2016**, *35*, 563.
[58] A. W. Kyri, G. Schnakenburg, R. Streubel, *Chem. Commun.* **2016**, *52*, 8593.
[59] F. Gleim, *Master Thesis*, Rheinische Friedrich-Wilhelms-Universität Bonn, Bonn, **2018**.
[60] a) N. Maigrot, L. Ricard, C. Charrier, P. Le Goff, F. Mathey, *Bull. Soc. Chim. Fr.* **1992**, *129*, 76; b) A. Espinosa Ferao, B. Deschamps, F. Mathey, *Bull. Soc. Chim. Fr.* **1993**, *130*, 695.
[61] a) W. Reif, H. Grassner, *Chem. Ing. Tech.* **1973**, *45*, 646; b) W. Bonrath, B. Gao, P. Houston, T. McClymont, M.-A. Müller, C. Schäfer, C. Schweiggert, J. Schütz, J. A. Medlock, *Org. Process Res. Dev.* **2023**, *27*, 1557.
[62] P. A. Byrne, D. G. Gilheany, *Chem. Soc. Rev.* **2013**, *42*, 6670.
[63] L. Kürti, B. Czakó, *Strategic applications of named reactions in organic synthesis*. *Background and detailed mechanisms*, Elsevier Academic, Burlington, MA, **2005**.
[64] A. K. Bhattacharya, G. Thyagarajan, *Chem. Rev.* **1981**, *81*, 415.
[65] G. Aksnes, R. Eriksen, S. Brandänge, T. Walle, B. Sjöberg, E. Bunnenberg, C. Djerassi, R. Records, *Acta Chem. Scand.* **1966**, *20*, 2463.
[66] F. Mathey, F. Mercier, *J. Chem. Soc., Chem. Commun.* **1980**, *0*, 191.
[67] A. Espinosa Ferao, *J. Phys. Chem. A* **2017**, *121*, 6517.
[68] H. R. Allcock, R. L. Kugel, *J. Am. Chem. Soc.* **1965**, *87*, 4216.
[69] a) U. Franz, O. Nuyken, K. Matyjaszewski, *Macromolecules* **1993**, *26*, 3723; b) G. Allen, C. J. Lewis, S. M. Todd, *Polymer* **1970**, *11*, 31.
[70] C. H. Honeyman, I. Manners, C. T. Morrissey, H. R. Allcock, *J. Am. Chem. Soc.* **1995**, *117*, 7035.
[71] H. R. Allcock, C. A. Crane, C. T. Morrissey, J. M. Nelson, S. D. Reeves, C. H. Honeyman, I. Manners, *Macromolecules* **1996**, *29*, 7740.

[72] L. Vanderark, T. Clark, E. Rivard, I. Manners, J. Slootweg, K. Lammertsma, *Synfacts* **2006**, *2006*, 1016.
[73] K. Naka, T. Umeyama, A. Nakahashi, Y. Chujo, *Macromolecules* **2007**, *40*, 4854.
[74] A. M. Priegert, B. W. Rawe, S. C. Serin, D. P. Gates, *Chem. Soc. Rev.* **2016**, *45*, 922.
[75] S. Kobayashi, J. Kadokawa, *Macromol. Rapid Commun.* **1994**, *15*, 567.
[76] J.-I. Kadokawa, S. Kobayashi, *Phosphorus, Sulfur, Silicon Relat. Elem.* **2002**, *177*, 1387.
[77] J. L. Hodgson, M. L. Coote, *Macromolecules* **2005**, *38*, 8902.
[78] F.-L. Jin, X. Li, S.-J. Park, *J. Ind. Eng. Chem.* **2015**, *29*, 1.
[79] C. A. May (Ed.) *Epoxy resins*. *Chemistry and technology*, M. Dekker, New York, **op. 1988**.
[80] F. E. Bailey, J. V. Koleske, *Alkylene oxides and their polymers*, Dekker, New York, **1991**.
[81] M. Ibrahim, E. Ramadan, N. E. Elsadek, S. E. Emam, T. Shimizu, H. Ando, Y. Ishima, O. H. Elgarhy, H. A. Sarhan, A. K. Hussein et al., *J. Control. Release* **2022**, *351*, 215.
[82] J. B. Rose, *J. Chem. Soc.* **1956**, 542.
[83] M. P. Dreyfuss, P. Dreyfuss in *Encyclopedia of Polymer Science and Technology* (Ed.: H. F. Mark), Wiley, **2002**.
[84] P. Dreyfuss, M. P. Dreyfuss in *Advances in Polymer Science*, *4/4* (Eds.: H.-J. Cantow, G. Dall'Asta, J. D. Ferry, W. Kern, G. Natta, C. G. Overberger, W. Prins, G. V. Schulz, W. P. Slichter, A. J. Staverman et al.), Springer Berlin Heidelberg, Berlin, Heidelberg, **1967**, pp. 528–590.
[85] D. Delfs, H. Meerwein, H. Morschel, German Patent DE914438C, **1939**.
[86] H. Meerwein, D. Delfs, H. Morschel, *Angew. Chem.* **1960**, *72*, 927.
[87] S. Kobayashi, M. Suzuki, T. Saegusa, *Polym. Bull.* **1981**, *4*, 315.
[88] S. Kobayashi, M. Huang, T. Saegusa, *Polym. Bull.* **1981**, *4*.
[89] a) M. Yoshifuji, T. Sato, N. Inamoto, *Chem. Lett.* **1988**, *17*, 1735; b) M. Yoshifuji, I. Shima, N. Inamoto, K. Hirotsu, T. Higuchi, *J. Am. Chem. Soc.* **1981**, *103*, 4587.
[90] C. Murcia García, *Dissertation*, Rheinische Friedrich-Wilhelms-Universität Bonn, Bonn, **2016**.
[91] a) T. Kawashima, N. Inamoto, *Bull. Chem. Soc. Jpn.* **1991**, *64*, 713; b) T. Kawashima, S. Nakayama, M. Yoshifuji, R. Okazaki, N. Inamoto, *Bull. Chem. Soc. Jpn.* **1991**, *64*, 711; c) T. S. Hafez, Y. O. El-Khoshnieh, M. R. Mahran, S. M. S. Atta, *Phosphorus, Sulfur, Silicon Relat. Elem.* **1991**, *56*, 165.
[92] T. Kawashima, H. Takami, R. Okazaki, *Chem. Lett.* **1994**, *23*, 1487.
[93] U. Dabrowska, J. Dabrowski, *Chem. Ber.* **1976**, *109*, 1779.
[94] C. A. P. Goodwin, B. L. L. Réant, G. F. Vettese, J. G. C. Kragskow, M. J. Giansiracusa, I. M. DiMucci, K. M. Lancaster, D. P. Mills, S. Sproules, *Inorg. Chem.* **2020**, *59*, 7571.
[95] S. R. Alvarado, I. A. Shortt, H.-J. Fan, J. Vela, *Organometallics* **2015**, *34*, 4023.
[96] J. H. Shin, B. M. Bridgewater, D. G. Churchill, G. Parkin, *Inorg. Chem.* **2001**, *40*, 5626.
[97] a) T. S. Cameron, B. Dahlèn, *J. Chem. Soc., Perkin Trans. 2* **1975**, 1737; b) D. G. Gilheany, *Chem. Rev.* **1994**, *94*, 1339.
[98] N. Kuhn, H. Schumann, *Phosphorus, Sulfur Relat. Elem.* **1986**, *26*, 199.
[99] I. A. Nuretdinov, E. I. Loginova, *Izv. Akad. Nauk, Ser. Khim.* **1973**, 2827.
[100] J. M. Brunel, B. Faure, M. Maffei, *Coord. Chem. Rev.* **1998**, *178-180*, 665.
[101] G. Wittig, U. Schöllkopf, *Chem. Ber.* **1954**, *87*, 1318.
[102] C. J. O'Brien, J. L. Tellez, Z. S. Nixon, L. J. Kang, A. L. Carter, S. R. Kunkel, K. C. Przeworski, G. A. Chass, *Angew. Chem. Int. Ed.* **2009**, *48*, 6836.
[103] a) T. A. Albright, W. J. Freeman, E. E. Schweizer, *J. Org. Chem.* **1975**, *40*, 3437; b) S. Li, G. Wang, *Phosphorus, Sulfur, Silicon Relat. Elem.* **1991**, *61*, 119.
[104] A. T. Royappa, A. L. Rheingold, W. C. Teuchtler, N. L. Auld, *J. Mol. Struct.* **2020**, *1202*, 127268.
[105] M. Bujak, A. Olejniczak, M. Podsiadło, *Acta Cryst.* **2022**, *78*, 868.
[106] a) G. A. Lawrance, *Chem. Rev.* **1986**, *86*, 17; b) I. Krossing, I. Raabe, *Angew. Chem., Int. Ed.* **2004**, *43*, 2066.
[107] S. Kobayashi, M. Suzuki, T. Saegusa, *Macromol.* **1984**, *17*, 107.
[108] A. Espinosa Ferao, *Calculations on 1,2-oxaphosphetane chemistry, unpublished results.*
[109] F. Gleim, G. Schnakenburg, A. E. Ferao, R. Streubel, *Chem. Commun.* **2024**, *60*, 2625.
[110] O. Dahl, *J. Chem. Soc., Perkin Trans. 1* **1978**, 947.

[111] I. J. Borowitz, S. Firstenberg, G. B. Borowitz, D. Schuessler, *J. Am. Chem. Soc.* **1972**, *94*, 1623.
[112] R. Baumgärtner, W. Sawodny, J. Goubeau, *Z. anorg. allg. Chem.* **1964**, *333*, 171.
[113] a) J. Gloede, B. Costisella, *Z. anorg. allg. Chem.* **1980**, *471*, 147; b) J. E. Nycz, R. Musiol, *Heteroat. Chem.* **2006**, *17*, 310.
[114] P. G. Jones, F. Ruthe, *CCDC 926017: Experimental Crystal Structure Determination*, Cambridge Crystallographic Data Centre, **2013**.
[115] J. Jeske, W.-W. Du Mont, P. G. Jones, *Chem. Eur. J.* **1999**, *5*, 385.
[116] P. C. Brehm, *Calculations on 1,2-oxaphosphetane chemistry, unpublished results.*
[117] W. Robien, University of Vienna, *(Spectral Data were obtained from John Wiley & Sons, Inc.)*.
[118] A. L. Allred, *J. Inorg. Nucl. Chem.* **1961**, *17*, 215.
[119] I. Fleming, *Molecular orbitals and organic chemical reactions*, Wiley, Hoboken, **2009**.
[120] a) W. J. Jolly, *Modern inorganic chemistry*, McGraw-Hill, New York, **1985**; b) N. Wiberg, A. F. Holleman, E. Wiberg, G. Fischer, *Inorganic Chemistry*, De Gruyter, Inc, Berlin/Boston, **1995**.
[121] M. J. Buckingham, G. E. Hawkes, I. M. Ismail, P. J. Sadler, *J. Chem. Soc., Dalton Trans.* **1982**, 1167.
[122] J. Coetzee, G. R. Eastham, A. M. Z. Slawin, D. J. Cole-Hamilton, *Org. Biomol. Chem.* **2012**, *10*, 3677.
[123] U. Kolczak, G. Rist, K. Dietliker, J. Wirz, *J. Am. Chem. Soc.* **1996**, *118*, 6477.
[124] V. Plack, J. R. Goerlich, A. Fischer, R. Schmutzler, *Z. anorg. allg. Chem.* **1999**, *625*, 1979.
[125] W. Wolfsberger, *J. Organomet. Chem.* **1986**, *317*, 167.
[126] P. Le Floch, A. Marinetti, L. Ricard, F. Mathey, *J. Am. Chem. Soc.* **1990**, *112*, 2407.
[127] F. Mercier, C. Hugel-Le Goff, F. Mathey, *Organometallics* **1988**, *7*, 955.
[128] P. Junker, J. M. Villalba Franco, G. Schnakenburg, V. Nesterov, R. T. Boere, Z.-W. Qu, R. Streubel, *Dalton Trans.* **2020**, *49*, 13544.
[129] a) J. Chatt, B. T. Heaton, *J. Chem. Soc., A* **1968**, 2745; b) A. Gallen, A. Riera, X. Verdaguer, A. Grabulosa, *Catal. Sci. Technol.* **2019**, *9*, 5504.
[130] T. Steiner, *Angew. Chem. Int. Ed.* **2002**, *41*, 48.
[131] P. Politzer, J. S. Murray, T. Clark, *Phys. Chem. Chem. Phys.* **2013**, *15*, 11178.
[132] W. Armarego, *Purification of Laboratory Chemicals, 8th Edition*, Butterworth-Heinemann, Amsterdam, **2017**.
[133] G. R. Fulmer, A. J. M. Miller, N. H. Sherden, H. E. Gottlieb, A. Nudelman, B. M. Stoltz, J. E. Bercaw, K. I. Goldberg, *Organometallics* **2010**, *29*, 2176.
[134] R. K. Harris, E. D. Becker, S. M. Cabral de Menezes, P. Granger, R. E. Hoffman, K. W. Zilm, *Pure Appl. Chem.* **2008**, *80*, 59.
[135] R. H. Blessing, *Acta Cryst.* **1995**, *A51*, 33.
[136] G. M. Sheldrick, *ShelXS97 and ShelXL97*, Germany, **1997**.
[137] O. V. Dolomanov, L. J. Bourhis, R. J. Gildea, J. A. K. Howard, H. Puschmann, *J Appl Crystallogr* **2009**, *42*, 339.
[138] P. A. Levene, *Org. Synth.* **1930**, *10*, 12.
[139] V. Plack, J. R. Goerlich, A. Fischer, H. Thönnessen, P. G. Jones, R. Schmutzler, *Z. anorg. allg. Chem.* **1995**, *621*, 1080.
[140] H. Saltzman, J. G. Sharefkin, *Org. Synth.* **1963**, *43*, 60.
[141] H. G. O. Becker, R. Beckert, *Organikum*. *Organisch-chemisches Grundpraktikum*, Wiley-VCH, Weinheim, **2009**.
[142] R. A. Zingaro, B. H. Steeves, K. Irgolic, *J. Organomet. Chem.* **1965**, *4*, 320.

7 Appendix

7.1 Crystal Data and Structure Refinement

7.1.1 [Pentacarbonyl{-2-(triphenylmethyl)-1,2-oxaphosphetane-κ*P*}molybdenum(0)] (7a)

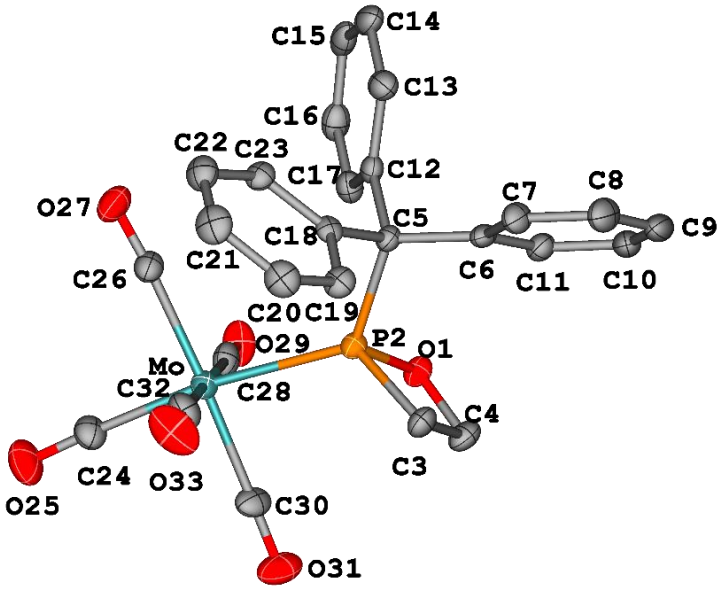

Figure 7.1: Molecular structures of **7a** in the solid state. Hydrogen atoms are omitted and the thermal ellipsoids are set at the 50% probability level.

Table 7.1: Crystal data and structure refinement for **7a**.

Identification code	GSTR768, FLG-359 // GXraymo_6902f
Crystal Habitus	clear colourless needle
Device Type	Bruker D8 Venture
Empirical formula	$C_{26}H_{19}O_6PMo$
Moiety formula	C26 H19 Mo O6 P
Formula weight	554.32
Temperature/K	100.0
Crystal system	monoclinic
Space group	$P2_1/c$
a/Å	9.4364(12)
b/Å	30.672(4)
c/Å	24.941(3)
α/°	90
β/°	94.189(5)
γ/°	90
Volume/Å^3	7199.5(15)
Z	12
ρ_{calc}g/cm^3	1.534

μ/mm^{-1}	0.653
F(000)	3360.0
Crystal size/mm^3	0.21 × 0.03 × 0.02
Absorption correction	empirical
Tmin; Tmax	0.5120; 0.7461
Radiation	MoKα (λ = 0.71073)
2Θ range for data collection/°	4.216 to 56°
Completeness to theta	0.999
Index ranges	-12 ≤ h ≤ 12, -40 ≤ k ≤ 40, -32 ≤ l ≤ 32
Reflections collected	115774
Independent reflections	17380 [R_{int} = 0.1230, R_{sigma} = 0.0861]
Data/restraints/parameters	17380/846/919
Goodness-of-fit on F^2	1.085
Final R indexes [I>=2σ (I)]	R_1 = 0.0689, wR_2 = 0.1525
Final R indexes [all data]	R_1 = 0.0897, wR_2 = 0.1627
Largest diff. peak/hole / e Å^{-3}	1.41/-1.17

Table 7.2: Bond Lengths for **7a**.

Atom	Atom	Length/Å	Atom	Atom	Length/Å
Mo	P2	2.4999(12)	C6'	C7'	1.392(7)
Mo	C24	2.005(5)	C6'	C11'	1.403(6)
Mo	C26	2.071(5)	C7'	C8'	1.384(7)
Mo	C28	2.052(5)	C8'	C9'	1.377(7)
Mo	C30	2.032(5)	C9'	C10'	1.391(7)
Mo	C32	2.050(5)	C10'	C11'	1.386(7)
P2	O1	1.661(3)	C12'	C13'	1.385(7)
P2	C3	1.845(5)	C12'	C17'	1.406(6)
P2	C5	1.895(5)	C13'	C14'	1.385(7)
O1	C4	1.467(6)	C14'	C15'	1.384(7)
O25	C24	1.153(7)	C15'	C16'	1.379(8)
O27	C26	1.136(6)	C16'	C17'	1.381(7)
O29	C28	1.143(6)	C18'	C19'	1.380(7)
O31	C30	1.140(6)	C18'	C23'	1.399(7)
O33	C32	1.133(7)	C19'	C20'	1.402(7)
C3	C4	1.548(7)	C20'	C21'	1.367(9)
C5	C6	1.535(6)	C21'	C22'	1.388(9)
C5	C12	1.546(6)	C22'	C23'	1.388(7)
C5	C18	1.549(6)	MoB	P2B	2.4871(12)
C6	C7	1.400(7)	MoB	C24B	2.028(5)
C6	C11	1.416(7)	MoB	C26B	2.090(5)
C7	C8	1.397(7)	MoB	C28B	2.047(5)
C8	C9	1.378(8)	MoB	C30B	2.020(5)
C9	C10	1.387(8)	MoB	C32B	2.046(6)
C10	C11	1.385(7)	P2B	O1B	1.660(3)
C12	C13	1.388(7)	P2B	C3B	1.844(5)
C12	C17	1.393(7)	P2B	C5B	1.915(5)

C13	C14	1.392(7)	O1B	C4B	1.463(6)
C14	C15	1.385(8)	O25B	C24B	1.140(6)
C15	C16	1.375(8)	O27B	C26B	1.126(6)
C16	C17	1.394(7)	O29B	C28B	1.141(6)
C18	C19	1.397(7)	O31B	C30B	1.152(6)
C18	C23	1.384(6)	O33B	C32B	1.144(7)
C19	C20	1.395(7)	C3B	C4B	1.536(6)
C20	C21	1.383(8)	C5B	C6B	1.545(6)
C21	C22	1.376(8)	C5B	C12B	1.536(6)
C22	C23	1.401(7)	C5B	C18B	1.542(6)
Mo'	P2'	2.4926(13)	C6B	C7B	1.384(7)
Mo'	C24'	2.025(5)	C6B	C11B	1.404(6)
Mo'	C26'	2.037(6)	C7B	C8B	1.396(7)
Mo'	C28'	2.049(6)	C8B	C9B	1.383(8)
Mo'	C30'	2.036(6)	C9B	C10B	1.372(8)
Mo'	C32'	2.023(7)	C10B	C11B	1.392(7)
P2'	O1'	1.658(4)	C12B	C13B	1.404(7)
P2'	C3'	1.841(5)	C12B	C17B	1.376(7)
P2'	C5'	1.906(5)	C13B	C14B	1.383(7)
O1'	C4'	1.471(6)	C14B	C15B	1.393(8)
O25'	C24'	1.152(6)	C15B	C16B	1.389(7)
O27'	C26'	1.149(8)	C16B	C17B	1.390(6)
O29'	C28'	1.147(7)	C18B	C19B	1.389(6)
O31'	C30'	1.147(8)	C18B	C23B	1.406(6)
O33'	C32'	1.156(8)	C19B	C20B	1.385(6)
C3'	C4'	1.530(7)	C20B	C21B	1.386(7)
C5'	C6'	1.531(6)	C21B	C22B	1.376(7)
C5'	C12'	1.536(6)	C22B	C23B	1.400(6)
C5'	C18'	1.549(6)			

Table 7.3: Bond Angles for **7a**.

Atom	Atom	Atom	Angle/˚	Atom	Atom	Atom	Angle/˚
C24	Mo	P2	172.15(16)	C7'	C6'	C5'	118.8(4)
C24	Mo	C26	88.6(2)	C7'	C6'	C11'	118.1(4)
C24	Mo	C28	91.1(2)	C11'	C6'	C5'	123.1(4)
C24	Mo	C30	88.2(2)	C8'	C7'	C6'	120.9(5)
C24	Mo	C32	89.4(2)	C9'	C8'	C7'	120.9(5)
C26	Mo	P2	99.29(14)	C8'	C9'	C10'	119.0(5)
C28	Mo	P2	89.25(14)	C11'	C10'	C9'	120.6(5)
C28	Mo	C26	88.5(2)	C10'	C11'	C6'	120.5(5)
C30	Mo	P2	83.96(15)	C13'	C12'	C5'	122.2(4)
C30	Mo	C26	175.8(2)	C13'	C12'	C17'	117.5(4)
C30	Mo	C28	88.9(2)	C17'	C12'	C5'	120.2(4)
C30	Mo	C32	90.3(2)	C14'	C13'	C12'	121.2(4)
C32	Mo	P2	90.12(15)	C15'	C14'	C13'	120.9(5)
C32	Mo	C26	92.3(2)	C16'	C15'	C14'	118.5(5)

C32	Mo	C28	179.1(2)	C15'	C16'	C17'	121.0(5)
O1	P2	Mo	111.44(13)	C16'	C17'	C12'	120.8(5)
O1	P2	C3	80.81(19)	C19'	C18'	C5'	124.4(5)
O1	P2	C5	107.48(19)	C19'	C18'	C23'	118.2(5)
C3	P2	Mo	119.13(18)	C23'	C18'	C5'	117.3(4)
C3	P2	C5	104.9(2)	C18'	C19'	C20'	120.6(6)
C5	P2	Mo	124.35(14)	C21'	C20'	C19'	120.5(6)
C4	O1	P2	95.3(3)	C20'	C21'	C22'	119.9(5)
C4	C3	P2	85.6(3)	C21'	C22'	C23'	119.6(6)
O1	C4	C3	98.0(3)	C22'	C23'	C18'	121.1(5)
C6	C5	P2	112.1(3)	O25'	C24'	Mo'	178.2(5)
C6	C5	C12	106.6(4)	O27'	C26'	Mo'	174.8(6)
C6	C5	C18	115.3(4)	O29'	C28'	Mo'	178.5(5)
C12	C5	P2	110.7(3)	O31'	C30'	Mo'	178.5(6)
C12	C5	C18	112.0(4)	O33'	C32'	Mo'	177.5(7)
C18	C5	P2	100.1(3)	C24B	MoB	P2B	172.97(15)
C7	C6	C5	124.1(4)	C24B	MoB	C26B	90.01(19)
C7	C6	C11	117.6(4)	C24B	MoB	C28B	90.9(2)
C11	C6	C5	118.2(4)	C24B	MoB	C32B	85.5(2)
C8	C7	C6	121.2(5)	C26B	MoB	P2B	95.36(13)
C9	C8	C7	120.3(5)	C28B	MoB	P2B	93.61(13)
C8	C9	C10	119.4(5)	C28B	MoB	C26B	90.0(2)
C11	C10	C9	121.2(5)	C30B	MoB	P2B	83.87(14)
C10	C11	C6	120.3(5)	C30B	MoB	C24B	91.3(2)
C13	C12	C5	118.4(4)	C30B	MoB	C26B	173.8(2)
C13	C12	C17	118.5(4)	C30B	MoB	C28B	83.9(2)
C17	C12	C5	123.1(4)	C30B	MoB	C32B	88.4(2)
C12	C13	C14	120.9(5)	C32B	MoB	P2B	89.25(14)
C15	C14	C13	119.8(5)	C32B	MoB	C26B	97.8(2)
C16	C15	C14	120.0(5)	C32B	MoB	C28B	171.4(2)
C15	C16	C17	120.1(5)	O1B	P2B	MoB	114.56(13)
C12	C17	C16	120.6(5)	O1B	P2B	C3B	80.39(19)
C19	C18	C5	120.2(4)	O1B	P2B	C5B	106.33(18)
C23	C18	C5	121.3(4)	C3B	P2B	MoB	115.17(16)
C23	C18	C19	118.1(4)	C3B	P2B	C5B	105.6(2)
C20	C19	C18	120.3(5)	C5B	P2B	MoB	125.52(14)
C21	C20	C19	120.7(5)	C4B	O1B	P2B	95.3(3)
C22	C21	C20	119.6(5)	C4B	C3B	P2B	85.8(3)
C21	C22	C23	119.8(5)	O1B	C4B	C3B	98.1(3)
C18	C23	C22	121.5(5)	C6B	C5B	P2B	110.6(3)
O25	C24	Mo	177.9(5)	C12B	C5B	P2B	112.1(3)
O27	C26	Mo	174.8(4)	C12B	C5B	C6B	106.9(3)
O29	C28	Mo	178.2(5)	C12B	C5B	C18B	112.1(4)
O31	C30	Mo	179.2(6)	C18B	C5B	P2B	102.4(3)
O33	C32	Mo	176.2(6)	C18B	C5B	C6B	112.8(4)
C24'	Mo'	P2'	174.29(16)	C7B	C6B	C5B	124.1(4)

C24'	Mo'	C26'	86.7(2)	C7B	C6B	C11B	117.9(4)
C24'	Mo'	C28'	88.8(2)	C11B	C6B	C5B	118.0(4)
C24'	Mo'	C30'	90.9(2)	C6B	C7B	C8B	120.7(5)
C26'	Mo'	P2'	98.78(16)	C9B	C8B	C7B	120.6(5)
C26'	Mo'	C28'	91.5(3)	C10B	C9B	C8B	119.6(5)
C28'	Mo'	P2'	89.37(14)	C9B	C10B	C11B	120.2(5)
C30'	Mo'	P2'	83.67(17)	C10B	C11B	C6B	121.0(5)
C30'	Mo'	C26'	177.2(2)	C13B	C12B	C5B	116.5(4)
C30'	Mo'	C28'	89.8(2)	C17B	C12B	C5B	125.3(4)
C32'	Mo'	P2'	90.10(18)	C17B	C12B	C13B	118.1(4)
C32'	Mo'	C24'	91.5(2)	C14B	C13B	C12B	121.4(5)
C32'	Mo'	C26'	91.4(3)	C13B	C14B	C15B	119.8(5)
C32'	Mo'	C28'	177.2(3)	C16B	C15B	C14B	119.2(4)
C32'	Mo'	C30'	87.3(3)	C15B	C16B	C17B	120.5(5)
O1'	P2'	Mo'	112.57(14)	C12B	C17B	C16B	121.1(5)
O1'	P2'	C3'	80.9(2)	C19B	C18B	C5B	119.5(4)
O1'	P2'	C5'	105.9(2)	C19B	C18B	C23B	118.3(4)
C3'	P2'	Mo'	116.34(16)	C23B	C18B	C5B	122.1(4)
C3'	P2'	C5'	104.3(2)	C20B	C19B	C18B	120.6(4)
C5'	P2'	Mo'	127.00(15)	C19B	C20B	C21B	121.3(5)
C4'	O1'	P2'	94.6(3)	C22B	C21B	C20B	118.8(4)
C4'	C3'	P2'	85.7(3)	C21B	C22B	C23B	120.9(5)
O1'	C4'	C3'	98.5(4)	C22B	C23B	C18B	120.2(4)
C6'	C5'	P2'	111.1(3)	O25B	C24B	MoB	176.6(5)
C6'	C5'	C12'	114.8(4)	O27B	C26B	MoB	175.5(5)
C6'	C5'	C18'	106.9(4)	O29B	C28B	MoB	174.3(4)
C12'	C5'	P2'	100.9(3)	O31B	C30B	MoB	176.0(4)
C12'	C5'	C18'	111.4(4)	O33B	C32B	MoB	173.4(5)
C18'	C5'	P2'	111.8(3)				

7.1.2 [Pentacarbonyl{-4,4-dimethyl-2-(triphenylmethyl)-1,2-oxaphosphetane-κ*P*}molybdenum(0)] (7b)

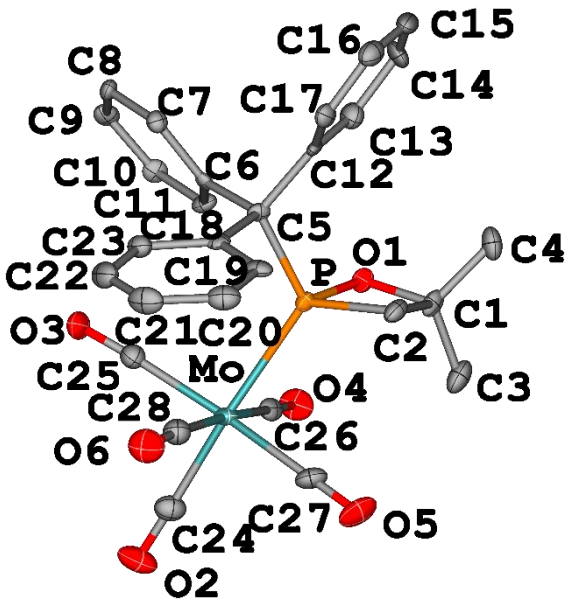

Figure 7.2: Molecular structures of **7b** in the solid state. Hydrogen atoms are omitted and the thermal ellipsoids are set at the 50% probability level.

Table 7.4: Crystal data and structure refinement for **7b**.

Identification code	GSTR755, FLG-308 // GXraymo_6850_0m0
Crystal Habitus	clear colourless needle
Device Type	Bruker D8 Venture
Empirical formula	$C_{28}H_{23}O_6PMo$
Moiety formula	C28 H23 Mo O6 P
Formula weight	582.37
Temperature/K	100.0
Crystal system	triclinic
Space group	P-1
a/Å	9.4957(6)
b/Å	18.3164(14)
c/Å	22.5419(16)
α/°	99.296(2)
β/°	92.701(2)
γ/°	95.011(2)
Volume/Å^3	3846.9(5)
Z	6
ρ_{calc}g/cm^3	1.508
μ/mm^{-1}	0.615
F(000)	1776.0
Crystal size/mm^3	0.6 × 0.01 × 0.01
Absorption correction	empirical
Tmin; Tmax	0.599645; 0.745985
Radiation	MoKα (λ = 0.71073)

2Θ range for data collection/°	3.668 to 55.998°
Completeness to theta	0.967
Index ranges	-12 ≤ h ≤ 12, -23 ≤ k ≤ 23, 0 ≤ l ≤ 29
Reflections collected	17274
Independent reflections	17274 [R_{int} = 0.1156, R_{sigma} = 0.1744]
Data/restraints/parameters	17274/30/979
Goodness-of-fit on F^2	0.996
Final R indexes [I>=2σ (I)]	R_1 = 0.0650, wR_2 = 0.1379
Final R indexes [all data]	R_1 = 0.1453, wR_2 = 0.1588
Largest diff. peak/hole / e $Å^{-3}$	2.23/-0.83

Table 7.5: Bond Lengths for **7b**.

Atom	Atom	Length/Å	Atom	Atom	Length/Å
Mo	P	2.5313(14)	C5'	C12'	1.534(7)
Mo	C24	2.009(6)	C5'	C18'	1.553(7)
Mo	C25	2.044(6)	C6'	C7'	1.408(7)
Mo	C26	2.042(6)	C6'	C11'	1.385(7)
Mo	C27	2.028(6)	C7'	C8'	1.399(7)
Mo	C28	2.053(6)	C8'	C9'	1.371(7)
P	O1	1.666(4)	C9'	C10'	1.381(8)
P	C1	2.344(5)	C10'	C11'	1.382(7)
P	C2	1.839(5)	C12'	C13'	1.387(8)
P	C5	1.896(5)	C12'	C17'	1.397(7)
O1	C1	1.500(6)	C13'	C14'	1.387(8)
O2	C24	1.142(7)	C14'	C15'	1.382(8)
O3	C25	1.144(6)	C15'	C16'	1.376(9)
O4	C26	1.159(6)	C16'	C17'	1.403(8)
O5	C27	1.152(6)	C18'	C19'	1.403(7)
O6	C28	1.136(6)	C18'	C23'	1.391(7)
C1	C2	1.551(7)	C19'	C20'	1.382(7)
C1	C3	1.518(7)	C20'	C21'	1.367(8)
C1	C4	1.509(7)	C21'	C22'	1.384(8)
C5	C6	1.546(7)	C22'	C23'	1.387(7)
C5	C12	1.543(7)	Mo1A	P1A	2.5258(14)
C5	C18	1.563(7)	Mo1A	C24A	2.003(6)
C6	C7	1.412(7)	Mo1A	C25A	2.058(6)
C6	C11	1.380(7)	Mo1A	C26A	2.039(6)
C7	C8	1.392(7)	Mo1A	C27A	2.047(6)
C8	C9	1.382(7)	Mo1A	C28A	2.052(6)
C9	C10	1.382(7)	P1A	O1A	1.665(4)
C10	C11	1.399(7)	P1A	C1A	2.337(5)
C12	C13	1.403(7)	P1A	C2A	1.843(5)
C12	C17	1.396(7)	P1A	C5A	1.905(5)
C13	C14	1.381(7)	O1A	C1A	1.500(6)
C14	C15	1.372(8)	O2A	C24A	1.143(6)
C15	C16	1.364(8)	O3A	C25A	1.134(7)

C16	C17	1.388(7)	O4A	C26A	1.145(6)
C18	C19	1.395(7)	O5A	C27A	1.152(6)
C18	C23	1.394(7)	O6A	C28A	1.141(6)
C19	C20	1.377(7)	C1A	C2A	1.543(7)
C20	C21	1.395(8)	C1A	C3A	1.519(7)
C21	C22	1.369(8)	C1A	C4A	1.514(7)
C22	C23	1.384(7)	C5A	C6A	1.543(7)
Mo'	P'	2.5147(14)	C5A	C12A	1.549(7)
Mo'	C24'	1.996(6)	C5A	C18A	1.559(7)
Mo'	C25'	2.064(6)	C6A	C7A	1.401(7)
Mo'	C26'	2.043(6)	C6A	C11A	1.390(7)
Mo'	C27'	2.045(6)	C7A	C8A	1.371(8)
Mo'	C28'	2.053(6)	C8A	C9A	1.391(8)
P'	O1'	1.668(4)	C9A	C10A	1.382(7)
P'	C1'	2.330(5)	C10A	C11A	1.364(7)
P'	C2'	1.815(5)	C12A	C13A	1.391(7)
P'	C5'	1.906(5)	C12A	C17A	1.389(7)
O1'	C1'	1.508(6)	C13A	C14A	1.393(7)
O2'	C24'	1.141(7)	C14A	C15A	1.374(8)
O3'	C25'	1.143(6)	C15A	C16A	1.379(8)
O4'	C26'	1.152(6)	C16A	C17A	1.382(7)
O5'	C27'	1.134(6)	C18A	C19A	1.387(7)
O6'	C28'	1.142(6)	C18A	C23A	1.400(7)
C1'	C2'	1.538(7)	C19A	C20A	1.406(7)
C1'	C3'	1.529(8)	C20A	C21A	1.382(7)
C1'	C4'	1.522(8)	C21A	C22A	1.390(8)
C5'	C6'	1.548(7)	C22A	C23A	1.369(7)

Table 7.6: Bond Angles for **7b**.

Atom	Atom	Atom	Angle/˚	Atom	Atom	Atom	Angle/˚
C24	Mo	P	172.68(17)	C1'	C2'	P'	87.6(3)
C24	Mo	C25	87.4(2)	C6'	C5'	P'	110.3(3)
C24	Mo	C26	88.9(2)	C6'	C5'	C18'	112.9(4)
C24	Mo	C27	91.9(2)	C12'	C5'	P'	113.3(3)
C24	Mo	C28	86.3(2)	C12'	C5'	C6'	104.1(4)
C25	Mo	P	94.21(16)	C12'	C5'	C18'	115.8(4)
C25	Mo	C28	87.1(2)	C18'	C5'	P'	100.7(3)
C26	Mo	P	83.93(15)	C7'	C6'	C5'	117.6(4)
C26	Mo	C25	93.4(2)	C11'	C6'	C5'	124.3(5)
C26	Mo	C28	175.1(2)	C11'	C6'	C7'	118.0(5)
C27	Mo	P	87.50(16)	C8'	C7'	C6'	120.4(5)
C27	Mo	C25	172.0(2)	C9'	C8'	C7'	120.0(5)
C27	Mo	C26	94.6(2)	C8'	C9'	C10'	120.0(5)
C27	Mo	C28	85.0(2)	C9'	C10'	C11'	120.4(5)
C28	Mo	P	100.87(16)	C10'	C11'	C6'	121.1(5)
O1	P	Mo	113.45(13)	C13'	C12'	C5'	119.4(5)

O1	P	C1	39.56(17)	C13'	C12'	C17'	118.2(5)
O1	P	C2	80.1(2)	C17'	C12'	C5'	122.3(5)
O1	P	C5	107.8(2)	C14'	C13'	C12'	121.4(6)
C1	P	Mo	119.52(14)	C15'	C14'	C13'	120.4(6)
C2	P	Mo	120.10(18)	C16'	C15'	C14'	119.0(6)
C2	P	C1	41.4(2)	C15'	C16'	C17'	121.1(6)
C2	P	C5	108.3(2)	C12'	C17'	C16'	119.8(6)
C5	P	Mo	119.82(17)	C19'	C18'	C5'	119.7(4)
C5	P	C1	120.3(2)	C23'	C18'	C5'	122.4(5)
C1	O1	P	95.4(3)	C23'	C18'	C19'	117.8(5)
O1	C1	P	45.0(2)	C20'	C19'	C18'	120.6(5)
O1	C1	C2	95.5(4)	C21'	C20'	C19'	121.0(5)
O1	C1	C3	108.2(4)	C20'	C21'	C22'	119.4(5)
O1	C1	C4	110.2(4)	C21'	C22'	C23'	120.3(5)
C2	C1	P	51.6(2)	C22'	C23'	C18'	120.9(5)
C3	C1	P	113.8(4)	O2'	C24'	Mo'	177.9(6)
C3	C1	C2	114.1(5)	O3'	C25'	Mo'	176.1(5)
C4	C1	P	133.9(4)	O4'	C26'	Mo'	178.8(5)
C4	C1	C2	116.3(4)	O5'	C27'	Mo'	173.5(5)
C4	C1	C3	111.2(5)	O6'	C28'	Mo'	174.0(5)
C1	C2	P	87.0(3)	C24A	Mo1A	P1A	171.76(18)
C6	C5	P	111.4(3)	C24A	Mo1A	C25A	88.0(2)
C6	C5	C18	112.6(4)	C24A	Mo1A	C26A	89.0(2)
C12	C5	P	113.9(3)	C24A	Mo1A	C27A	88.0(2)
C12	C5	C6	105.1(4)	C24A	Mo1A	C28A	89.8(2)
C12	C5	C18	114.0(4)	C25A	Mo1A	P1A	99.36(15)
C18	C5	P	100.0(3)	C26A	Mo1A	P1A	87.88(16)
C7	C6	C5	117.3(4)	C26A	Mo1A	C25A	85.4(2)
C11	C6	C5	123.8(4)	C26A	Mo1A	C27A	95.0(2)
C11	C6	C7	118.6(4)	C26A	Mo1A	C28A	173.7(2)
C8	C7	C6	119.7(5)	C27A	Mo1A	P1A	84.72(16)
C9	C8	C7	121.1(5)	C27A	Mo1A	C25A	175.9(2)
C8	C9	C10	119.3(5)	C27A	Mo1A	C28A	91.1(2)
C9	C10	C11	120.3(5)	C28A	Mo1A	P1A	94.14(15)
C6	C11	C10	120.9(5)	C28A	Mo1A	C25A	88.5(2)
C13	C12	C5	118.2(5)	O1A	P1A	Mo1A	114.31(13)
C17	C12	C5	124.0(5)	O1A	P1A	C1A	39.74(17)
C17	C12	C13	117.5(5)	O1A	P1A	C2A	79.8(2)
C14	C13	C12	120.6(5)	O1A	P1A	C5A	106.1(2)
C15	C14	C13	120.9(6)	C1A	P1A	Mo1A	118.91(14)
C16	C15	C14	119.3(5)	C2A	P1A	Mo1A	120.07(17)
C15	C16	C17	121.1(5)	C2A	P1A	C1A	41.2(2)
C16	C17	C12	120.5(5)	C2A	P1A	C5A	108.1(2)
C19	C18	C5	119.9(4)	C5A	P1A	Mo1A	120.63(16)
C23	C18	C5	121.8(5)	C5A	P1A	C1A	120.1(2)
C23	C18	C19	118.2(5)	C1A	O1A	P1A	95.0(3)

C20	C19	C18	120.9(5)	O1A	C1A	P1A	45.22(19)
C19	C20	C21	120.4(6)	O1A	C1A	C2A	95.6(4)
C22	C21	C20	119.0(6)	O1A	C1A	C3A	107.6(4)
C21	C22	C23	121.1(5)	O1A	C1A	C4A	109.1(4)
C22	C23	C18	120.5(5)	C2A	C1A	P1A	51.9(2)
O2	C24	Mo	178.7(5)	C3A	C1A	P1A	113.3(4)
O3	C25	Mo	176.2(5)	C3A	C1A	C2A	116.2(5)
O4	C26	Mo	179.2(5)	C4A	C1A	P1A	134.2(4)
O5	C27	Mo	175.1(5)	C4A	C1A	C2A	116.0(4)
O6	C28	Mo	173.8(5)	C4A	C1A	C3A	110.7(4)
C24'	Mo'	P'	172.35(18)	C1A	C2A	P1A	86.8(3)
C24'	Mo'	C25'	89.1(2)	C6A	C5A	P1A	101.0(3)
C24'	Mo'	C26'	89.2(2)	C6A	C5A	C12A	114.4(4)
C24'	Mo'	C27'	89.0(2)	C6A	C5A	C18A	113.0(4)
C24'	Mo'	C28'	88.6(2)	C12A	C5A	P1A	112.5(3)
C25'	Mo'	P'	94.30(15)	C12A	C5A	C18A	105.9(4)
C26'	Mo'	P'	83.85(15)	C18A	C5A	P1A	110.1(3)
C26'	Mo'	C25'	92.2(2)	C7A	C6A	C5A	121.6(5)
C26'	Mo'	C27'	94.3(2)	C11A	C6A	C5A	121.6(5)
C26'	Mo'	C28'	177.4(2)	C11A	C6A	C7A	116.7(5)
C27'	Mo'	P'	88.38(15)	C8A	C7A	C6A	120.9(5)
C27'	Mo'	C25'	173.2(2)	C7A	C8A	C9A	121.6(5)
C27'	Mo'	C28'	84.4(2)	C10A	C9A	C8A	117.2(5)
C28'	Mo'	P'	98.32(16)	C11A	C10A	C9A	121.5(5)
C28'	Mo'	C25'	89.0(2)	C10A	C11A	C6A	121.9(5)
O1'	P'	Mo'	114.58(14)	C13A	C12A	C5A	123.4(5)
O1'	P'	C1'	40.18(18)	C17A	C12A	C5A	118.5(5)
O1'	P'	C2'	80.5(2)	C17A	C12A	C13A	117.8(5)
O1'	P'	C5'	107.9(2)	C12A	C13A	C14A	120.7(5)
C1'	P'	Mo'	119.72(16)	C15A	C14A	C13A	120.5(6)
C2'	P'	Mo'	119.48(18)	C14A	C15A	C16A	119.2(5)
C2'	P'	C1'	41.3(2)	C15A	C16A	C17A	120.6(5)
C2'	P'	C5'	106.9(2)	C16A	C17A	C12A	121.1(5)
C5'	P'	Mo'	120.30(16)	C19A	C18A	C5A	123.6(4)
C5'	P'	C1'	119.9(2)	C19A	C18A	C23A	118.1(5)
C1'	O1'	P'	94.2(3)	C23A	C18A	C5A	118.2(4)
O1'	C1'	P'	45.6(2)	C18A	C19A	C20A	120.6(5)
O1'	C1'	C2'	95.5(4)	C21A	C20A	C19A	120.2(5)
O1'	C1'	C3'	108.2(4)	C20A	C21A	C22A	119.1(5)
O1'	C1'	C4'	109.4(4)	C23A	C22A	C21A	120.7(5)
C2'	C1'	P'	51.1(2)	C22A	C23A	C18A	121.2(5)
C3'	C1'	P'	115.2(4)	O2A	C24A	Mo1A	177.8(6)
C3'	C1'	C2'	116.3(5)	O3A	C25A	Mo1A	173.8(5)
C4'	C1'	P'	133.1(4)	O4A	C26A	Mo1A	175.2(5)
C4'	C1'	C2'	115.8(5)	O5A	C27A	Mo1A	178.5(5)
C4'	C1'	C3'	110.3(5)	O6A	C28A	Mo1A	176.2(5)

7.1.3 2-(Triphenylmethyl)-1,2-oxaphosphetane (8a)

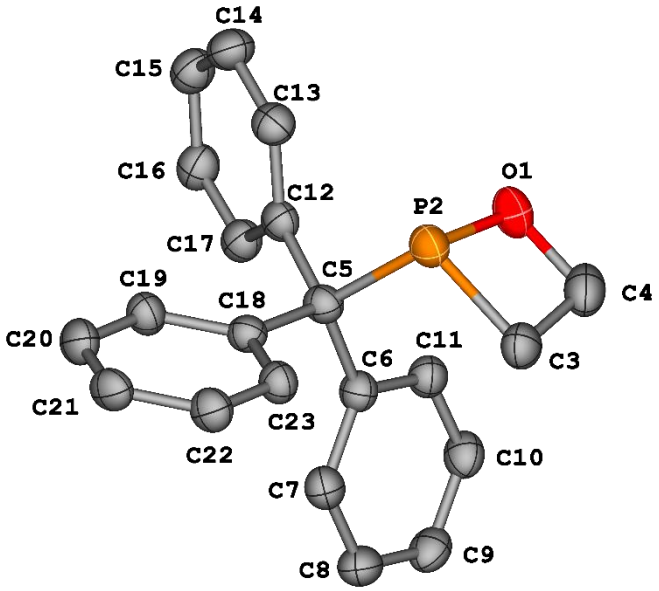

Figure 7.3: Molecular structures of **8a** in the solid state. Hydrogen atoms are omitted and the thermal ellipsoids are set at the 50% probability level.

Table 7.7: Crystal data and structure refinement for **8a**.

Identification code	GSTR746, FLG-326 // GXray6808
Crystal Habitus	clear colourless plate
Device Type	STOE IPDS-2T
Empirical formula	$C_{21}H_{19}OP$
Moiety formula	C21 H19 O P
Formula weight	318.33
Temperature/K	123(2)
Crystal system	triclinic
Space group	P-1
a/Å	8.1143(10)
b/Å	8.9827(13)
c/Å	12.4136(16)
α/°	94.652(11)
β/°	90.566(10)
γ/°	113.742(10)
Volume/Å^3	824.6(2)
Z	2
ρ_{calc}g/cm^3	1.282
μ/mm^{-1}	0.169
F(000)	336.0
Crystal size/mm^3	0.25 × 0.14 × 0.03
Absorption correction	integration
Tmin; Tmax	0.8198; 0.9942
Radiation	MoKα (λ = 0.71073)

2Θ range for data collection/°	4.976 to 50.496°
Completeness to theta	0.994
Index ranges	-9 ≤ h ≤ 9, -10 ≤ k ≤ 10, -14 ≤ l ≤ 14
Reflections collected	7553
Independent reflections	7553 [R_{int} = 0.0757, R_{sigma} = 0.0981]
Data/restraints/parameters	7553/0/209
Goodness-of-fit on F^2	0.910
Final R indexes [I>=2σ (I)]	R_1 = 0.0611, wR_2 = 0.1392
Final R indexes [all data]	R_1 = 0.1409, wR_2 = 0.1720
Largest diff. peak/hole / e $Å^{-3}$	0.67/-0.41

Table 7.8: Bond Lengths for **8a**.

Atom	Atom	Length/Å	Atom	Atom	Length/Å
P2	O1	1.670(3)	C10	C11	1.379(6)
P2	C3	1.849(4)	C12	C13	1.391(6)
P2	C4	2.318(5)	C12	C17	1.396(6)
P2	C5	1.923(5)	C13	C14	1.387(6)
O1	C4	1.468(5)	C14	C15	1.391(7)
C3	C4	1.541(6)	C15	C16	1.383(6)
C5	C6	1.528(5)	C16	C17	1.387(6)
C5	C12	1.540(6)	C18	C19	1.394(6)
C5	C18	1.533(6)	C18	C23	1.402(6)
C6	C7	1.398(6)	C19	C20	1.383(6)
C6	C11	1.394(6)	C20	C21	1.379(6)
C7	C8	1.390(6)	C21	C22	1.380(6)
C8	C9	1.373(6)	C22	C23	1.383(6)
C9	C10	1.380(6)			

Table 7.9: Bond Angles for **8a**.

Atom	Atom	Atom	Angle/˚	Atom	Atom	Atom	Angle/˚
O1	P2	C3	80.47(18)	C8	C9	C10	119.5(4)
O1	P2	C4	39.12(16)	C11	C10	C9	120.4(4)
O1	P2	C5	104.29(18)	C10	C11	C6	121.4(4)
C3	P2	C4	41.52(18)	C13	C12	C5	121.5(4)
C3	P2	C5	105.5(2)	C13	C12	C17	117.4(4)
C5	P2	C4	112.47(18)	C17	C12	C5	121.0(4)
C4	O1	P2	95.0(3)	C14	C13	C12	121.7(4)
C4	C3	P2	85.8(3)	C13	C14	C15	119.8(4)
O1	C4	C3	98.3(3)	C16	C15	C14	119.4(4)
C6	C5	P2	112.4(3)	C15	C16	C17	120.2(5)
C6	C5	C12	111.5(3)	C16	C17	C12	121.5(4)
C6	C5	C18	113.1(3)	C19	C18	C5	122.9(4)
C12	C5	P2	106.5(3)	C19	C18	C23	117.2(4)
C18	C5	P2	103.6(3)	C23	C18	C5	120.0(4)
C18	C5	C12	109.3(3)	C20	C19	C18	121.1(4)

C7	C6	C5	122.4(4)	C21	C20	C19	120.9(4)
C11	C6	C5	120.2(4)	C20	C21	C22	119.0(4)
C11	C6	C7	117.4(4)	C21	C22	C23	120.4(4)
C8	C7	C6	120.9(4)	C22	C23	C18	121.4(4)
C9	C8	C7	120.5(4)				

Table 7.10: Torsion Angles for **8a**.

A	B	C	D	Angle/˚	A	B	C	D	Angle/˚
P2	O1	C4	C3	5.3(3)	C7	C8	C9	C10	-0.9(7)
P2	C3	C4	O1	-4.8(3)	C8	C9	C10	C11	-0.1(7)
P2	C5	C6	C7	115.8(4)	C9	C10	C11	C6	1.5(7)
P2	C5	C6	C11	-63.1(5)	C11	C6	C7	C8	0.7(7)
P2	C5	C12	C13	-35.9(5)	C12	C5	C6	C7	-124.8(4)
P2	C5	C12	C17	147.2(4)	C12	C5	C6	C11	56.3(5)
P2	C5	C18	C19	133.8(4)	C12	C5	C18	C19	20.6(6)
P2	C5	C18	C23	-45.6(4)	C12	C5	C18	C23	-158.8(4)
O1	P2	C3	C4	4.3(3)	C12	C13	C14	C15	0.2(7)
C3	P2	O1	C4	-4.5(3)	C13	C12	C17	C16	0.0(7)
C5	P2	O1	C4	-108.2(3)	C13	C14	C15	C16	0.2(7)
C5	P2	C3	C4	106.6(3)	C14	C15	C16	C17	-0.5(7)
C5	C6	C7	C8	-178.3(4)	C15	C16	C17	C12	0.4(7)
C5	C6	C11	C10	177.2(4)	C17	C12	C13	C14	-0.3(7)
C5	C12	C13	C14	-177.2(4)	C18	C5	C6	C7	-1.2(6)
C5	C12	C17	C16	176.9(4)	C18	C5	C6	C11	179.9(4)
C5	C18	C19	C20	180.0(4)	C18	C5	C12	C13	75.4(5)
C5	C18	C23	C22	179.9(4)	C18	C5	C12	C17	-101.4(5)
C6	C5	C12	C13	-158.8(4)	C18	C19	C20	C21	0.5(7)
C6	C5	C12	C17	24.3(5)	C19	C18	C23	C22	0.5(6)
C6	C5	C18	C19	-104.2(5)	C19	C20	C21	C22	-0.4(7)
C6	C5	C18	C23	76.4(5)	C20	C21	C22	C23	0.3(7)
C6	C7	C8	C9	0.6(7)	C21	C22	C23	C18	-0.4(7)
C7	C6	C11	C10	-1.7(7)	C23	C18	C19	C20	-0.6(6)

7.1.4 2-(Triphenylmethyl)-1,2-oxaphosphetane P-sulfide (11a)

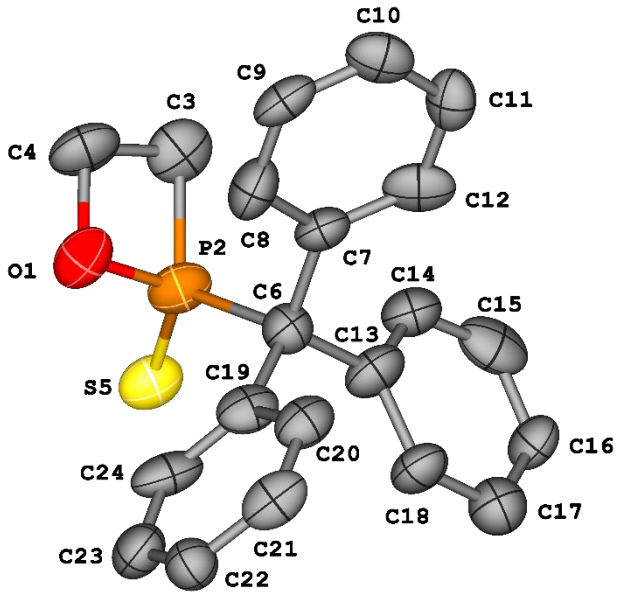

Figure 7.4: Molecular structures of **11a** in the solid state. Hydrogen atoms are omitted and the thermal ellipsoids are set at the 50% probability level.

Table 7.11: Crystal data and structure refinement for **11a**.

Identification code	GSTR785, FLG-399 // GXray7060
Crystal Habitus	clear colourless plank
Device Type	STOE STADIVARI
Empirical formula	$C_{21}H_{19}OPS$
Moiety formula	C21 H19 O P S
Formula weight	350.41
Temperature/K	100
Crystal system	triclinic
Space group	P-1
a/Å	9.2693(19)
b/Å	11.021(3)
c/Å	18.294(4)
α/°	73.025(17)
β/°	83.985(16)
γ/°	77.267(17)
Volume/Å^3	1741.8(6)
Z	4
ρ_{calc}g/cm^3	1.336
μ/mm^{-1}	2.54
F(000)	736.0
Crystal size/mm^3	0.15 × 0.05 × 0.02
Absorption correction	multi-scan
Tmin; Tmax	0.1987; 0.8623
Radiation	CuKα (λ = 1.54186)

2Θ range for data collection/°	8.562 to 140.902°
Completeness to theta	0.994
Index ranges	-7 ≤ h ≤ 11, -13 ≤ k ≤ 13, -19 ≤ l ≤ 22
Reflections collected	65511
Independent reflections	65511 [R_{int} = 0.8514, R_{sigma} = 0.2691]
Data/restraints/parameters	65511/24/433
Goodness-of-fit on F^2	1.170
Final R indexes [I>=2σ (I)]	R_1 = 0.1747, wR_2 = 0.4022
Final R indexes [all data]	R_1 = 0.3324, wR_2 = 0.4825
Largest diff. peak/hole / e $Å^{-3}$	1.17/-0.69

Table 7.12: Bond Lengths for **11a**.

Atom	Atom	Length/Å	Atom	Atom	Length/Å
S5	P2	1.923(6)	S5'	P2'	1.929(5)
P2	O1	1.631(12)	P2'	O1'	1.621(12)
P2	C3	1.802(18)	P2'	C3'	1.79(2)
P2	C6	1.906(15)	P2'	C6'	1.900(16)
O1	C4	1.458(19)	O1'	C4'	1.514(19)
C3	C4	1.52(2)	C3'	C4'	1.56(3)
C6	C7	1.57(2)	C6'	C7'	1.59(2)
C6	C13	1.58(2)	C6'	C13'	1.50(2)
C6	C19	1.52(2)	C6'	C19'	1.58(2)
C7	C8	1.41(2)	C7'	C8'	1.39(2)
C7	C12	1.37(2)	C7'	C12'	1.41(2)
C8	C9	1.40(2)	C8'	C9'	1.38(2)
C9	C10	1.36(2)	C9'	C10'	1.40(3)
C10	C11	1.39(2)	C10'	C11'	1.39(2)
C11	C12	1.42(2)	C11'	C12'	1.42(2)
C13	C14	1.37(2)	C13'	C14'	1.39(2)
C13	C18	1.40(2)	C13'	C18'	1.38(2)
C14	C15	1.40(2)	C14'	C15'	1.36(2)
C15	C16	1.37(2)	C15'	C16'	1.42(2)
C16	C17	1.38(2)	C16'	C17'	1.40(2)
C17	C18	1.41(2)	C17'	C18'	1.34(2)
C19	C20	1.43(2)	C19'	C20'	1.41(2)
C19	C24	1.36(2)	C19'	C24'	1.34(2)
C20	C21	1.41(2)	C20'	C21'	1.44(2)
C21	C22	1.38(2)	C21'	C22'	1.32(2)
C22	C23	1.40(2)	C22'	C23'	1.37(2)
C23	C24	1.39(2)	C23'	C24'	1.44(2)

Table 7.13: Bond Angles for **11a**.

Atom	Atom	Atom	Angle/˚	Atom	Atom	Atom	Angle/˚
O1	P2	S5	116.9(5)	O1'	P2'	S5'	114.8(5)
O1	P2	C3	82.4(7)	O1'	P2'	C3'	84.1(8)

O1	P2	C6	104.7(6)	O1'	P2'	C6'	107.0(7)
C3	P2	S5	119.0(5)	C3'	P2'	S5'	118.8(6)
C3	P2	C6	112.5(7)	C3'	P2'	C6'	111.7(8)
C6	P2	S5	116.0(5)	C6'	P2'	S5'	115.8(5)
C4	O1	P2	93.6(9)	C4'	O1'	P2'	93.6(10)
C4	C3	P2	84.9(10)	C4'	C3'	P2'	85.8(10)
O1	C4	C3	98.8(13)	O1'	C4'	C3'	96.3(14)
C7	C6	P2	107.1(10)	C7'	C6'	P2'	106.7(10)
C7	C6	C13	112.3(11)	C13'	C6'	P2'	111.4(12)
C13	C6	P2	104.1(9)	C13'	C6'	C7'	109.7(12)
C19	C6	P2	109.8(10)	C13'	C6'	C19'	114.1(13)
C19	C6	C7	110.2(11)	C19'	C6'	P2'	105.1(10)
C19	C6	C13	113.1(13)	C19'	C6'	C7'	109.5(13)
C8	C7	C6	117.4(13)	C8'	C7'	C6'	123.9(14)
C12	C7	C6	122.7(14)	C8'	C7'	C12'	121.2(14)
C12	C7	C8	119.6(14)	C12'	C7'	C6'	114.8(15)
C9	C8	C7	117.6(14)	C9'	C8'	C7'	118.5(14)
C10	C9	C8	122.8(15)	C8'	C9'	C10'	122.7(15)
C9	C10	C11	120.4(15)	C11'	C10'	C9'	118.7(15)
C10	C11	C12	117.4(14)	C10'	C11'	C12'	120.2(16)
C7	C12	C11	122.1(16)	C7'	C12'	C11'	118.7(17)
C14	C13	C6	120.6(15)	C14'	C13'	C6'	123.6(14)
C14	C13	C18	117.8(16)	C18'	C13'	C6'	120.3(14)
C18	C13	C6	121.6(14)	C18'	C13'	C14'	116.2(14)
C13	C14	C15	121.7(16)	C15'	C14'	C13'	121.7(15)
C16	C15	C14	119.4(15)	C14'	C15'	C16'	121.9(15)
C15	C16	C17	121.1(16)	C17'	C16'	C15'	114.8(15)
C16	C17	C18	118.4(17)	C18'	C17'	C16'	122.6(16)
C13	C18	C17	121.4(15)	C17'	C18'	C13'	122.8(15)
C20	C19	C6	116.8(13)	C20'	C19'	C6'	118.6(14)
C24	C19	C6	125.0(13)	C24'	C19'	C6'	120.6(14)
C24	C19	C20	118.0(14)	C24'	C19'	C20'	120.8(15)
C21	C20	C19	119.8(14)	C19'	C20'	C21'	118.8(14)
C22	C21	C20	121.2(14)	C22'	C21'	C20'	117.8(16)
C21	C22	C23	117.7(14)	C21'	C22'	C23'	125.2(16)
C24	C23	C22	121.4(15)	C22'	C23'	C24'	116.8(15)
C19	C24	C23	121.9(15)	C19'	C24'	C23'	120.6(16)

7.1.5 2-(Triphenylmethyl)-1,2-oxaphosphetane P-borane (14a)

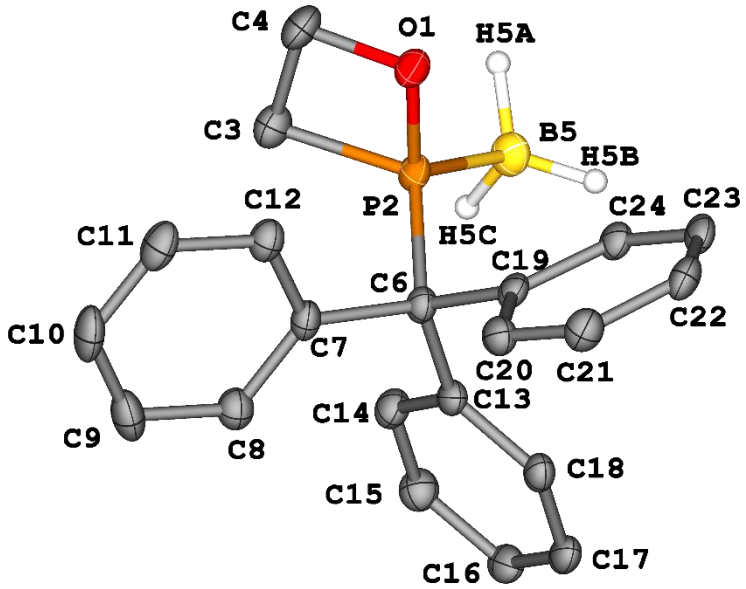

Figure 7.5: Molecular structures of **14a** in the solid state. Hydrogen atoms are omitted unless bound to boron and the thermal ellipsoids are set at the 50% probability level.

Table 7.14: Crystal data and structure refinement for **14a**.

Identification code	GSTR769, FLG-363 // GXraycu_6906f
Crystal Habitus	clear colourless plank
Device Type	Bruker D8 Venture
Empirical formula	$C_{21}H_{22}BOP$
Moiety formula	C21 H22 B O P
Formula weight	332.16
Temperature/K	100.0
Crystal system	monoclinic
Space group	$P2_1/n$
a/Å	8.9875(8)
b/Å	21.0205(17)
c/Å	9.7305(7)
α/°	90
β/°	105.463(4)
γ/°	90
Volume/Å^3	1771.8(3)
Z	4
ρ_{calc}g/cm^3	1.245
μ/mm^{-1}	1.383
F(000)	704.0
Crystal size/mm^3	0.18 × 0.06 × 0.01
Absorption correction	multi-scan
Tmin; Tmax	0.5085; 0.7536
Radiation	CuKα (λ = 1.54178)
2Θ range for data collection/°	8.412 to 135.498°

Completeness to theta	0.996
Index ranges	-10 ≤ h ≤ 10, -25 ≤ k ≤ 25, -11 ≤ l ≤ 11
Reflections collected	34870
Independent reflections	3195 [R_{int} = 0.0788, R_{sigma} = 0.0397]
Data/restraints/parameters	3195/0/226
Goodness-of-fit on F^2	1.055
Final R indexes [I>=2σ (I)]	R_1 = 0.0508, wR_2 = 0.1318
Final R indexes [all data]	R_1 = 0.0559, wR_2 = 0.1365
Largest diff. peak/hole / e $Å^{-3}$	0.60/-0.46

Table 7.15: Bond Lengths for **14a**.

Atom	Atom	Length/Å	Atom	Atom	Length/Å
P2	O1	1.6395(15)	C11	C12	1.385(3)
P2	C3	1.817(2)	C13	C14	1.396(3)
P2	B5	1.907(2)	C13	C18	1.397(3)
P2	C6	1.895(2)	C14	C15	1.384(3)
O1	C4	1.491(3)	C15	C16	1.390(3)
C3	C4	1.543(3)	C16	C17	1.380(3)
C6	C7	1.541(3)	C17	C18	1.393(3)
C6	C13	1.538(3)	C19	C20	1.396(3)
C6	C19	1.539(3)	C19	C24	1.397(3)
C7	C8	1.392(3)	C20	C21	1.386(3)
C7	C12	1.403(3)	C21	C22	1.387(3)
C8	C9	1.396(3)	C22	C23	1.390(3)
C9	C10	1.382(4)	C23	C24	1.385(3)
C10	C11	1.391(4)			

Table 7.16: Bond Angles for **14a**.

Atom	Atom	Atom	Angle/˚	Atom	Atom	Atom	Angle/˚
O1	P2	C3	82.74(9)	C9	C10	C11	119.5(2)
O1	P2	B5	115.71(10)	C12	C11	C10	120.0(2)
O1	P2	C6	106.53(8)	C11	C12	C7	121.1(2)
C3	P2	B5	112.36(11)	C14	C13	C6	119.91(17)
C3	P2	C6	113.56(9)	C14	C13	C18	117.92(18)
C6	P2	B5	119.96(10)	C18	C13	C6	122.17(18)
C4	O1	P2	93.42(12)	C15	C14	C13	121.45(19)
C4	C3	P2	85.09(13)	C14	C15	C16	120.1(2)
O1	C4	C3	97.87(15)	C17	C16	C15	119.17(19)
C7	C6	P2	106.83(12)	C16	C17	C18	120.91(19)
C13	C6	P2	105.22(13)	C17	C18	C13	120.44(19)
C13	C6	C7	113.37(16)	C20	C19	C6	120.32(17)
C13	C6	C19	110.99(15)	C20	C19	C24	118.09(19)
C19	C6	P2	108.56(13)	C24	C19	C6	121.39(17)
C19	C6	C7	111.48(16)	C21	C20	C19	120.99(19)

C8	C7	C6	122.51(18)	C20	C21	C22	120.47(19)
C8	C7	C12	118.21(18)	C21	C22	C23	119.0(2)
C12	C7	C6	119.23(18)	C24	C23	C22	120.59(19)
C7	C8	C9	120.5(2)	C23	C24	C19	120.82(19)
C10	C9	C8	120.6(2)				

7.1.6 2-Bromoethyl(2-methoxy-2-oxoethyl)(triphenylmethyl)phosphane oxide (19a)

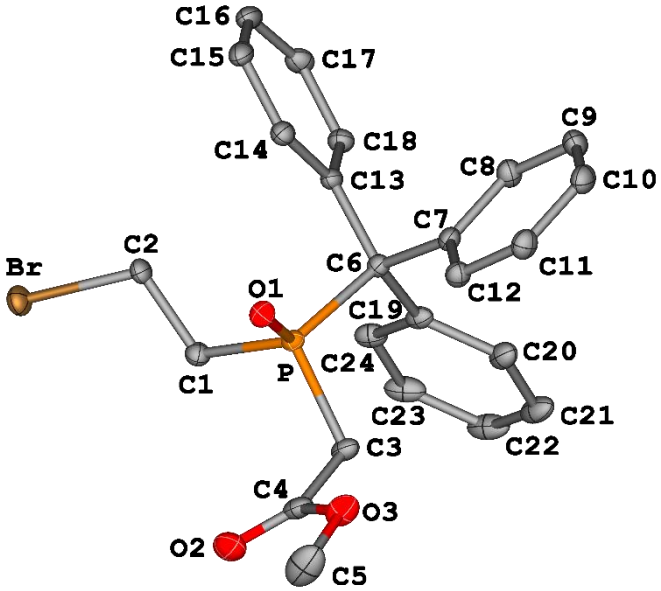

Figure 7.6: Molecular structures of **19a** in the solid state. Hydrogen atoms are omitted and the thermal ellipsoids are set at the 50% probability level.

Table 7.17: Crystal data and structure refinement for **19a**.

Identification code	GSTR752, FLG-327 // GXraymo_6825f
Crystal Habitus	clear colourless plate
Device Type	Bruker D8 Venture
Empirical formula	$C_{24}H_{24}BrO_3P$
Moiety formula	C24 H24 Br O3 P
Formula weight	471.31
Temperature/K	100
Crystal system	triclinic
Space group	P-1
a/Å	9.5566(7)
b/Å	10.8740(7)
c/Å	12.1513(8)
α/°	97.716(3)
β/°	112.057(3)
γ/°	109.430(3)
Volume/Å^3	1054.03(13)
Z	2

ρ_{calc}g/cm^3	1.485
μ/mm^{-1}	2.049
F(000)	484.0
Crystal size/mm^3	0.48 × 0.32 × 0.04
Absorption correction	empirical
Tmin; Tmax	0.6550; 0.7460
Radiation	MoKα (λ = 0.71073)
2Θ range for data collection/°	3.786 to 60.054°
Completeness to theta	0.999
Index ranges	-13 ≤ h ≤ 13, -15 ≤ k ≤ 15, -17 ≤ l ≤ 17
Reflections collected	45848
Independent reflections	6159 [R_{int} = 0.0504, R_{sigma} = 0.0298]
Data/restraints/parameters	6159/0/263
Goodness-of-fit on F^2	1.049
Final R indexes [I>=2σ (I)]	R_1 = 0.0259, wR_2 = 0.0641
Final R indexes [all data]	R_1 = 0.0299, wR_2 = 0.0661
Largest diff. peak/hole / e Å^{-3}	0.50/-0.46

Table 7.18: Bond Lengths for **19a**.

Atom	Atom	Length/Å	Atom	Atom	Length/Å
Br	C2	1.9604(13)	C9	C10	1.391(2)
P	O1	1.4841(10)	C10	C11	1.387(2)
P	C1	1.8254(14)	C11	C12	1.397(2)
P	C3	1.8290(14)	C13	C14	1.4024(19)
P	C6	1.8809(14)	C13	C18	1.3949(19)
O2	C4	1.206(2)	C14	C15	1.3922(19)
O3	C4	1.3375(19)	C15	C16	1.391(2)
O3	C5	1.446(2)	C16	C17	1.384(2)
C1	C2	1.5195(19)	C17	C18	1.3951(19)
C3	C4	1.5043(19)	C19	C20	1.397(2)
C6	C7	1.5468(18)	C19	C24	1.407(2)
C6	C13	1.5443(18)	C20	C21	1.399(2)
C6	C19	1.5391(19)	C21	C22	1.381(3)
C7	C8	1.4029(19)	C22	C23	1.388(3)
C7	C12	1.3943(19)	C23	C24	1.389(2)
C8	C9	1.386(2)			

Table 7.19: Bond Angles for **19a**.

Atom	Atom	Atom	Angle/˚	Atom	Atom	Atom	Angle/˚
O1	P	C1	109.49(6)	C9	C8	C7	121.24(13)
O1	P	C3	112.11(6)	C8	C9	C10	119.99(14)
O1	P	C6	114.89(6)	C11	C10	C9	119.43(13)
C1	P	C3	104.05(7)	C10	C11	C12	120.70(13)
C1	P	C6	111.32(6)	C7	C12	C11	120.31(13)
C3	P	C6	104.36(6)	C14	C13	C6	118.62(12)

C4	O3	C5	116.43(14)	C18	C13	C6	122.82(12)
C2	C1	P	112.67(9)	C18	C13	C14	118.40(12)
C1	C2	Br	110.83(9)	C15	C14	C13	120.64(13)
C4	C3	P	109.14(9)	C16	C15	C14	120.26(14)
O2	C4	O3	124.97(14)	C17	C16	C15	119.52(13)
O2	C4	C3	124.84(14)	C16	C17	C18	120.44(14)
O3	C4	C3	110.19(13)	C13	C18	C17	120.67(13)
C7	C6	P	111.22(9)	C20	C19	C6	120.92(13)
C13	C6	P	107.72(9)	C20	C19	C24	117.61(13)
C13	C6	C7	105.70(10)	C24	C19	C6	121.23(12)
C19	C6	P	106.06(9)	C19	C20	C21	120.80(15)
C19	C6	C7	111.26(11)	C22	C21	C20	120.79(15)
C19	C6	C13	114.91(11)	C21	C22	C23	119.15(14)
C8	C7	C6	116.21(12)	C22	C23	C24	120.48(16)
C12	C7	C6	125.46(12)	C23	C24	C19	121.17(15)
C12	C7	C8	118.33(13)				

Table 7.20: Torsion Angles for **19a**.

A	B	C	D	Angle/˚	A	B	C	D	Angle/˚
P	C1	C2	Br	-155.74(7)	C6	C19	C24	C23	-173.97(13)
P	C3	C4	O2	80.98(16)	C7	C6	C13	C14	-64.98(15)
P	C3	C4	O3	-98.52(12)	C7	C6	C13	C18	110.38(14)
P	C6	C7	C8	-171.04(10)	C7	C6	C19	C20	17.07(17)
P	C6	C7	C12	8.54(17)	C7	C6	C19	C24	-168.72(12)
P	C6	C13	C14	54.00(14)	C7	C8	C9	C10	0.2(2)
P	C6	C13	C18	-130.64(12)	C8	C7	C12	C11	0.3(2)
P	C6	C19	C20	-104.00(13)	C8	C9	C10	C11	-0.3(2)
P	C6	C19	C24	70.21(14)	C9	C10	C11	C12	0.3(2)
O1	P	C1	C2	56.63(11)	C10	C11	C12	C7	-0.3(2)
O1	P	C3	C4	35.97(12)	C12	C7	C8	C9	-0.2(2)
O1	P	C6	C7	43.16(11)	C13	C6	C7	C8	-54.41(15)
O1	P	C6	C13	-72.23(10)	C13	C6	C7	C12	125.17(14)
O1	P	C6	C19	164.26(8)	C13	C6	C19	C20	137.12(13)
C1	P	C3	C4	-82.26(11)	C13	C6	C19	C24	-48.66(17)
C1	P	C6	C7	168.33(9)	C13	C14	C15	C16	-1.3(2)
C1	P	C6	C13	52.94(10)	C14	C13	C18	C17	-2.5(2)
C1	P	C6	C19	-70.57(10)	C14	C15	C16	C17	-0.8(2)
C3	P	C1	C2	176.64(10)	C15	C16	C17	C18	1.3(2)
C3	P	C6	C7	-80.02(10)	C16	C17	C18	C13	0.4(2)
C3	P	C6	C13	164.60(9)	C18	C13	C14	C15	3.0(2)
C3	P	C6	C19	41.08(10)	C19	C6	C7	C8	70.96(15)
C5	O3	C4	O2	1.3(2)	C19	C6	C7	C12	-109.46(15)
C5	O3	C4	C3	-179.18(13)	C19	C6	C13	C14	171.94(12)
C6	P	C1	C2	-71.50(11)	C19	C6	C13	C18	-12.69(18)
C6	P	C3	C4	160.93(10)	C19	C20	C21	C22	-0.1(2)
C6	C7	C8	C9	179.40(13)	C20	C19	C24	C23	0.4(2)

C6	C7	C12	C11	-179.32(13)	C20	C21	C22	C23	0.5(2)
C6	C13	C14	C15	178.55(12)	C21	C22	C23	C24	-0.4(2)
C6	C13	C18	C17	-177.91(13)	C22	C23	C24	C19	-0.1(2)
C6	C19	C20	C21	174.08(13)	C24	C19	C20	C21	-0.3(2)

7.1.7 2-bromoethyl (2-oxo-2-phenylethyl)(triphenylmethyl)phosphane oxide (19b)

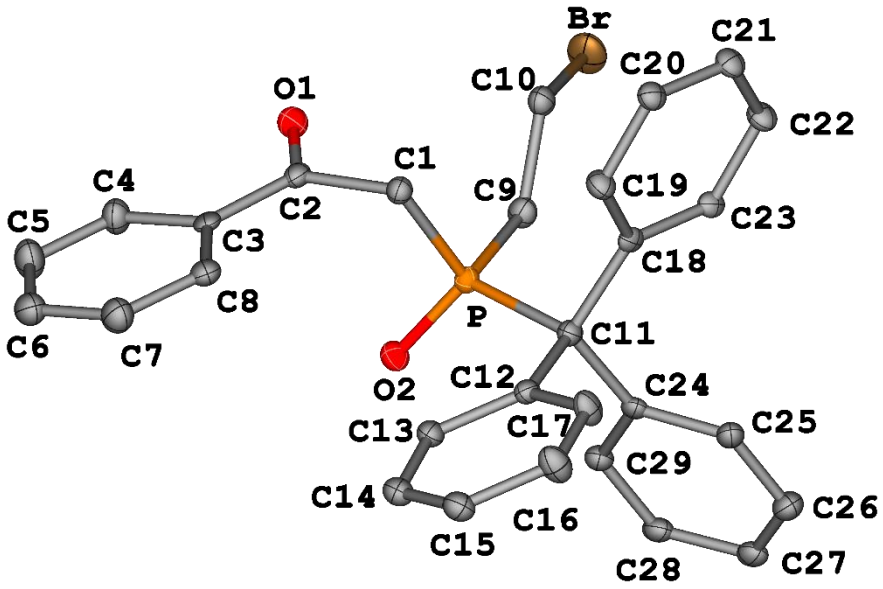

Figure 7.7: Molecular structures of **19b** in the solid state. Hydrogen atoms are omitted and the thermal ellipsoids are set at the 50% probability level.

Table 7.21: Crystal data and structure refinement for **19b**.

Identification code	GSTR760, FLG-350 // GXraymo_6861f
Crystal Habitus	clear colourless needle
Device Type	Bruker D8 Venture
Empirical formula	$C_{29}H_{26}O_2PBr$
Moiety formula	C29 H26 Br O2 P
Formula weight	517.38
Temperature/K	100
Crystal system	triclinic
Space group	P-1
a/Å	8.9276(15)
b/Å	10.5777(17)
c/Å	14.307(2)
α/°	69.469(6)
β/°	84.259(7)
γ/°	72.909(7)
Volume/Å^3	1209.4(3)
Z	2
ρ_{calc}g/cm^3	1.421

μ/mm^{-1}	1.790
F(000)	532.0
Crystal size/mm^3	0.28 × 0.14 × 0.06
Absorption correction	empirical
Tmin; Tmax	0.487803; 0.746069
Radiation	MoKα (λ = 0.71073)
2Θ range for data collection/°	4.28 to 51.996°
Completeness to theta	0.987
Index ranges	-10 ≤ h ≤ 10, -11 ≤ k ≤ 13, 0 ≤ l ≤ 17
Reflections collected	4735
Independent reflections	4735 [R_{int} = ?, R_{sigma} = 0.1317]
Data/restraints/parameters	4735/264/299
Goodness-of-fit on F^2	1.078
Final R indexes [I>=2σ (I)]	R_1 = 0.0874, wR_2 = 0.2096
Final R indexes [all data]	R_1 = 0.1510, wR_2 = 0.2394
Largest diff. peak/hole / e Å^{-3}	1.48/-1.04

Table 7.22: Bond Lengths for **19b**.

Atom	Atom	Length/Å	Atom	Atom	Length/Å
Br	C10	1.971(8)	C12	C13	1.400(11)
P	O2	1.500(6)	C12	C17	1.394(11)
P	C1	1.832(8)	C13	C14	1.409(11)
P	C9	1.813(8)	C14	C15	1.366(12)
P	C11	1.868(8)	C15	C16	1.402(11)
O1	C2	1.228(10)	C16	C17	1.391(12)
C1	C2	1.528(10)	C18	C19	1.387(11)
C2	C3	1.476(11)	C18	C23	1.398(11)
C3	C4	1.417(11)	C19	C20	1.408(11)
C3	C8	1.400(12)	C20	C21	1.368(11)
C4	C5	1.385(12)	C21	C22	1.378(11)
C5	C6	1.370(13)	C22	C23	1.402(11)
C6	C7	1.380(12)	C24	C25	1.406(11)
C7	C8	1.393(12)	C24	C29	1.405(11)
C9	C10	1.510(11)	C25	C26	1.380(11)
C11	C12	1.558(11)	C26	C27	1.380(12)
C11	C18	1.554(11)	C27	C28	1.387(11)
C11	C24	1.537(10)	C28	C29	1.398(11)

Table 7.23: Bond Angles for **19b**.

Atom	Atom	Atom	Angle/˚	Atom	Atom	Atom	Angle/˚
O2	P	C1	109.6(3)	C24	C11	C18	112.4(6)
O2	P	C9	108.5(4)	C13	C12	C11	122.5(7)
O2	P	C11	114.9(3)	C17	C12	C11	119.2(7)
C1	P	C11	106.3(4)	C17	C12	C13	118.2(7)
C9	P	C1	108.8(4)	C12	C13	C14	119.9(7)

C9	P	C11	108.6(4)	C15	C14	C13	121.0(8)
C2	C1	P	105.8(5)	C14	C15	C16	119.7(8)
O1	C2	C1	118.3(7)	C17	C16	C15	119.4(8)
O1	C2	C3	121.8(7)	C16	C17	C12	121.7(8)
C3	C2	C1	119.8(7)	C19	C18	C11	120.8(7)
C4	C3	C2	117.9(8)	C19	C18	C23	118.8(7)
C8	C3	C2	124.4(7)	C23	C18	C11	120.1(7)
C8	C3	C4	117.8(7)	C18	C19	C20	120.4(7)
C5	C4	C3	120.0(8)	C21	C20	C19	119.8(7)
C6	C5	C4	121.1(8)	C20	C21	C22	120.9(8)
C5	C6	C7	120.3(8)	C21	C22	C23	119.6(8)
C6	C7	C8	119.7(9)	C18	C23	C22	120.4(7)
C7	C8	C3	121.1(8)	C25	C24	C11	120.4(7)
C10	C9	P	121.6(6)	C29	C24	C11	122.5(7)
C9	C10	Br	109.3(5)	C29	C24	C25	117.0(7)
C12	C11	P	111.1(5)	C26	C25	C24	121.5(8)
C18	C11	P	104.6(5)	C27	C26	C25	120.9(8)
C18	C11	C12	111.0(6)	C26	C27	C28	119.2(8)
C24	C11	P	111.7(5)	C27	C28	C29	120.4(8)
C24	C11	C12	106.2(6)	C28	C29	C24	121.0(7)

Table 7.24: Torsion Angles for **19b**.

A	B	C	D	Angle/˚	A	B	C	D	Angle/˚
P	C1	C2	O1	-75.9(8)	C11	C12	C13	C14	175.9(7)
P	C1	C2	C3	105.3(7)	C11	C12	C17	C16	-176.8(8)
P	C9	C10	Br	-173.3(4)	C11	C18	C19	C20	-175.1(7)
P	C11	C12	C13	24.3(9)	C11	C18	C23	C22	175.6(7)
P	C11	C12	C17	-159.0(6)	C11	C24	C25	C26	176.9(7)
P	C11	C18	C19	83.7(8)	C11	C24	C29	C28	-176.8(7)
P	C11	C18	C23	-89.9(7)	C12	C11	C18	C19	-36.2(10)
P	C11	C24	C25	162.5(6)	C12	C11	C18	C23	150.2(7)
P	C11	C24	C29	-22.5(10)	C12	C11	C24	C25	-76.2(8)
O1	C2	C3	C4	8.7(11)	C12	C11	C24	C29	98.8(8)
O1	C2	C3	C8	-171.9(7)	C12	C13	C14	C15	1.0(12)
O2	P	C1	C2	-36.2(6)	C13	C12	C17	C16	0.1(13)
O2	P	C9	C10	140.5(6)	C13	C14	C15	C16	-0.4(13)
O2	P	C11	C12	-58.5(6)	C14	C15	C16	C17	-0.4(13)
O2	P	C11	C18	-178.2(5)	C15	C16	C17	C12	0.6(14)
O2	P	C11	C24	59.9(6)	C17	C12	C13	C14	-0.9(12)
C1	P	C9	C10	21.4(8)	C18	C11	C12	C13	140.2(7)
C1	P	C11	C12	62.9(6)	C18	C11	C12	C17	-43.1(10)
C1	P	C11	C18	-56.8(6)	C18	C11	C24	C25	45.3(10)
C1	P	C11	C24	-178.7(5)	C18	C11	C24	C29	-139.6(7)
C1	C2	C3	C4	-172.5(7)	C18	C19	C20	C21	1.3(12)
C1	C2	C3	C8	6.9(12)	C19	C18	C23	C22	1.8(12)
C2	C3	C4	C5	-180.0(8)	C19	C20	C21	C22	-1.6(13)

C2	C3	C8	C7	-179.8(8)	C20	C21	C22	C23	2.1(12)
C3	C4	C5	C6	-1.3(14)	C21	C22	C23	C18	-2.2(12)
C4	C3	C8	C7	-0.4(12)	C23	C18	C19	C20	-1.4(12)
C4	C5	C6	C7	1.7(14)	C24	C11	C12	C13	-97.4(8)
C5	C6	C7	C8	-1.4(13)	C24	C11	C12	C17	79.3(9)
C6	C7	C8	C3	0.8(13)	C24	C11	C18	C19	-154.9(7)
C8	C3	C4	C5	0.6(12)	C24	C11	C18	C23	31.5(10)
C9	P	C1	C2	82.3(6)	C24	C25	C26	C27	-1.2(12)
C9	P	C11	C12	179.9(5)	C25	C24	C29	C28	-1.5(12)
C9	P	C11	C18	60.1(6)	C25	C26	C27	C28	0.7(12)
C9	P	C11	C24	-61.7(6)	C26	C27	C28	C29	-0.7(12)
C11	P	C1	C2	-160.9(5)	C27	C28	C29	C24	1.1(12)
C11	P	C9	C10	-94.0(7)	C29	C24	C25	C26	1.5(12)

7.1.8 2-iodoethyl(methyl)triphenylmethyl)phosphane oxide (19c)

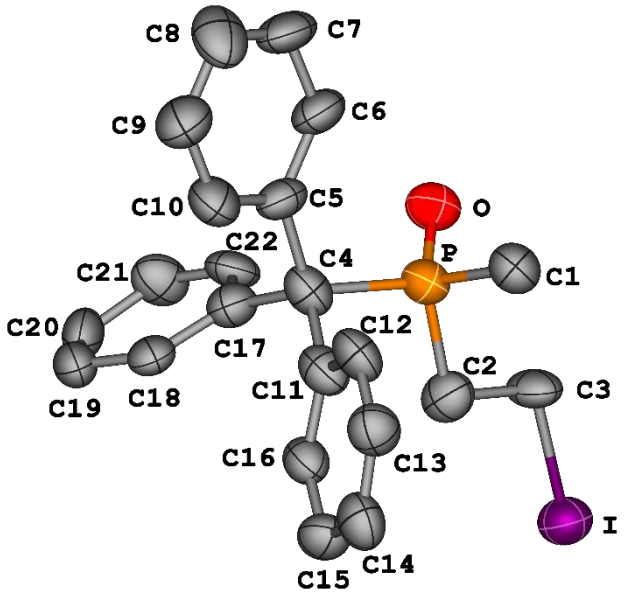

Figure 7.8: Molecular structures of **19c** in the solid state. Hydrogen atoms are omitted and the thermal ellipsoids are set at the 50% probability level.

Table 7.25: Crystal data and structure refinement for **19c**.

Identification code	GSTR830, FLG-352 // GXray7821_1
Crystal Habitus	clear colourless plank
Device Type	STOE Stadivari
Empirical formula	$C_{22}H_{22}IOP$
Moiety formula	C22 H22 I O P
Formula weight	460.26
Temperature/K	100
Crystal system	triclinic
Space group	P-1
a/Å	8.5094(6)

b/Å	9.6625(5)
c/Å	12.4574(8)
α/°	87.025(5)
β/°	71.262(5)
γ/°	89.857(5)
Volume/Å^3	968.57(11)
Z	2
ρ_{calc}g/cm^3	1.578
μ/mm^{-1}	13.809
F(000)	460.0
Crystal size/mm^3	0.3 × 0.1 × 0.03
Absorption correction	multi-scan
Tmin; Tmax	0.0070; 0.0178
Radiation	Cu Kα (λ = 1.54186)
2Θ range for data collection/°	7.504 to 135.492°
Completeness to theta	0.994
Index ranges	-10 ≤ h ≤ 5, -11 ≤ k ≤ 11, -14 ≤ l ≤ 13
Reflections collected	41947
Independent reflections	3500 [R_{int} = 0.0878, R_{sigma} = 0.0277]
Data/restraints/parameters	3500/0/228
Goodness-of-fit on F^2	2.489
Final R indexes [I>=2σ (I)]	R_1 = 0.1654, wR_2 = 0.4682
Final R indexes [all data]	R_1 = 0.1699, wR_2 = 0.4789
Largest diff. peak/hole / e Å^{-3}	6.70/-2.73

Table 7.26: Bond Lengths for **19c**.

Atom	Atom	Length/Å	Atom	Atom	Length/Å
I	C3	2.165(15)	C9	C10	1.38(3)
P	O	1.502(12)	C11	C12	1.40(2)
P	C1	1.820(17)	C11	C16	1.39(2)
P	C2	1.852(19)	C12	C13	1.38(3)
P	C4	1.899(18)	C13	C14	1.40(3)
C2	C3	1.52(2)	C14	C15	1.37(2)
C4	C5	1.55(2)	C15	C16	1.42(2)
C4	C11	1.53(3)	C17	C18	1.41(2)
C4	C17	1.53(2)	C17	C22	1.40(2)
C5	C6	1.40(3)	C18	C19	1.41(2)
C5	C10	1.39(3)	C19	C20	1.36(3)
C6	C7	1.40(2)	C20	C21	1.40(3)
C7	C8	1.36(3)	C21	C22	1.36(2)
C8	C9	1.37(3)			

Table 7.27: Bond Angles for **19c**.

Atom	Atom	Atom	Angle/˚	Atom	Atom	Atom	Angle/˚
O	P	C1	110.7(7)	C7	C8	C9	119(2)

O	P	C2	110.5(7)	C8	C9	C10	120(2)
O	P	C4	115.0(8)	C9	C10	C5	121.9(18)
C1	P	C2	105.2(9)	C12	C11	C4	122.3(16)
C1	P	C4	108.6(8)	C16	C11	C4	119.4(14)
C2	P	C4	106.3(8)	C16	C11	C12	118.3(17)
C3	C2	P	107.9(12)	C13	C12	C11	119.7(18)
C2	C3	I	110.0(11)	C12	C13	C14	122.6(16)
C5	C4	P	111.8(11)	C15	C14	C13	118.4(19)
C11	C4	P	102.2(12)	C14	C15	C16	119.7(17)
C11	C4	C5	112.5(13)	C11	C16	C15	121.2(15)
C17	C4	P	110.3(11)	C18	C17	C4	120.1(14)
C17	C4	C5	104.3(14)	C22	C17	C4	125.0(15)
C17	C4	C11	116.0(13)	C22	C17	C18	114.9(14)
C6	C5	C4	124.5(15)	C19	C18	C17	122.6(14)
C10	C5	C4	118.6(15)	C20	C19	C18	119.1(13)
C10	C5	C6	116.9(15)	C19	C20	C21	119.0(14)
C7	C6	C5	120.4(19)	C22	C21	C20	120.7(15)
C8	C7	C6	121(2)	C21	C22	C17	122.8(15)

Table 7.28: Torsion Angles for **19c**.

A	B	C	D	Angle/˚	A	B	C	D	Angle/˚
P	C2	C3	I	179.7(7)	C5	C4	C17	C22	87.6(19)
P	C4	C5	C6	21.6(19)	C5	C6	C7	C8	1(3)
P	C4	C5	C10	-160.3(12)	C6	C5	C10	C9	1(3)
P	C4	C11	C12	89.3(17)	C6	C7	C8	C9	1(3)
P	C4	C11	C16	-89.6(15)	C7	C8	C9	C10	-1(3)
P	C4	C17	C18	149.9(12)	C8	C9	C10	C5	0(3)
P	C4	C17	C22	-33(2)	C10	C5	C6	C7	-1(2)
O	P	C2	C3	46.5(14)	C11	C4	C5	C6	135.9(15)
O	P	C4	C5	-58.2(13)	C11	C4	C5	C10	-46.0(19)
O	P	C4	C11	-178.8(9)	C11	C4	C17	C18	34(2)
O	P	C4	C17	57.3(14)	C11	C4	C17	C22	-148.1(16)
C1	P	C2	C3	-73.0(13)	C11	C12	C13	C14	2(3)
C1	P	C4	C5	66.5(13)	C12	C11	C16	C15	-2(2)
C1	P	C4	C11	-54.1(12)	C12	C13	C14	C15	-5(3)
C1	P	C4	C17	-178.0(12)	C13	C14	C15	C16	5(3)
C2	P	C4	C5	179.2(11)	C14	C15	C16	C11	-1(2)
C2	P	C4	C11	58.6(11)	C16	C11	C12	C13	2(3)
C2	P	C4	C17	-65.3(14)	C17	C4	C5	C6	-97.6(17)
C4	P	C2	C3	171.9(12)	C17	C4	C5	C10	80.5(17)
C4	C5	C6	C7	176.7(16)	C17	C4	C11	C12	-150.7(17)
C4	C5	C10	C9	-177.2(17)	C17	C4	C11	C16	30(2)
C4	C11	C12	C13	-176.9(16)	C17	C18	C19	C20	8(2)
C4	C11	C16	C15	176.8(15)	C18	C17	C22	C21	2(2)
C4	C17	C18	C19	174.5(15)	C18	C19	C20	C21	-11(3)
C4	C17	C22	C21	-175.9(18)	C19	C20	C21	C22	10(3)

C5	C4	C11	C12	-31(2)	C20	C21	C22	C17	-5(3)
C5	C4	C11	C16	150.3(15)	C22	C17	C18	C19	-3(2)
C5	C4	C17	C18	-89.9(17)					

7.1.9 2-Bromoethyl(2-oxopropyl)(triphenylmethyl)phosphane oxide (19f)

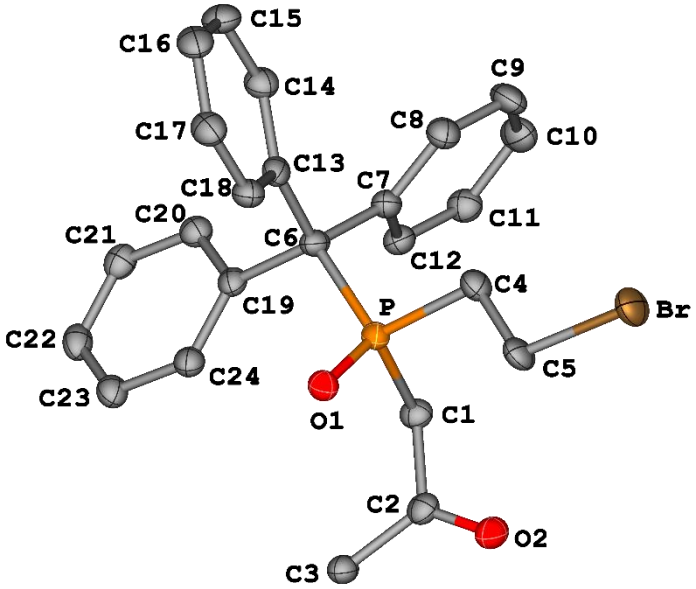

Figure 7.9: Molecular structures of **19f** in the solid state. Hydrogen atoms are omitted and the thermal ellipsoids are set at the 50% probability level.

Table 7.29: Crystal data and structure refinement for **19f**.

Identification code	GSTR813, FLG-457 // GXray7409
Crystal Habitus	clear colourless block
Device Type	STOE STADIVARI
Empirical formula	$C_{24}H_{24}BrO_2P$
Moiety formula	C24 H24 Br O2 P
Formula weight	455.31
Temperature/K	100
Crystal system	triclinic
Space group	P-1
a/Å	8.8789(4)
b/Å	9.5863(4)
c/Å	13.4826(5)
α/°	84.831(3)
β/°	87.383(3)
γ/°	65.062(3)
Volume/Å^3	1036.32(8)
Z	2
ρ_{calc}g/cm^3	1.459
μ/mm^{-1}	3.563
F(000)	468.0
Crystal size/mm^3	0.21 × 0.2 × 0.12

Absorption correction	multi-scan
Tmin; Tmax	0.2209; 0.2978
Radiation	CuKα (λ = 1.54186)
2Θ range for data collection/°	10.208 to 140.976°
Completeness to theta	0.987
Index ranges	-10 ≤ h ≤ 4, -11 ≤ k ≤ 11, -15 ≤ l ≤ 16
Reflections collected	15691
Independent reflections	3862 [R_{int} = 0.0486, R_{sigma} = 0.0410]
Data/restraints/parameters	3862/0/254
Goodness-of-fit on F^2	1.047
Final R indexes [I>=2σ (I)]	R_1 = 0.0541, wR_2 = 0.1413
Final R indexes [all data]	R_1 = 0.0664, wR_2 = 0.1529
Largest diff. peak/hole / e $Å^{-3}$	1.70/-0.71

Table 7.30: Bond Lengths for **19f**.

Atom	Atom	Length/Å	Atom	Atom	Length/Å
Br	C5	1.960(3)	C9	C10	1.382(6)
P	O1	1.488(3)	C10	C11	1.384(6)
P	C1	1.838(4)	C11	C12	1.397(5)
P	C4	1.823(4)	C13	C14	1.401(5)
P	C6	1.886(3)	C13	C18	1.392(5)
O2	C2	1.217(4)	C14	C15	1.393(5)
C1	C2	1.516(5)	C15	C16	1.386(6)
C2	C3	1.502(5)	C16	C17	1.371(6)
C4	C5	1.518(5)	C17	C18	1.391(5)
C6	C7	1.541(5)	C19	C20	1.397(5)
C6	C13	1.547(5)	C19	C24	1.394(5)
C6	C19	1.552(5)	C20	C21	1.384(5)
C7	C8	1.404(5)	C21	C22	1.399(6)
C7	C12	1.393(5)	C22	C23	1.366(6)
C8	C9	1.392(5)	C23	C24	1.408(5)

Table 7.31: Bond Angles for **19f**.

Atom	Atom	Atom	Angle/˚	Atom	Atom	Atom	Angle/˚
O1	P	C1	110.50(15)	C9	C8	C7	120.8(4)
O1	P	C4	110.02(16)	C10	C9	C8	120.5(4)
O1	P	C6	116.91(15)	C9	C10	C11	119.9(4)
C1	P	C6	105.62(16)	C10	C11	C12	119.6(4)
C4	P	C1	106.16(17)	C7	C12	C11	121.7(3)
C4	P	C6	107.02(16)	C14	C13	C6	119.9(3)
C2	C1	P	110.0(2)	C18	C13	C6	122.0(3)
O2	C2	C1	120.1(3)	C18	C13	C14	117.8(3)
O2	C2	C3	123.0(3)	C15	C14	C13	120.8(4)
C3	C2	C1	116.9(3)	C16	C15	C14	120.2(4)
C5	C4	P	108.7(2)	C17	C16	C15	119.4(3)

C4	C5	Br	110.8(2)	C16	C17	C18	120.8(4)
C7	C6	P	104.2(2)	C17	C18	C13	120.9(3)
C7	C6	C13	112.8(3)	C20	C19	C6	118.5(3)
C7	C6	C19	112.1(3)	C24	C19	C6	123.1(3)
C13	C6	P	111.6(2)	C24	C19	C20	118.3(3)
C13	C6	C19	106.0(3)	C21	C20	C19	120.7(3)
C19	C6	P	110.3(2)	C20	C21	C22	120.7(4)
C8	C7	C6	121.2(3)	C23	C22	C21	119.0(3)
C12	C7	C6	121.2(3)	C22	C23	C24	120.8(4)
C12	C7	C8	117.5(3)	C19	C24	C23	120.5(3)

7.1.10 Bromo(2-bromoethyl)(triphenylmethyl)phosphane oxide (34b)

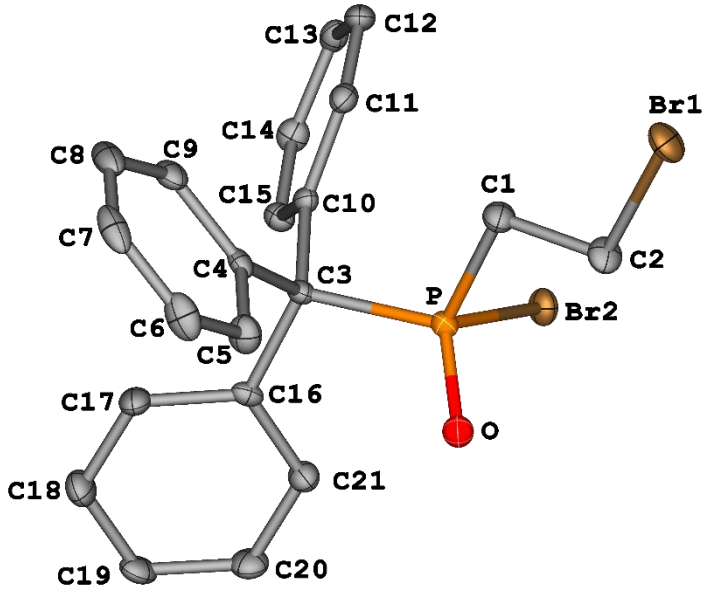

Figure 7.10: Molecular structures of **34b** in the solid state. Hydrogen atoms are omitted and the thermal ellipsoids are set at the 50% probability level.

Table 7.32: Crystal data and structure refinement for **34b**.

Identification code	GSTR820, FLG-479 // GXraymo_7603f
Crystal Habitus	clear colourless plate
Device Type	Bruker D8 Venture
Empirical formula	$C_{21}H_{19}OPBr_2$
Moiety formula	C21 H19 Br2 O P
Formula weight	478.15
Temperature/K	100.0
Crystal system	orthorhombic
Space group	Pbcn
a/Å	15.5180(5)
b/Å	14.8016(7)
c/Å	16.4458(8)
α/°	90
β/°	90

γ/°	90
Volume/Å^3	3777.5(3)
Z	8
ρ_{calc}g/cm^3	1.682
μ/mm^{-1}	4.383
F(000)	1904.0
Crystal size/mm^3	0.3 × 0.1 × 0.04
Absorption correction	multi-scan
Tmin; Tmax	0.5881; 0.7462
Radiation	MoKα (λ = 0.71073)
2Θ range for data collection/°	3.802 to 55.99°
Completeness to theta	1.000
Index ranges	-20 ≤ h ≤ 18, -19 ≤ k ≤ 19, -21 ≤ l ≤ 21
Reflections collected	41588
Independent reflections	4567 [R_{int} = 0.0552, R_{sigma} = 0.0288]
Data/restraints/parameters	4567/0/226
Goodness-of-fit on F^2	1.044
Final R indexes [I>=2σ (I)]	R_1 = 0.0265, wR_2 = 0.0607
Final R indexes [all data]	R_1 = 0.0359, wR_2 = 0.0646
Largest diff. peak/hole / e Å^{-3}	0.46/-0.28

Table 7.33: Bond Lengths for **34b**.

Atom	Atom	Length/Å	Atom	Atom	Length/Å
Br1	C2	1.962(2)	C8	C9	1.388(3)
Br2	P	2.2191(6)	C10	C11	1.404(3)
P	O	1.4761(15)	C10	C15	1.386(3)
P	C1	1.824(2)	C11	C12	1.385(3)
P	C3	1.890(2)	C12	C13	1.395(3)
C1	C2	1.515(3)	C13	C14	1.385(3)
C3	C4	1.546(3)	C14	C15	1.395(3)
C3	C10	1.536(3)	C16	C17	1.394(3)
C3	C16	1.549(3)	C16	C21	1.394(3)
C4	C5	1.397(3)	C17	C18	1.391(3)
C4	C9	1.393(3)	C18	C19	1.383(3)
C5	C6	1.387(3)	C19	C20	1.380(3)
C6	C7	1.379(4)	C20	C21	1.389(3)
C7	C8	1.382(4)			

Table 7.34: Bond Angles for **34b**.

Atom	Atom	Atom	Angle/˚	Atom	Atom	Atom	Angle/˚
O	P	Br2	111.76(7)	C6	C7	C8	119.4(2)
O	P	C1	112.04(10)	C7	C8	C9	120.6(2)
O	P	C3	114.19(9)	C8	C9	C4	120.5(2)
C1	P	Br2	101.65(7)	C11	C10	C3	120.11(18)
C1	P	C3	110.48(10)	C15	C10	C3	121.61(18)

C3	P	Br2	105.86(7)	C15	C10	C11	118.15(19)
C2	C1	P	108.60(15)	C12	C11	C10	121.1(2)
C1	C2	Br1	110.05(15)	C11	C12	C13	120.1(2)
C4	C3	P	106.15(14)	C14	C13	C12	119.2(2)
C4	C3	C16	107.67(16)	C13	C14	C15	120.5(2)
C10	C3	P	107.65(13)	C10	C15	C14	120.8(2)
C10	C3	C4	114.06(17)	C17	C16	C3	117.95(18)
C10	C3	C16	111.48(17)	C21	C16	C3	123.91(19)
C16	C3	P	109.65(14)	C21	C16	C17	118.06(19)
C5	C4	C3	119.00(19)	C18	C17	C16	121.1(2)
C9	C4	C3	122.21(19)	C19	C18	C17	120.1(2)
C9	C4	C5	118.3(2)	C20	C19	C18	119.5(2)
C6	C5	C4	120.8(2)	C19	C20	C21	120.6(2)
C7	C6	C5	120.4(2)	C20	C21	C16	120.7(2)

7.1.11 Iodo(2-iodoethyl)(triphenylmethyl)phosphane oxide (34c)

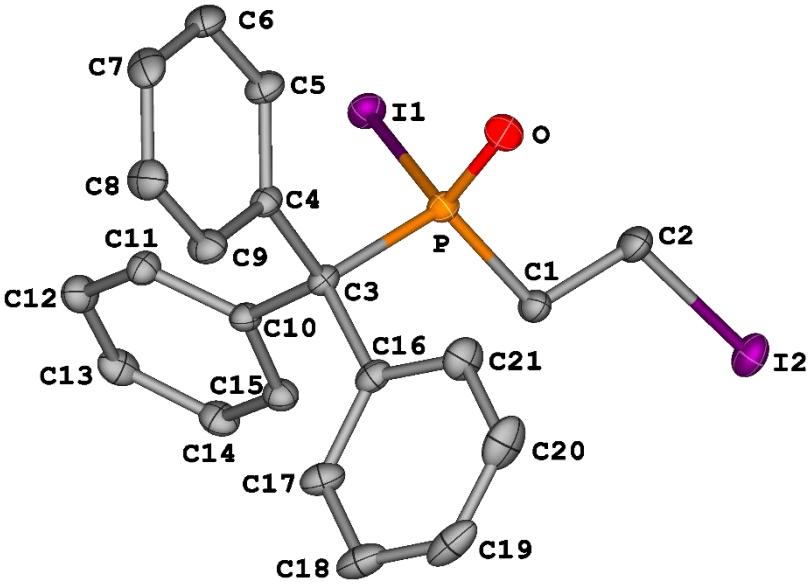

Figure 7.11: Molecular structures of **34c** in the solid state. Hydrogen atoms are omitted and the thermal ellipsoids are set at the 50% probability level.

Table 7.35: Crystal data and structure refinement for **34c**.

Identification code	GSTR822, FLG-508 // GXraymo_7684f
Crystal Habitus	clear colourless plank
Device Type	Bruker D8 Venture
Empirical formula	$C_{21}H_{19}OPI_2$
Moiety formula	C21 H19 I2 O P
Formula weight	572.13
Temperature/K	100.00
Crystal system	orthorhombic
Space group	Pbcn
a/Å	15.6572(3)

b/Å	15.0040(4)
c/Å	16.6917(4)
α/°	90
β/°	90
γ/°	90
Volume/Å^3	3921.22(16)
Z	8
ρ_{calc}g/cm^3	1.938
μ/mm^{-1}	3.296
F(000)	2192.0
Crystal size/mm^3	0.2 × 0.08 × 0.02
Absorption correction	multi-scan
Tmin; Tmax	0.6050; 0.7464
Radiation	MoKα (λ = 0.71073)
2Θ range for data collection/°	3.76 to 65.05°
Completeness to theta	0.998
Index ranges	-23 ≤ h ≤ 21, -22 ≤ k ≤ 22, -25 ≤ l ≤ 25
Reflections collected	58418
Independent reflections	7118 [R_{int} = 0.0454, R_{sigma} = 0.0260]
Data/restraints/parameters	7118/0/226
Goodness-of-fit on F^2	1.056
Final R indexes [I>=2σ (I)]	R_1 = 0.0291, wR_2 = 0.0746
Final R indexes [all data]	R_1 = 0.0361, wR_2 = 0.0786
Largest diff. peak/hole / e Å^{-3}	1.89/-1.30

Table 7.36: Bond Lengths for **34c**.

Atom	Atom	Length/Å	Atom	Atom	Length/Å
I1	P	2.4565(6)	C8	C9	1.401(4)
I2	C2	2.157(3)	C10	C11	1.390(3)
P	O	1.480(2)	C10	C15	1.402(3)
P	C1	1.840(2)	C11	C12	1.396(3)
P	C3	1.898(2)	C12	C13	1.390(4)
C1	C2	1.516(4)	C13	C14	1.389(4)
C3	C4	1.544(3)	C14	C15	1.388(4)
C3	C10	1.534(3)	C16	C17	1.392(4)
C3	C16	1.548(3)	C16	C21	1.388(4)
C4	C5	1.396(3)	C17	C18	1.393(4)
C4	C9	1.393(4)	C18	C19	1.382(5)
C5	C6	1.397(3)	C19	C20	1.377(5)
C6	C7	1.390(4)	C20	C21	1.396(4)
C7	C8	1.370(4)			

Table 7.37: Bond Angles for **34c**.

Atom	Atom	Atom	Angle/˚	Atom	Atom	Atom	Angle/˚
O	P	I1	112.59(8)	C8	C7	C6	119.7(2)

O	P	C1	111.66(11)	C7	C8	C9	120.5(3)
O	P	C3	114.04(11)	C4	C9	C8	120.9(2)
C1	P	I1	100.92(8)	C11	C10	C3	121.6(2)
C1	P	C3	110.52(11)	C11	C10	C15	118.2(2)
C3	P	I1	106.23(7)	C15	C10	C3	119.9(2)
C2	C1	P	107.85(17)	C10	C11	C12	120.6(2)
C1	C2	I2	110.63(17)	C13	C12	C11	120.4(2)
C4	C3	P	109.46(16)	C14	C13	C12	119.7(2)
C4	C3	C16	108.45(18)	C15	C14	C13	119.6(2)
C10	C3	P	107.30(15)	C14	C15	C10	121.5(2)
C10	C3	C4	111.63(18)	C17	C16	C3	121.1(2)
C10	C3	C16	113.33(19)	C21	C16	C3	120.0(2)
C16	C3	P	106.49(16)	C21	C16	C17	118.5(2)
C5	C4	C3	123.5(2)	C16	C17	C18	120.4(3)
C9	C4	C3	118.3(2)	C19	C18	C17	120.5(3)
C9	C4	C5	118.0(2)	C20	C19	C18	119.5(3)
C4	C5	C6	120.9(2)	C19	C20	C21	120.2(3)
C7	C6	C5	120.1(2)	C16	C21	C20	120.8(3)

Table 7.38: Torsion Angles for **34c**.

A	B	C	D	Angle/˚	A	B	C	D	Angle/˚
I1	P	C1	C2	74.51(18)	C4	C3	C16	C21	-70.4(3)
I1	P	C3	C4	-86.70(15)	C4	C5	C6	C7	0.2(4)
I1	P	C3	C10	34.61(15)	C5	C4	C9	C8	0.5(4)
I1	P	C3	C16	156.26(13)	C5	C6	C7	C8	0.1(4)
P	C1	C2	I2	178.08(12)	C6	C7	C8	C9	0.0(4)
P	C3	C4	C5	28.6(3)	C7	C8	C9	C4	-0.3(4)
P	C3	C4	C9	-155.2(2)	C9	C4	C5	C6	-0.5(4)
P	C3	C10	C11	-109.2(2)	C10	C3	C4	C5	-90.0(3)
P	C3	C10	C15	64.5(2)	C10	C3	C4	C9	86.1(3)
P	C3	C16	C17	-139.3(2)	C10	C3	C16	C17	-21.5(3)
P	C3	C16	C21	47.4(3)	C10	C3	C16	C21	165.1(2)
O	P	C1	C2	-45.3(2)	C10	C11	C12	C13	-1.7(4)
O	P	C3	C4	37.90(18)	C11	C10	C15	C14	3.6(4)
O	P	C3	C10	159.20(15)	C11	C12	C13	C14	2.9(4)
O	P	C3	C16	-79.14(17)	C12	C13	C14	C15	-0.9(4)
C1	P	C3	C4	164.66(15)	C13	C14	C15	C10	-2.5(4)
C1	P	C3	C10	-74.04(17)	C15	C10	C11	C12	-1.6(4)
C1	P	C3	C16	47.62(18)	C16	C3	C4	C5	144.4(2)
C3	P	C1	C2	-173.39(17)	C16	C3	C4	C9	-39.4(3)
C3	C4	C5	C6	175.7(2)	C16	C3	C10	C11	133.5(2)
C3	C4	C9	C8	-175.8(2)	C16	C3	C10	C15	-52.8(3)
C3	C10	C11	C12	172.3(2)	C16	C17	C18	C19	-0.9(4)
C3	C10	C15	C14	-170.3(2)	C17	C16	C21	C20	1.4(4)
C3	C16	C17	C18	-173.2(2)	C17	C18	C19	C20	-0.1(4)
C3	C16	C21	C20	175.0(2)	C18	C19	C20	C21	1.8(4)

C4	C3	C10	C11	10.7(3)	C19	C20	C21	C16	-2.5(4)
C4	C3	C10	C15	-175.6(2)	C21	C16	C17	C18	0.3(4)
C4	C3	C16	C17	103.0(3)					

7.1.12 [Pentacarbonyl{2-((hydroxy(triphenylmethyl)phosphino)ethyl-acetate-κP}tungsten(0)] (55a)

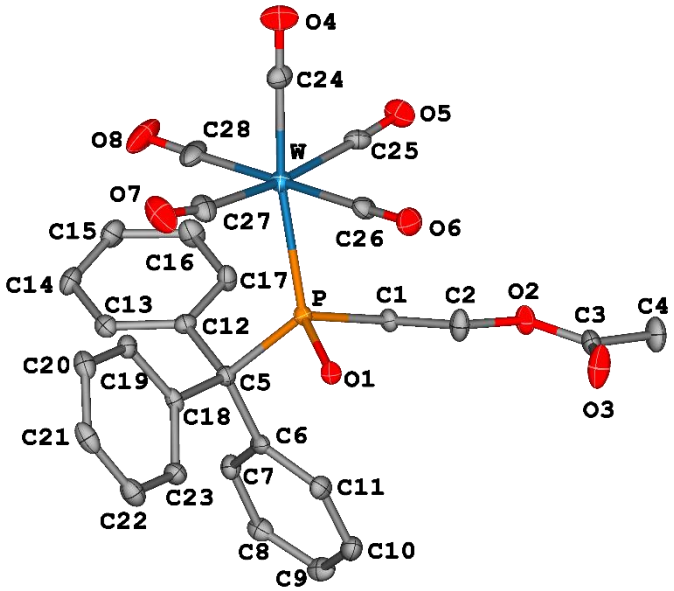

Figure 7.12: Molecular structures of **55a** in the solid state. Hydrogen atoms are omitted and the thermal ellipsoids are set at the 50% probability level.

Table 7.39: Crystal data and structure refinement for **55a**.

Identification code	GSTR834, FLG-549 // GXraymo_7934f_pl
Crystal Habitus	clear yellowish colourless plate
Device Type	Bruker D8 Venture
Empirical formula	$C_{28}H_{23}O_8PW$
Moiety formula	C28 H23 O8 P W
Formula weight	702.28
Temperature/K	100
Crystal system	triclinic
Space group	P-1
a/Å	9.7746(8)
b/Å	11.8024(10)
c/Å	11.8049(9)
α/°	80.283(3)
β/°	78.201(3)
γ/°	85.911(3)
Volume/Å^3	1313.00(19)
Z	2
ρ_{calc}g/cm^3	1.776
μ/mm^{-1}	4.510

F(000)	688.0
Crystal size/mm^3	0.18 × 0.16 × 0.04
Absorption correction	multi-scan
Tmin; Tmax	0.3616; 0.7463
Radiation	MoKα (λ = 0.71073)
2Θ range for data collection/°	3.504 to 56°
Completeness to theta	1.000
Index ranges	-12 ≤ h ≤ 12, -15 ≤ k ≤ 15, -15 ≤ l ≤ 15
Reflections collected	46391
Independent reflections	6335 [R_{int} = 0.0941, R_{sigma} = 0.0902]
Data/restraints/parameters	6335/0/343
Goodness-of-fit on F^2	1.046
Final R indexes [I>=2σ (I)]	R_1 = 0.0421, wR_2 = 0.1029
Final R indexes [all data]	R_1 = 0.0451, wR_2 = 0.1054
Largest diff. peak/hole / e Å^{-3}	2.46/-1.49

Table 7.40: Bond Lengths for **55a**.

Atom	Atom	Length/Å	Atom	Atom	Length/Å
W	P	2.5458(11)	C5	C12	1.537(6)
W	C24	2.007(5)	C5	C18	1.538(6)
W	C25	2.055(5)	C6	C7	1.385(6)
W	C26	2.033(5)	C6	C11	1.411(6)
W	C27	2.060(5)	C7	C8	1.400(6)
W	C28	2.054(5)	C8	C9	1.382(7)
P	O1	1.614(3)	C9	C10	1.387(7)
P	C1	1.857(4)	C10	C11	1.386(6)
P	C5	1.940(4)	C12	C13	1.403(6)
O2	C2	1.465(5)	C12	C17	1.397(6)
O2	C3	1.334(5)	C13	C14	1.398(6)
O3	C3	1.204(6)	C14	C15	1.387(7)
O4	C24	1.142(6)	C15	C16	1.387(7)
O5	C25	1.134(6)	C16	C17	1.392(7)
O6	C26	1.142(6)	C18	C19	1.401(6)
O7	C27	1.131(7)	C18	C23	1.400(6)
O8	C28	1.136(6)	C19	C20	1.387(7)
C1	C2	1.515(6)	C20	C21	1.387(7)
C3	C4	1.495(7)	C21	C22	1.397(7)
C5	C6	1.542(6)	C22	C23	1.381(7)

Table 7.41: Bond Angles for **55a**.

Atom	Atom	Atom	Angle/˚	Atom	Atom	Atom	Angle/˚
C24	W	P	171.22(13)	C18	C5	P	102.0(3)
C24	W	C25	87.4(2)	C18	C5	C6	112.6(4)
C24	W	C26	87.32(19)	C7	C6	C5	120.8(4)
C24	W	C27	85.1(2)	C7	C6	C11	117.2(4)

C24	W	C28	91.62(19)	C11	C6	C5	122.0(4)
C25	W	P	89.83(13)	C6	C7	C8	122.1(4)
C25	W	C27	172.49(18)	C9	C8	C7	119.4(4)
C26	W	P	84.49(14)	C8	C9	C10	120.0(4)
C26	W	C25	92.80(19)	C11	C10	C9	120.1(4)
C26	W	C27	87.1(2)	C10	C11	C6	121.2(4)
C26	W	C28	177.26(19)	C13	C12	C5	121.4(4)
C27	W	P	97.63(14)	C17	C12	C5	120.5(4)
C28	W	P	96.71(14)	C17	C12	C13	117.8(4)
C28	W	C25	89.7(2)	C14	C13	C12	120.4(4)
C28	W	C27	90.3(2)	C15	C14	C13	120.8(4)
O1	P	W	112.09(12)	C16	C15	C14	119.2(4)
O1	P	C1	97.91(18)	C15	C16	C17	120.0(5)
O1	P	C5	101.86(18)	C16	C17	C12	121.6(4)
C1	P	W	111.49(14)	C19	C18	C5	120.2(4)
C1	P	C5	105.81(19)	C23	C18	C5	122.9(4)
C5	P	W	124.19(13)	C23	C18	C19	116.8(4)
C3	O2	C2	115.4(4)	C20	C19	C18	121.9(4)
C2	C1	P	109.6(3)	C21	C20	C19	120.3(4)
O2	C2	C1	106.6(4)	C20	C21	C22	118.7(5)
O2	C3	C4	111.9(4)	C23	C22	C21	120.7(5)
O3	C3	O2	124.1(4)	C22	C23	C18	121.6(4)
O3	C3	C4	124.0(4)	O4	C24	W	178.5(4)
C6	C5	P	112.5(3)	O5	C25	W	176.5(4)
C12	C5	P	107.7(3)	O6	C26	W	177.1(4)
C12	C5	C6	108.8(4)	O7	C27	W	171.9(5)
C12	C5	C18	113.0(3)	O8	C28	W	176.5(5)

Table 7.42: Torsion Angles for **55a**.

A	B	C	D	Angle/˚	A	B	C	D	Angle/˚
W	P	C1	C2	80.4(3)	C7	C8	C9	C10	1.7(7)
P	C1	C2	O2	-173.8(3)	C8	C9	C10	C11	-0.4(7)
P	C5	C6	C7	-142.8(4)	C9	C10	C11	C6	-1.9(7)
P	C5	C6	C11	39.2(5)	C11	C6	C7	C8	-1.3(7)
P	C5	C12	C13	-137.8(4)	C12	C5	C6	C7	-23.5(5)
P	C5	C12	C17	48.6(5)	C12	C5	C6	C11	158.6(4)
P	C5	C18	C19	71.2(4)	C12	C5	C18	C19	-44.2(5)
P	C5	C18	C23	-104.3(4)	C12	C5	C18	C23	140.3(4)
O1	P	C1	C2	-37.2(3)	C12	C13	C14	C15	0.4(7)
C2	O2	C3	O3	0.2(7)	C13	C12	C17	C16	3.0(7)
C2	O2	C3	C4	-178.8(4)	C13	C14	C15	C16	2.4(7)
C3	O2	C2	C1	-163.2(4)	C14	C15	C16	C17	-2.5(8)
C5	P	C1	C2	-141.9(3)	C15	C16	C17	C12	-0.3(8)
C5	C6	C7	C8	-179.3(4)	C17	C12	C13	C14	-3.0(6)
C5	C6	C11	C10	-179.3(4)	C18	C5	C6	C7	102.6(5)
C5	C12	C13	C14	-176.7(4)	C18	C5	C6	C11	-75.3(5)

C5	C12	C17	C16	176.8(4)	C18	C5	C12	C13	-25.9(6)
C5	C18	C19	C20	-174.7(4)	C18	C5	C12	C17	160.5(4)
C5	C18	C23	C22	174.9(4)	C18	C19	C20	C21	-0.1(7)
C6	C5	C12	C13	99.9(5)	C19	C18	C23	C22	-0.8(6)
C6	C5	C12	C17	-73.6(5)	C19	C20	C21	C22	-1.1(7)
C6	C5	C18	C19	-168.0(4)	C20	C21	C22	C23	1.4(7)
C6	C5	C18	C23	16.5(6)	C21	C22	C23	C18	-0.4(7)
C6	C7	C8	C9	-0.9(7)	C23	C18	C19	C20	1.0(6)
C7	C6	C11	C10	2.6(7)					

7.2 Compound abbreviations of target molecules

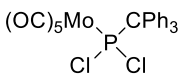

4

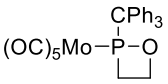

7a

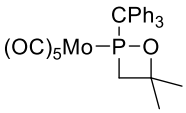

7b

8a

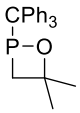

8b

10a

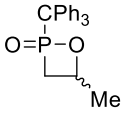

10c,c'

11a

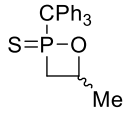

11c,c'

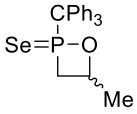

12c,c'

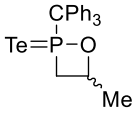

13c,c'

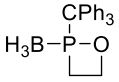

14a

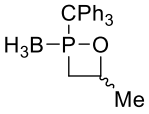

14c,c'

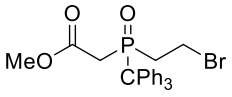

19a

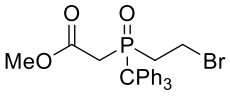

19b

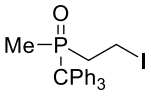

19c

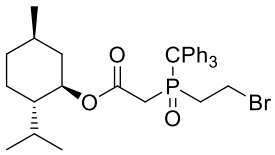

19d,d'

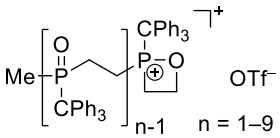

22^{n}

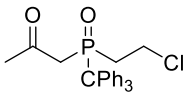

19e

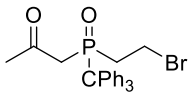

19f

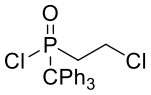

34a

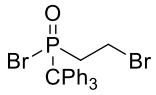

34b

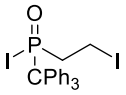

34c

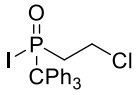

36a

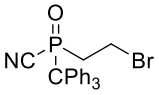

37a

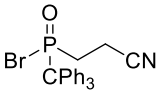

37b

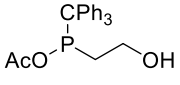

38a

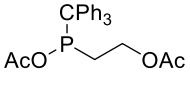

39a

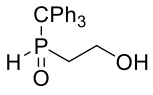

40a

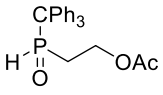

41a

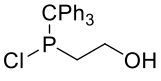

38b

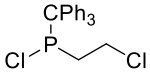

39b

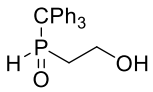

40b

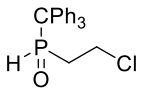

41b

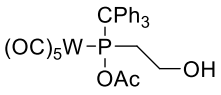

54a

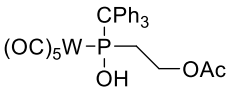

55a

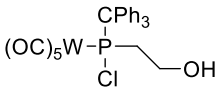

54b

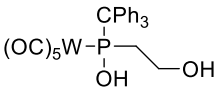

55b

Figure 7.13: Compound abbreviations of target molecules.

7.3 List of Figures

7.4 List of Schemes

7.5 List of Tables